



**University of
Sheffield**

The role of integrins in the spatial
organisation of the mammary gland

Priya Narayanan

A thesis submitted in fulfilment of the requirements for the degree of Doctor
of Philosophy

Department of Oncology and Metabolism

May 2023

For all the animals who unwittingly sacrifice their lives in the name of research.

Declaration

The work in this thesis has not been submitted in support of an application of any degree or qualification at the University of Sheffield or any other University or Institute of learning.

Priya Narayanan
May 2023

Acknowledgements

My PhD has been the most challenging period in my life, and I would not have been able to complete it without the support and love of many people over the past 3.5 years.

Foremost, I am grateful to my supervisors, Dr Nasreen Akhtar and Dr Alexander Fletcher, for providing guidance and support throughout my studies. Some of my favourite meetings were ones in which we discussed completely random things unrelated to my research. I am also thankful for the pastoral support of my advisor Karen Sisley.

I am beyond grateful to all the technicians in the O&M department and staff at the LMF that have helped me along the way. Particularly Matthew Fisher for all his support with the mouse work and Sarah Waite for providing help with experimental questions. I would like to thank Dr Stanley Strawbridge and Dr Jessica Crawshaw for providing advice and suggestions on the modelling work.

I would also like to thank the past and current members of the Akhtar and Fletcher groups who have helped me with experimental/modelling work. I am also grateful to members of the Jessop Wing office for cheering me up when experiments did not work, making those bad days more bearable.

I am thankful to my parents for being just a phone call away whenever I needed them and for sending me care packages throughout my studies. Lastly, I want to thank my best friend and now fiancé, Juan-Philip Marx, for being my pillar of strength and always finding time to help debug my MATLAB scripts despite doing a PhD himself.

I walk away from my PhD not only having furthered my knowledge but also having met incredible people who have challenged and nurtured me, to whom I will always be indebted.

Thank you all.

Abstract

The mammary epithelium is organised into a bilayer of inner polarised luminal epithelial (LE) lining the lumen space and outer myoepithelial (ME) cells, surrounded by a laminin-rich extracellular matrix (ECM). Although this architectural design is found in numerous internal organs, the processes involved in forming the concentric bilayer remain unknown. β 1-integrin, a receptor that detects the ECM, is expressed more in ME than LE cells. We hypothesised that i) affinity to the ECM or ii) repulsion at the apical membrane drives ME cell positioning towards the ECM. I begin this thesis by validating lineage-specific β 1-integrin deletion mouse models before characterising lumen formation in organoid cultures. I explore the role of ME β 1-integrin-ECM signalling in polarity orientation and lumen formation to understand the differences between *in vivo* and *in vitro* data. Genetic deletion of β 1-integrin in LE or ME cells did not affect cell positioning in primary culture organoids. I further tested by overlaying 2D cells with an exogenous ECM to relocate ECM affinity and disrupt the apical membrane. In WT culture, ME cells were positioned next to the top surface due to their affinity to the ECM, but β 1-integrin^{-/-} ME cells failed. β 1-integrin deletion in LE cells inhibited apical membrane disruption in response to an ECM overlay and significantly reduced ME relocation. These findings support our hypotheses; however, further investigations are needed to establish the hierarchy of the two mechanisms. Using the experimental data, I developed a computational model to run predictive simulations of cell sorting under different integrin expressions. This identified integrins are required for establishing and maintaining cell positioning. Finally, I tested to what extent cell positioning and cell lineage-specific β 1-integrin are essential for normal tissue function using organoid and collagen gel contraction assays. Overall, my thesis provides novel insights into the multifaceted role of integrins in the spatial organisation and function of the mammary gland.

Table of contents

Declaration	3
Acknowledgements	4
Abstract	5
Table of contents	6
List of Figures	10
List of Tables	13
List of Abbreviations	14
1 Introduction	15
1.1 Mammary gland development	15
1.1.1 Embryonic and prepubertal development.....	15
1.1.2 Pubertal development	16
1.1.3 Development during adulthood.....	17
1.2 Structure of the gland	18
1.2.1 Mammary BM composition	19
1.2.2 Mammary tissue cells	20
1.2.2.1 Cap cells	20
1.2.2.2 Body cells	20
1.2.2.3 Luminal epithelial cells	20
1.2.2.4 Myoepithelial cells	20
1.2.2.5 Mammary stem cells.....	21
1.3 MEC-ECM interactions – adhesion receptors	22
1.3.1 Integrins	22
1.3.1.1 Integrin structure	22
1.3.1.2 Integrin-ECM adhesion and signalling.....	24
1.3.1.3 Integrin expression in the mammary gland	26
1.4 β1-integrin role in mammary gland development	26
1.4.1 Apical-basal polarity.....	26
1.4.2 Cell proliferation	27
1.4.3 Lactational differentiation	28
1.4.4 Cellular apoptosis.....	29
1.4.5 Stem cell maintenance.....	29
1.5 β4-integrin role in mammary gland development	30
1.6 Integrin role in breast cancer	32
1.7 Potential mechanisms involved in spatial organisation of mammary tissue	34
1.7.1 Oriented cell division	36
1.7.2 Cell movement.....	38
1.8 Summary	38
1.9 Hypothesis and Aims	39
2 Methods	41
2.1 β1-integrin^{-/-} mice	41
2.1.1 Licensing and husbandry.....	41

2.1.2 Mouse models	41
2.1.3 Murine mammary gland isolation.....	41
2.2 Primary cell culture	42
2.2.1 Monolayer cell culture	43
2.2.2 ECM-overlay assay	44
2.2.3 Repulsion test assay.....	44
2.2.4 Organoid formation assay.....	44
2.2.5 Organoid contraction assay	45
2.2.6 Collagen gel contraction assay.....	46
2.2.7 Replating assay	46
2.2.8 EdU proliferation assay	46
2.3 Standard cell culture procedures	47
2.3.1 Acid-etching coverslips	47
2.3.2 Passaging and culturing cells	47
2.3.3 Freezing cells.....	47
2.4 Molecular Biology	48
2.4.1 RNA Isolation	48
2.4.2 cDNA synthesis	48
2.4.3 TaqMan qPCR.....	48
2.4.3.1 Analysis	49
2.5 Immunostaining	49
2.5.1 Antibodies	49
2.5.2 Immunofluorescence staining 3D organoids and 2D cells.	50
2.5.3 Whole mount mammary gland immunofluorescence staining	51
2.5.4 Imaging and quantification	51
2.6 Statistical analysis	52
3 Lineage specific $\beta 1$-integrin^{fx/fx} primary organoids as a model system to study the role	
<i>$\beta 1$-integrin in lumen formation.</i>	53
3.1 Introduction	53
3.2 Results	55
3.2.1 Primary mammary co-culture organoids recapitulate <i>in vivo</i> mammary tissue.	55
3.2.2 Characterisation of inducible deletion of $\beta 1$ -integrin gene in myoepithelial cells	57
3.2.3 Characterisation of inducible deletion of $\beta 1$ -integrin gene in luminal cells	59
3.2.4 Loss of $\beta 1$ -integrin in ME cells perturbs lumen formation in organoids embedded in a type I collagen gel but not laminin-rich BM.....	61
3.2.5 Deletion of $\beta 1$ -integrin in luminal cells perturbs lumen formation in organoids embedded in a laminin-rich BM and type I collagen.	66
3.2.6 The absence of WT ME cells in LE $\beta 1$ -integrin KO organoids inverts apical polarity when plated on top of a laminin-rich BM.	69
3.3 Discussion	71
4 The effect of lineage specific deletion of $\beta 1$-integrin in mammary epithelial cell sorting	
4.1 Introduction	73
4.2 Results	75
4.2.1 $\beta 1$ -integrin deletion in myoepithelial cells does not affect its positioning when embedded in laminin-rich BM	75
4.2.2 Laminin deposition and assembly is compromised in ME $\beta 1$ -integrin deleted organoids.	78
4.2.3 $\beta 1$ -integrin deletion in luminal cells does not affect cell sorting in a laminin-rich BM or in type I collagen gel	81

4.2.4 β 1-integrin deletion in ME or LE cells alone does not disrupt MEC positioning in alveolar structures	83
4.2.5 MECs re-plated in Matrigel organise into inner LE and outer ME.	86
4.2.6 ME cells position closer to the new cell-ECM interface.	91
4.2.7 The presence of an apical membrane overrides ME cell affinity to the ECM.	93
4.2.8 MEC plated on top of a confluent epithelial layer move towards the ECM.	95
4.2.9 ME cells reposition next to the new cell-ECM interface even in the absence of oriented cell division.	97
4.2.10 Inhibition of cell proliferation does not affect spatial organisation of MECs in 3D culture.	99
4.3 Discussion	101
5 Development of an in-silico model to study cell sorting in the mammary gland.	105
5.1 Introduction	105
5.1.1 Cell-based modelling methods	107
5.1.2 Aims	108
5.2 Methods	109
5.2.1 Initial and boundary conditions	109
5.2.2 Cell types	110
5.2.3 Mechanical forces	110
5.2.4 Cell-cell repulsion (F_{ccr})	110
5.2.5 Cell-cell adhesion (F_{cca})	111
5.2.6 Cell-ECM forces (F_{cea})	111
5.2.7 Cell division	112
5.2.8 Cell death	113
5.2.9 Cell polarity	114
5.2.10 Data output	114
5.2.11 The software	114
5.2.11.1 Installation	115
5.2.11.2 GitHub	116
5.3 Results	116
5.3.1 2D culture reference model	116
5.3.1.1 2D culture morphology of a population comprising of two cell types.	117
5.3.1.2 2D culture morphology with addition of stem cells	120
5.3.2 Knockout of control mechanisms	122
5.3.2.1 Oriented cell division	122
5.3.2.2 Anchorage-dependent growth	124
5.3.2.3 Anoikis	126
5.3.3 Organoid reference model	127
5.3.3.1 Morphology and growth kinetics	127
5.3.4 Integrin expression variation	129
5.3.5 Integrins are necessary for establishing and maintaining cell positioning.	136
5.3.6 Summary of simulated organoid cases	140
5.4 Discussion	140
6 β1-integrin is required for myoepithelial cell contractility	143
6.1 Introduction	143
6.2 Results	144
6.2.1 β 1-integrin deletion in ME cells impairs its morphology and transcription of ME cell differentiation markers.	144
6.2.2 Deletion of β 1-integrin in ME cells affects its contractility.	147
6.2.3 ME cells cause contraction of collagen gels regardless of oxytocin presence.	153
6.2.4 Collagen gel contractility is affected by loss of β 1-integrin in LE cells.	155

6.3 Discussion	158
7 General Discussion	162
7.1 Overview	162
7.2 Critical appraisal of key methodology.....	166
7.3 Future work	167
7.4 Conclusion	169
8 References	170

List of Figures

Figure 1: Schematic of mammary gland morphogenesis in mice.....	17
Figure 2: The mammary gland structure.....	18
Figure 3: Integrin heterodimer.....	23
Figure 4: Integrin family and their heterodimers.....	23
Figure 5: Schematic representation of key integrin signalling pathways.....	25
Figure 6: Cell sorting models.....	35
Figure 7: Tamoxifen inducible $\beta 1$ -integrin gene expression.....	42
Figure 8: Organoid formation in laminin-rich BM matrix.....	56
Figure 9: 4-OHT treatment of $\beta 1$ -Integrin ^{fx/fx} : K14-CreER MECs knocks out $\beta 1$ -Integrin in ME cells.....	58
Figure 10: 4-OHT treatment of $\beta 1$ -Integrin ^{fx/fx} : K18-CreER MECs knocks out $\beta 1$ -Integrin in LE cells.....	60
Figure 11: ME $\beta 1$ -Integrin deletion does not affect lumen formation in organoids embedded in a laminin-rich BM.....	63
Figure 12: ME $\beta 1$ -Integrin deletion does not affect apical-basal polarity of alveolar organoids embedded in a laminin-rich BM.....	64
Figure 13: ME $\beta 1$ -Integrin deletion perturbs lumen formation in organoids embedded in type I collagen. ...	65
Figure 14: LE $\beta 1$ -Integrin deletion perturbs lumen formation in alveolar organoids.....	67
Figure 15: Apical-basal polarity is partially inverted in LE $\beta 1$ -integrin ^{fx/fx} alveolar organoids.....	68
Figure 16: Lumen formation and apical-basal polarity is significantly impaired in LE $\beta 1$ -integrin ^{fx/fx} alveolar organoids plated on top of a laminin-rich BM.....	70
Figure 17: ME $\beta 1$ -integrin ^{fx/fx} ductal organoids embedded in a laminin-rich BM form with inner LE and outer ME.....	77
Figure 18: ME $\beta 1$ -Integrin deletion reduces LM111 deposition.....	80
Figure 19: LE $\beta 1$ -integrin ^{fx/fx} ductal organoids form with inner LE and outer ME.....	82
Figure 20: ME $\beta 1$ -integrin ^{fx/fx} alveolar organoids form with inner LE and outer ME.....	84
Figure 21: LE $\beta 1$ -integrin ^{fx/fx} alveolar organoids form with inner LE and outer ME.....	85
Figure 22: Diagram explaining the rational of the 2D to 3D experiment.....	87
Figure 23: Dissociating 2D culture removes pre-assembled mammary structures.....	87

Figure 24: MEC sorting is not disrupted in ME $\beta 1$ -integrin ^{fx/fx} alveolar organoids.....	89
Figure 25: MEC sorting is not disrupted in LE $\beta 1$ -integrin ^{fx/fx} alveolar organoids.	90
Figure 26: ME cells position next to a new ECM interface.....	92
Figure 27: In the presence of an apical membrane fewer ME cells are positioned next to the new ECM interface.....	94
Figure 28: MEC added to a confluent Eph4 2D culture adhere and integrate.	96
Figure 29: Inhibition of cell proliferation reduces the number of ME cell positioned next to the new ECM interface.....	98
Figure 30: Inhibition of cell proliferation does not affect MEC sorting in 3D culture.	100
Figure 31: Schematics of different cell-based modelling approaches.	107
Figure 32: Simulation of WT MEC reference model.	118
Figure 33: Height distribution of ME and LE cells in the reference population.	118
Figure 34: Growth kinetics of WT MEC reference model.....	119
Figure 35: Addition of mammary stem cells better recapitulates in vitro culture.....	121
Figure 36: Knockout of oriented planar cell division does not alter cell positioning.	123
Figure 37: Knockout of anchorage dependent growth does not alter cell positioning.	125
Figure 38: Knockout of anoikis does not alter cell positioning.	126
Figure 39: Snapshot of WT organoid reference model at t = 120 hr.	128
Figure 40: Growth kinetics of WT organoid reference model.....	129
Figure 41: 3D organoid computational model recapitulates in vitro culture of organoids without $\beta 1$ -integrin in ME or LE cells.....	131
Figure 42: $\beta 1$ -integrin knockout in both cell types does not affect MEC sorting in simulated organoids.....	132
Figure 43: $\beta 4$ -integrin knockout in ME and/or LE cells does not affect MEC sorting in simulated organoids.	133
Figure 44: Spatial organisation of organoids with differential integrin expression.....	135
Figure 45: Loss of integrin function simulations from WT organoids.....	137
Figure 46: Gain of integrin function simulations from $\beta 1$ and $\beta 4$ KO organoids.....	139
Figure 47: ME $\beta 1$ -integrin ^{fx/fx} cell area is smaller than WT ME cells in 3D culture.....	145
Figure 48: ME $\beta 1$ -integrin deletion downregulates ACTA2 gene expression.....	146
Figure 49: Oxytocin induces contraction of alveolar organoids.....	148

Figure 50: ME β 1-integrin deletion reduces the number of contractions per minute in alveolar organoids. 148

Figure 51: Automatisation of organoid contraction analysis using MATLAB helps detect minute changes not visible to the naked eye. 149

Figure 52: Morphology of ME β 1-integrin^{fx/fx} cells is different to WT ME cells when treated with oxytocin. 150

Figure 53: MECs exhibit contractile phenotype even in the absence of oxytocin in collagen gels. 152

Figure 54: Contractile properties are markedly attenuated in ME β 1-integrin^{fx/fx} cells from pregnant mice. 153

Figure 55: MECs cultured in collagen gel largely formed spherical organoids. 154

Figure 56: Contractile properties are markedly attenuated in ME β 1-integrin^{fx/fx} cells from virgin mice. 154

Figure 57: Contractile properties are markedly attenuated in LE β 1-integrin^{fx/fx} cells from pregnant mice. . 156

Figure 58: ME cell area is not affected by β 1-integrin deletion in LE cells. 157

Figure 59: Working model of how integrins modulate differentiation and contractility of ME cells. 161

List of Tables

Table 1: Integrin expression in the mammary gland.....	26
Table 2: TaqMan gene expression assay probes, gene name and assay ID.....	49
Table 3: Primary antibodies used in this study, source, and concentration.....	50
Table 4: Table of parameters used for 2D culture in silico simulations.....	117
Table 5: Table of parameters used for 3D culture in silico simulations.....	127
Table 6: Combinations of β1 and β4 expression in luminal and myoepithelial cells.....	130
Table 7: Summarises the simulated organoid cases with different integrin expressions.....	140

List of Abbreviations

4-OHT	4-hydroxytamoxifen
α SMA	alpha Smooth Muscle Actin
β 1-integrin	Beta 1-integrin
β 4-integrin	Beta 4-integrin
BM	Basement membrane
cDNA	complementary DNA
CHO	Chinese Hamster Ovary
CreER	Cre-Estrogen Receptor
CT	Cycle threshold
DNA	Deoxyribonucleic acid
ECM	Extracellular Matrix
EDTA	Ethylenediaminetetraacetic acid
EDU	5-ethynyl-2'-deoxyuridine
EGF	Epidermal growth factor
ERK	Extracellular signal-regulated kinase
FAK	Focal adhesion kinase
FBS	Foetal Bovine Serum
FGF	Fibroblast growth factor
GFP	Green fluorescent protein
IF	Immunofluorescence
ILK	Integrin-linked kinase
K8/18	Keratin 8/18
Keratin 14	Keratin 14
LE	Luminal Epithelial
LM	Laminin
MaSC	Mammary Stem Cells
MAPK1	Mitogen Activated Protein Kinase-1
ME	Myoepithelial cells
MECs	Mammary Epithelial Cells
PAK	p21 interacting exchange factor Associated Kinase
PBS	Phosphate Buffered Saline
PKC ζ	Protein Kinase C zeta
qPCR	quantitative PCR
Rac	Ras-related C3 botulinum toxin substrate
RNA	Ribose Nucleic Acid
RPM	Revolutions Per Minute
scRNAseq	Single cell RNA sequencing
SEM	Standard Error of the Mean
TEB	Terminal End Bud
WT	Wild Type
ZO1	Zonular Occludens-1

1 Introduction

In this thesis, I will examine the role of integrins receptors that detects the extracellular matrix (ECM) in spatial organisation of the mammary gland. Mammary tissue is made up of a network of branched ducts connected to milk producing lobular alveoli. Each structure is spatially ordered with inner luminal epithelial cells and outer myoepithelial cells, surrounded by a thin layer of specialised extracellular matrix (ECM), termed the basement membrane (BM). However, this architectural design is not unique to the mammary gland; it is also found in the prostate, salivary, lacrimal, and sweat glands. Despite this, the processes involved in forming the concentric bilayer structure remains unknown. Understanding the mechanisms involved in spatial organisation of the mammary tissue during development, also has important implications within the cancer and regenerative medicine fields. For example, early stage of breast cancer is characterised by a loss in tissue architecture with an abnormal growth of tumour cells filling the hollow spaces of the tissue. Data increasingly suggest that in invasive breast carcinoma the myoepithelial cell layer is lost along with the surrounding BM enabling cancer cells to disseminate to other organs (Dornier et al., 2017). Therefore, understanding how this tumour suppressing bilayer structure develops is important in tackling breast cancer.

In this introduction chapter, I will give an overview of the mammary gland morphogenesis, integrin structure and its role in the mammary gland. I will then discuss the mechanisms we hypothesise to be involved in forming the concentric bilayer structure.

1.1 Mammary gland development

Mammary tissue is a unique glandular structure because, although the stroma is formed before birth, the epithelium only becomes fully developed postnatally.

1.1.1 Embryonic and prepubertal development

In mice, development of the mammary tissue starts around embryonic day 10; a ductal tree-like structure forms from a small rudiment known as the anlage (Hogg et al., 1983). Elongation

of embryonic branches is driven by directional cell migration and is supported rather than directly powered by cell proliferation (Myllymäki et al., 2023).

Before birth, this structure repolarises, forming simple epithelial tubes that remain in a quiescent state until the onset of puberty in female embryos (Hogg et al., 1983). However, in male embryos the mammary rudiment is compressed irreversibly in response to androgen signaling around embryonic day 14 (Dunbar et al., 1999). This contrasts to humans, where mammary gland development remains indistinguishable between males and females until puberty.

1.1.2 Pubertal development

During puberty, under the influence of hormones and other growth factors such as FGF10 and TGF- β 1, the mammary anlage undergoes branching morphogenesis to generate an extensive ductal network in humans and mice (Williams and Daniel, 1983, Lindström et al., 2022, Neumann et al., 2023). Expansion of the ductal network is driven by terminal end buds (TEBs) that encapsulate the leading front of primary ducts. TEBs are comprised of cap cells, which form the outer layer, and body cells, which form a multilayered inner core (Figure 1) (Williams and Daniel, 1983).

Direction of ductal extension was conventionally thought to be due to global signals and alignment of type I collagen. However more recently Nerger and colleagues (2021), revealed increased stiffness from ECM accumulation near TEB constrains the bifurcation angle of TEB, which subsequently regulates the orientation of epithelial growth. Knockout mice models of estrogen receptor- α fail to develop TEBs and fail to undergo branching morphogenesis, which suggests that estrogen is an important regulator of proliferation and morphogenesis during puberty (Mallepell et al., 2006).

Cells within TEBs undergo rapid proliferation via the GPRC6A/PI3K/AKT/mTOR signaling pathway activated by L-arginine (Ge et al., 2022). These cells have significantly lower levels of cell adhesion and lack cell polarity, enabling ductal elongation and stromal expansion (Ewald et al., 2012, Williams and Daniel, 1983). Increasingly, data suggest that radial intercalation is the primary mechanism by which the stratified epithelium resolves back to a bi-layered

structure (Neumann et al., 2018). However, the molecular mechanisms involved are still elusive.

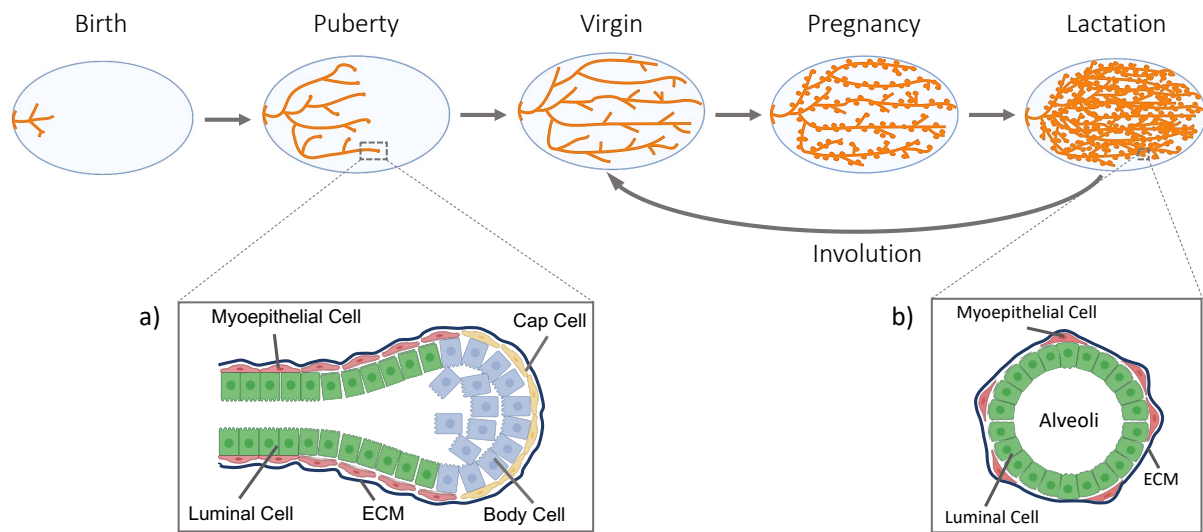


Figure 1: Schematic of mammary gland morphogenesis in mice. A schematic of the stages of mammary gland development from pre-puberty through to pregnancy, lactation, and involution. During puberty, **(a)** terminal end bud form which invade the mammary fat pad forming branches. During pregnancy and lactation, the mammary gland undergoes lateral branching forming **(b)** lobular alveoli at the end of the ducts. Following lactation, the mammary gland regresses back to its non-pregnant state through apoptosis and tissue remodelling.

1.1.3 Development during adulthood

With each menstrual cycle, the mammary epithelium undergoes proliferation and apoptosis in response to hormonal and matrix regulatory factors (Fata et al., 2001). However, during pregnancy intense proliferation of the alveolar epithelium rapidly forms structures known as alveoli to aid milk production (Figure 1). Transformation of tubular branches into spherical alveoli is induced by switch in surface tension from axial to circumferential through collective rotation of MECs (Fernandez et al., 2021).

Following weaning, the mammary gland undergoes involution due to the loss of lactogenic hormones (Figure 1). Involution is the process by which the mammary gland regresses back to its non-lactating state. This period is characterised by apoptosis of epithelial cells and remodelling of the ECM by several proteases such as metalloproteinase 3 (Talhouk et al., 1991).

1.2 Structure of the gland

The virgin human mammary gland is made up of a series of hollow primary ducts with lateral secondary and tertiary branches interspersed within the stroma (Figure 2). Upon stimulation of lactogenic hormones, the mammary gland undergoes prolific expansion to form hollow milk-producing alveoli at the end of ducts (Figure 2) (Briskin and O'Malley, 2010, Sternlicht et al., 2006). Single lumen formation is essential for the transport of milk from the alveoli to the nipple during lactation via the lactiferous ducts.

The mammary epithelium consists of luminal epithelial (LE) cells (ductal and alveolar) that form the luminal compartment and myoepithelial cells that form the basal compartment (Figure 2). The myoepithelial (ME) cells are surrounded by a thin layer of ECM known as the BM, that separates the basal compartment from the fibrous stroma composed of adipocytes, immune cells, fibroblasts, blood vessels and ECM proteins, the most abundant of which is type I collagen. Production and spatial organisation of type I collagen is driven by phosphorylation of eukaryotic initiation factor 4E in the stroma (Preston et al., 2022).

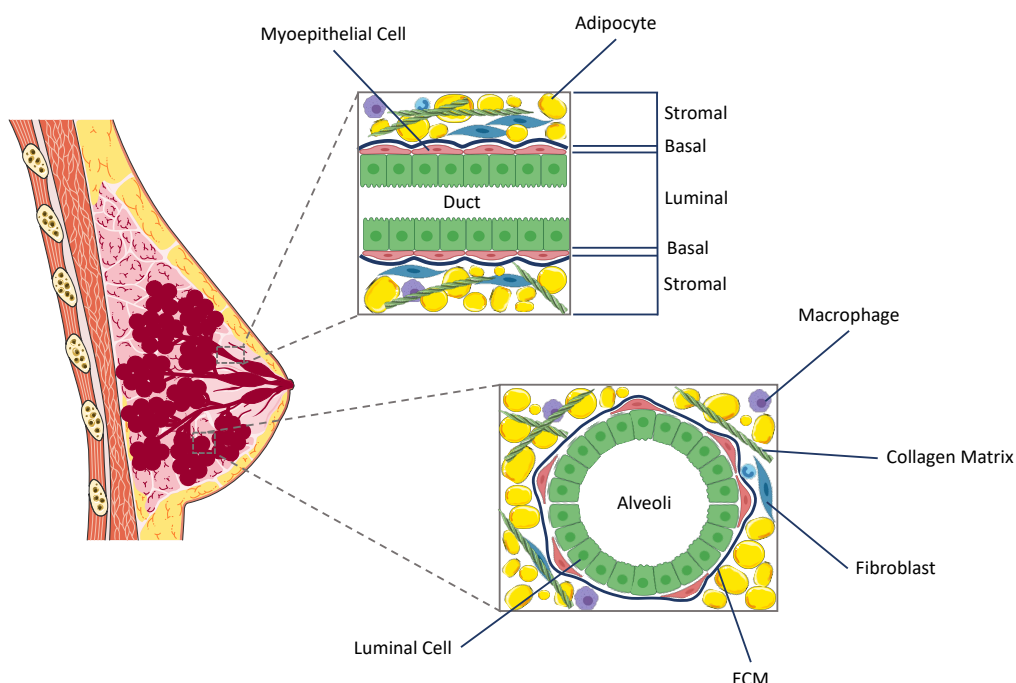


Figure 2: The mammary gland structure. The mammary gland is composed of two major cell types, luminal cells (luminal compartment) and myoepithelial cells (basal compartment). The extracellular matrix (ECM) separates cells of the stromal compartment e.g., immune cells, fibroblasts, and adipocytes from the basal compartment. The stromal compartment is also highly rich in collagens.

In mice the BM around ducts is surrounded by a thick layer of fibroblast embedded collagen. The remaining stromal area is filled with adipocytes.

1.2.1 Mammary BM composition

The breast BM is composed of proteoglycans and glycoproteins, such as laminins (LM), collagens, fibronectin, and tenascins (Muschler and Streuli, 2010). Nidogen and proteoglycans, such as perlecan, link networks of LM and polymeric collagen IV to form the BM (Jayadev and Sherwood, 2017).

As well as acting as a structural barrier, the ECM plays an important role in supporting both mammary tissue architecture and function. *In vivo* studies have revealed the composition and thickness of the BM is altered at the tip of the TEB compared to static areas such as the duct, which promotes ductal elongation (Paine and Lewis, 2017). Similarly, the composition of the BM is altered during various stages of development and pregnancy (Schedin et al., 2004). For example, in the adult mammary glands, the most common LM isoforms found are LM-111, -332, -511 and -521. However, during mammary gland development LM-211, -411 and -421 are also expressed. Macrophages have been implicated in maintaining the homeostasis and the remodelling of the ECM through protease production and controlling fibroblast activity (Wang et al., 2020). However, further studies are needed to identify the functional consequences of altered ECM in the mammary gland by the macrophages.

One of the major contributors to the BM are ME cells; they synthesise components such as collagen IV, LM-111, LM-332 and fibronectin (Warburton et al., 1982). A recent study by Englund and colleagues (2021) has shown LE cells also synthesise and deposit BM components such as LM- α 5 and LM- α 4. Interestingly adhesion to LM- α 5 containing LMs such as LM-521 directs progenitor cells towards a luminal cell fate; this suggests LE cells can regulate progenitor cell multipotency through stable factors such as LMs in the mammary gland (Englund et al., 2022).

1.2.2 Mammary tissue cells

1.2.2.1 Cap cells

Cap cells are specialised undifferentiated epithelial cells that form the outer layer of the TEB (Figure 1) (Williams and Daniel, 1983). Cap cells undergo a transient epithelial-to-mesenchymal transition (EMT) to aid the invasion of the mammary fat pad (Nelson et al., 2006, Kouros-Mehr and Werb, 2006). The plasticity of these epithelial cells is maintained by *Ovo-like 2*, a transcriptional regulator of EMT genes (Watanabe et al., 2014). Cap cells eventually differentiate to give rise to ME cells. However, cap cells that migrate into the TEB body undergo apoptosis (Dawson et al., 2021, Paine et al., 2016).

1.2.2.2 Body cells

In contrast, body cells fill the interior of the TEB (Figure 1) (Williams and Daniel, 1983). The lumen is formed following apoptosis of inner body cells and differentiation of the outer body cells give rise to luminal epithelial cells.

1.2.2.3 Luminal epithelial cells

LE cells line the lumen of the mammary ducts in virgins and the lumen of alveoli during pregnancy (Figure 2). During pregnancy, the LE cells rapidly undergo functional differentiation following activation of the STAT5-mediated prolactin signalling pathway regulated by the ECM (Streuli et al., 1995). LE cells within the alveoli synthesise and secrete milk following downregulation of progesterone which triggers the formation of impermeable tight junctions (Nguyen et al., 2001). A change in the permeability of tight junctions during lactation is important to prevent leakage and store milk proteins between nursing periods.

1.2.2.4 Myoepithelial cells

ME cells are another type of epithelial cells present in the mammary tissue. They contain smooth muscle actin and smooth muscle myosin, which enables contractile forces (Haaksma et al., 2011). The ME cells are further differentiated into ductal and alveolar ME cells. Alveolar ME cells are stellate shaped with multi-processes, they form a discontinuous basket-like meshwork around alveoli. However, during pregnancy and lactation, these ME cells fully enclose the alveoli (Emerman and Vogl, 1986). Adherence to other ME cells and the BM

through integrin-focal adhesions, desmosomes and hemidesmosomes ensures contractions of adjacent alveolar ME cells are synchronised to aid smooth milk ejection. In contrast, ductal ME cells are spindle-shaped and lie parallel to the luminal epithelial cells fully encompassing the ducts (Figure 2). Contraction of the ductal ME cells in response to oxytocin enables milk flow in the ducts by increasing the diameter of the lumen and reducing the length of the ducts (Emerman and Vogl, 1986).

1.2.2.5 Mammary stem cells

The presence of a mammary stem cell (MaSC) population has been postulated from early mammary transplantation studies, which formed outgrowths in donor mice after up to seven consecutive transplants (Daniel et al., 1968). Transcription factors such as p63 are key regulators of MaSC activity (Chakrabarti et al., 2014). Knockout of $\Delta Np63$, an isoform of p63 depletes MaSC-enriched basal cells affecting polarity and lumen formation in the pubertal mammary gland (Kumar et al., 2019).

The use of a multi-parameter cell sorting technique has led to the identification and purification of a distinct population of MaSCs, $Lin^- CD29^{hi} CD24^+$, capable of repopulating a fully functioning mammary gland from a single cell, suggesting MaSCs are multipotent (Stingl et al., 2006, Shackleton et al., 2006). The cellular markers used are $\beta 1$ -integrin (CD29) and heat-stable antigen (CD24), which are markers for basal and luminal cells, respectively.

Several important cellular fate mapping, lineage tracing, single cell transplantation and single cell RNA sequencing (scRNAseq) studies have shown cells during early stages of embryonic development can give rise to both LE and ME cells (Wuidart et al., 2018, Van Keymeulen et al., 2011, Lilja et al., 2018). However, towards the end of embryonic development these MaSCs switch from multipotency to unipotency and the unipotent fate is maintained through heterotypic communication between LE and ME cells (Centonze et al., 2020). On the contrary, lineage tracing studies in the pubertal gland has revealed a population of bipotent stem cells ($CD29^{hi} CD24^{hi} CD49^{hi} EpCAM^{lo}$) within the luminal layer that can give rise to both luminal and differentiated myoepithelial cells (Rios et al., 2014). Given discrepancies in lineage tracing studies on the mammary cell hierarchy, more comprehensive studies using scRNAseq are required to better understand the role and potency of these MaSCs in the mammary gland.

Construction of integrated datasets of mouse and human MEC obtained by scRNAseq suggest postnatally LE and ME cells arise from unipotent progenitors (Saeki et al., 2021).

1.3 MEC-ECM interactions – adhesion receptors

Cell-ECM interactions play an important role during development and growth of the mammary gland. ECM adhesion receptors such as integrins, dystroglycans and syndecans provide a link between the matrix and the cell cytoskeleton. *In vitro* studies by Schedin and colleagues (2004) have revealed that cell-ECM interactions have profound effect on cellular behaviour. For example, MECs cultured on nulliparous ECM form hollow spherical organoids, however, when cultured on involution day 4-6 ECM the cells fail to survive and die (Schedin et al., 2004).

Studies have shown that integrins, the major cell-ECM adhesion receptors, are essential for modulating cell proliferation, differentiation, stem cell maintenance, polarity orientation and directing branching morphogenesis during mammary gland development (Ma et al., 2022, Olabi et al., 2018, Akhtar and Streuli, 2013, Jeanes et al., 2012, Akhtar and Streuli, 2006, Naylor et al., 2005, Li et al., 2005).

1.3.1 Integrins

1.3.1.1 Integrin structure

Integrins are a class of cell surface receptor which mediate cell-cell and cell-ECM interactions. Integrins are heterodimeric molecules composed of an alpha (α) and a beta (β) subunit, held together by non-covalent bonds (Figure 3). In the mammary gland, fibroblast growth factor receptor 2 protects β 1-integrin from degradation in MECs (Mieczkowski et al., 2022). *In vivo*, the 18 α - and 8 β -subunits can combine to form 24 different functionally active $\alpha\beta$ heterodimeric receptors (Figure 4).

The α - and β -subunits have a large extracellular and short intracellular domain with a single transmembrane domain. The extracellular domain binds to ligands whilst the intracellular domain binds to a large complex of cytoskeletal proteins, cell-signalling proteins, and scaffolding proteins. The major ligands for integrins are ECM components such as laminins,

collagen, and fibronectin. Other ligands include counter receptors of the immunoglobulin superfamily such as intercellular adhesion molecules and vascular cell-adhesion molecules (Humphries et al., 2006).

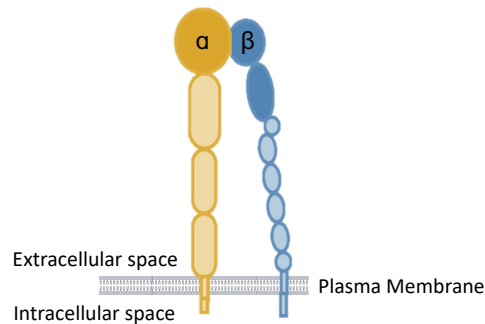


Figure 3: Integrin heterodimer. Schematic diagram of an activated integrin heterodimer.

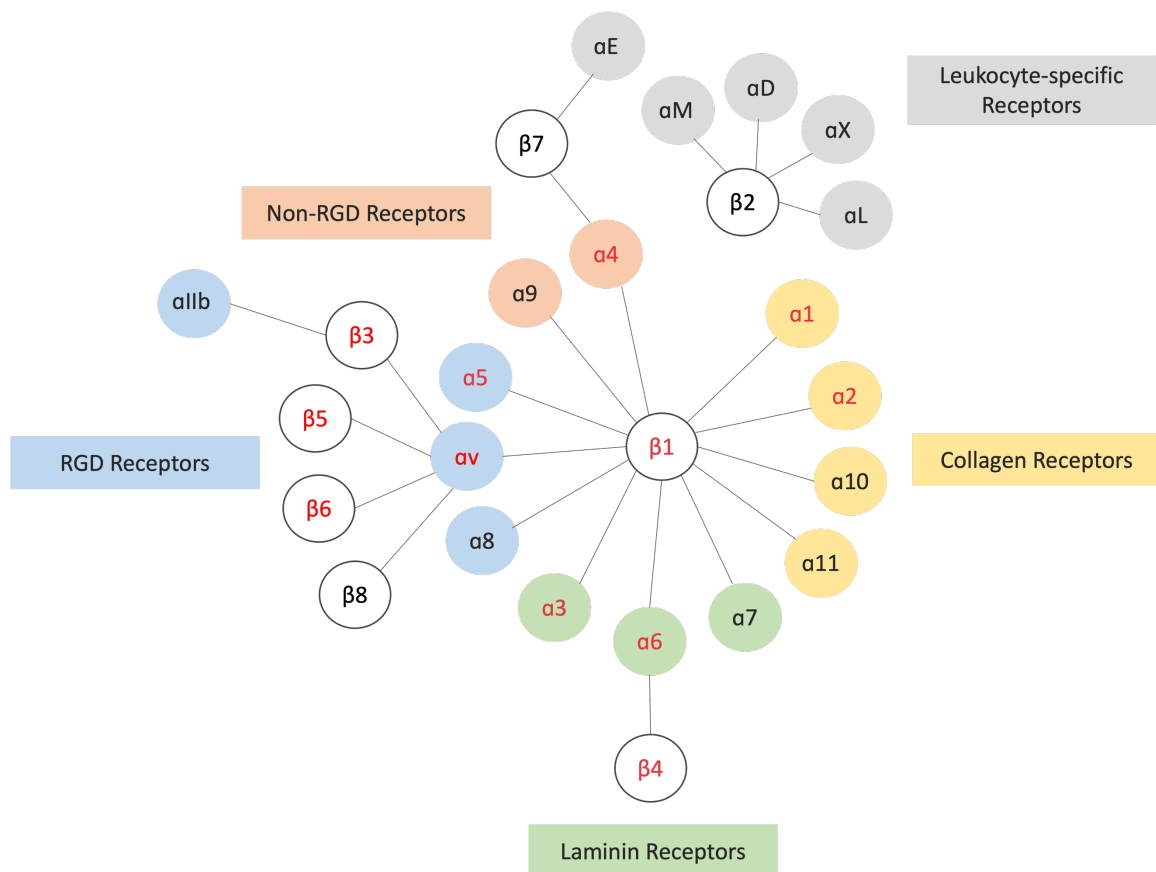


Figure 4: Integrin family and their heterodimers. In vertebrates, there are 24 integrin heterodimer receptors composed of an α and β subunit. The integrin family can be divided into four subfamilies: laminin-binding integrin (green), collagen-binding integrin (yellow), RGD-binding integrin (blue), non-RGD matrix-binding integrin (peach) and leukocyte-binding integrin (grey). The α -subunit in red is found in the mammary gland with the associated β -subunit also in red, $\beta 1$ and/or $\beta 4$.

1.3.1.2 Integrin-ECM adhesion and signalling

Integrin activation is bi-directional; it can be activated from the outside by insoluble ligand binding or from the inside by cytoskeletal adapter protein binding. Binding of adapter proteins such as talin, triggered by intracellular signals, to the cytoplasmic domain of β -integrin promotes a conformational change, integrin transition from an inactive folded state into an open active state primed for ligand binding. Similarly, binding of ECM components or divalent cations, such as Mg^{2+} or Ca^{2+} , to the extracellular integrin domain promotes a partial conformational change, that increases ligand affinity and modifies protein-binding sites on the cytoplasmic domain.

ECM binding to $\beta 1$ - and $\beta 3$ -integrin heterodimers, induces integrin clustering and aggregation on the cell membrane forming focal complexes, which can mature into actin-dependent focal adhesion (FA). Formation of mature FA is also dependent on cytoskeletal binding proteins such as paxillin, α -actinin, vinculin, α -parvin, PINCH and filamin binding to the intracellular β -integrin domain (Wiesner et al., 2005). Intracellular signalling pathways are activated through the recruitment of signalling proteins such as focal adhesion kinases (FAK), integrin-linked kinase (ILK), and Src-family protein tyrosine kinases (SFKs) to the adhesion complex (Geiger et al., 2009) (Figure 5).

Disruption of any of the components of the integrin-actin cytoskeleton linkage, such as talin, vinculin, FAK, Arp2/3 complex, phosphatidylinositol (4,5)-bisphosphate (PIP2) or α -actinin, affects cell adhesion stability and dynamics (Zhang et al., 2008, Xu et al., 1998).

In contrast, ECM binding to $\beta 4$ -integrin heterodimers form hemidesmosomes, which anchor cytokeratin intermediate filaments through plectin molecules (Reznicek et al., 1998).

1.3.1.3 Integrin expression in the mammary gland

Within the mammary epithelium, $\beta 1$ -integrin is the most commonly expressed integrin; it can form heterodimers with six different α -subunits (Figure 4) (Lahlou and Muller, 2011). The laminin binding $\alpha 6\beta 4$ integrin receptor is also present in mammary epithelial cells. Immunohistochemical analysis has shown $\beta 1$, $\beta 4$, $\alpha 2$, $\alpha 3$ and $\alpha 6$ and integrin subunits are expressed by both LE and ME. Additionally, ME cells also express the subunits $\beta 3$, $\beta 5$, $\alpha 1$, $\alpha 5$ and $\alpha \nu$ (Taddei et al., 2003). The integrin heterodimers are primarily localised on the surface of ME cells near the ECM, however, the $\beta 1$, $\alpha 2$, $\alpha 3$ and $\alpha 6$ subunits also localise on the lateral surfaces of LE cells (Prince et al., 2002; Shaw, 1999). Table 1 shows a summary of integrins expressed in the mammary gland, their localisation, and ligands.

Table 1: Integrin expression in the mammary gland. Colours indicate laminin affinity to integrin: grey = low, black = medium, red = high. Font size is proportional to laminin affinity strength. Data taken from (Nishiuchi et al., 2006).

Integrin	Localisation	Ligands
$\alpha 1\beta 1$	Basal surface of ME cells	Collagen I, Collagen IV
$\alpha 2\beta 1$	Basal and lateral surfaces of ME and LE cells	Collagen I, Collagen IV
$\alpha 3\beta 1$	Basal and lateral surfaces of ME and LE cells	Laminin-211, 221, 332, -311, -321, -511, -521, -522, -523
$\alpha 5\beta 1$	Basal surface of ME cells	Fibronectin
$\alpha 6\beta 1$	Basal and lateral surfaces of ME and LE cells	Laminin-111, -211, 221, -332, -311, -321, -411, -421, -511, -521, -522, -523
$\alpha 6\beta 4$	Basal surface of ME and LE cells	Laminin-332, -311, -321, -511, -521, -522, -523
$\alpha \nu\beta 3$	Basal surface of ME cells, luminal progenitor cells	Vitronectin, Fibronectin

1.4 $\beta 1$ -integrin role in mammary gland development

1.4.1 Apical-basal polarity

Epithelial cell polarisation is dependent on interactions with the ECM involving integrin heterodimers. The role of $\beta 1$ -integrin in cell polarisation has been studied extensively in

Madin-Darby Canine Kidney (MDCK) epithelial cells. Yu et al., (2005) showed that β 1-integrin interacts with collagen I gel to orient the polarity of MDCK cells, via Rac1 signalling and organisation of laminin into a basement membrane-like structure around the periphery of the cyst. β 1-integrin-Rac signalling downregulates the Rho-ROCK-Ezrin pathway at the ECM interface enabling phosphorylation of podocalyxin and NHERF1 by PKC β II (Bryant et al., 2014, Yu et al., 2008). Dissociation from Ezrin triggers the endocytosis of podocalyxin-NHERF1 from the ECM interface; this complex is re-routed to form a new apical face on the opposite side of the cell (Bryant et al., 2014, Yu et al., 2008).

However, in the mammary epithelia, the polarity orientation mechanism appears to differ downstream of β 1-integrin-ECM interaction. Akhtar and Streuli (2013) identified that β 1-integrin organises microtubules through integrin-linked kinase (ILK), which promotes endocytic removal of apical components incorrectly located at the cell-matrix interface. The apical components are then re-routed to assemble a new apical face on the opposite side of the cell next to the apical lumen and position the Golgi sub-apically, governing the orientation of polarity (Akhtar and Streuli, 2013). Loss of β 1-integrin in MEC inverts the cell polarity despite an intact basement membrane, suggesting additional roles for this integrin in polarity orientation downstream of BM deposition (Akhtar and Streuli, 2013).

1.4.2 Cell proliferation

As mentioned earlier, β 1-integrin signalling is an important regulator of cell proliferation. β 1-integrin knock-down studies in various cell types have shown an upregulation of different cyclin-dependent kinases such as p16^{Ink4a} and p21^{Cip1} (Aszodi et al., 2003). p21^{Cip1} is a CDK inhibitor and therefore acts as a regulator of cell cycle progression at the G1 and S phase. Therefore, upregulation of p21^{Cip1} expression results in a proliferative block.

Similar β 1-integrin knock-down studies in lactating mammary gland have shown an upregulation of p21^{Cip1} expression, blocking alveolar proliferation (Li et al., 2005). Further *in vivo* analysis revealed the levels of FAK, an important mediator in integrin-mediated signalling pathways was reduced (Li et al., 2005). This suggests β 1-integrin signalling via FAK downregulates the expression of p21^{Cip1}, enabling cell cycle progression.

More recently, (Jeanes et al., 2012) showed that cell proliferation was perturbed in β 1-integrin null cells through disruption of the GTPase Rac1. Rac1 activity is required for nuclear translocation of phospho-Erk, where it can activate transcription factors such as Elk-1. Therefore, Erk translocation mediated by Rac1 is essential for cell cycle progression from G₁ to S phase.

1.4.3 Lactational differentiation

Lactational differentiation is an important process that occurs during pregnancy; luminal epithelial cells undergo differentiation forming alveolar epithelial cells capable of synthesising milk during lactation. *In vivo* studies show deletion of β 1-integrin within luminal cells prior to pregnancy, reduces lobular alveoli development significantly (Naylor et al., 2005). However, deletion of β 1-integrin mid-pregnancy, following differentiation of luminal cells, resulted in fewer defects in alveolar morphology, luminal cells were correctly polarised, and a BM was deposited (Naylor et al., 2005, Li et al., 2005). Despite this, milk production is insufficient to nurse the pups, growth rate is lower compared to the WT control pups, due to smaller alveoli, and filling of the lumen with epithelial cells. Moreover, this phenotype is not rescued with subsequent pregnancies; mutant pups from second pregnancy have dramatically reduced growth compared to WT control pups (Naylor et al., 2005).

Furthermore, genetic approaches have revealed β 1-integrin-mediated Rac1 signalling is important for the nuclear translocation of Stat5, a transcription factor required for differentiation of mammary epithelial cells (Naylor et al., 2005, Akhtar and Streuli, 2006, Akhtar et al., 2009, Rooney et al., 2016). This suggests that β 1-integrin has a direct role in lactogenesis through modulating differentiation. Whether β 1-integrin mediated perturbation of alveolar formation directly affects lactogenesis is yet to be established. The perturbed architecture might misplace some of the signalling components needed for lactation. Therefore, more studies are required to address whether lactational defects are connected to perturbed architecture.

1.4.4 Cellular apoptosis

Following weaning, the mammary gland undergoes involution during which milk production ceases, and the mammary gland regresses due to apoptosis, necrosis, and autophagy of alveolar epithelial cells. Studies by Boudreau and colleagues (1995) first highlighted the importance of β 1-integrin-ECM ligation in driving involution. Cell culture experiments revealed mammary epithelial cells grown on laminin rich ECM suppressed caspase-mediated apoptosis compared to cells grown directly on tissue culture plates, which displayed characteristics of apoptosis (Boudreau et al., 1995). However, the addition of β 1-integrin antibodies or overexpression of MMP-3, which degrades the ECM, enhanced apoptosis of cells cultured on exogenous ECM (Boudreau et al., 1995).

In vivo analysis of mammary tissue sections revealed no significant difference in the structure or composition of the BM, or the expression of β 1-integrin, during the transition from lactation to involution (Prince et al., 2002). Instead, they discovered a significant reduction of ligand-binding β 1-integrin during the induction of apoptosis (Prince et al., 2002). These findings suggest β 1-integrin signalling is important for the transduction of survival signals from the ECM, and loss of β 1-integrin ligation to the ECM induces apoptosis. Interestingly, our lab group has recently shown that involution occurs independently of β 1-integrin in the mammary gland via Rac1 mediated autophagy of alveolar epithelial cells (Mironov et al., 2023).

1.4.5 Stem cell maintenance

β 1-integrin has long been associated as a marker and regulator of stem cells such as epidermal, hematopoietic and spermatogonial (Brizzi et al., 2012). However, a growing body of data suggests β 1-integrin is also a determinant of mammary epithelial stemness. For example, in basal and MaSCs, expression of α 2 β 1 integrins is enriched, but in luminal cells α 1 β 1 and α 8 β 1 integrins are more abundant (Ji et al., 2011).

Whilst symmetric division is important to maintain and amplify the stem cell population, asymmetric division is important for producing differentiated cells. In mammary epithelia deletion of β 1-integrin in K14 positive basal cells alters the cell division axis from a symmetric

division to an asymmetric one; rather than just producing basal daughter cells, proliferating basal cells also gave rise to luminal daughter cells (Taddei et al., 2008). This suggests β 1-integrin mediated signalling has an important role in maintaining the mammary stem cell niche through controlling symmetric and asymmetric cell division.

Li and colleagues (2005) found that selective deletion of β 1-integrin from the luminal epithelium in mice undergoing a second pregnancy led to reduced density of lobuloalveolar units. Further analysis using the mammary transplantation technique, showed that β 1-integrin null cells in the mammary epithelia were unable to repopulate following pregnancy (Li et al., 2005). Similarly, ablation of β 1-integrin specifically from cells in the basal compartment, e.g., ME cells and MaSCs, impaired the cells' ability to regenerate mammary epithelium upon transplantation into cleared fat pads of syngeneic mice (Taddei et al., 2008).

Furthermore, *in vitro* stem cell assays using murine mammary epithelial cells, have also implicated β 1-integrin in maintaining bipotent basal cells and luminal progenitor cells populations (Olabi et al., 2018). Analysis of β 1-integrin downstream signalling pathways revealed maintenance and self-renewal of bipotent cells is dependent on Rac1 mediated activation of the Wnt pathway, thereby activating transcription of stem cell-related genes (Olabi et al., 2018). In contrast, maintenance and self-renewal of luminal progenitor cell population occurs in a Rac1-independent manner (Olabi et al., 2018).

More recently the contribution of specific integrin dimers involved in mammary stem cell regulation was analysed by Romagnoli and colleagues. Deletion of both laminin binding integrins, α 3 β 1 and α 6 β 1, in basal cells lead to myosin II-mediated activation of p53 and subsequently impaired the basal cell's ability to repopulate cleared mammary fat pads (Romagnoli et al., 2019). Whilst the importance of p53 in mammary stem cell regulation has been implicated in earlier studies by (Chiche et al., 2013, Cicalese et al., 2009), the molecular mechanisms involving myosin II-mediated activation of p53 remains to be elucidated.

1.5 β 4-integrin role in mammary gland development

α 6 β 4-integrin is expressed primarily in basal cells where it adheres the laminins to intermediate filaments through the assembly of hemidesmosomes (Sonnenberg et al., 1991).

Despite intermediate filaments not possessing intrinsic polarity, studies in MDCK cells have shown $\alpha6\beta4$ -integrin is involved in guiding apico-basal cell polarisation, by promoting Rac-1 activity-mediated basal cues (Myllymäki et al., 2011). Furthermore, in 3D culture, inhibition of $\beta4$ -integrin disrupted hemidesmosome formation and subsequently perturbed ECM-directed polarity resulting in disorganised mammary gland colonies (Weaver et al., 2002, Weaver et al., 1997). However, *in vivo* analysis shows mammary epithelial cells can still establish polarity and form concentric bi-layered structures, in transplanted mammary tissue that lack $\alpha6$ integrin. Antibody staining was used to confirm the transplanted tissue lacked $\alpha6$ integrin and the outgrowth did not arise from WT cells (Klinowska et al., 2001). Given $\alpha6$ integrin forms a heterodimer with $\beta1$ and $\beta4$ -integrin, this suggests $\alpha6\beta4$ -integrin is not important for cell sorting or establishing cell polarity (Klinowska et al., 2001). One possible explanation is that in the absence of $\alpha6\beta4$ integrin an alternate integrin such as $\alpha3\beta1$ could be mediating cell sorting and polarity orientation.

Similarly, *in vivo* studies and cell culture assays provide conflicting results on the role of $\alpha6\beta4$ -integrin in branching morphogenesis. It has been shown that blocking of $\alpha6$ integrin in Matrigel cell culture resulted in inhibition of hemidesmosome formation and impeded branching morphogenesis (Stahl et al., 1997). Conversely, Klinowska and colleagues reported, branching morphogenesis *in vivo* is not dependent on $\alpha6\beta4$ -integrin. However, more recently, Li et al (2015) found that mammary gland development in $\beta4$ -integrin knockout mice is significantly impaired due to downregulation of parathyroid hormone related protein (PTHrP) expression in epithelial cells. Addition of exogenous PTHrP rescues this phenotype; mammary buds elongate and undergo branching morphogenesis in $\beta4$ -integrin knockout mice (Li et al., 2015). These data reveal a novel role of $\beta4$ -integrin in controlling branching morphogenesis through regulating the paracrine activity of PTHrP with the mesenchyme.

Given the importance of $\beta4$ -integrin in the development of other epithelial tissues, it would be surprising if $\alpha6\beta4$ -integrin were not important in mammary gland development, as Klinowska and colleagues suggest. A recent study by Walker et al., (2020) highlights a novel role of $\beta4$ -integrin in stem cell maintenance and alveologenesis. Whilst some immunofluorescence studies have suggested $\beta4$ -integrin expression is restricted to ME cells, scRNAseq has identified $\beta4$ -integrin is also expressed by alveolar progenitor cells (Walker et

al., 2020). Furthermore, deletion of $\beta 4$ -integrin *in vivo* impaired alveolar development and milk production (Walker et al., 2020). This suggests $\beta 4$ -integrin might be important in mammary gland development. However, further studies are required to identify whether the function and signalling of $\beta 4$ -integrin differs between myoepithelial cells and alveolar progenitor cells.

1.6 Integrin role in breast cancer

The role of $\beta 1$ - and $\beta 4$ -integrin in breast tumorigenesis has been shown in both *in vitro* studies using breast cancer cell lines and *in vivo* mouse studies. Deletion of $\beta 1$ -integrin in mammary tumour cells impaired the proliferative capacity of the cancer cells resulting in dormancy; also, significantly fewer hyperplastic mammary lesions developed (White et al., 2004). These observations are consistent with findings from previous studies in which inhibition of $\beta 1$ -integrin binding activity in cancer cells blocked cell proliferation and induced apoptosis (Park et al., 2008, Wang et al., 2002, Weaver et al., 1997). $\beta 1$ -integrin suppresses activation of the tumour suppressor p53 promoting cell proliferation and survival (Bui et al., 2022).

Similarly, $\alpha 6\beta 4$ -integrin also suppresses cell apoptosis. $\beta 4$ -integrin mediated activation of the PI3K-Akt pathway upregulates vascular endothelial growth factor translation, promoting angiogenesis and cell survival through an autocrine signalling pathway in breast carcinoma cells (Chung et al., 2002). Also, in invasive cancer cells, $\alpha 6\beta 4$ -integrin localises and associates with F-actin at the leading-edge promoting cell migration and invasion (Rabinovitz et al., 1999).

However, there is still some controversy in the links between $\beta 1$ -integrin and breast cancer; as some studies have shown that inhibition of $\beta 1$ -integrin activity promotes cell proliferation (Howlett et al., 1995). Discrepancies between these studies could be a result of different cell densities used, differences in $\beta 1$ -integrin blocking techniques and the use of different cell lines, which express different $\beta 1$ -integrin heterodimers. For example, while $\alpha 3\beta 1$ integrin promotes breast tumorigenesis (Cagnet et al., 2014), $\alpha 2\beta 1$ integrin suppresses breast cancer metastasis (Ramirez et al., 2011). This suggests the role of $\beta 1$ -integrin in breast cancer is highly dependent on the stage of disease progression and its heterodimer, possibly due to the plasticity of the receptor.

Similarly, early studies in breast cancer patients, have given contradictory results on the expression of $\beta 1$ -integrin and its association with patient prognosis. Whilst in some subsets of breast cancer $\beta 1$ -integrin expression is absent (Jonjic et al., 1993, Gonzalez et al., 1999); in well- to moderately differentiated infiltrating carcinomas, $\beta 1$ -integrin is highly expressed (Koukoulis et al., 1991, Zutter et al., 1993, Jonjic et al., 1993). Similarly, studies have reported either a positive correlation (Gonzalez et al., 1999), no association (Berry et al., 2004) or a negative correlation (Yao et al., 2007) between $\beta 1$ -integrin expression and likelihood of survival. The discrepancy in $\beta 1$ -integrin expression levels might be because comparisons were made between cancerous mammary tissue and normal tissue, where $\beta 1$ -integrin expression is higher in myoepithelial cells. However, in invasive breast cancer, this cell type is lost and the expression of $\beta 1$ -integrin on cancer cell surface is dispersed. Therefore, it is important future studies use an alternate method to immunohistochemical analysis to assess $\beta 1$ -integrin expression.

Unlike $\beta 1$ -integrin there is limited clinical data on $\beta 4$ -integrin. Analysis of $\beta 4$ -integrin mRNA expression in breast tumours using in situ hybridisation, revealed a correlation with both tumour size and tumour grade (Diaz et al., 2005). However, they found no prognostic significance between $\beta 4$ -integrin and laminin-5 in early breast cancer, suggesting $\alpha 6\beta 4$ -integrin has an important role in breast cancer tumour progression. More recently, (Lu et al., 2008) found mRNA and protein expression of $\alpha 6\beta 4$ is not homogenous in breast cancer but rather it is associated most significantly with “basal-like” breast cancer.

Both *in vitro* and *in vivo* studies, suggest that $\beta 1$ - and $\beta 4$ -integrin are involved in breast cancer development and progression through increased cell proliferation, invasion, and suppression of apoptosis. However, there has been no work done to analyse the role of integrins in positioning MEC lineages as inner luminal and outer myoepithelial, which exhibits many tumour suppression properties (Barsky 2003, Jones et al., 2003, Shao et al., 1998). Data increasingly suggest that in invasive breast carcinoma the ME cell layer is lost along with the surrounding ECM enabling cancer cells to metastasize (Dornier et al., 2017). Therefore, understanding how this tumour suppressing bilayer structure develops is important in tackling breast cancer.

1.7 Potential mechanisms involved in spatial organisation of mammary tissue.

We are proposing affinity to the ECM and/or repulsion at the apical membrane drives the spatial organisation of mammary epithelial cell lineages through oriented cell division and/or cell movement.

Early studies by Townes and Holtfrete in gastrulating amphibians revealed embryonic cells contained self-sorting ability; when different embryonic regions are mixed, they sort into distinct populations. In 1963, Steinberg proposed the differential adhesion hypothesis based on thermodynamic principles to explain cell sorting affinities to explain the experimental results. An experimental study using chick retinal cells suggests that cells gather by adhering to cells of similar adhesion to maximise their intercellular adhesion and concurrently minimise interfacial free energy, thereby producing a more thermodynamically stable tissue structure (Figure 5A). Furthermore, studies using embryonic lung tissue provided the first direct evidence that differential expression of cadherins within cell aggregates promotes cell sorting to minimise surface tension (Figure 5B) (Nose et al., 1988).

However, numerical simulations by (Brodland, 2002) suggest that cell sorting is not solely dependent on cell-cell adhesion but is also governed by cell contractility, this hypothesis is known as the differential interfacial tension. The model suggests cell sorting is driven by actin cytoskeleton mediated cortical tension (Figure 5C). Furthermore, experimental analyses using gastrulating zebrafish embryos have shown that actomyosin contractility is critical in the sorting of germ-layer progenitor cells (Krieg et al., 2008). More recently, Revell et al., (2019) developed a force-based three-dimensional model to better understand the effect of differential interfacial tension in 3D cell aggregate. Their model shows a lower amount of differential interfacial tension is required compared to differential adhesion to drive cell sorting (Revell et al., 2019). This suggests the primary driver of cell sorting is interfacial tension asymmetries.

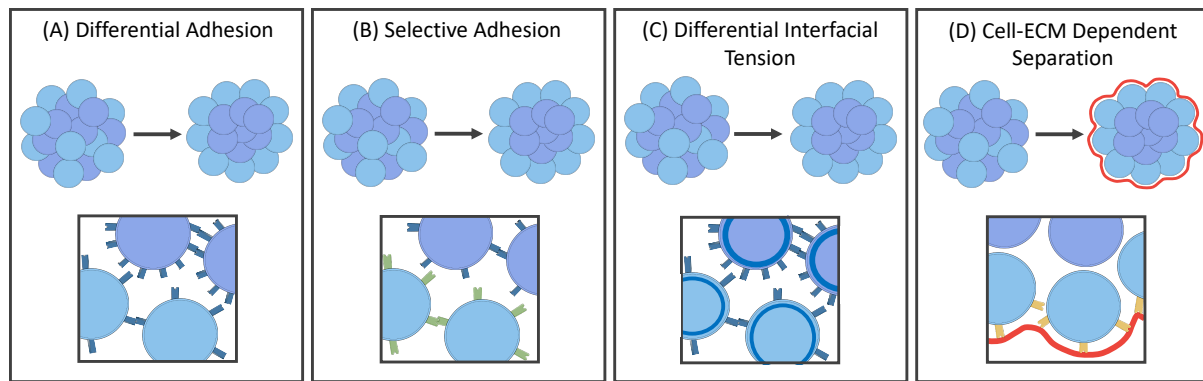


Figure 6: Cell sorting models. (A) The differential adhesion hypothesis proposes cells will sort based on expression levels of the same adhesion complex. (B) The selective adhesion model predicts cells will sort based on differential expression of cadherin molecules. (C) The differential interfacial tension hypothesis suggests cell sorting is also dependent on cytoskeleton-mediated cortical tension. (D) Cell-ECM adhesion mediated by integrins dominates cell sorting in some tissues.

However, a downfall of all these models is that they fail to consider the influence of cell-ECM interactions found in *in vivo*. In the presence of fibronectin, an ECM component, $\alpha 5\beta 1$ integrin expressing Chinese hamster ovary (CHO) cells form spherical 3D aggregates even in the absence of cadherins (Robinson et al., 2003).

Moreover, Cerchiarri and colleagues (2015) found that concentric self-organisation of the mammary gland is dependent on interfacial energy of the tissue-ECM boundary, rather than differential cell-cell adhesion (Figure 5D). Mathematical modelling suggests that despite perturbation of cell-cell adhesion, cells are still able to self-organise and form the correct tissue architecture (Cerchiarri et al., 2015). This suggests that in the presence of ECM, binary cohesive interactions between myoepithelial cells and the ECM, dominate cell sorting in mammary tissue (Figure 5D). Since Cerchiarri's model makes no assumptions about the ECM properties, such as composition and stiffness, it is possible that self-organisation of the tissue can occur in the presence of any boundary type; however, this does require further investigation theoretically and experimentally.

New insights from *C. elegans*, *Drosophila* and the mouse aorta show that molecules such as collagens, zona pellucida (ZP) domain proteins, nidogen, ABC transporter and glycoproteins are secreted apically via proteinaceous membrane channels or through evaginations "blebs" of the plasma membrane. The translucent nature of luminal components under light microscopy and proneness to degrade when fixed has meant the identity of these

components and their role in morphogenesis remains poorly understood in developing vertebrate organs.

In the *Drosophila* trachea, apically secreted Piopio (Pio) interacts with Dumpy (Dp) to form a structural network in the luminal space that helps control cell rearrangement to resolve multilayer structures during morphogenesis (Jaźwińska et al., 2003). Moreover, the apical matrix has shown to provide a constraining force along the apical surface of the epithelium driving cell shape changes, oriented cell division and intercalation of cells during *Drosophila* limb development (Diaz-de-la-Loza et al., 2018, Ray et al., 2015). Similarly, in vertebrates negatively charged sialic acid found on the glycoprotein, Podocalyxin, causes an electrostatic repulsion at the apical interface of developing mouse aorta initiating lumen formation (Strilic et al., 2010). These studies suggest a similar force at the apical membrane in the mammary gland could be driving cell positioning.

1.7.1 Oriented cell division

Spindle orientation plays an important role in determining the position of the daughter cell during cell division. Whilst planar division maintains a single epithelial layer, orthogonal (apico-basal axis) division induces stratification. Recent studies *in vivo* and *in vitro* have uncovered the role of cortical cues and cell-cell adhesion in positioning the mitotic spindle.

Cell culture studies by Toyoshima and Nishida (2007) showed that spindle orientation in both HeLa and NRK cells grown on fibronectin or collagen was parallel to the cell-ECM plane, whereas in cells plated on poly-L-lysine or treated with RGD peptide or anti- β 1-integrin antibody, the spindle was misoriented. Furthermore, they found that spindle orientation is dependent on remodelling of the actin cytoskeleton by myosin X and stabilisation of the astral microtubules by the protein EB1 (Toyoshima and Nishida, 2007). Similarly, in β 1-integrin knockout mice, spindle orientation was randomised in basal epidermal cells due to aberrant apical localisation of nuclear mitotic apparatus (NuMA), LGN and α PKC (Lechler and Fuchs). The LGN-NuMA complex associates with astral spindle microtubules at the cortex, providing mechanical force to orientate the spindle. These studies show that β 1-integrin mediated cell-ECM adhesion is important in orientating the mitotic spindle parallel to the substrate plane, and thus, dictates the directionality of the ensuing cell division.

However, physical manipulation studies using murine skin explants show orientation of cell division is dependent on cell shape rather than apical localisation of the NuMA complex (Box et al., 2019). Exogenous strain (25%) applied using a stretch chamber promoted basal cell elongation along the axis of strain and cell division was shifted toward planar division. This suggests cell division axis orientation can be altered by basal cells depending on extrinsic cues. In contrast, a different study found low levels of axial stretch (12%) in MDCK cells orients the cell division axis parallel to the stretch axis despite no difference in overall cell shape when stretched (Hart et al., 2017). Further analysis showed E-cadherin mediated localisation of LGN perpendicular to the stretch axis is important in tension-oriented cell division independent of cell shape (Hart et al., 2017).

Within the mammary gland, oriented cell division is important for lobuloalveolar development and ductal elongation. Taddei et al (2008) found that mice lacking β 1-integrin in basal mammary epithelial cells had altered cell division axis, producing both basal and luminal cells rather than contributing solely to the basal cell population. Furthermore, alveologenesis in these β 1-integrin knockout mice was retarded. This shows that β 1-integrin-dependent oriented cell division, of basal epithelial cells, is important in producing entire functional alveoli.

During development, mammary ducts are elongated through stratified TEB structures. In contrast to other epithelial organs in which stratification occurs through basally positioned cells, in the mammary gland stratification is initiated on the apical side in luminal cells (Huebner et al., 2014). Interestingly, in common with cancerous epithelial cells, these internal daughter cells lack apicobasal polarity and junctional complexes, (Huebner et al., 2014). However, unlike cancerous epithelial cells, these highly motile cells are unable to invade the ECM, but just aid ductal elongation through spatial control of phosphorylated ERK1/2 (Huebner et al., 2014). Similarly, the organisation and expansion of the mammalian lung airways is dependent on ERK1/2 signalling mediated orientation of the mitotic spindle parallel to the airway longitudinal axis (Tang et al., 2011). However, further studies are necessary to identify if integrin-dependent mechanisms for spindle orientation are important during stratification in the mammary gland.

1.7.2 Cell movement

Experimental studies using different systems, such as mammary ducts, mouse salivary glands and kidneys suggest cell movement as a mechanism for spatial organisation of cells (Mori et al., 2009, Huebner et al., 2016, Larsen et al., 2006, Chi et al., 2009). *In vitro* collagen gel overlay assays show luminal structure formation is dependent on β 1-integrin-mediated collective cell migration of MDCK cells (Ishida et al., 2014). Furthermore, computational modelling suggests stiffness of the ECM is also an important determinant of lumen formation; rigid ECM perturbed cell migration and subsequently lumen formation (Ishida et al., 2014).

A recent study by Neuman et al (2018) showed that migrating cells within the mammary tissue form protrusions with high levels of PI3K activity and F-actin at their leading edge, creating a posterior tension gradient and allowing epithelial cells to intercalate. Intercalation is the process in which cells exchange neighbours, promoting morphogenesis during metazoan development. Studies in *Xenopus* have shown that intercalation contributes to convergent extension during gastrulation and thinning of the multi-layered epithelium during organogenesis (Sedzinski et al., 2016). Within the mammary tissue, luminal epithelial cells intercalate into the basal surface layer, aiding ductal elongation and resolving the multilayer epithelium into a bilayer (Neumann et al., 2018). However, the molecular mechanisms responsible for intercalation of mammary epithelial cells remains unknown.

Interestingly, in *Xenopus*, β 1-integrin-mediated adhesion to fibronectin drives radial intercalation through localisation of Dishevelled to the cell membrane (Marsden et al., 2001). Similarly, the ECM has been identified important in *Drosophila* wing development. (Diaz-de-la-Loza et al., 2018) found that degradation of the apical and basal ECM in *Drosophila* wings triggers planar polarisation of Myosin-II which drives cell intercalation. Therefore, β 1-integrin-mediated adhesion to the ECM or the lack thereof might contribute to intercalation during mammary tissue morphogenesis.

1.8 Summary

Both *in vitro* and *in vivo* studies, suggest that β 1- and β 4-integrin expression play an important role in breast tissue development and cancer progression through modulation of cell

polarisation, proliferation, functional differentiation, and apoptosis. However, there has been much less work analysing the role of β 1- and β 4-integrin in positioning mammary epithelial cells as inner luminal and outer myoepithelial. This study will provide a better understanding of the mechanisms involved in forming this concentric bilayer structure which acts as a powerful tumour suppressor.

1.9 Hypothesis and Aims

We hypothesise that (i) a higher affinity to the ECM or (ii) repulsion at the apical membrane drives ME cell positioning towards the ECM.

To understand the molecular mechanism that drives spatial organisation in the mammary gland, I will be using primary mammary epithelial cell cultures derived from mice. Given there are currently no established cell lines that can be induced to differentiate into luminal and myoepithelial cells, primary cell culture is the only option as it best recapitulates *in vivo* mammary tissue organisation and function. Also *in vitro* studies using primary mammary epithelial cells will ensure we can study in detail the mechanisms that drive ME cell positioning towards the ECM as its easier to manipulate and is more tractable experimentally.

Given there are over 15 different β 1- and β 4-integrin combination between LE and ME cells testing all these experimentally is not feasible. Therefore, alongside experimental studies, cell-based computational modelling will be used to study the processes and the role of different integrins in spatial organisation of mammary tissue. This will help reduce and replace the number of animals required embracing the 3Rs. Moreover, computational modelling has many advantages which will be discussed in full in chapter 5.

The objective of this thesis was to understand the role and contribution of LE and ME integrins in the spatial organisation of the mammary gland.

The aims of the project are to:

1. Validate the inhouse developed mouse models to check for lineage specific perturbation of β 1-integrin in LE or ME cells specifically *in vitro* (chapter 3).

2. Characterise lumen formation of lineage specific β 1-integrin KO primary MEC organoids embedded in laminin rich ECM or type I collagen (chapter 3).
3. Test the effect of β 1-integrin deletion in sorting of primary MECs using organoids embedded in laminin rich ECM or type I collagen, and ECM-overlay assays (chapter 4).
4. Develop and validate a cell-based computational model to understand the interplay of cellular mechanisms such as oriented cell division, anchorage dependent growth and anoikis (chapter 5).
5. Using the newly established computational model, explore the relative contribution of β 1- and β 4-integrin in LE and ME cells in driving MEC sorting and maintaining their position (chapter 5).
6. Assess the functional importance of cell positioning and β 1-integrin in the mammary gland during lactation, through organoid and collagen gel contraction assays (chapter 6).

The outcome of these aims is presented in the following results chapters.

2 Methods

2.1 β 1-integrin^{-/-} mice

2.1.1 Licensing and husbandry

All the mice used in this study were handled in accordance with UK legislation under the Animals (Scientific Procedures) Act 1986. All procedures were approved by the University of Sheffield Ethics Committee and carried out under the UK Home office Project License (PP1836785) held by Dr. Nasreen Akhtar.

The mice were kept at 22°C with 40-60% of humidity and had a 12-hour photoperiod. The mice were given *ad libitum* access to water and food.

2.1.2 Mouse models

Our lab has generated a β 1-integrin^{fx/fx}: YFP: K14-CreERTM and a β 1-integrin^{fx/fx}: YFP: K8-CreERTM mouse model in which β 1-integrin gene deletion is induced specifically within myoepithelial cells using K14-CreER promoter or luminal cells using the K8-CreER promoter respectively (Figure 5). The YFP (Yellow Fluorescent Protein) reporter gene was used to detect CreER activity. *In vitro*, cell culture studies will compare untreated (control) with +4-OHT treated mammary epithelial cell harvested from K14-CreERTM or K8-CreERTM mice.

2.1.3 Murine mammary gland isolation

Mice were culled by cervical dislocation. The mammary glands were harvested, and the samples were either fixed in 10% (w/v) formalin solution (Sigma-Aldrich Cat no. HT501128) or the epithelial cells were isolated for primary cell culture. Mammary gland samples were extracted from 8-12-week-old virgin mice to study ductal structures whilst samples from 15.5-17.5-day pregnant mice were used to study alveoli structures.

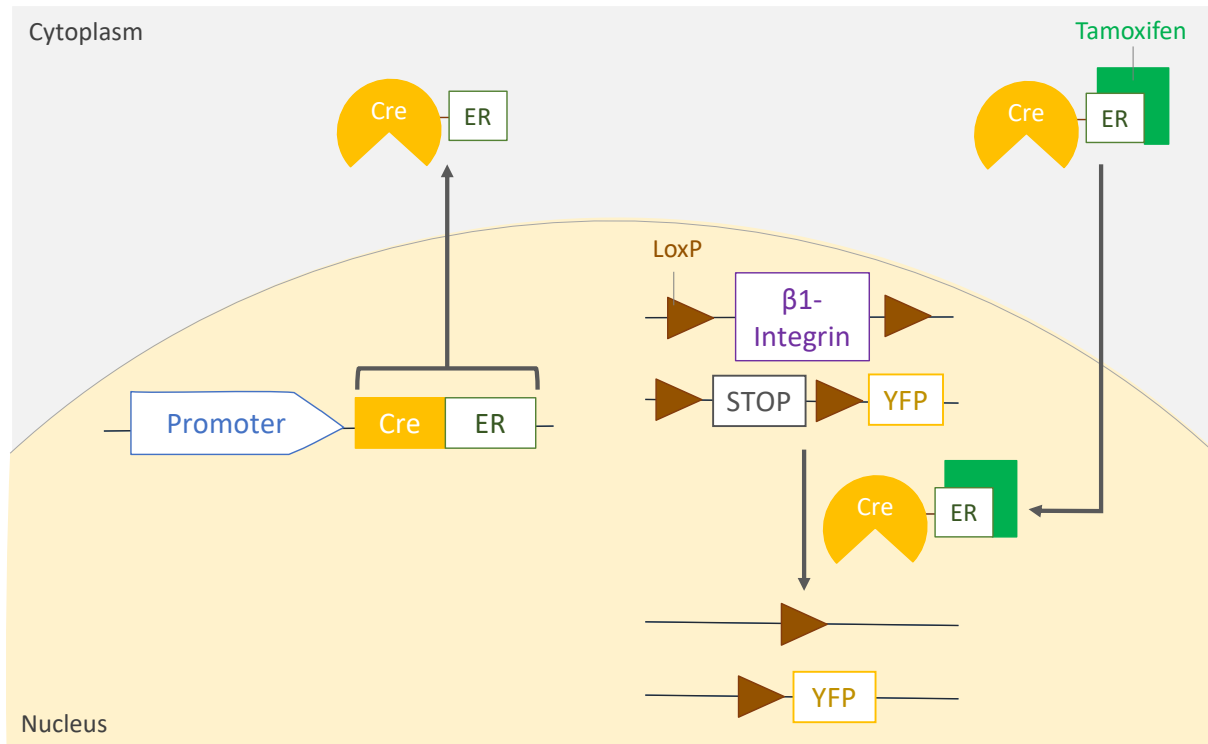


Figure 7: Tamoxifen inducible $\beta 1$ -integrin gene expression. CreER expression is confined to the cytoplasm in myoepithelial cells or luminal cells from the $\beta 1$ -integrin^{fx/fx}: YFP: K14-CreERTM or $\beta 1$ -integrin^{fx/fx}: YFP: K8-CreERTM, respectively. Addition of tamoxifen causes translocation of the Cre-ER protein to the nucleus where it catalyses the recombination of the $\beta 1$ -integrin DNA sequence flanked by the loxP sites, causing a loss of $\beta 1$ -integrin expression. CreER activity is detected using the reporter YFP (Yellow Fluorescent Protein) which gets expressed following deletion of the 'Stop' DNA sequence flanked by the loxP sites.

2.2 Primary cell culture

The extracted mammary gland was minced using a scalpel and digested using a collagenase buffer (47.5 ml of H₂O + 490 mg F-10 medium (Sigma-Aldrich, Cat no. N6635-IL), 60 mg of NaHCO₃ (Sigma-Aldrich, Cat no. 13433), 130 mg HEPES-Na (Thermo Scientific, Cat no. 215000250), 75 mg of trypsin (Gibco, Cat no. 27250018), 150 mg of collagenase A (Roche, Cat no. 11088793001), 2.5 ml of FBS (biosera, Cat no. FB-1001)) for 40 minutes at 37°C to hydrolyse the collagen and dissociate the tissue. The dissociated tissue was centrifuged for 2 mins at 400 RPM. The pellet was re-digested in the collagenase buffer for 15 mins at 37°C, whilst the supernatant was spun for 2 mins at 400 RPM.

The following sets of spins were done to remove other cell types such as fibroblasts and hematopoietic cells, thus leaving only mammary epithelial cell organoids. The pellet was

labelled P1 and kept on ice, the supernatant was spun for 10 minutes at 1500 RPM. The supernatant was discarded and the pellet from this spin was labelled P-A and kept on ice. Following the second collagenase digestion, the cells were spun for 4 mins at 900 RPM. The pellet obtained was labelled P2 and kept on ice, the supernatant was spun for 10 minutes at 1500 RPM. The supernatant was discarded and the pellet from this spin was labelled P-B and kept on ice. P-A and P-B were combined and resuspended in Ham's F12 medium (Sigma-Aldrich, UK); the cells were spun for 4 minutes at 900 RPM. The supernatant was discarded, and the pellet was labelled P3 and kept on ice. P1, P2 and P3 were combined and resuspended in F-12, the cells were spun for 4 minutes at 900 RPM. This step was repeated three times to remove traces of digestive enzymes. The effluents were spun down to collect the MECs.

2.2.1 Monolayer cell culture

To culture cells in 2D, plastic plates were conditioned for 2 h at 37°C with 2× serum fetuin: Ham's F-12 medium (Lonza, Cat no. LZBE12-615F), 20% FBS, 1mg/ml fetuin (Sigma-Aldrich, Cat no. F2379), 50 U/ml penicillin/streptomycin (Lonza, Cat no. LZDE17-603E), 5µg/ml human recombinant insulin (Sigma-Aldrich, Cat no. I9278), 1µg/ml hydrocortisone (Sigma-Aldrich, Cat no. H0888), and 3ng/ml epidermal growth factor (EGF) (Sigma-Aldrich, Cat no. E1257). Cells were resuspended in equal volume in Ham's F-12 medium and seeded onto plastic plates directly or onto coverslips.

Cells were fed on alternate days with Ham's F-12 media supplemented with 10% FBS, 50 U/ml penicillin/streptomycin, 5µg/ml insulin, 1µg/ml hydrocortisone, and 3ng/ml EGF. To induce β 1-integrin gene deletion in cells the cells were treated with 100nM 4-hydroxytamoxifen (4-OHT) (Sigma-Aldrich, Cat no. H7904) dissolved in ethanol. The treatment was administered at the time of plating and at the next feed.

The cells were fixed on day five, to ensure β 1-integrin was knocked out, using 4% formaldehyde in PBS.

2.2.2 ECM-overlay assay

For ECM-overlay assays, media was removed from cells in 2D culture on day three and overlaid with diluted Matrigel (BD Biosciences, Cat no. 354234) (1:25) in cold DMEM/F12 (Lonza, Cat no. LZBE12) media supplemented with 10% FBS, 50 U/ml penicillin/streptomycin, 5µg/ml insulin, 1µg/ml hydrocortisone, and 3ng/ml EGF for 48 hr. To inhibit cell proliferation 1µg/ml of aphidicolin (Sigma-Aldrich, Cat no. 178273) in DMSO was added to the media, EdU assay was used to confirm inhibition of proliferation (section 2.2.7). The cells were then fixed and immunostained.

2.2.3 Repulsion test assay

For testing the apical domain repulsion hypothesis, Eph4 cells were labelled for 30 mins at 37°C with 5µM with the fluorescent dye CellTracker Red CMTPX (Invitrogen, Cat no. C34552) in serum free medium, and cells were transferred into petri dish to form a confluent monolayer for ~2 days. 24 hr prior to the addition of MEC, media was changed to +/- low calcium media to disrupt tight junctions (DMEM (with Ca²⁺ Gibco, Cat no. 11960044), (without Ca²⁺: Gibco, Cat no. 21068028), 1% penicillin/streptomycin, 5µg/ml insulin, 2.49mM L-glutamine). 5µM Ca²⁺ was added to the DMEM media, without calcium, to produce low calcium media. MEC cultured in 2D were trypsinised and labelled for 30 mins at 37°C with 5µM with the fluorescent dye CellTracker Green CMFDA (Invitrogen, Cat no. C2925) in serum free medium, and cells were plated on top of the Eph4 cells. The cells were then fixed after 24 hr and immunostained.

2.2.4 Organoid formation assay

To culture MECs in collagen, 95µl of collagen I gel solution was prepared on ice, (86.3% (v/v) commercial rat tail collagen I; 2.9% (v/v) sodium bicarbonate; 10.8% 10X DMEM-F12 (Gibco, Cat no. 42400028). Coverslip in 24-well plates was coated with 15µl collagen I gel and allowed to set at 37°C for 40 minutes. The remaining 80µl of collagen I gel solution was kept on ice to polymerise and avoid gelling. The MECs were resuspended in 80µl collagen I solution and plated on top of the set collagen I gel. Collagen gels were allowed to set at 37°C for 1 hour before organoid media (DMEM/F12 medium supplemented with 50 U/ml

penicillin/streptomycin, 5µg/ml insulin, 1µg/ml hydrocortisone, and 3ng/ml EGF) was added to the wells.

For organoid cultures in a laminin-rich reconstituted basement membrane, Matrigel was thawed overnight at 4°C on ice. For embedded experiments MECs were resuspended in 80µl of Matrigel and plated onto coverslips in 24-well plates. The Matrigel was allowed to set at 37°C for 1 hour before organoid media was added. For on top experiments, 80µl of Matrigel was plated onto coverslips in 24-well plates and allowed to set at 37°C for 1 hour. MECs resuspended in organoid media was then added to the wells.

4-OHT was added to induce β 1-integrin gene deletion in cells during the first two feeds.

Cells were fed on alternate days and fixed on day five once organoids with lumens had formed and to ensure β 1-integrin turnover.

2.2.5 Organoid contraction assay

MEC from pregnant mice were embedded in 80µl Matrigel and cultured for 4 days in organoid media supplemented with 1mg/mL mouse recombinant prolactin (Sigma-Aldrich, Cat no. SRP4688). To induce contractions of organoids, 1µM of oxytocin (Sigma-Aldrich, Cat no. O3251) dissolved in DMEM/12 media, was added on day 4 and incubated for 1 hour. For analysis of organoid contraction, the organoids were imaged every second using brightfield microscopy for 120 seconds.

Organoid contraction was analysed using a custom MATLAB code. To summarise, the video was input into MATLAB and separated into frames, the organoids were cropped to minimise noise and converted to greyscale images. The initial frame was used as the reference frame and all subsequent frames were then compared to the reference frame to determine differences in each pixel. Pixel differences in a control organoid were used as a threshold to exclude any pixel change due to noise.

2.2.6 Collagen gel contraction assay

For our collagen gel contraction assay we chose to use the attached-matrix model where the collagen gel is adhered to a rigid substrate, glass coverslip, throughout the experiment. Collagen gels were photographed at the time of plating once the gels were set and again at the time of fixing, on day 5, once organoids were fully formed. The percentage of collagen gel contraction was calculated by $\frac{\text{original size of gel} - \text{final size of gel}}{\text{original size of gel}} * 100$. Although this model restricts horizontal contraction of the collagen gel, we found that gels still contracted in all directions.

2.2.7 Replating assay

For replating assays, media was removed from cells in 2D culture on day three, and the cells were washed in 5mM PBS-EDTA. The cells were incubated in PBS-EDTA at 37°C for 30 seconds to disengage attached cells. The cells were then incubated in trypsin at 37°C for 30 seconds. The dissociated cells were centrifuged for 2 mins at 1200 RPM. The supernatant was discarded, and cells were replated in Matrigel or type I collagen, at a cell density of 1×10^5 per well in 24-well plates with coverslips.

Cells were fed on alternate days and were fixed on day five once organoids with lumens had formed.

2.2.8 EdU proliferation assay

Cell proliferation in MECs was assayed using a Click-iT™ Plus EdU Alexa Fluor® 647 Imaging Kit (Invitrogen, Cat no. C10640) according to manufacturer's protocol. Cells were incubated with 10µM EdU reagent in complete DMEM/F12 media at 37°C for 2 hours prior to fixation. Click-iT™ reaction cocktail was added to coverslips for 30 minutes following secondary antibody incubation and prior to Hoechst incubation. The number of EdU positive nuclei were counted from 8 fields of view and expressed as a percentage of the total number of nuclei.

2.3 Standard cell culture procedures

2.3.1 Acid-etching coverslips

Coverslips were treated with concentrated nitric acid (Fisher Scientific, Cat no, 10654732) for 5 mins to improve cell adhesion and attachment of exogenous ECM. Nitric acid was discarded safely by diluting in water. Acid treated coverslips were washed in running tap water for 2 hr to remove all traces of nitric acid. The coverslips were washed in distilled water twice, and then ethanol prior to storing in a glass bottle containing ethanol.

2.3.2 Passaging and culturing cells

Eph4 cell line was cultured in DMEM/F12 media, supplemented with 5% FBS, 1% penicillin/streptomycin and 5ug/ml insulin. Media was changed every 2-3 days.

The Eph4 cells were passaged when 80% confluency was reached. Complete media was removed, cells were washed 2 times with 1x PBS, trypsin was added to the flasks and cells were incubated at 37°C for 3 minutes. Complete media was added to stop the effect of trypsin. Cells were then centrifuged at 1200 RPM for 3 minutes. The pellet was resuspended in complete media and replated at the optimal density.

The Eph4 cells were replaced by younger frozen aliquots after 10 passages to avoid significant changes to cell marker expression and functionality.

2.3.3 Freezing cells

Pelleted cells were resuspended in freezing media containing: 60% complete media, 10% DMSO (Sigma-Aldrich, Cat no. D2650) and 30% FBS and transferred to cryovials. Cryovials were frozen at -80°C for the first 24 hours before being transferred to liquid nitrogen for long-term storage.

Cells were defrosted quickly in a 37°C water-bath and diluted in complete media in a 15ml falcon tube. The tube was then centrifuged at 1200 RPM for 3 minutes. The pellet was

resuspended in complete media and replated at the optimal density into a T-75 flask. Cells were passaged at least twice before being used for experiments.

2.4 Molecular Biology

2.4.1 RNA Isolation

RNA was isolated from cells in 2D cultures using peqGOLD TriFast™ (peqlab, Cat no. 30-2010) as per manufactures instructions. To summarise cells were lysed directly in the culture dish using TriFast. Chloroform was added to the tubes and incubated for 5 minutes, RNA was phase separated from DNA and proteins by centrifugation at 12000g for 15 minutes at 4°C. RNA in the aqueous phase was precipitated using isopropanol and centrifugation at 12000g for 10 minutes at 4°C. The RNA pellet was washed twice with 75% ethanol by vortexing and centrifugation at 12000g for 10 minutes at 4°C. The pellet was allowed to air dry before resuspending it in RNAase-free water. The RNA concentration and 260/280 ratio was determined using a Nanodrop. All RNA was stored at -80°C till cDNA synthesis.

2.4.2 cDNA synthesis

Single-stranded cDNA was synthesised from total RNA using the High-Capacity RNA-to-cDNA™ Kit (Applied Biosystems, Cat no. 10704217) according to manufacturer's protocol. In brief 20ul of reverse transcription mix containing buffer mix, enzyme mix, RNA sample and quantity sufficient nuclease-free H₂O were placed into a thermal cycler for an hour at 37°C followed by 5 minutes at 95°C to denature the enzymes. cDNA was then stored at -20°C for up to a month or at 4°C for up to a week.

2.4.3 TaqMan qPCR

16µl of PCR reaction mix containing 5µl RNase-free water, 1µl TaqMan® gene expression assay probes (Table 2) and 10µl TaqMan® gene expression master mix (Applied Biosystems Cat no. 4369016) was transferred into a rotor-gene style tube. 4µl of cDNA was added to the side of the well. The tubes were sealed with caps and tapped gently on a counter surface to mix all the components at the bottom of the well. The tubes were placed in a Rotor-Gene Q

real-time PCR System and the cDNA was amplified. Mitogen Activated Protein Kinase 1 was used as the housekeeping gene to act as an internal control for gene expression.

The following thermal conditions and stages were used hold for 2 minutes at 50°C, hold for 10 minutes at 95°C to ensure all the complex targets are denatured and then 40 cycles of 15 seconds at 95°C to denature all dsDNA then a minute at 60°C to promote primer binding to the template and subsequent elongation.

Table 2: TaqMan gene expression assay probes, gene name and assay ID.

Gene name	Probe name	Assay ID
Mitogen Activated Protein Kinase 1	MAPK1	Mm00442479_m1
SMA	Acta2	Mm00725412_s1
p63	Trp63	Mm00495793_m1
Keratin 5	Krt5	Mm01305291_g1
Keratin 14	Krt14	Mm00516876_m1

2.4.3.1 Analysis

Amplification and melting curves were analysed to ensure there was >90% efficiency in amplification of the specific target and there were no primer-dimer artefacts (Figure S1). Relative quantification of the qPCR data was carried out using the $2\Delta\Delta C_t$ method. C_t values of technical repeats were averaged and then normalised relative to the housekeeping gene MAPK1 average, ΔC_t . The fold change was calculated by $2^{-(\Delta C_t)}$.

2.5 Immunostaining

2.5.1 Antibodies

Primary antibodies used in this study have been described in table 3. Conjugated A647 Anti-Laminin-5 (Merck, Cat no. MAB19562) (1:200). GFP anti-Tag (Fisher Scientific, Cat no. 10474172) (1:200), Phalloidin-TRITC (Sigma-Aldrich, Cat no. P151) (1:1000).

Secondary antibodies used include anti-rat IgG, Rhodamine Red-X (Jackson Immunolabs, Cat no. 112-295-167), anti-mouse IgG, Cyanine Dyes (Cy2) (Jackson Immunolabs, Cat no. 115-225-146), anti-mouse IgG, Rhodamine Red-X (Jackson Immunolabs, Cat no. 115-295-166), anti-

guinea pig IgG, Alexa Fluora 488, (Jackson Immunolabs, Cat no. 706-545-148), anti-rabbit IgG, Rhodamine Red-X (Jackson Immunolabs, Cat no. 111-295-144). They were used at 1:500 dilution.

Table 3: Primary antibodies used in this study, source, and concentration.

Antibody	Source	Dilution
β 1 integrin	Millipore, Cat no. MAB1997	1:100
Laminin 111	Gifted Antibody	1:500
β 4 integrin (clone CD104)	BD Pharmingen, Cat no. 550544	1:100
ZO1 (clone R40.76)	Millipore, Cat no. MAB1520	1:200
Cre Recombinase (clone 2D8)	Millipore, Cat no. MAB3120	1:200
Smooth Muscle Actin (clone 1A4)	Sigma-Aldrich, Cat no. A2547	1:400
PKC Zeta C-20	Santa Cruz, Cat no. SC216	1:200
Keratin 14	Biologend, Cat no. 905031	1:400
Keratin 8/18	Progen, Cat no. GP11	1:400

Nuclei were stained with 4 μ g/ml Hoechst 33258 (Sigma-Aldrich, Cat no. 11534886).

2.5.2 Immunofluorescence staining 3D organoids and 2D cells.

Media was removed from cultured organoids and washed in phosphatase-buffered saline (PBS) three times. The organoid structures were fixed using 4% (v/v) formalin solution (Generon, Cat no. 18814-20) for 10 minutes. Samples were washed in PBS three times, and then permeabilised in 0.2% triton (Sigma-Aldrich, Cat no. T8787) in PBS for 7 minutes at RT. Samples were then washed in PBS three times and blocked in 10% goat serum (LabTech, Cat no. GO-605) in PBS for 1 hours at RT. Primary antibodies were added or TRITC-phalloidin in 5% goat serum in PBS were added to the samples and incubated for 2 hours at RT. Samples were washed in PBS six times before adding the fluorescent secondary antibodies in 5% goat serum in PBS. Following a 2-hour incubation the samples were washed once in PBS and incubated with Hoechst for 3 minutes at RT. The samples were washed in PBS five times before mounting using ProLong Gold Antifade Mountant (Invitrogen, Cat no. 11539306).

2.5.3 Whole mount mammary gland immunofluorescence staining

Small sections (~2-5 mm²) were spread onto Poly-L-Lysine slides and immersed into 10% (v/v) formalin solution for 30 minutes. Samples were then washed in PBS three times, and then permeabilised in 0.2% triton in PBS for 30 minutes at RT. Samples were then washed in PBS three times and blocked in 10% goat serum in PBS for 2 hours at RT. Primary antibodies were added or TRITC-phalloidin in 5% goat serum in PBS were added to the samples and left overnight at 4°C or for 2 hours at RT respectively in a humid chamber. Samples were washed in PBS five times before adding the fluorescent secondary antibodies in 5% goat serum in PBS and Hoechst. Following a 3-hour incubation the samples were washed five times in PBS and mounted using ProLong Gold Antifade Mountant.

2.5.4 Imaging and quantification

Unstained live cells in 2D and 3D culture were imaged using a 20x or 40x objective on the DMI1 inverted brightfield microscope. Lumen formation counts were performed down the microscope, a minimum of 25 organoids were counted per condition. Lumen area was calculated using the ImageJ software. The lumen was defined by manually tracing around its perimeter using the area selection tool and then measured.

IF 2D cell cultures, 3D organoids and WM mammary tissue samples were imaged using a x20 or x40 oil objective lens on the Zeiss LSM880 Airyscan within a few days of staining. Confocal images of organoids were taken through its midsection or the top of the organoid. Images were subsequently processed for presentation using ImageJ software. For Z stacks ZEN Black software was used to determine the optimal number of Z sections. Z-stacks were taken to create 3D renderings which provide a greater depth of field and allows for better analysis of tissue organisation. 3D rendering, and videos were developed using Arivis software. A minimum of 8 organoids or fields of view were imaged per condition.

Monochromatic z-slices were coloured with a rainbow array and stacked to produce depth-coded confocal image (Lee et al., 2022). The rainbow colours represent actin filaments at different depths; apical = red, middle = green, basal = blue.

Quantification of β 1-integrin fluorescence intensity in ME cells, defined by the perimeter manually traced around the cell, was calculated using the measure tool in ImageJ software to obtain the area integrated intensity value. A region next to the cell that has no fluorescence was measured to provide the background fluorescence value. The corrected total cell fluorescence was calculated by integrated density – mean fluorescence of background readings.

Quantification of LM-111 fluorescence intensity, defined by the perimeter manually traced around the organoid, was calculated using the measure tool in ImageJ software to obtain the area integrated intensity value. A region next to the organoid that has no fluorescence was measured to provide the background fluorescence value. The corrected total cell fluorescence was calculated like above.

The area and perimeter of ME cells from IF stained images were quantified using ImageJ. The perimeter of the ME cell was traced around manually using the area selection tool or automatically using the wand tool. The measurements were calculated based on the selected ME cell and displayed in a results table.

2.6 Statistical analysis

All statistical analysis was carried out using GraphPad PRISM[®] software V8. Results are expressed as the mean \pm Standard Error of Mean (SEM). The number of organoids/cells analysed is stated in the figure legends.

Statistical significance of difference was analysed using an unpaired Student's t-test for comparing two groups and One-way ANOVA statistical test was used when comparing more than two groups. Statistical significance was defined as p-values below ≤ 0.05 (*) for all data.

3 Lineage specific $\beta 1$ -integrin^{fx/fx} primary organoids as a model system to study the role $\beta 1$ -integrin in lumen formation.

3.1 Introduction

The mammary gland is made up of a network of branched hollow ducts connected to hollow milk producing alveoli. The mammary epithelium exhibits a bilayer structure consisting of an inner layer of secretory luminal (LE) cells surrounded by a layer of contractile myoepithelial (ME) cells adjacent to the extracellular matrix (ECM). This architecture is essential for normal tissue function, and loss of tissue organisation is associated with cancer and other diseases. For example, initial stages of breast cancer, such as epithelial atypia and carcinoma in situ, are often characterised by partial or complete lumen filling (Harris et al., 1999). Moreover, the loss of ME cells is a distinct sign of invasive carcinoma (Bofin et al., 2004). However, the molecular mechanisms involved in mammary tissue structure organisation and its maintenance are not fully understood. Therefore, understanding the mechanism of the spatial organisation during normal development may provide insight into the mechanisms that initiate breast cancer and help identify potential targets to treat the disease.

Primary organoid cultures have been used widely to study mammary gland morphogenesis since the late 1970s, as this cell culture model best recapitulates *in vivo* development and function (Emerman et al., 1979). For example, mammary epithelial cells (MEC) cultured in laminin-rich basement membrane (LrBM) form 3D polarised organoids with LE cells lining the lumen and ME cells on the outside. Organotypic cultures have been used to identify mechanisms involved in ductal elongation and branching morphogenesis (Huebener et al., 2016, Ewald et al., 2008, Sumbal and Koledova, 2019). MECs organoids are also great models of lactation; stimulation with lactogenic hormones causes the synthesis and secretion of milk proteins into the lumen, analogous to MECs during lactation *in vivo* (Sumbal et al., 2020, Akhtar et al., 2016). Accordingly, in this thesis, I will use primary murine organoids to study the mechanisms involved in the spatial organisation of the mammary gland.

Over the last 25 years, studies from our lab and others have shown the importance of $\beta 1$ -integrin in many aspects of MEC function, including polarisation, proliferation, survival, and

functional differentiation (Akhtar and Streuli, 2013, Jeanes et al., 2012, Akhtar and Streuli, 2006, Naylor et al., 2005). These studies have helped identify that cell-ECM interactions contribute to mammary gland morphogenesis. However, little is known about the role of β 1-integrin in the spatial organisation of the mammary gland, lumen formation and cell sorting.

Lumen formation is tightly coupled to cell polarity. Epithelial cells have three distinct domains; the apical surface faces the lumen; the basal surface interacts with the ECM and the lateral surface connects epithelial cells laterally. Apical-basal polarity is established and maintained by asymmetric cortical distribution of three complementary dynamic complexes PAR, Scribble and Crumbs. Cell polarisation also requires cues from the ECM to orient epithelial cell polarity. The role of β 1-integrin in polarity orientation has been studied in Madin-Darby canine kidney (MDCK) cells in some detail. Studies suggest β 1-integrin mediated signalling via Rac1 orients apical polarity (Yu et al., 2005, deLeon et al., 2012, O'Brien et al., 2001). However, in the mammary gland Rac1 appears to be dispensable, instead the β 1-integrin-ILK signalling pathway is utilised for organising cell polarity (Akhtar and Streuli, 2013). Polarisation of microtubules along the apico-basal axis regulates the endocytic removal of apical components from the outer membrane establishing the basal domain and placement of the Golgi apparatus sub-apically for polarised trafficking of proteins (Akhtar and Streuli 2013).

Mammary organoids with β 1-integrin deletion have inverted polarity, the apical membrane faces the surrounding ECM, and perturbed lumen formation (Akhtar and Streuli 2013). However, the contribution of LE and ME β 1-integrin in polarity orientation and lumen formation is not well understood. Although progressive loss of cell polarity is a hallmark of breast cancer, polarity is rarely inverted *in vivo*. Despite abnormal lumen formation in mammary tissue from LE β 1-integrin KO mouse models, the apical polarity is not inverted albeit mispositioned (Akhtar and Streuli 2013). Laminin assembly is known to direct apical polarisation (O'Brien et al., 2001, Yu et al., 2005); the deposition and assembly of laminins by WT ME cells could activate an alternate integrin signalling pathway in β 1-integrin null LE cells, preventing polarity inversion.

The aim of this chapter was to validate the inhouse developed mouse models to check for lineage specific perturbation of β 1-integrin in LE or ME cells specifically *in vitro* and

characterise lumen formation of lineage specific β 1-integrin KO primary MEC organoids embedded in laminin rich ECM or type I collagen.

In all, the work in this chapter validates two lineage specific β 1-integrin mouse models to be employed in the following chapters. I also characterise the effect of β 1-integrin deletion in lumen formation to better understand the differences between the *in vivo* and *in vitro* data. Moreover, given *in vitro* lumen structures have been shown to affect the levels of several secreted factors and cellular function (Bischel et al., 2014), it was important to characterise if this physiologically relevant mammary gland structure is affected in our lineage specific β 1-integrin KO organoid models for our following studies.

3.2 Results

3.2.1 Primary mammary co-culture organoids recapitulate *in vivo* mammary tissue.

The initial aim of the study was to culture 3D organoids that recapitulate *in vivo* mammary tissue organisation. The bilayer mammary epithelium consists of inner LE cells which express keratin 8 and 18 (K8, K18) and outer ME cells which express smooth muscle actin (SMA) and keratin 14 (K14). Primary MEC isolated from virgin female mice were embedded in Matrigel, an exogenous laminin-rich BM that recapitulates the ECM *in vivo*, for four days. Figure 8A shows pre-assembled mammary structure at the time of plating.

3D renderings (Figure 8B) and Z-stack images (Figure 8B) shows 3D mammary organoid embedded in Matrigel form a hollow lumen with inner LE (K18) and outer ME (SMA, K14) cell positioning, comparable to *in vivo* mammary tissue (Figure 8D). Consistent with previous findings, β 1- and β 4-integrin was basolateral with higher levels expressed next to the ECM (Figure 8E, F).

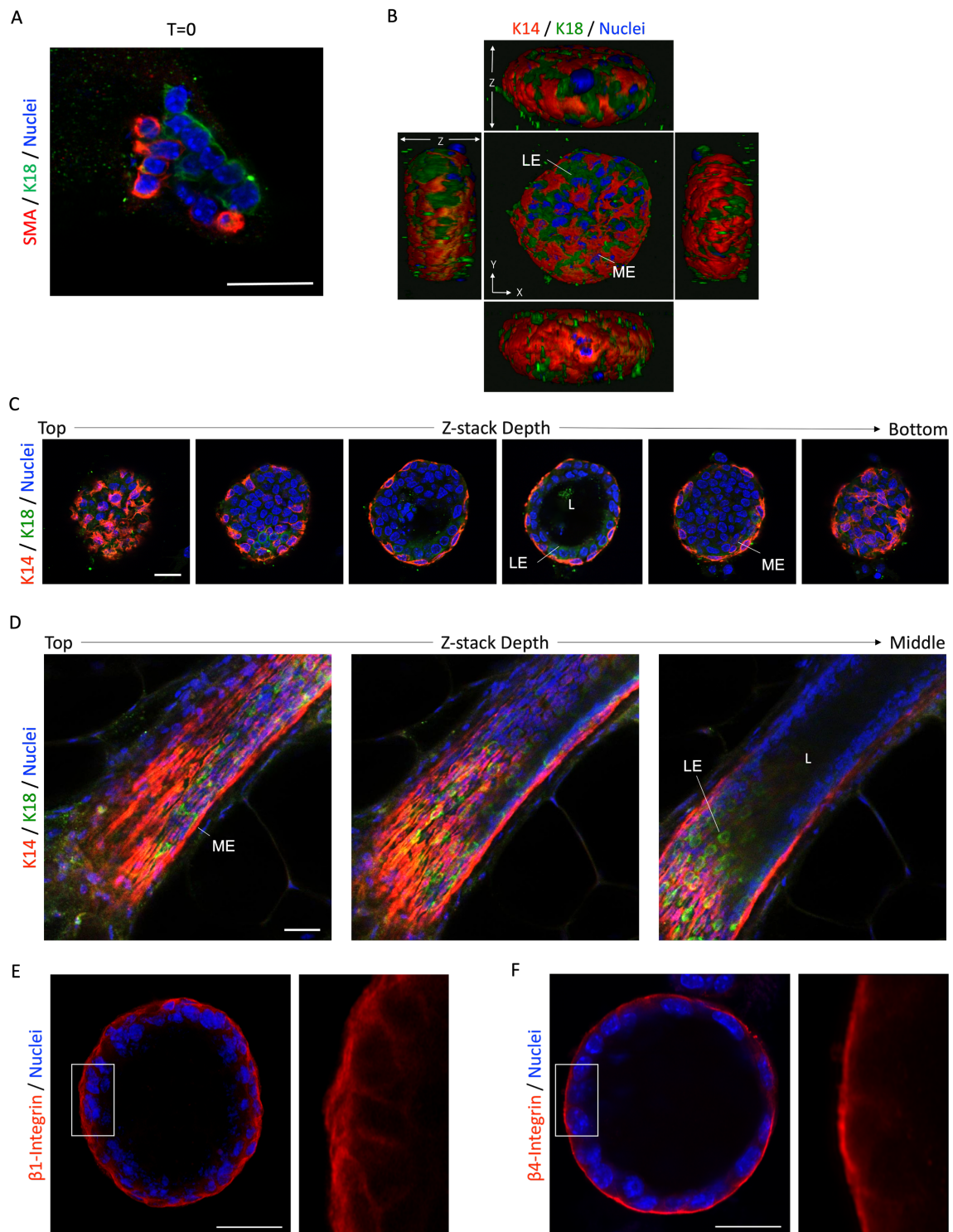


Figure 8: Organoid formation in laminin-rich BM matrix. WT MECs were embedded in a laminin-rich BM (Matrigel) and cultured in organoid forming media for 4 days. **(A)** Representative confocal image of MECs at T=0, fixed after the Matrigel had solidified (~40 mins). SMA (red), K18 (green). Bar: 20 μ m. **(B)** 3D rendering of WT organoid and **(C)** z-stack section stained for K14 (red) and K18 (green). **(D)** Virgin WT wholemount mammary gland stained for K14 (red) and K18 (green). **(E)** 4-day old MECs stained for β 1-integrin (red). Bar: 10 μ m. **(F)** 4-day old MECs stained for β 4-integrin (red). Bar: 20 μ m. Insets are 6x zoom.

3.2.2 Characterisation of inducible deletion of β 1-integrin gene in myoepithelial cells

β 1-integrin gene deletion in our conditional KO mouse models is regulated by the expression pattern of the Cre recombinase, which is driven by cell “specific” promoters e.g., K14 – ME marker or K8 – LE marker. In response to 4-hydroxytamoxifen (4-OHT), the Cre-ERT fusion protein is activated and translocates to the nucleus to induce recombination of the floxed DNA sequences, β 1-integrin, and “STOP” which induces expression of the reporter YFP.

To demonstrate efficient deletion of β 1-integrin in ME cells *in vitro*, MECs were isolated from virgin female β 1-integrin^{fx/fx}: YFP: K14-CreERTM (BK14) mice and cultured in both 2-dimensional (2D) cultures on coverslips and in 3-dimensional (3D) cultures in Matrigel for 5 days.

Cells were grown in a 2D system to form a monolayer culture. The cells were either left untreated or treated with 4-OHT at the time of plating and on day 2, to induce β 1-integrin gene deletion specifically in ME cells. Using immunofluorescence analysis, I show that Cre recombinase expression is found in the cytoplasm of ME cells specifically and upon treatment of 4-OHT, the fused CreER protein, translocate into the nucleus (Figure 9A). Lineage specific deletion of β 1-integrin was confirmed at the protein level of fixed cells in 2D culture on day 5 (Figure 9B). Quantification of β 1-integrin IF staining confirmed β 1-integrin deletion in ME cells when treated with 4-OHT, as there was a significant reduction in fluorescence intensity between WT and ME β 1 KO cultures (Figure 9C).

Immunofluorescence staining of 4-OHT treated organoid culture, shows a loss of β 1-integrin expression in ME cells specifically, with LE cells still expressing β 1-integrin (Figure 9D).

These data demonstrate specific deletion of β 1-integrin from ME cells in both 2D and 3D culture using the Cre-ERT system.

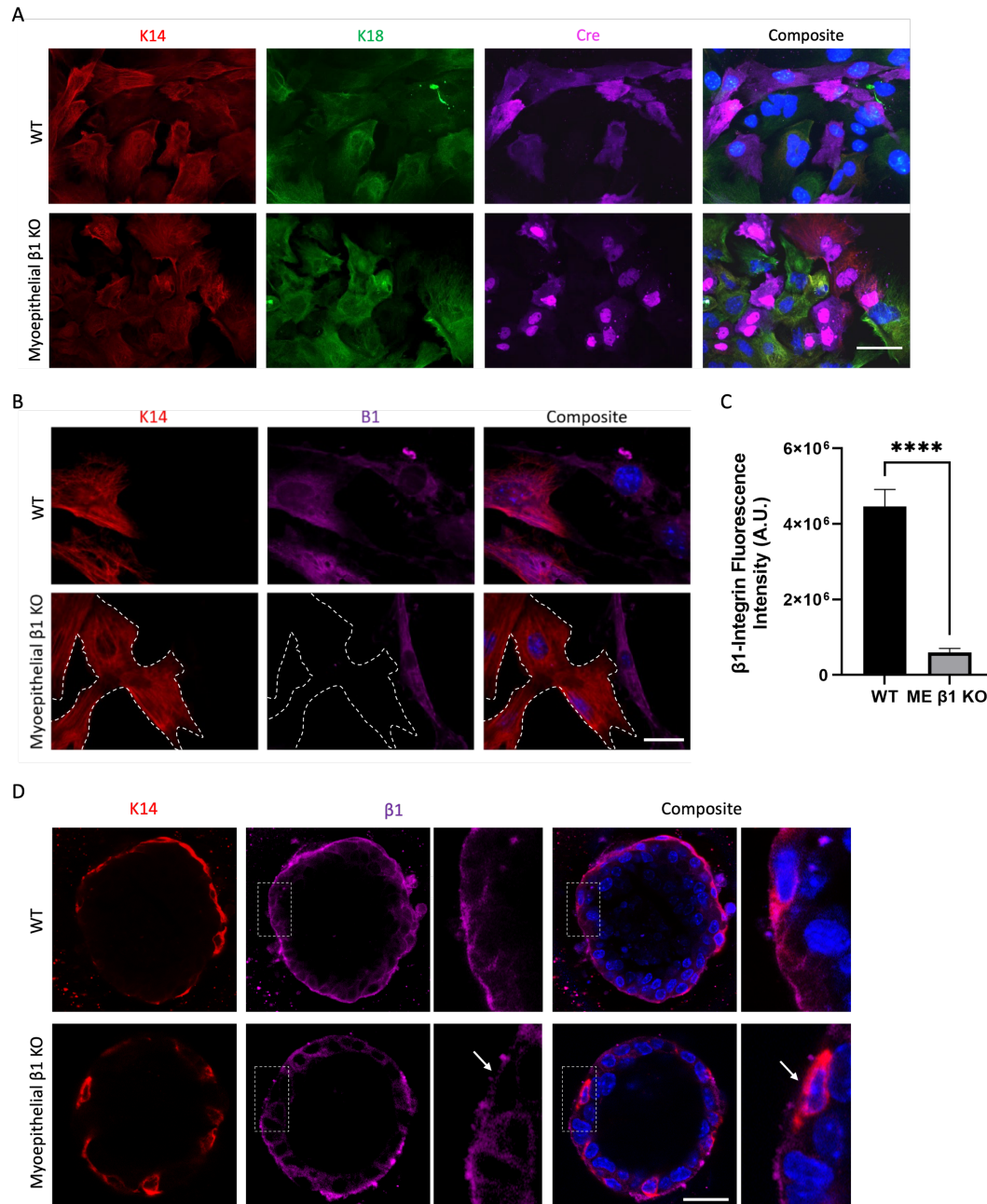


Figure 9: 4-OHT treatment of $\beta 1$ -Integrin^{flox/flox}: K14-CreER MECs knocks out $\beta 1$ -Integrin in ME cells. MEC isolated from BK14 mice were cultured for 5 days (A-B) in 2D on coverslips or (D) embedded in a laminin-rich BM (Matrigel), +/- 4-OHT. Representative images of (A) MECs stained for K14 (red), K18 (green), and CRE (magenta), (B) MECs stained for K14 (red) and $\beta 1$ (magenta), and (D) organoids stained for K14 (red) and $\beta 1$ -integrin (magenta). Insets are 2x zoom. Bar: 20 μ m. White arrow shows where $\beta 1$ -integrin has been lost in ME cells only. (C) Quantification $\beta 1$ -integrin IF intensity in K14 positive cells (ME cells). Data show mean \pm SEM. N = 35 cells. Statistical significant was determined by a Students T-test where **** P < 0.0001.

3.2.3 Characterisation of inducible deletion of β 1-integrin gene in luminal cells

I determined efficient deletion of β 1-integrin from LE cells using MECs from virgin female β 1-integrin^{fx/fx}: YFP: K8-CreERTM (BK8) mice. The use of LE cell specific promoter K8 ensured β 1-integrin gene deletion was induced specifically within LE cells when treated with 4-OHT.

The cells were cultured in both 2D on coverslips and in Matrigel for 5 days. Immunofluorescence staining of 2D MECs shows Cre recombinase expression is found in the cytoplasm of LE cells specifically and upon treatment of 4-OHT, the fused CreER protein, translocate into the nucleus (Figure 10A). Lineage specific deletion of β 1-integrin was confirmed at the protein level of fixed cells in 2D culture on day 5 (Figure 10A-B). Quantification of β 1-integrin IF staining confirmed β 1-integrin deletion in LE cells when treated with 4-OHT, as there was a significant reduction in fluorescence intensity between WT and LE β 1 KO cultures (Figure 10C).

Similarly, in 3D culture addition of 4-OHT induced deletion of β 1-integrin in luminal cells and caused induction of the YFP reporter gene (Figure 10D). The disparity of YFP expression in LE cells when treated with 4-OHT, could be due to variable sensitivity to Cre by the different promoters (Reizis 2019). Cre activity at the β 1-integrin site may not guarantee recombination at the YFP site due to accessibility of Cre recombinase and unequal locus activity. These data demonstrate specific deletion of β 1-integrin from LE cells in both 2D and 3D culture is achievable using the Cre-ERT system.

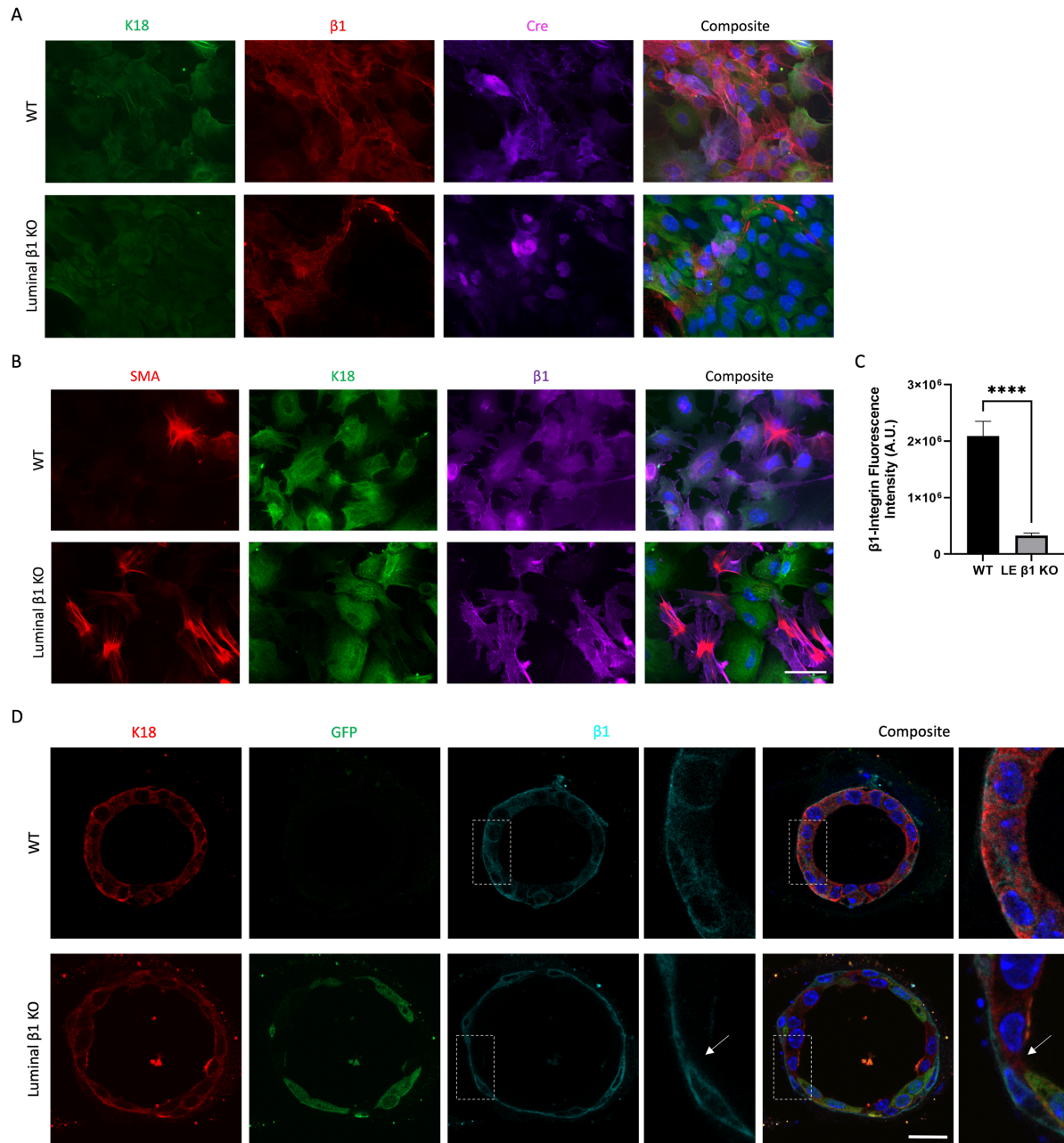


Figure 10: 4-OHT treatment of $\beta 1$ -Integrin^{flox/flox}: K18-CreER MECs knocks out $\beta 1$ -Integrin in LE cells. MEC isolated from BK8 mice were cultured for 5 days (A-B) in 2D on coverslips or (D) embedded in a laminin-rich BM (Matrigel), +/- 4-OHT. Representative images of (A) MECs stained for K18 (green), $\beta 1$ (red) and CRE (magenta), (B) MECs stained for SMA (red), K18 (green) and $\beta 1$ (magenta), and (D) organoids stained for K18 (red) and GFP (green), $\beta 1$ -integrin (cyan). Bar: 20 μ m. White arrow shows where $\beta 1$ -integrin has been lost in LE cells only. (C) Quantification $\beta 1$ -integrin IF intensity in K18 positive cells (LE cells). Data show mean \pm SEM. N = 35 cells. Statistical significant was determined by a Students T-test where **** P < 0.0001.

3.2.4 Loss of β 1-integrin in ME cells perturbs lumen formation in organoids embedded in a type I collagen gel but not laminin-rich BM.

Previously in the lab we have shown β 1-integrin null organoids have perturbed lumen formation and inverted polarity (Akhtar et al., 2013). Similarly, *in vivo* deletion of LE β 1-integrin results in failed lumen formation, however, the polarity is not inverted (Akhtar et al., 2013). How LE cells integrate signals from ME and the ECM to orient polarity and drive lumen formation is unclear. Therefore, it was important to characterise lumen formation using lineage specific β 1-integrin *ex vivo* cultures to better understand the differences between the *in vitro* and *in vivo* studies.

WT ME cells could be depositing ECM components that activates an alternate integrin signalling pathway in β 1-integrin null LE cells to maintain polarity orientation but is insufficient to permit lumen formation. To test this, I examined lumen formation in organoids from virgin and pregnant BK14 mice. In virgin mice the mammary tissue is filled with branching structures known as ducts whereas in response to hormonal changes during pregnancy milk-secreting alveoli are produced. Given there are structural and functional differences between ducts and alveoli, organoids from both virgin and pregnant were examined.

Figure 11A shows representative brightfield images of BK14 ductal and alveolar organoids embedded in Matrigel +/- 4-OHT. Analysis of lumen showed ~80% of WT and ME β 1-integrin KO organoids had lumen formation (Figure 11B). Similarly, there was no significant difference in lumen formation in the alveolar organoid (Figure 11C). The area of the lumens was then assessed using image ImageJ to determine if β 1-integrin deletion altered the size of the organoids (Figure 11D). However, there was no significant difference between the size of WT and β 1-integrin KO organoids (Figure 11E). Interestingly, there was a significant difference in lumen size between ductal and alveolar organoids (Figure 11E). Suggesting the *in vitro* expansion capacity of alveolar (pregnant) MECs is restricted in the absence of hormones needed for alveologenesis during pregnancy. This data highlights the importance of diverse cues from the mammary tissue microenvironment in driving lumen formation.

IF staining of alveolar organoids shows that WT organoids develop lumen with basolateral β 1-integrin, apical f-actin, and PKC (Figure 12A). Deletion of ME β 1-integrin did not affect lumen formation or apical polarity orientation in the presence of exogenous laminins (Figure 12B).

To determine the mechanism of ME mediated lumen formation, BK14 MECs were cultured in the absence of exogenous laminins, to assess the importance of laminin deposition by ME cells. Figure 13A shows representative brightfield images of BK14 ductal organoids embedded in type I collagen +/- 4-OHT. IF staining shows more clearly organoid structure (Figure 13B). Lumen formation in WT organoids cultured in collagen gels was ~60% which is lower than that seen in WT organoids embedded in Matrigel (Figure 13C). Also, lumen formation in ME β 1-integrin KO organoids was ~15%, which was significantly lower than the already reduced level of lumen formation in WT organoids embedded in collagen (Figure 13C). Alveolar organoids also had perturbed lumen formation in the absence of β 1-integrin in ME cells (Figure 13D). Given ME cells are the major contributors to the ECM, laminin deposition might be impaired in the absence of β 1-integrin, resulting in insufficient LE cell-laminin engagement to permit lumen formation.

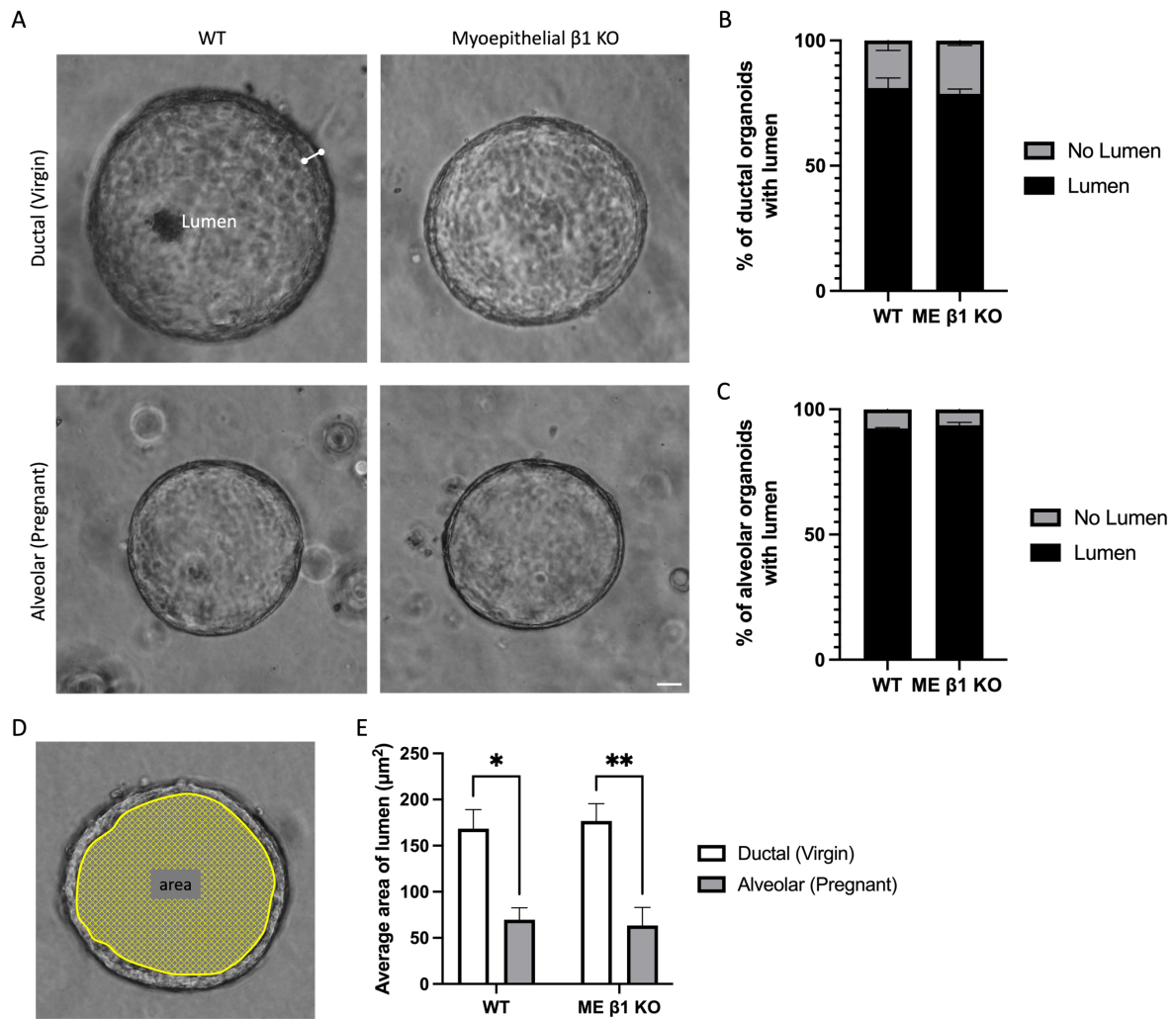


Figure 11: ME $\beta 1$ -Integrin deletion does not affect lumen formation in organoids embedded in a laminin-rich BM. MEC isolated from virgin or pregnant BK14 mice were embedded in laminin-rich BM (Matrigel) and cultured for 5 days +/- 4-OHT. **(A)** Representative brightfield images of organoids formed on day 5. The line between the two points highlights the MEC layer. Bar: 20 μm . Quantification of **(B)** virgin and **(C)** pregnant WT, $\beta 1$ -KO ME organoids with lumens, N = 3 independent experiments, 50 organoids per condition. Statistical significant was determined by a one way ANOVA. **(D)** Lumen area was calculated by drawing around the perimeter of the lumen and using the measure tool in ImageJ. **(E)** Quantification of virgin and pregnant WT, $\beta 1$ -KO ME organoid average lumen size. N = 3 independent experiments, 10 organoids per condition. +/- SEM. Statistical significant was determined by a one way ANOVA where * $P < 0.05$, ** $P < 0.01$.

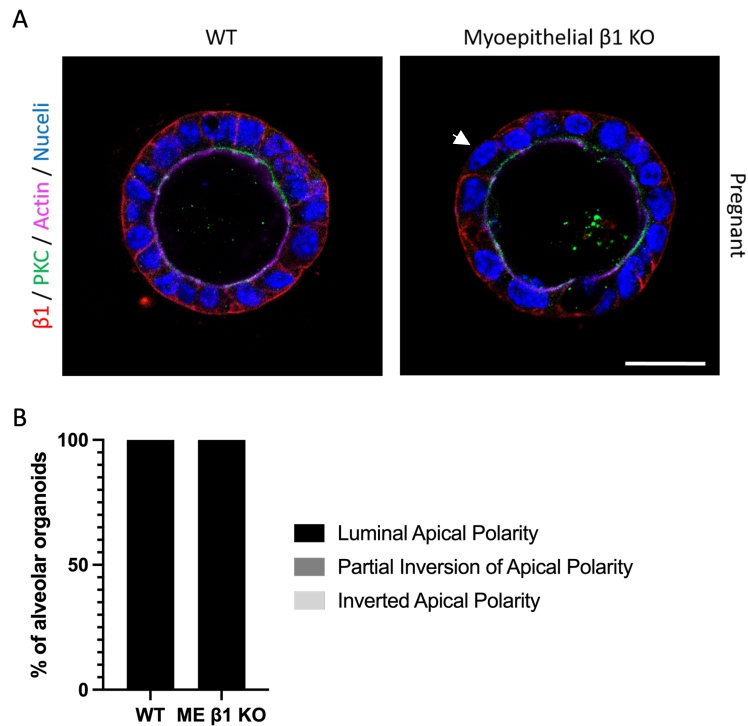


Figure 12: ME β 1-Integrin deletion does not affect apical-basal polarity of alveolar organoids embedded in a laminin-rich BM. MEC isolated from pregnant BK14 mice were embedded in laminin-rich BM (Matrigel) and cultured for 5 days +/- 4-OHT. **(A)** Representative confocal images of organoids on day 5 stained with β 1 (red), aPKC (green) an apical polarity marker, and actin (magenta). Arrow shows ME cell with β 1-integrin loss. Bar: 20 μ m. **(B)** Quantification of apical polarity in WT and ME β 1 KO organoids embedded in Matrigel, N = 3 independent experiments, 10 organoids per condition. Statistical significant was determined by a one way ANOVA.

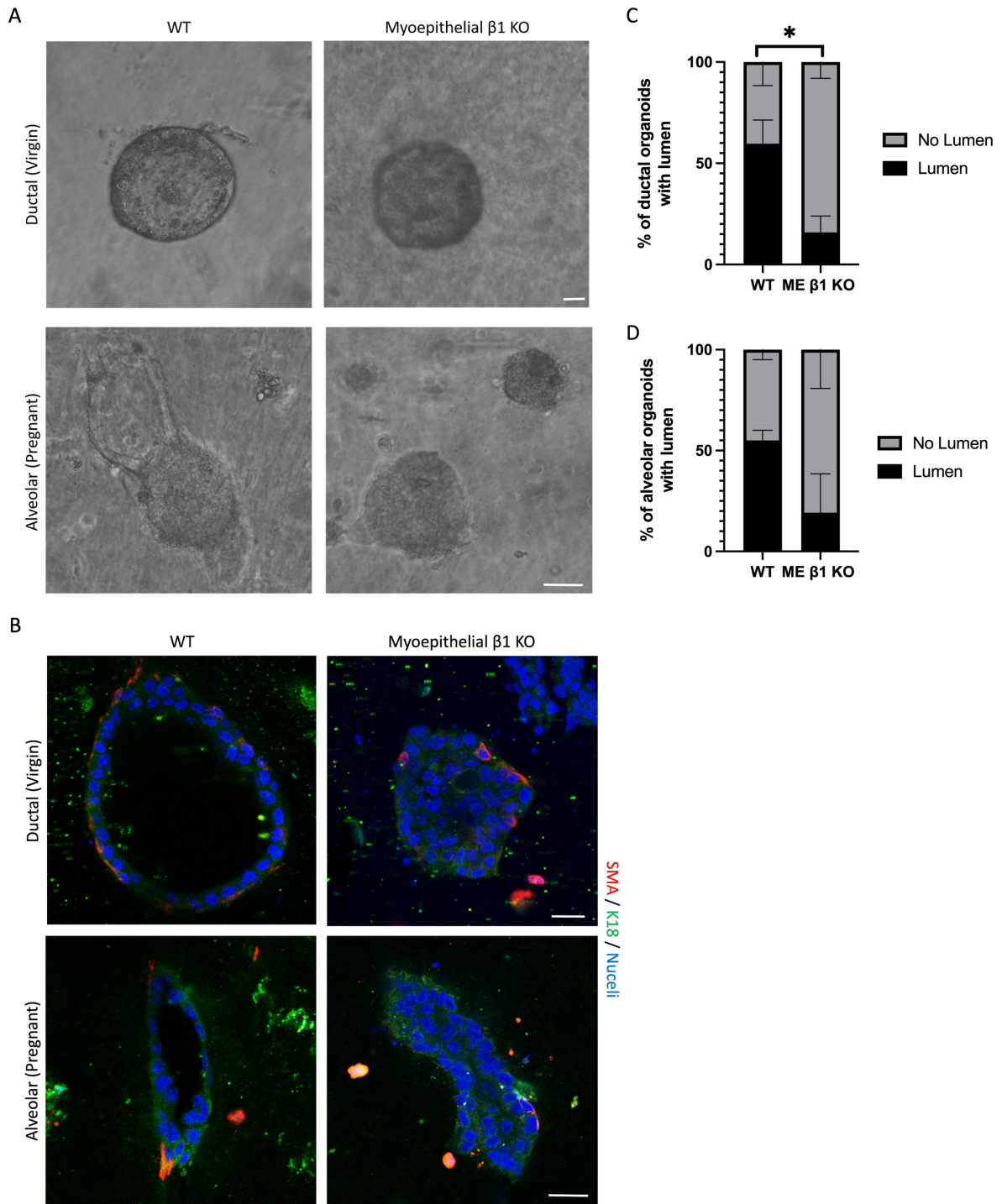


Figure 13: ME β 1-Integrin deletion perturbs lumen formation in organoids embedded in type I collagen. MEC isolated from virgin or pregnant BK14 mice were embedded in type I collagen and cultured for 5 days +/- 4-OHT. **(A)** Representative brightfield images of organoids formed on day 5. Bar: 20 μ m. **(B)** Representative confocal images of organoids on day 5 stained for SMA (red) and K18 (green). Bar: 20 μ m. Quantification of **(C)** virgin (3 independent experiments) and **(D)** pregnant WT, β 1-KO ME organoids with lumens, N = 2 independent experiments, 10 organoids per condition. Statistical significant was determined by a one way ANOVA where * $P < 0.05$.

3.2.5 Deletion of β 1-integrin in luminal cells perturbs lumen formation in organoids embedded in a laminin-rich BM and type I collagen.

LE β 1-integrin deleted mouse models have perturbed lumen formation despite retention of apical polarity orientation in the mammary gland (Akhtar and Streuli 2013). To test if WT ME cells in ex vivo cultures is sufficient for polarity orientation of LE cells and lumen formation, I used MECs from BK8 as it allows for LE cell specific β 1-integrin deletion.

Firstly, I assessed lumen formation in organoids from virgin and pregnant BK8 mice. Figure 14A shows representative brightfield images of BK8 ductal and alveolar organoids embedded in Matrigel +/- 4-OHT. Analysis of lumen formation in ductal (virgin) organoids showed ~90% of WT and ~80% LE β 1-integrin KO organoids had lumen formation (Figure 14B). However, in alveolar (pregnant) organoids deletion of β 1-integrin in LE cells significantly disrupted lumen formation compared to the WT organoids (Figure 14C).

Although there was no significant difference in lumen formation in ductal (virgin) organoids, there was a difference in the size of lumen between WT and LE β 1-integrin KO organoids (Figure 14D). Like the BK14 organoids there was a significant difference in lumen size between WT ductal (virgin) and alveolar (pregnant) organoids (Figure 14D). However, there was no difference in size between the KO organoids (Figure 14D).

Similarly, lumen formation in alveolar organoids was significantly impaired when cultured in a collagen matrix (Figure 14G).

Given apical polarity is not inverted *in vivo* in the presence of WT ME cells, the apical-basal polarity in BK8 alveolar (pregnant) organoids was assessed. Although the apical membrane was partially inverted in a significant percentage of β 1-integrin KO LE organoids compared to WT organoids, 85% of the organoids still had luminal apical polarity (Figure 15A-B). This could be because by the time β 1-integrin is turned over the organoids have already established polarity and formed lumens (Akhtar and Streuli 2013). Therefore, lumen formation and polarity orientation were examined by analysing organoids plated on top of Matrigel.

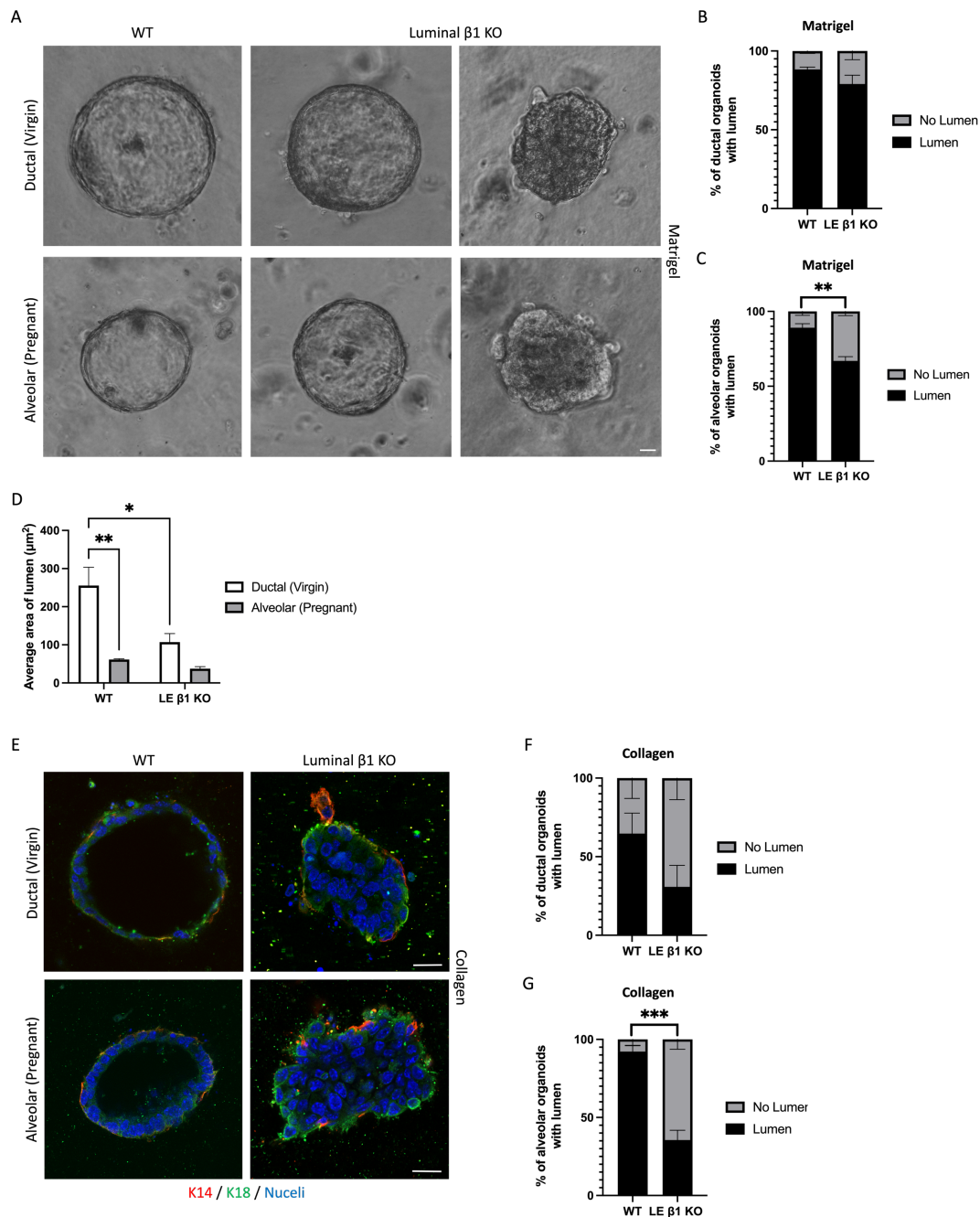


Figure 14: LE $\beta 1$ -Integrin deletion perturbs lumen formation in alveolar organoids. MEC isolated from virgin or pregnant BK8 mice were embedded in laminin-rich BM (Matrigel) or type I collagen and cultured for 5 days +/- 4-OHT. **(A)** Representative brightfield images of organoids formed on day 5 with and without lumen following $\beta 1$ -integrin KO in LE. Bar: 20 μm . Quantification of **(B)** virgin and **(C)** pregnant organoids in Matrigel with lumens, $N = 3$ independent experiments, 50 organoids per condition. **(D)** Quantification of virgin and pregnant WT, LE $\beta 1$ KO organoid average lumen size. $N = 3$ independent experiments, 10 organoids per condition. **(E)** Representative confocal images of organoids cultured in type I collagen gel stained for SMA (red) and K18 (green). Bar: 20 μm . Quantification of **(F)** virgin and **(G)** pregnant organoids in collagen with lumens, $N = 3$ independent experiments, 10 organoids per condition. All data are shown as mean +/- SEM and statistical significant was determined by a one way ANOVA where ** $P < 0.01$, *** $P < 0.001$.

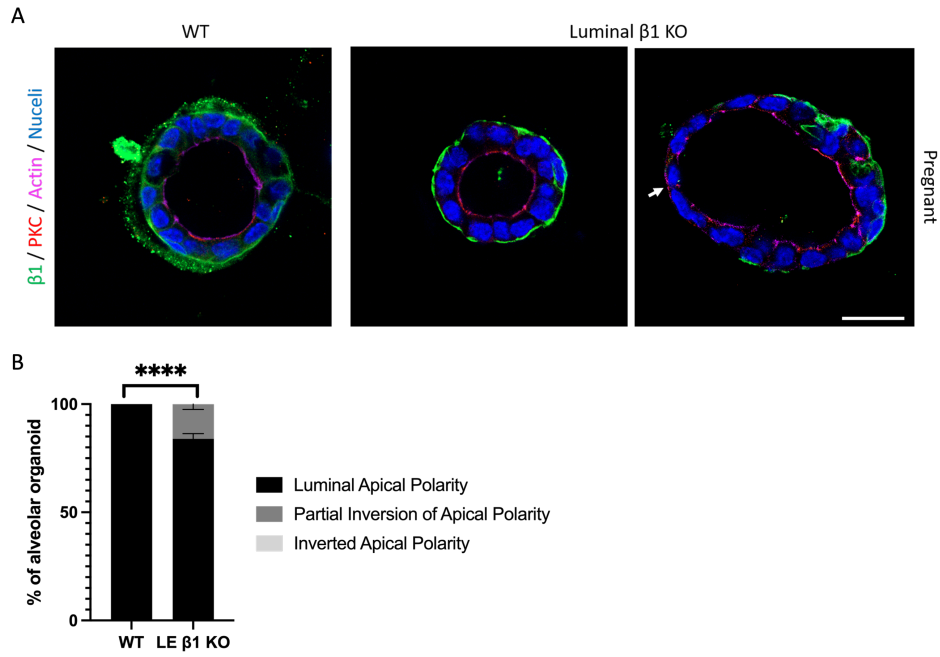


Figure 15: Apical-basal polarity is partially inverted in LE $\beta 1$ -integrin^{fl/fl} alveolar organoids. MEC isolated from pregnant BK8 mice were embedded in laminin-rich BM (Matrigel) and cultured for 5 days +/- 4-OHT. **(A)** Representative confocal images of organoids on day 5 stained with $\beta 1$ (green), aPKC (red) an apical polarity marker, and actin (magenta). Bar: 20 μ m. **(B)** Quantification of WT and $\beta 1$ -KO LE organoids embedded in Matrigel with either luminal or inverted polarity, N = 3 independent experiments, 25 organoids per condition. All data are shown as mean +/- SEM and statistical significant was determined by a one way ANOVA where **** P < 0.0001.

3.2.6 The absence of WT ME cells in LE β 1-integrin KO organoids inverts apical polarity when plated on top of a laminin-rich BM.

Cells plated on top of Matrigel are not fully encapsulated in the matrix, the MECs have rotate in the ECM to cover themselves, therefore it takes longer for MECs to form polarised organoids with lumen. This provides sufficient time for β 1-integrin turnover in LE cells allowing more profound effects on lumen formation and polarisation to be seen.

As speculated only 30% of KO organoids plated on top formed lumens which was significantly lower than organoids embedded in Matrigel (Figure 16A-B). However, like previous *in vivo* data the apical polarity was not inverted in LE β 1 KO organoids that were surrounded by WT ME cells. The luminal apical polarity was only partially inverted in over 50% of the organoids (Figure 16D).

Interestingly, in areas where ME cells were absent the apical polarity was inverted (Figure 16C). ME cells are the main contributors of ECM synthesis and assembly in the mammary gland (Warburton et al., 1982). Therefore, ME cell mediated laminin deposition could be engaging with an alternate integrin signalling pathway in LE cells to control apical-basal polarity orientation. In chapter 4, I examine laminin deposition and the effect of β 1-integrin deletion in ME cells.

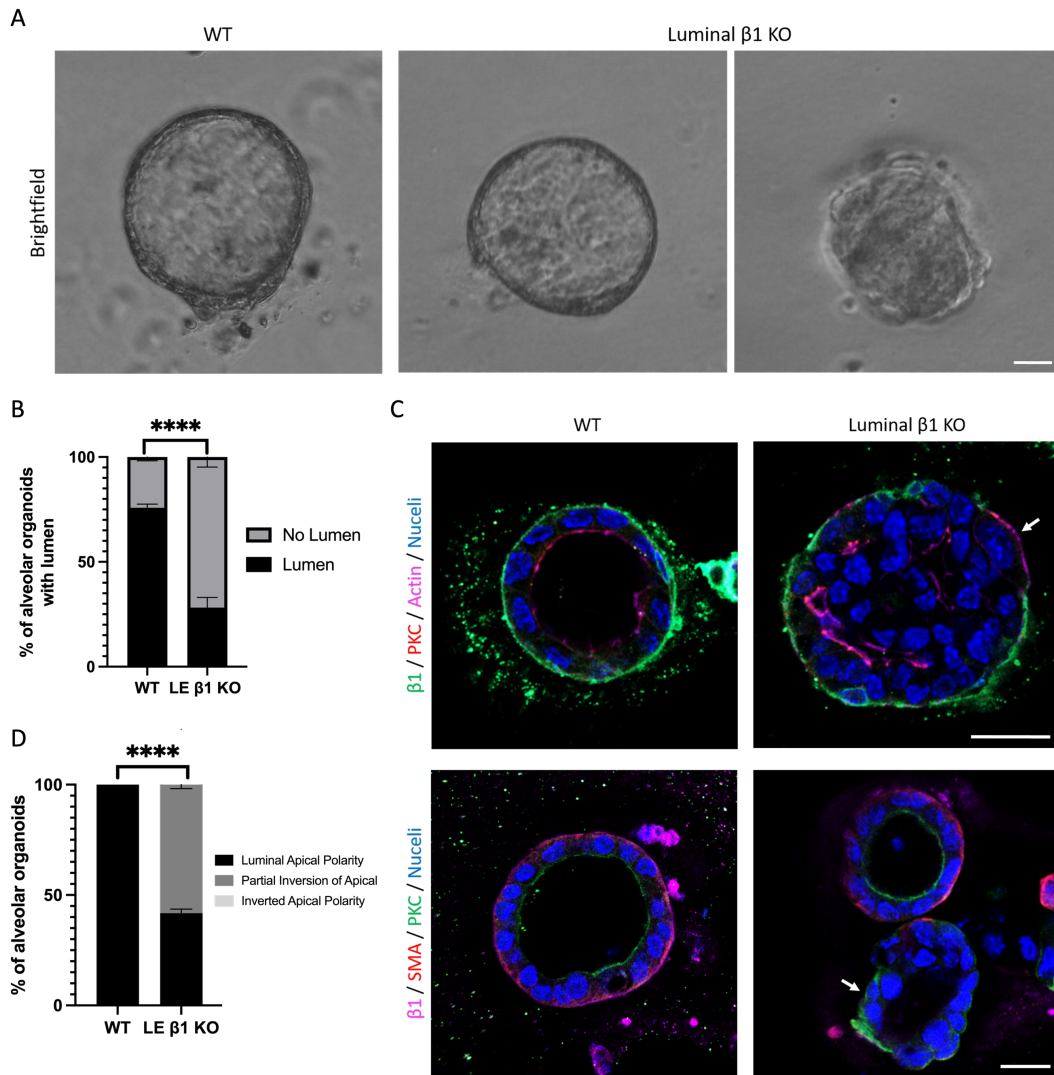


Figure 16: Lumen formation and apical-basal polarity is significantly impaired in LE $\beta 1$ -integrin^{fx/fx} alveolar organoids plated on top of a laminin-rich BM. MEC isolated from pregnant BK8 mice were plated on top of a laminin-rich BM (Matrigel) and cultured for 5 days +/- 4-OHT. **(A)** Representative brightfield images of organoids formed on day 5 with and without lumen following $\beta 1$ -integrin KO in LE. Bar: 20 μ m. **(B)** Quantification of WT, $\beta 1$ -KO LE organoid with lumens when plated on top of Matrigel, N = 3 independent experiments, 50 organoids per condition. **(C)** Representative confocal images of organoids stained with $\beta 1$ (green), aPKC (red), and Actin (magenta) or with $\beta 1$ (magenta), SMA (red), and aPKC (green). White arrows indicate where the apical polarity is inverted. Bar: 20 μ m. **(D)** Quantification of WT and $\beta 1$ -KO LE organoids embedded in Matrigel with either luminal or inverted polarity, N = 3 independent experiments, 25 organoids per condition. All data are shown as mean +/- SEM and statistical significant was determined by a one way ANOVA where **** P < 0.0001.

3.3 Discussion

To investigate the role of β 1-integrin in the spatial organisation of the mammary gland, our lab has generated two 4-OHT inducible mouse models to specifically delete the β 1-integrin gene in ME or LE cells within primary culture. This ensures only the consequences of the loss of β 1-integrin are investigated, without the addition of artefacts that might arise otherwise from FACS and replating of cells. This system is also more robust than transcriptional downregulation which can result in partial down regulation of protein products. Therefore, key conclusions can be made about integrin-mediated events in spatial organisation of the mammary tissue only.

The work presented in this chapter validates β 1-integrin^{fx/fx}: YFP: K14-CreERTM and β 1-integrin^{fx/fx}: YFP: K18-CreERTM mouse models as a tractable system for deleting β 1-integrin specifically in ME or LE cells *in vitro*. Consistent with previous studies, I have shown that WT ductal primary organoids form a polarised bilayer structure with basolateral β 1-integrin expression.

Lumen expansion is an important step in ductal and alveolar morphogenesis. In the human mammary gland, the diameter of the ducts differs between 1.2-2.5 mm depending on whether they are primary or tertiary ducts, whereas the diameter of the alveoli is 0.12 mm (Bannister 1995, Hartman 1991). The difference in lumen diameter between ducts and alveoli could be because ducts need to transport large volumes of milk to the nipple during lactation. Interestingly organoids from virgin (ductal) and pregnant (alveolar) mice recapitulated this size difference even in the absence of hormonal signals. Several mechanisms including regulation of cell number have been proposed to regulate lumen size. For example, in vertebrates increased cell proliferation driven by VEGF can produce abnormally large blood vessels (Lee et al., 2005). Similarly, the size of neural tube organoids is proportional to the number of cells in the organoid (Fattah et al., 2021). However, in *Drosophila* the lumen size of the trachea is unaltered despite a fourfold increase in cell number, rather, lumen size appears to be controlled by the apical membrane (Beitel and Krasnow, 2000). Other studies have also shown lumen size is controlled by apical polarity orientation in the *Drosophila* salivary gland and trachea (Kerman et al., 2008, Myat and Andrew, 2002).

In the mammary gland, β 1-integrin-ECM signalling governs polarity orientation and the subsequent development of the lumen (Akhtar et al., 2013). In this chapter, I investigated the role of ME β 1-integrin-ECM signalling in polarity orientation and lumen formation because, in the presence of WT ME cells *in vivo*, the apical polarity is not inverted; however, lumen formation is still impaired (Akhtar et al., 2013). Moreover, other studies have suggested a role for ME cells in epithelial polarity orientation. (Rodrigues et al., 2021, Hill and Yeh, 2005, Luna-Moré et al., 1994, Akhtar and Streuli, 2013). In this study I show in the absence of WT ME cells the apical membrane is only partially inverted in LE β 1-integrin KO alveolar organoids despite impaired lumen formation. It is probable that WT ME cells could be depositing ECM components that engage an alternative integrin, such as β 4-integrin in LE β 1-integrin KO cells that provide cues for polarity orientation but is insufficient for lumen formation. Future studies testing the role of β 4-integrin in polarity orientation and lumen formation is needed to validate this.

Moreover, deletion of β 1-integrin in ME cells significantly perturbed lumen formation in ductal and alveolar organoids embedded in type I collagen gel, probably due to the absence of laminin cues needed for lumen formation. In the mammary gland several cell types contribute to ECM synthesis and assembly, however, ME cells are the major contributors to the ECM; they express high levels of α 1 and α 3 laminin subunits (Englund et al., 2021). In the absence of β 1-integrin, ME cell's ability to deposit laminins might have been compromised. Studies in keratinocytes have shown integrins are important for laminin synthesis and deposition (Margadant et al., 2009, deHart et al., 2003). Moreover, human MEC co-culture studies have shown organoids fail to form a lumen in the presence of ME cells unable to synthesise sufficient laminin-111 (Gudjonsson et al., 2002). Therefore, in the next chapter, I will examine if laminin deposition is affected when β 1-integrin is deleted in ME cells to validate if lumen formation is perturbed due to LE cells being unable to engage with laminins.

In all, I have demonstrated lineage specific deletion of β 1-integrin can be achieved *in vitro* and will be using these embedded organoid models to test the role of β 1-integrin in MEC sorting in the next chapter. Furthermore, I have shown WT ME cells with β 1-integrin are essential for polarity orientation of LE cells and lumen formation.

4 The effect of lineage specific deletion of β 1-integrin in mammary epithelial cell sorting

4.1 Introduction

During morphogenesis, different cell populations can self-organise to form discrete cellular compartments through a process known as cell sorting. Epithelial tissues such as the prostate, lacrimal, mammary, salivary, and sweat glands comprise of two population of heterogenous cell types that concentrically arrange to form two distinct layers. The mammary gland is composed of luminal (LE) cells that surround the lumen, myoepithelial (ME) cells that lie adjacent to the ECM and mammary stem cells (MaSCs).

Despite cells in the mammary gland undergoing constant rearrangement with each oestrous cycle, pregnancy, lactation, and involution, the tissue architecture is rarely lost. Several models have been proposed to explain the mechanisms of cell sorting, including the differential adhesion hypothesis (Foty et al., 1996, Steinberg, 1962a, Steinberg, 1962b, Steinberg, 1962c), the differential surface contraction hypothesis (Harris, 1976), and the differential interfacial tension hypothesis (Brodland, 2002). The central idea behind all these theories is that cell-cell adhesion drives cell sorting. For example, weakly adhesive cells will surround highly adhesive cells to achieve the most energetically favourable configuration.

A major contributor to mammary epithelial integrity is cell-cell adhesion. In mature ducts, LE cells connect to each other through E-cadherins, desmosomes, tight junctions, and gap junctions (Pitelka et al., 1973). Whereas ME cells connect to each other only through P-cadherins (Daniel et al., 1995). LE and ME cells are linked through desmosomes and gap junctions (Pitelka et al., 1973). During morphogenesis, the quantity and organisation of these cell-cell adhesion molecules dynamically varies. For example, unpublished transmission electron microscopy data from our lab shows desmosomes are absent between LE and ME in the alveoli during pregnancy and lactation. Therefore, distinct mechanisms of cell sorting may exist between the ducts and alveoli in the mammary gland.

Cell sorting studies using human MECs revealed that antibody-based disruption of E-cadherin or P-cadherin subsequently inhibits sorting of LE and ME cells into a bilayer (Chanson et al.,

2011). Furthermore, the bilayer organisation of engineered human MECs aggregates was disrupted by the addition of peptides blocking the cell adhesion recognition (CAR) sites on desmosomes (Runswick et al., 2001). However, given these studies either used microwells with nonfouling coating to prevent cells adhering to the well, or rotary culture, the absence of cell-cell adhesion might have had a more profound effect on MEC positioning than in the presence of ECM. Studies in the developing mammary gland have shown loss of cell-cell adhesion proteins such as E- and P-cadherin does not affect MEC positioning (Boussadia et al., 2002, Radice et al., 1997). Moreover, Cerchiari et al., (2014) demonstrated that spatial organisation of the mammary gland can be achieved even, in the absence of cell-cell adhesion. Suggesting other forces and mechanisms could be involved in driving cell sorting such as cell-ECM affinity.

Integrins are a family of $\alpha\beta$ heterodimer receptors that mediate cell-ECM interactions. Within the mammary gland, $\beta 1$ -integrin is the most expressed integrin; it can form heterodimers with six different α -subunits. MECs also express the $\alpha 6\beta 4$ integrin receptor. Mammary stem cells, LE progenitors and ME progenitors express a characteristic set of integrins, $\beta 1$ (CD29^{high}) and $\alpha 6$ (CD49f^{high}), $\beta 1$ (CD29^{low}) and $\beta 3$ (CD61^{high}), $\beta 1$ (CD29^{high}) respectively, which suggests integrins might have a functional role in driving cell sorting during mammary gland development (Shehata et al., 2012). Recent, lineage tracing, single cell transplantation and single cell RNA sequencing studies have shown, cells during early stages of embryonic development can give rise to both LE and ME cells (Pal et al., 2021, Ying and Beronja, 2020, Wuidart et al., 2018). Lineage segregation of LE and ME cells occurs concomitantly with the formation of microlumens and branching in the embryonic mammary gland. However, correct spatial organisation, inner LE and outer ME is only achieved in the pre-pubertal gland ~day 5 postnatal (Wuidart et al., 2018).

We propose the initial establishment of cell positioning is driven by cell sorting and the subsequent maintenance of cell positioning is dependent on oriented cell division planar to the ECM. Spatial cues from cell-ECM adhesion complexes have been implicated in directing spindle orientation (Matsumura et al., 2016, Fink et al., 2011, Toyoshima and Nishida, 2007). Moreover, in the mammary gland, basal cells lacking $\beta 1$ -integrin have altered cell division orientation resulting in progeny cells being found in the luminal compartment (Taddei et al., 2008).

Just as cell-ECM affinity could be driving MEC cell sorting, repulsive forces at the apical membrane could be promoting cell sorting. During drosophila limb development apically, secreted molecules provide a constraining force driving cell shape changes, oriented cell division and intercalation of cells (Diaz-de-la-Loza et al., 2018, Ray et al., 2015). Therefore, a similar force could be present in the mammary gland driving ME cells away from the apical membrane. Alternatively, the formation of a structural network in the luminal space could be binding and presenting or sequestering cytokines that helps control cell rearrangement to resolve multilayer structures during morphogenesis (Jazwinska et al., 2003).

Thus, we hypothesised that integrin mediated affinity to the ECM or repulsion at the apical membrane drives ME cell positioning. The aim of this chapter was to test the effect of β 1-integrin deletion in sorting of primary MECs using organoids embedded in laminin rich BM or type I collagen, and ECM-overlay assays. To do this, lineage specific CreERT/LoxP mouse models were used to delete β 1-integrin in LE or ME cells specifically and assess cell sorting using 3D and 2D cultures.

In this chapter, I have shown that deletion of β 1-integrin in any one cell lineage is insufficient to disrupt MEC sorting suggesting other integrins might be involved. This chapter highlights ME cell affinity to the matrix and repulsion at the apical membrane drive ME cell positioning.

4.2 Results

4.2.1 β 1-integrin deletion in myoepithelial cells does not affect its positioning when embedded in laminin-rich BM

To test whether perturbing β 1-integrin levels in myoepithelial cells affects cell positioning, mammary epithelial cells were isolated from virgin β 1-integrin^{fx/fx}: YFP: K14-CreERTM (BK14) mice and embedded in Matrigel to form 3D organoids of ductal structures.

Immunofluorescence staining showed that both WT and ME β 1 KO organoids formed a bilayer structure with luminal cells positioned next to the lumen and myoepithelial cells positioned next to the ECM (Figure 17A).

These results indicate that loss of β 1-integrin in myoepithelial cells does not affect formation of the concentric bilayer structure (Figure 17A-B). Moreover, the number of ME cells around

the organoids is unaltered (Figure 17C). However, this could be in part due to the presence of pre-assembled ductal structures at the time of plating. Given these cell clusters already have a bilayer structure, β 1-integrin mediated myoepithelial-ECM interactions may not be required to drive spatial organisation forming a bilayer organoid. Also, it is probable β 4-integrin could be engaging with either exogenous laminin in Matrigel or endogenous laminin deposited by WT luminal cells and subsequently aid organisation of the mammary tissue.

Analysis of β 4-integrin showed basal expression contiguous to the ECM in both WT and β 1-integrin KO organoids (Figure 17D). This suggests β 4-integrin mediated binding to laminins could be compensating for the lack of β 1-integrin cell-ECM binding driving spatial organisation in the mammary gland.

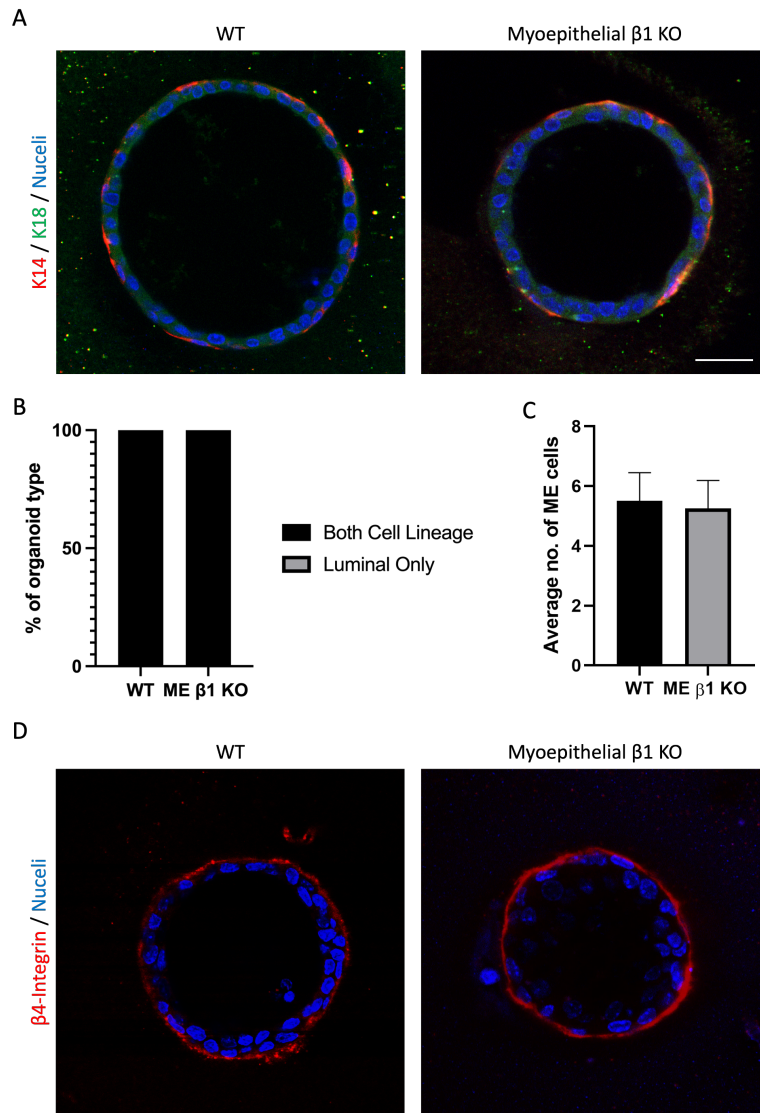


Figure 17: ME $\beta 1$ -integrin^{fx/fx} ductal organoids embedded in a laminin-rich BM form with inner LE and outer ME. MEC isolated from virgin BK14 mice were embedded in laminin-rich BM (Matrigel) and cultured for 5 days +/- 4-OHT. **(A)** Representative confocal images of organoids with inner luminal and outer ME. K14 (red) and K18 (green). Bar: 20 μ m. **(B)** Quantification of WT, ME $\beta 1$ KO organoid with both LE and ME cell, N = 3 independent experiments, 10 organoids per condition. Data is shown as mean +/- SEM and statistical significant was determined by a one way ANOVA. **(C)** Quantification of the number of ME cells (nuclei surrounded by K14/SMA staining) in WT and ME $\beta 1$ KO organoid using mid-section images, N = 3 independent experiments, 10 organoids per condition. Data is shown as mean +/- SEM and statistical significant was determined by a Students T-test. **(D)** 5-day old primary MEC organoids stained for $\beta 4$ -integrin (red).

4.2.2 Laminin deposition and assembly is compromised in ME β 1-integrin deleted organoids.

β 4-integrin can bind to laminin-332, -311, -321, -511, -521, -522, and -523 but not collagen (Yamada and Sekiguchi, 2015, Taddei et al., 2003). To assess if β 4-integrin could be mediating spatial organisation by binding to deposited endogenous laminins, I embedded the cells in type I collagen gels. MECs were cultured for five days in organoid forming media +/- 4-OHT to assess organoid formation.

Organoids formed with inner luminal and outer myoepithelial when cultured in type I collagen gel regardless of β 1-integrin expression in ME cells, suggesting spatial organisation of MEC could be driven by endogenous laminin deposition (Figure 18A).

To validate this, the expression and deposition of LM332 was studied. Englund et al., 2021 have shown previously that laminin α 3 is expressed by both ME cells and LE cells in mature ducts. Using immunofluorescence staining, I detected expression of LM332 in both ME and LE cells in the untreated and treated organoids (Figure 18B). However, I was unable to detect the secreted form of LM332, which could be in part due to the nature of the antibody used in this study (Figure 18B). The antibody used in this study was directed against an immunogen within the internal region of the laminin gamma 2 chain, therefore the signal might have been undetectable compared to if an antibody capable of detecting the entire laminin was used. Therefore, alternative antibodies capable of detecting the entire secreted form of LM332 need to be tested.

Studies by deHart et al., (2003, 2004) and Margadant et al., 2009 in keratinocytes have indicated that α 3 β 1 and α 6 β 1 integrin respectively modulates laminin deposition *in vitro*. Given myoepithelial cells are the main depositors of the ECM (Warburton et al., 1982), I wanted to see if deletion of β 1-integrin compromises ECM deposition and assembly in the mammary gland. As laminin α 1 has been shown to be expressed by ME cells specifically, I assessed the deposition of LM111 in collagen gel. LM111 was localised along the outer edge of the organoids, in line with previous *in vivo* studies (Paine and Lewis, 2017, Englund et al., 2019). However, loss of β 1-integrin perturbed LM111 deposition (Figure 18C-D).

It is possible other laminins such as LM332 or LM521 could be deposited by the WT LE cells guiding spatial organisation. Taken together these data suggest that β 4-integrin could be involved in modulating spatial organisation in the absence of β 1-integrin.

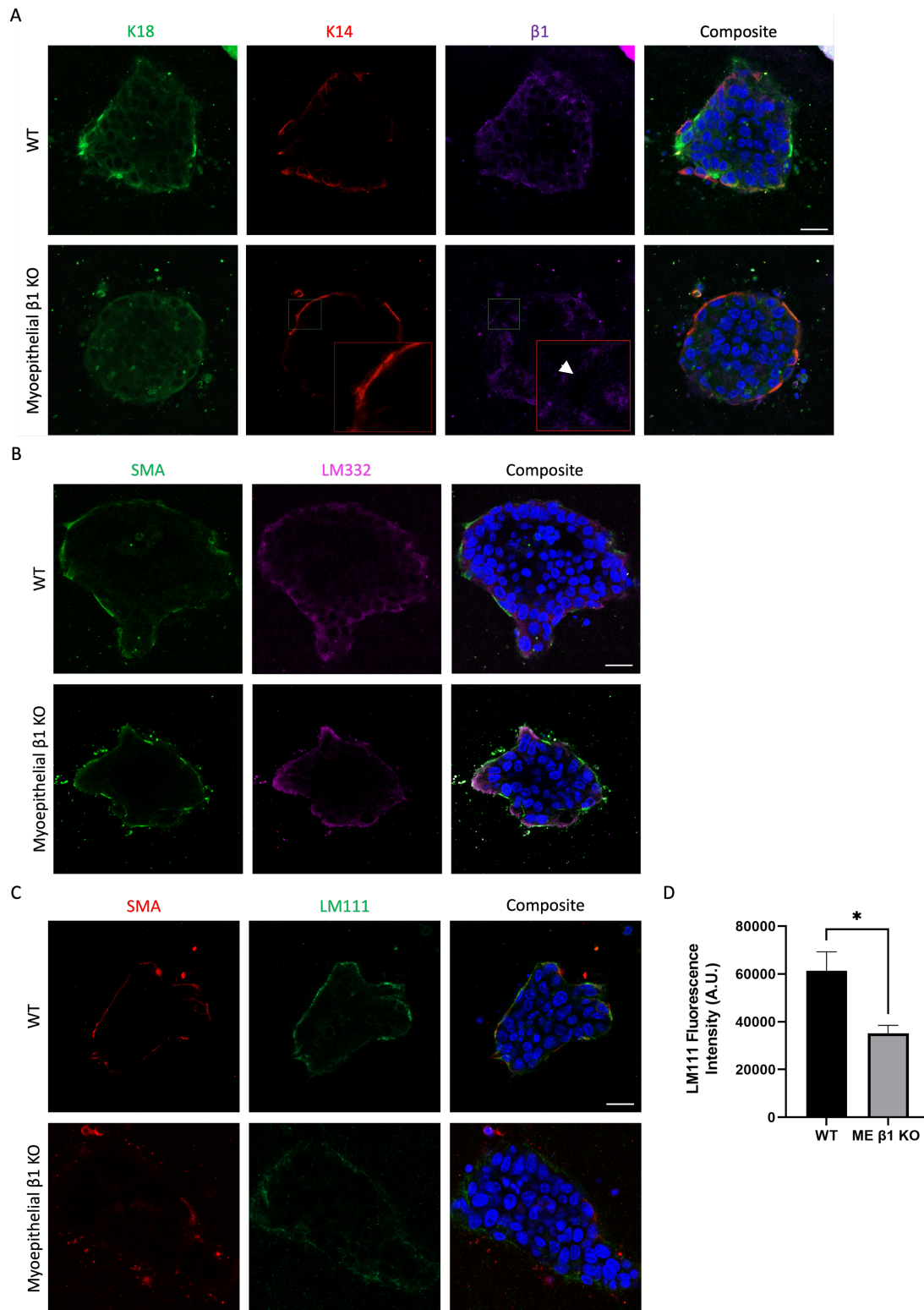


Figure 18: ME $\beta 1$ -Integrin deletion reduces LM111 deposition. MEC isolated from virgin BK14 mice were embedded in laminin-rich BM (Matrigel) and cultured for 5 days +/- 4-OHT. Representative confocal images of organoids stained with **(A)** K18 (green), K14 (red) and $\beta 1$ -integrin (magenta), **(B)** SMA (green) and LM332 (magenta), **(C)** SMA (red) and LM111 (green). Bar: 20 μ m. White arrow indicates loss of $\beta 1$ -integrin. **(D)** Quantification LM111 IF intensity. Data show mean \pm SEM. N = 3 independent experiments, minimum 5 organoids. Statistical significant was determined by a Students T-test where * P < 0.05.

4.2.3 β 1-integrin deletion in luminal cells does not affect cell sorting in a laminin-rich BM or in type I collagen gel

To test whether perturbing β 1-integrin levels in LE cells affects cell positioning, mammary epithelial cells were isolated from virgin β 1-integrin^{fx/fx}: YFP: K8-CreERTM (BK8) mice and embedded in Matrigel to form 3D organoids of ductal structures.

Immunofluorescence staining showed LE β 1-integrin KO organoids still formed a bilayer of inner LE and outer ME when embedded in Matrigel (Figure 19A-B). There was no significant difference in the number of ME cells present on the surface of the WT and treated organoids (Figure 19C).

Similarly, organoids cultured in type I collagen formed organoids with correct spatial organisation (Figure 19D). The deposition of LM111 was assessed using immunofluorescence and there was no difference between the WT and LE β 1-integrin KO samples (Figure 19D).

These data suggest that loss of β 1-integrin in LE cells alone is insufficient to disrupt spatial organisation of the two cell lineages. Previous studies have shown LE and ME cells in the resting mammary ducts are linked through desmosomes (Ewald et al., 2012, Pitelka et al., 1973). Therefore, it is possible this cell-cell adhesion molecule could be modulating spatial organisation and maintaining correct cell positioning even in the absence of cell-ECM adhesion.

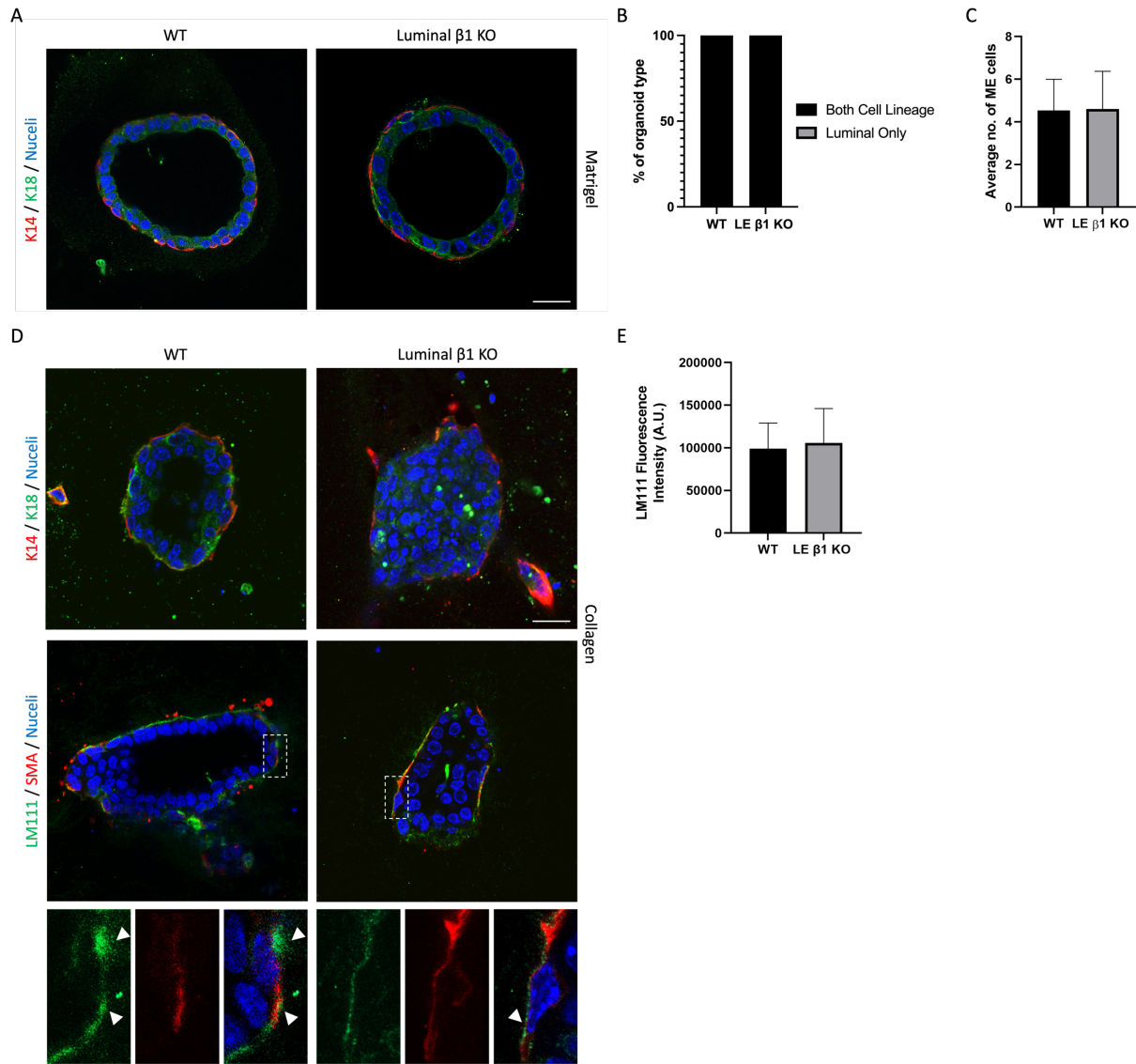


Figure 19: LE $\beta 1$ -integrin^{flox/flox} ductal organoids form with inner LE and outer ME. MEC isolated from virgin BK8 mice were embedded in laminin-rich BM (Matrigel) or type I collagen and cultured for 5 days +/- 4-OHT. **(A)** Representative confocal images of organoids embedded in Matrigel with inner luminal and outer ME. K14 (red) and K18 (green). **(B)** Quantification of WT, LE $\beta 1$ KO organoid with both LE and ME cell, N = 3 independent experiments, 20 organoids per condition. Data is shown as mean +/- SEM and statistical significant was determined by a one way ANOVA. **(C)** Quantification of the number of ME cells (nuclei surrounded by K14/SMA staining) in WT and LE $\beta 1$ KO organoid using mid-section images N = 3 independent experiments, 9 organoids per condition. Data is shown as mean +/- SEM and statistical significant was determined by a Students T-test. **(D)** Representative confocal images of organoids embedded in collagen stained with with K14 (red) and K18 (green), LM111 (green) and SMA (red). 2x zoom inset, arrows highlight where laminin staining is around ME cells. Bar: 20 μ m. **(E)** Quantification LM111 IF intensity. N = 3 independent experiments, minimum 5 organoids. Data is shown as mean +/- SEM and statistical significant was determined by a Students T-test.

4.2.4 β 1-integrin deletion in ME or LE cells alone does not disrupt MEC positioning in alveolar structures

Unpublished data from our lab shows desmosomes do not form between ME and LE cells in alveoli. To test if cell sorting is dependent on β 1-integrin mediated affinity to the ECM or driven by desmosome adhesion, MEC from pregnant mice were used as the mammary tissue undergoes massive tissue remodelling resulting in the formation of lots of alveoli. Therefore, the role of β 1-integrin in the spatial organisation of the mammary gland can be studied in the absence of desmosome adhesion.

MECs were harvested from pregnant (day 15-18) BK14 mice and embedded in Matrigel or type I collagen. Immunofluorescence staining showed MEC formed organoids, when embedded in laminin rich matrix, with inner LE and outer ME (Figure 20A). Interestingly, not all the alveolar organoids had both LE and ME cells (Figure 20B). This could be due to the fewer number of ME cells present in alveolar structures compared to ductal structures. However, the number of ME cells found on the surface of the organoids was not altered (Figure 20C). Similarly, MEC cultured in collagen formed bilayer organoids regardless of β 1-integrin expression (Figure 20D).

I then assessed spatial organisation in alveolar structures in the absence of β 1-integrin in LE cells. To study this, MEC from pregnant BK8 mice were harvested and embedded in Matrigel or type I collagen. Immunofluorescence staining showed MEC embedded in Matrigel, and collagen formed bilayer organoids, with inner LE and outer ME cells (Figure 21A, D). Like the BK14 alveolar structures there were several organoids without both cell type. However, in the absence of β 1-integrin in LE cells there were significantly more organoids with both LE and ME cells (Figure 21B). Likewise, there was also significantly more ME cells found on the surface of organoids lacking β 1-integrin (Figure 21C). This suggests β 1-integrin KO LE cells depend on ME cells for organoid formation.

Overall, the data suggests β 1-integrin might not play a major role in the spatial organisation of the mammary gland. However, it is possible I might not be seeing any effects on cell sorting due to pre-assembled structures at the time of plating. Given these cell clusters are already

spatially organised, deletion of $\beta 1$ -integrin in either cell lineage may not have impacted spatial organisation.

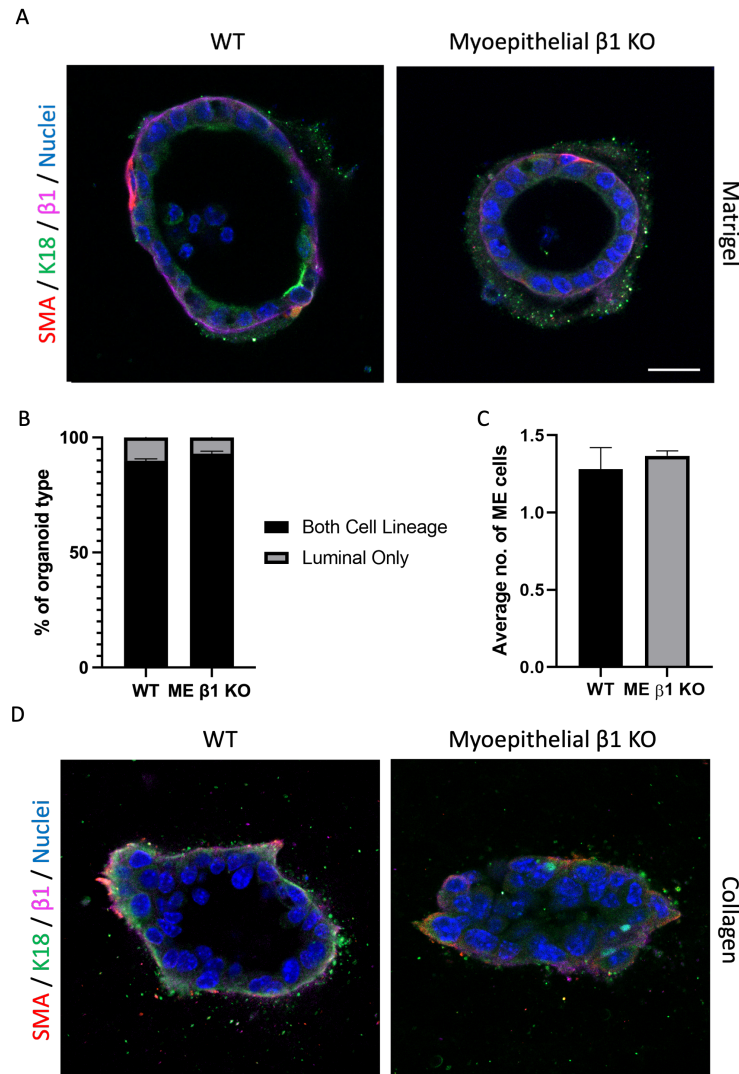


Figure 20: ME $\beta 1$ -integrin^{fx/fx} alveolar organoids form with inner LE and outer ME. MEC isolated from pregnant BK14 mice were embedded in laminin-rich BM (Matrigel) or type I collagen and cultured for 5 days +/- 4-OHT. Representative confocal images of organoids with inner luminal and outer ME in **(A)** Matrigel and **(D)** collagen. SMA (red) and K18 (green) and $\beta 1$ -integrin (magenta). Bar: 20 μ m. **(B)** Quantification of WT, ME $\beta 1$ KO organoid with both LE and ME cell, N = 3 independent experiments, 20 organoids per condition. Data is shown as mean +/- SEM and statistical significant was determined by a one way ANOVA. **(C)** Quantification of the number of ME cells (nuclei surrounded by K14/SMA staining) in WT and ME $\beta 1$ KO organoid using mid-section images, N = 3 independent experiments, 9 organoids per condition. Data is shown as mean +/- SEM and statistical significant was determined by a Students T-test.

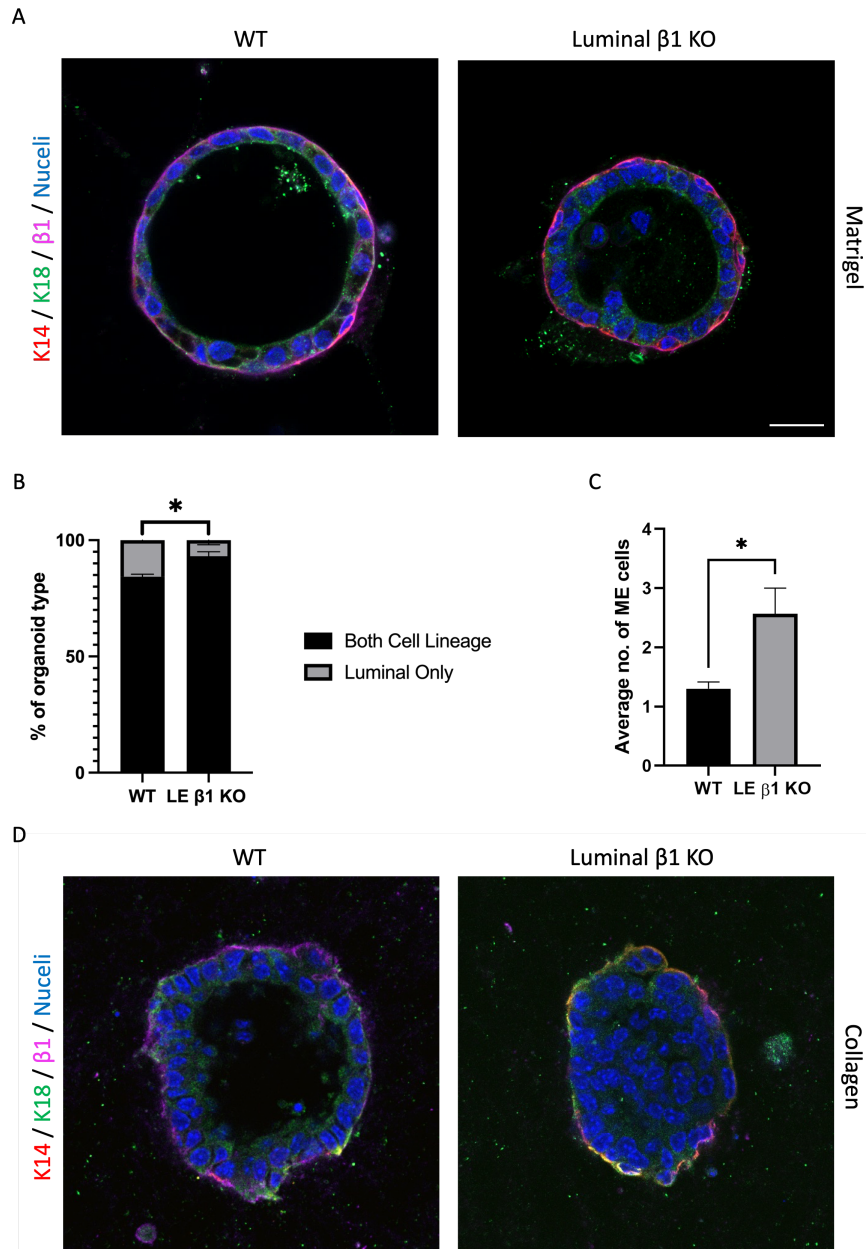


Figure 21: LE $\beta 1$ -integrin^{fx/fx} alveolar organoids form with inner LE and outer ME MEC isolated from pregnant BK8 mice were embedded in laminin-rich BM (Matrigel) or type I collagen and cultured for 5 days +/- 4-OHT. Representative confocal images of organoids with inner luminal and outer ME in **(A)** Matrigel and **(D)** collagen. K14 (red) and K18 (green) and $\beta 1$ -integrin (magenta). Bar: 20 μ m. **(B)** Quantification of WT, ME $\beta 1$ KO organoid with both LE and ME cell, N = 3 independent experiments, 25 organoids per condition. Data is shown as mean +/- SEM and statistical significant was determined by a one way ANOVA where * P < 0.05. **(C)** Quantification of the number of ME cells (nuclei surrounded by K14/SMA staining) in WT and ME $\beta 1$ KO organoid using mid-section images, N = 3 independent experiments, 9 organoids per condition. Data is shown as mean +/- SEM and statistical significant was determined by a Students T-test where * P < 0.05.

4.2.5 MECs re-plated in Matrigel organise into inner LE and outer ME.

To test whether inner LE and outer ME positioning in the organoid cultures was due to pre-assembled mammary structures at the time of plating, MECs were cultured on plastic for three days to produce a monolayer culture, removing pre-assembled clusters (Figure 22). Monolayered cells were detached and replated in Matrigel for five days to form organoids and subsequently assessed for bilayer formation.

When cultured on plastic plates the MEC structures formed a 2D monolayer and displayed a classic cobblestone morphology (Figure 23A). Following dissociation, MEC clusters varied in size from three to thirty cells, some of which had both luminal and ME cells or just contained luminal cells (Figure 23B, C).

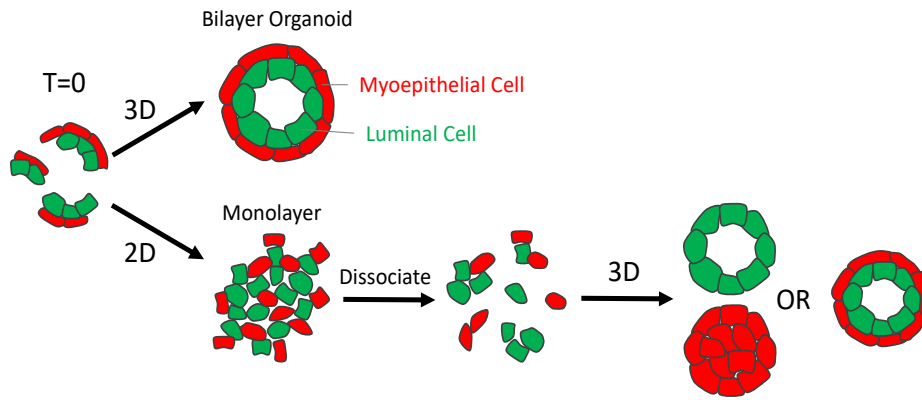


Figure 22: Diagram explaining the rationale of the 2D to 3D experiment. $T=0$ depicts MEC clusters isolated from murine mammary tissue.

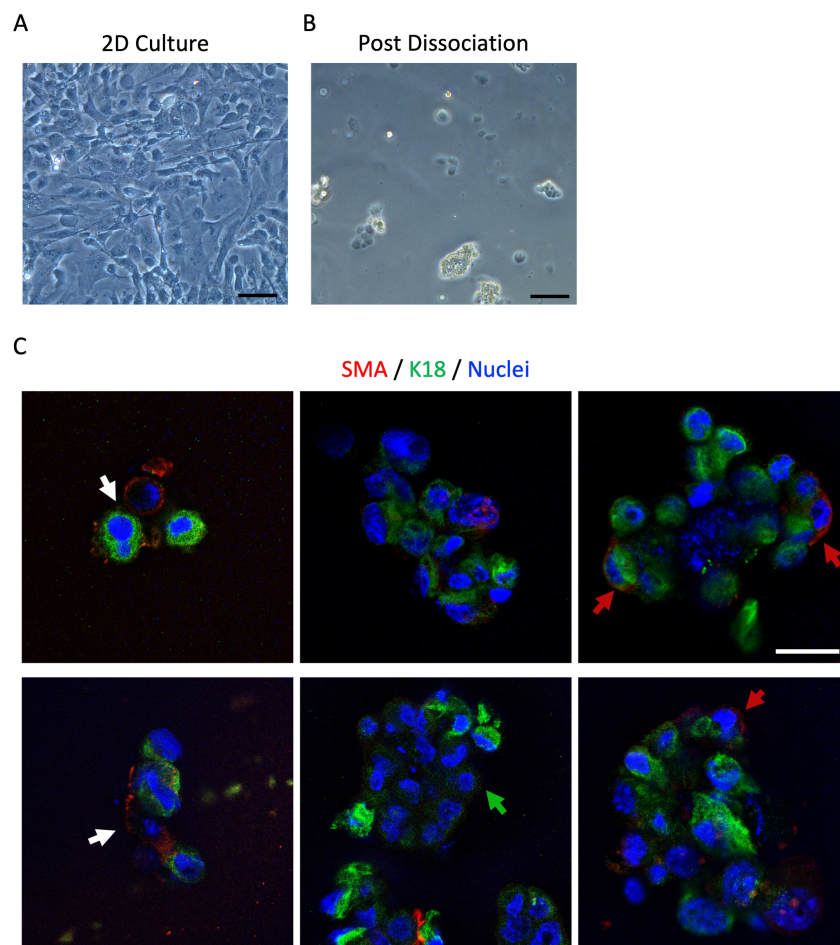


Figure 23: Dissociating 2D culture removes pre-assembled mammary structures. Representative brightfield images of (A) MEC grown in a monolayer for 3 days prior to (B) replating in Matrigel. Bar: $10\mu\text{m}$. (C) Representative confocal images of MECs replated in Matrigel and fixed after the Matrigel had solidified (~ 40 mins). SMA (red), K18 (green). Green arrow indicates luminal only clusters. Red arrows show ME cells on the edge of the cell cluster. White arrow indicates clusters with both cell types randomly organised. Bar: $20\mu\text{m}$.

Following re-plating in Matrigel, the MECs from pregnant BK14 mice still formed organoids (Figure 24A). Immunofluorescence staining showed that WT and β 1-integrin KO cultures formed two distinct types of organoids: luminal cell organoids, and mixed organoids containing both cell type (Figure 24A). There was no statistical difference in the percentage of each organoid type between the WT and β 1-integrin KO cultures (Figure 24B). In addition to cross sectional images, z-stacks were used to assess if the two cell lineages in the mixed type organoids had correctly spatially organised to form inner LE and outer ME. Figure 24C shows representative 3D renderings of WT and β 1-integrin KO ME organoid from z-stacks. Analysis revealed ME cells positioned next to the ECM regardless of β 1-integrin expression in ME cells (Figure 24C-D).

Similarly, MECs from pregnant BK8 mice formed organoids when replated in Matrigel from 2D culture (Figure 25A). Less than 15% of the β 1-integrin KO organoids had lumen formation, which is significantly lower than the WT (Figure 25B). Like the K14 mice replating experiment only two types of organoids were found: luminal only or mixed type organoids (Figure 25C). Analysis of cross-sectional images and z-stacks showed that ME cells in mixed type organoids still positioned next to the ECM (Figure 25D-E).

This suggests that deletion of β 1-integrin in ME cells alone is insufficient to disrupt spatial organisation as other laminin binding receptors such as β 4-integrin or dystroglycan could be engaging with either exogenous laminin in Matrigel or endogenous laminin deposited by WT luminal cells and subsequently aiding organisation of the mammary tissue.

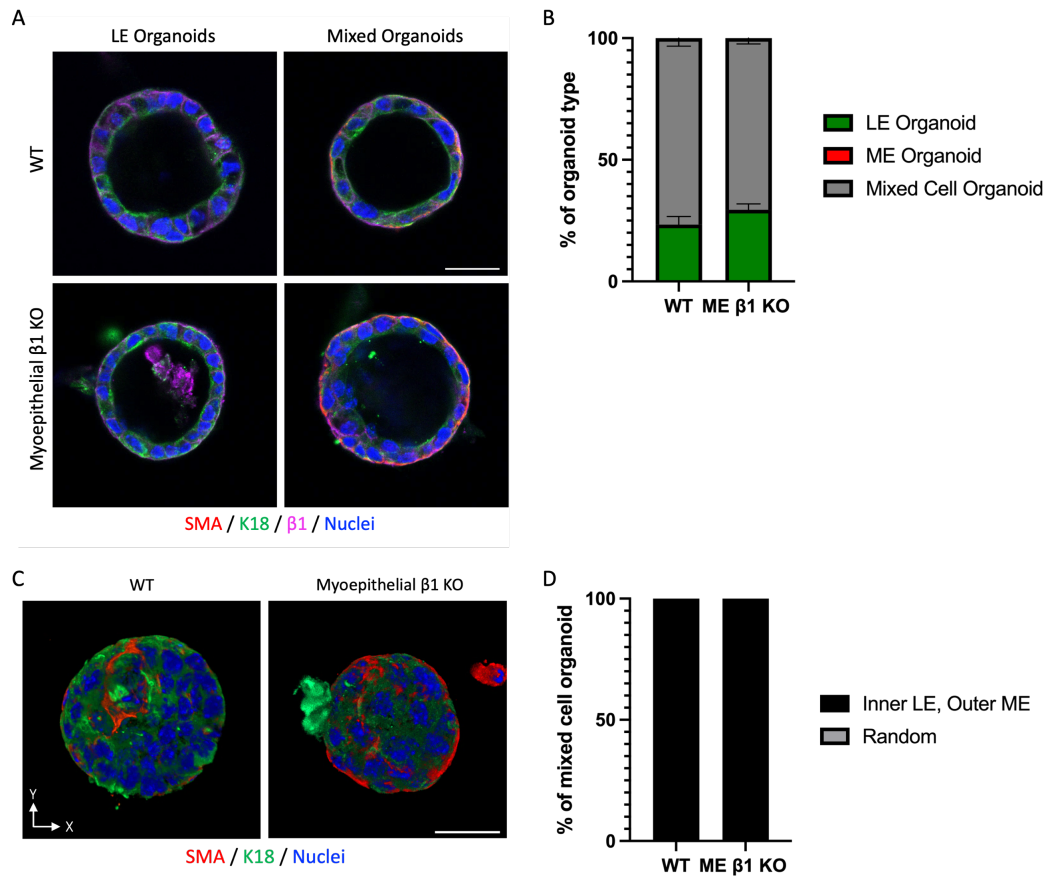


Figure 24: MEC sorting is not disrupted in ME $\beta 1$ -integrin^{fx/fx} alveolar organoids. (A) Representative confocal images of pregnant BK14 MEC cultured in 2D and replated in Matrigel stained with SMA (red), K18 (green) and B1 (magenta). (B) Quantification of mixed, myoepithelial, and luminal epithelial organoids in WT, ME $\beta 1$ KO conditions. N = 3 independent experiments, 25 organoids per condition. (C) 3D rendering of WT and ME $\beta 1$ KO condition mixed cell type organoids stained for SMA (red) and K18 (green). Bar: 25 μ m (D) Quantification of the number of mixed type organoid with inner LE and outer ME structure or random organisation. N = 3 independent experiments, 25 organoids per condition. All data are shown as mean +/- SEM and statistical significant was determined by a one way ANOVA.

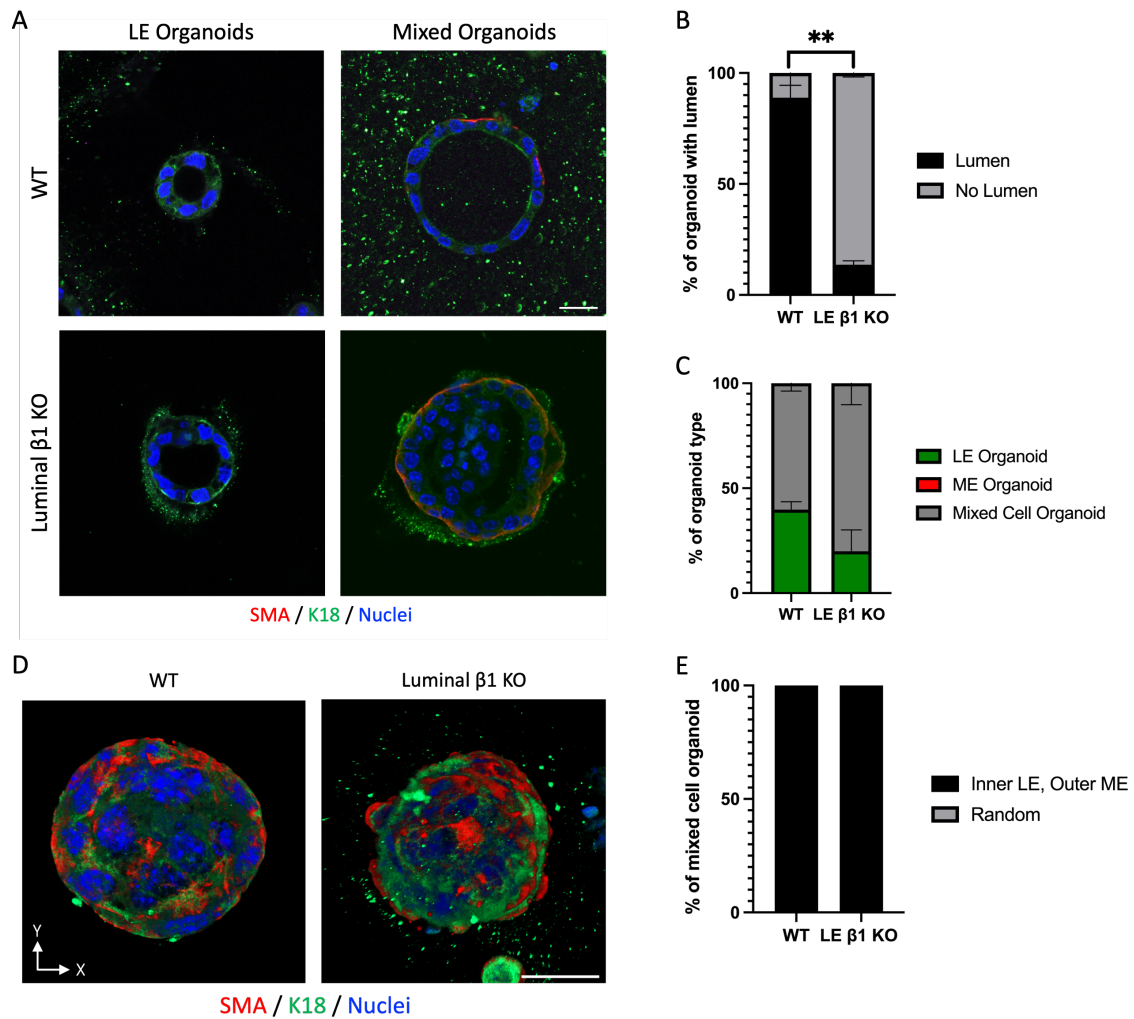


Figure 25: MEC sorting is not disrupted in LE $\beta 1$ -integrin^{f/fx} alveolar organoids. (A) Representative confocal images of pregnant BK8 MEC cultured in 2D and replated in Matrigel stained with SMA (red), K18 (green). Bar: 20 μ m (B) Quantification of WT, LE $\beta 1$ KO organoid with lumens when plated on top of Matrigel, N = 3 independent experiments, 50 organoids per condition. (C) Quantification of mixed, myoepithelial, and luminal epithelial organoids in WT, ME $\beta 1$ KO conditions. N = 3 independent experiments, 25 organoids per condition. (D) 3D renderings of WT and ME $\beta 1$ KO condition mixed cell type organoids stained for SMA (red) and K18 (green). Bar: 20 μ m (E) Quantification of the number of mixed type organoid with inner LE and outer ME structure or random organisation. N = 3 independent experiments, 25 organoids per condition. All data are shown as mean +/- SEM and statistical significant was determined by a one way ANOVA where ** P < 0.01.

4.2.6 ME cells position closer to the new cell-ECM interface.

In a complementary strategy to the 3D organoid experiments, 2D cultures were used to perform overlay experiments with ECM to test our hypothesis. The overlay assay was first developed in 1995 to study mammary differentiation in which cells were seeded in 2D and then treated with soluble ECM proteins (Streuli et al., 1995). The assay has since been used to experimentally manipulate the apical membrane by creating a new cell-ECM interface through the addition of ECM proteins to the media (Akhtar et al., 2013). Thus, this approach will allow us to test our hypothesis and help determine if ME cell positioning is driven by affinity to the matrix or repulsion at the apical membrane.

MEC cells were cultured on plastic for three days to form a polarised monolayer culture with ZO1 at the apical junctions (Figure 26A). 3D renderings of z-stacks and depth-coded confocal images of SMA showed that ME cells preferentially adhered to the endogenous ECM even in the absence of β 1-integrin (Figure 26B-C).

The cells were then overlaid with Matrigel diluted in media to create a new cell-ECM interface. Creation of new cell-ECM interface disrupted the apical membrane tight junctions in WT and ME β 1 KO cultures (Figure 26A). In the presence of a new ECM cue more ME cells were found closer to this interface (Figure 26B-C). There were significantly fewer ME cells on the bottom next to the endogenous ECM (Figure 26D).

When β 1-integrin, the main ECM binding receptor, was deleted in ME cells there was a significant decrease in the number of ME cells positioned next to the new ECM interface compared to WT ME cells (Figure 26D). Suggesting β 1-integrin-ECM interaction drives ME cell positioning towards the new ECM cue.

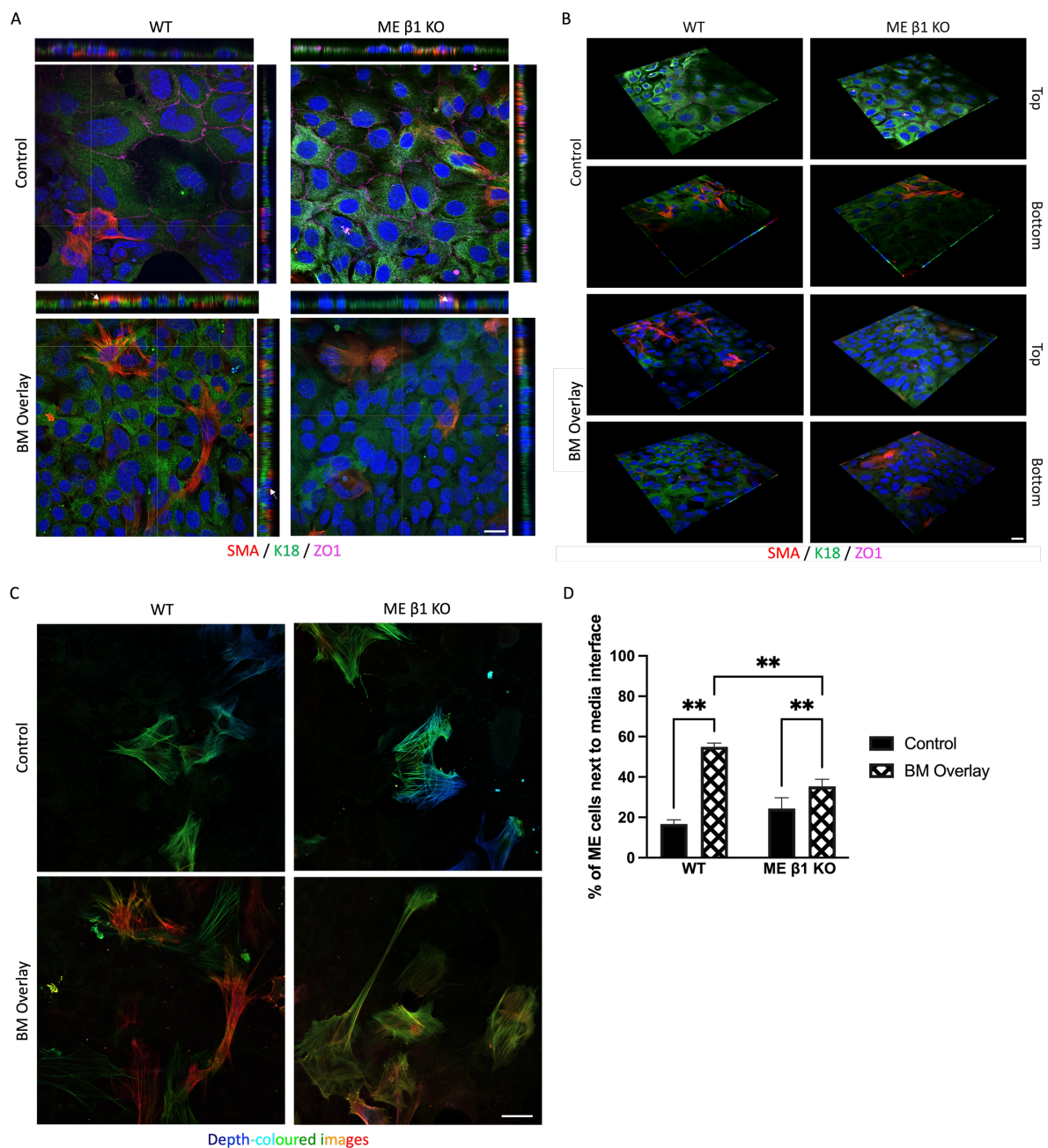


Figure 26: ME cells position next to a new ECM interface. (A) Representative confocal images of MECs overlaid with ECM matrix for 48 hours to create a new cell-ECM interface. xz and yz cross-sections of images are shown for visualisation of relative MEC positioning. MECs were stained with SMA (red) and K18 (green) and ZO1 (magenta). Bar: 20 μ m. (B) Representative 3D renderings of z-stacks showing the top and bottom view. SMA (red) and K18 (green) and ZO1 (magenta). Bar: 20 μ m. (C) Depth-coloured images of ME z-stack. Monochromatic z-slices from figure A of ME cells were coloured with a rainbow array and the images were stacked. The rainbow colours represent smooth muscle actin filaments at different depths; apical = red, middle = green, basal = blue. (Lee et al., 2022). (D) Histogram represents mean values of N = 3 independent experiments. Data is shown as mean +/- SEM and statistical significant was determined by a one way ANOVA where **p < 0.01.

4.2.7 The presence of an apical membrane overrides ME cell affinity to the ECM.

To test whether repulsion at the apical membrane drives ME cell positioning towards the ECM, I overlaid LE $\beta 1$ KO 2D cell culture with Matrigel, as previously in the lab we have shown that when you overlay with BM and delete $\beta 1$ -integrin in both cell lineages the apical membrane is not lost (Akhtar and Streuli, 2013). Here I see the same thing when overlaid with ECM and $\beta 1$ -integrin is deleted in LE cells the apical membrane was not disrupted (Figure 27A). Although there is a greater percentage of ME cells next to the new ECM interface even in the presence of an apical membrane, it is significantly less than the WT (Figure 27B-D). This suggests that repulsion at the apical membrane could be overriding the cues from the ECM when determining cell positioning of ME cells.

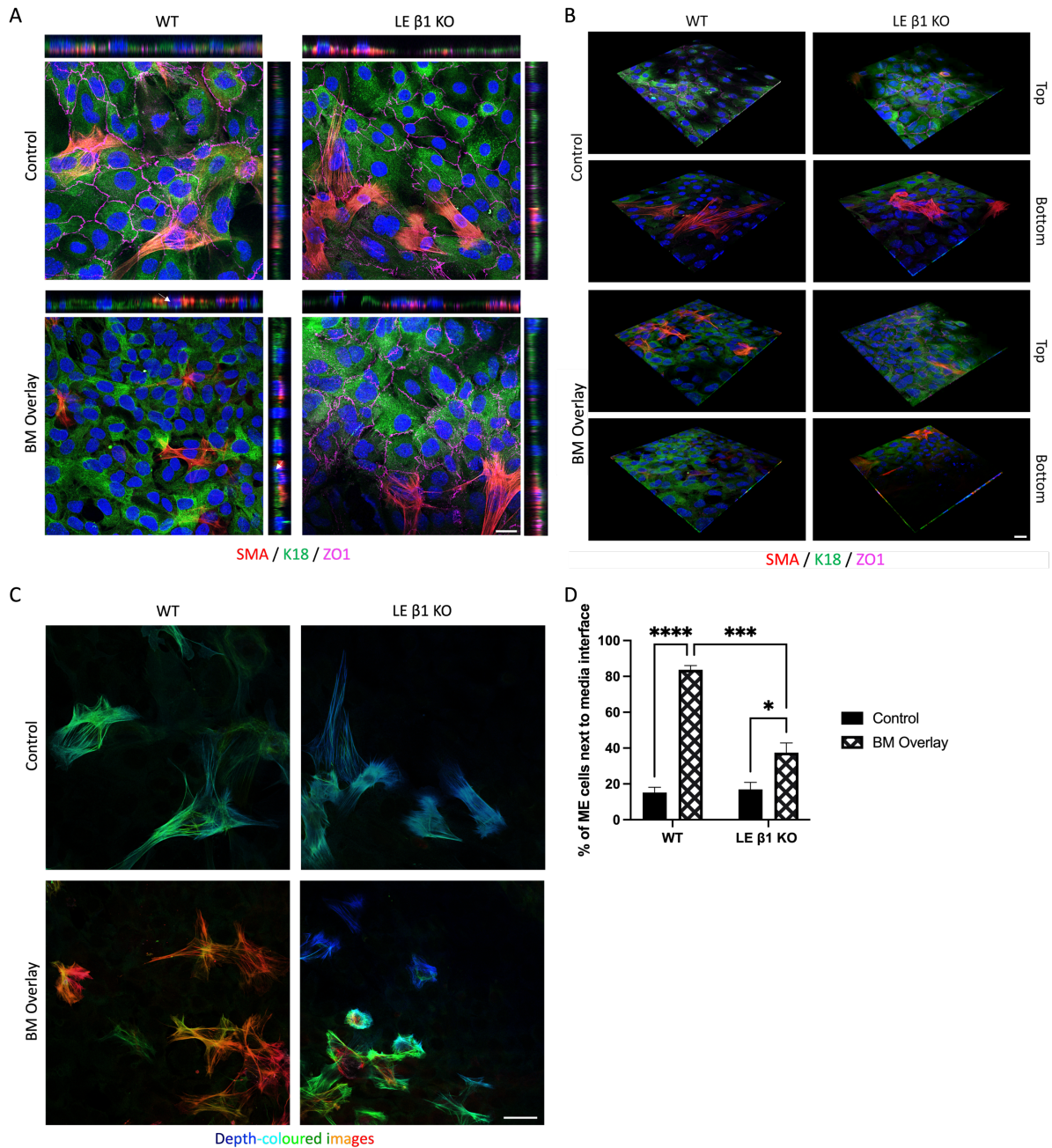


Figure 27: In the presence of an apical membrane fewer ME cells are positioned next to the new ECM interface. (A) Representative confocal images of MECs overlaid with ECM matrix for 48 hours to create a new cell-ECM interface. xz and yz cross-sections of images are shown for visualisation of relative MEC positioning. MECs were stained with SMA (red) and K18 (green) and ZO1 (magenta). Bar: 20 μ m. (B) Representative 3D renderings of z-stacks showing the top and bottom view. SMA (red) and K18 (green) and ZO1 (magenta). Bar: 20 μ m. (C) Depth-coloured images of ME z-stack. Monochromatic z-slices from figure A of ME cells were coloured with a rainbow array and the images were stacked. The rainbow colours represent smooth muscle actin filaments at different depths; apical = red, middle = green, basal = blue. (D) Histogram represents mean values of N = 3 independent experiments. Data is shown as mean +/- SEM and statistical significant was determined by a one way ANOVA where * $p < 0.05$; *** $p < 0.001$; **** $p < 0.0001$.

4.2.8 MEC plated on top of a confluent epithelial layer move towards the ECM.

We speculate that components secreted at the apical surface of the mammary epithelium form a matrix that provides a constraining or electrostatic repulsive force driving ME cells towards the ECM. To further investigate why ME cells fail to position next to the new cell-ECM interface in the presence of an apical membrane, I tested if primary MEC attach to a polarised epithelial layer when plated on top. Eph4 cells were cultured for 4 days to form a confluent monolayer, red cell tracker dye was then added to mark Eph4 cells. MECs cultured in 2D were trypsinised and dissociated. The MECs were marked with green cell tracker dye before adding to the Eph4 culture media. The cells were cultured for 24 hours before fixing and staining with ZO1.

MEC in suspension, when added to a confluent Eph4 monolayer, adhered to the apical membrane, and started forming protrusions (Figure 28A). MEC position was determined by looking at the body of the MEC in relation to the body of the Eph4 cells. Quantification showed only a small percentage of MECs remained on top of the Eph4 cells whilst the majority of MECs integrated or moved below the Eph4 cells (Figure 28C). These findings suggest that although MECs can adhere to an apical membrane, they actively migrate away from this interface closer to the endogenous ECM deposited by the Eph4 cells.

To confirm the role of apical repulsion in driving spatial organisation, I disrupted the apical membrane of the Eph4 monolayer and then plated MECs on top. Low Ca²⁺ media was added 24 hours prior to the addition of MECs to disrupt the tight junctions. Compared to the control sample fewer number of MECs were attached to the Eph4 cells despite disrupting the apical membrane (Figure 28B). This could be in part because calcium is required for cell-cell and cell-ECM adhesion and the lack thereof in the media could be inhibiting MEC from adhering to the Eph4 cells and or the ECM. Despite disruption to the apical membrane, MECs still moved away from the top surface towards the bottom (Figure 28D). This suggests that components secreted at the apical surface rather than the surface itself could be driving cell positioning. Moreover, these results show that cell migration is involved in positioning MECs closer to the ECM.

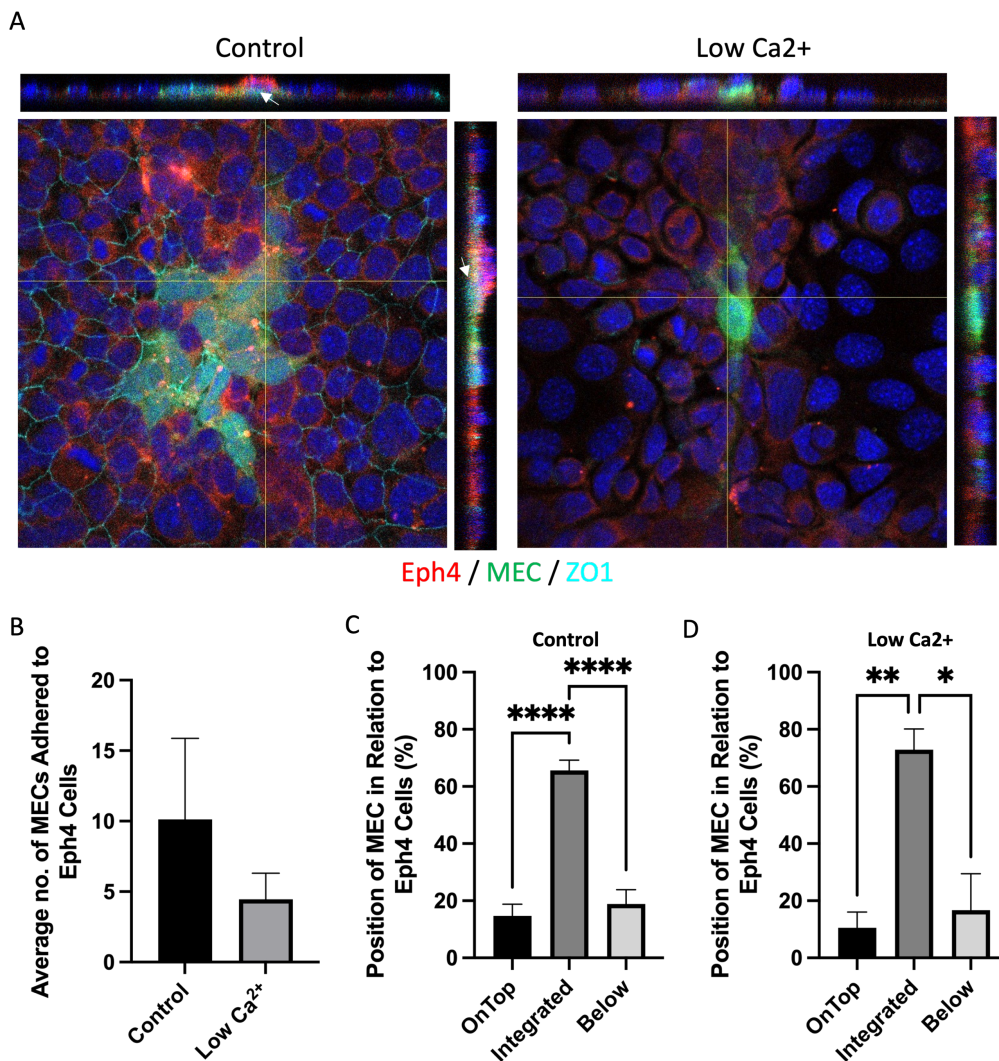


Figure 28: MEC added to a confluent Eph4 2D culture adhere and integrate. (A) Representative confocal images of Eph4 cells with MECs added to the culture media for 24 hr. xz and yz cross-sections of images are shown for visualisation of MEC positioning relative to Eph4 cells. Coverslips were stained with ZO1 (cyan). White arrow shows MEC on bottom. **(B)** Histogram represents the average number of MECs adhered to Eph4 cells. Data is shown as mean +/- SEM and statistical significant was determined by a Students T-test. **(C)** Histogram represents the position of MECs in relation to the Eph4 cells in normal media. N = 5 independent experiments. Data is shown as mean +/- SEM and statistical significant was determined by a one way ANOVA where **** $p < 0.0001$. **(D)** Histogram represents the position of MECs in relation to the Eph4 cells in low Ca²⁺ media. N = 3 independent experiments. Data is shown as mean +/- SEM and statistical significant was determined by a one way ANOVA where * $p < 0.05$; ** $p < 0.01$;

4.2.9 ME cells reposition next to the new cell-ECM interface even in the absence of oriented cell division.

To determine if oriented cell division is also involved in spatial organisation, I inhibited cell division using aphidicolin, which blocks the cell cycle at early S phase.

To confirm inhibition of cell proliferation I did an EdU assay to measure cell division in the presence and absence of aphidicolin. When overlaid with Matrigel cell proliferation was significantly increased compared to the control and samples treated with aphidicolin had no EdU positive cells confirming inhibition of proliferation (Figure 29A-B).

As seen before in the presence of a Matrigel overlay, a significant number of ME cells were positioned next to this new interface compared to the control, where majority of the ME cells were on the bottom (Figure 29C-D). Even in the absence of proliferation a significant number of ME cells were positioned next to the new interface (Figure 29C-D). However, this was significantly lower than just the overlay. This suggests that both cell migration and oriented cell division might play a role in driving ME cell positioning. It would be interesting to determine if ME cells divide perpendicular to the ECM, or they migrate towards the ECM cue and then divide planar, or if it is a combination of both.

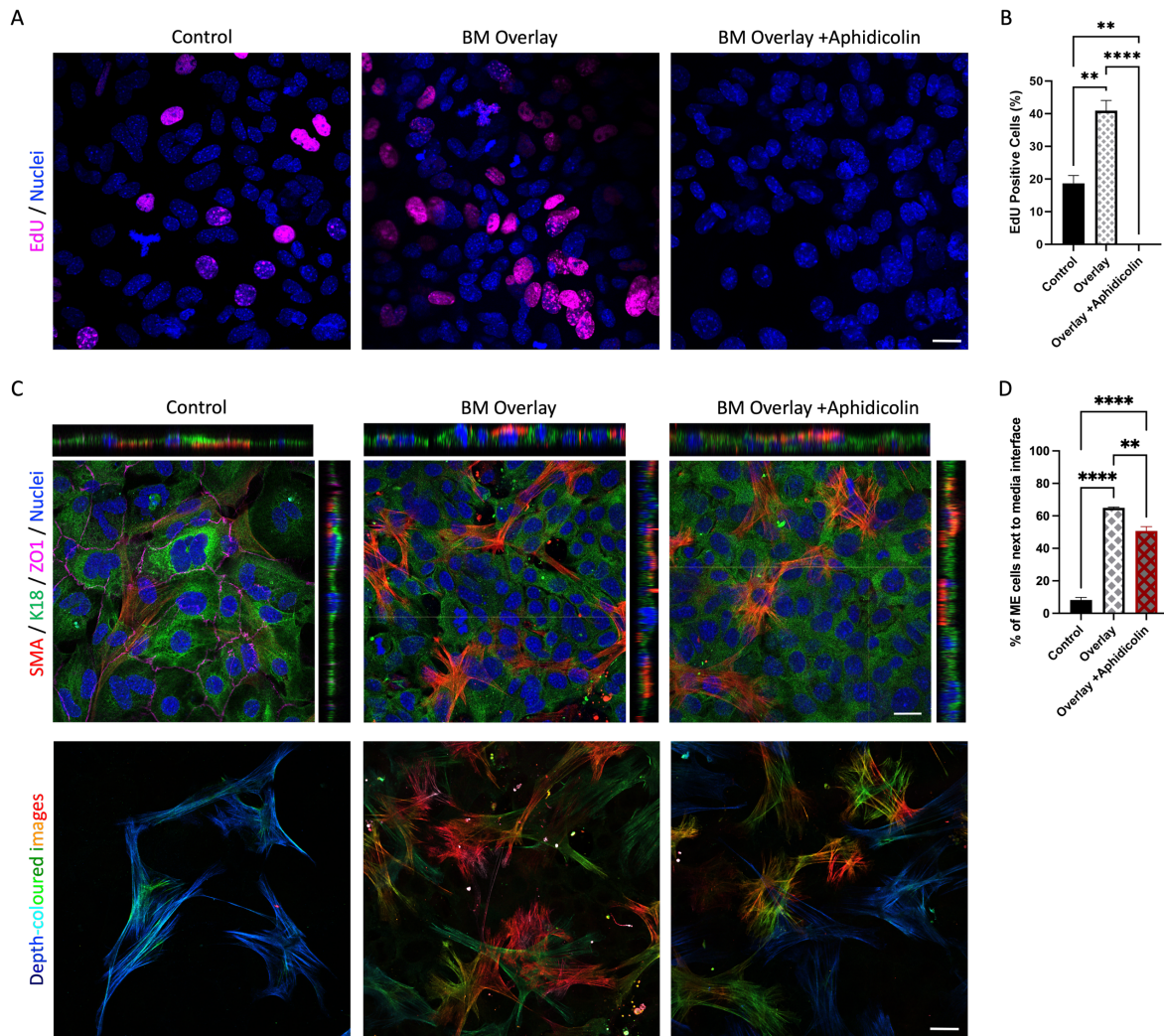


Figure 29: Inhibition of cell proliferation reduces the number of ME cell positioned next to the new ECM interface. (A) Representative confocal images of EdU assay of MECs overlaid with Matrigel in the presence and absence of aphidicolin. EdU (magenta). Control refers to samples without BM or aphidicolin in the media. Bar: 20 μ m. (B) Histogram represents the percentage of EdU positive cell. N = 3 coverslips, 8 fields of view per coverslip. (C) Representative confocal images of MECs were overlaid with ECM matrix for 48 hours to create a new cell-ECM interface. xz and yz cross-sections of images are shown for visualisation of relative MEC positioning. MECs were stained with SMA (red) and K18 (green) and ZO1 (apical tight junction marker) (magenta). Depth-coloured images of ME z-stack. Monochromatic z-slices from figure A of ME cells were coloured with a rainbow array and the images were stacked. The rainbow colours represent smooth muscle actin filaments at different depths; apical = red, middle = green, basal = blue. Bar: 20 μ m. (D) Histogram represents mean values of N = 3 independent experiments. All data are shown as mean +/- SEM and statistical significant was determined by a one way ANOVA where ** $p < 0.01$; **** $p < 0.0001$.

4.2.10 Inhibition of cell proliferation does not affect spatial organisation of MECs in 3D culture.

To investigate the interplay of cell movement and proliferation on spatial organisation of MECs in 3D culture, cell proliferation was inhibited to test whether ME cell positioning is from proliferating stem cells or cell rearrangement. Preassembled structures were removed by culturing cells in 2D for 3 days and then replated in Matrigel.

Inhibition of proliferation at the time of plating arrested organoids as small cysts (Figure 30A). Control organoids were significantly larger than aphidicolin treated organoids (Figure 30B). Organoids inhibited with cell proliferation still spatially organised as inner LE and outer ME even in the absence of β 1-integrin in ME cells (Figure 30C-D). This data suggests that MEC cells can spatially organise through cell movement in the absence of oriented cell division.

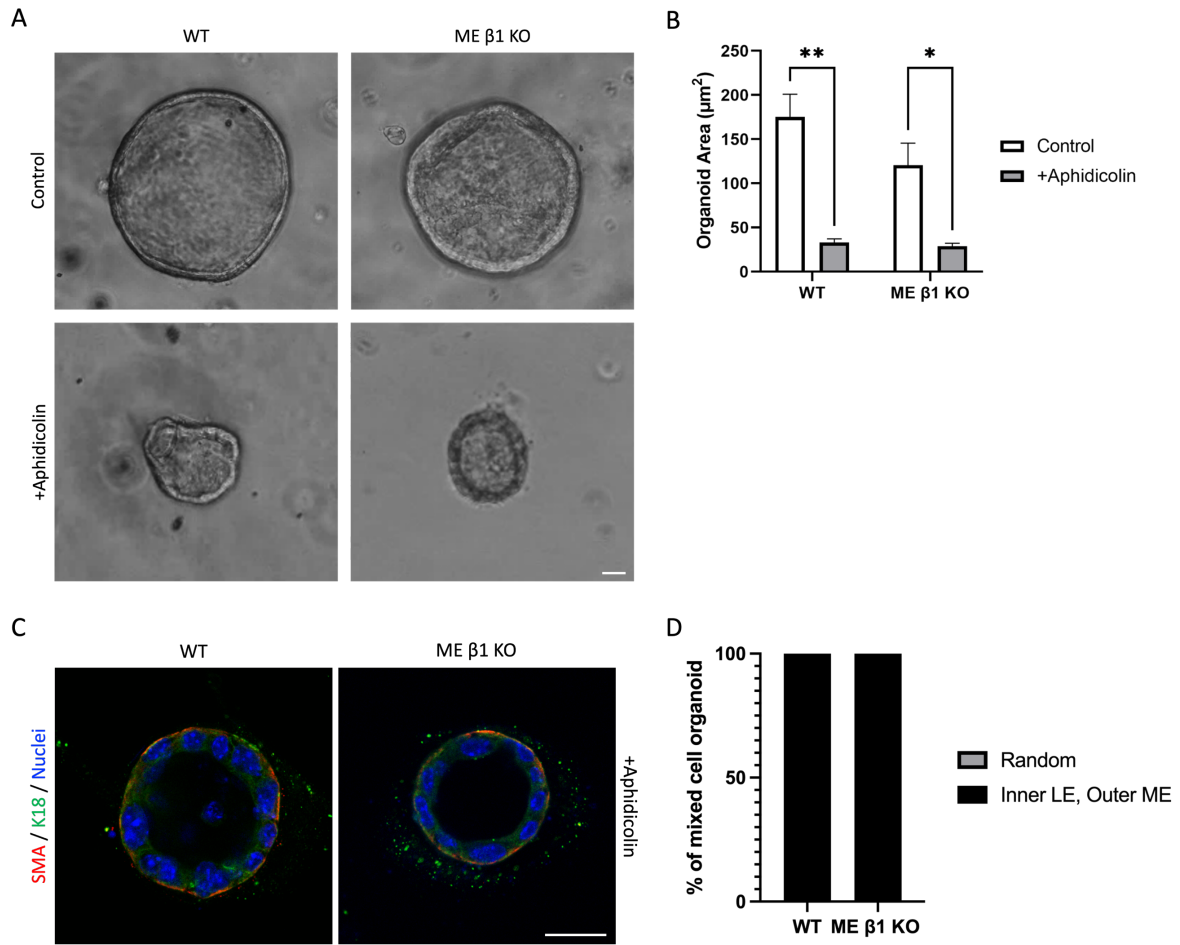


Figure 30: Inhibition of cell proliferation does not affect MEC sorting in 3D culture. (A) Representative brightfield images of organoids replated in Matrigel +/- aphidicolin. Bar: 20 μm . (B) Graph shows the average size of organoids from N = 3 independent experiments, minimum 8 organoids per condition. (C) Representative confocal images of MECs replated in Matrigel +/- aphidicolin, stained with SMA (red) and K18 (green). Bar: 20 μm . (D) Graph shows the percentage of organoids with inner LE and outer ME positioning versus random cell positioning from N = 3 independent experiments, 10 organoids per condition. Data is shown as mean +/- SEM and statistical significant was determined by a one way ANOVA where ** P<0.01, *** P<0.001.

4.3 Discussion

During embryonic development of the mammary gland, progenitor cells of the basal and luminal compartment are initially specified in partially overlapping domains, eventually these cells segregate into separate compartments to form inner luminal and outer myoepithelial in contact with the stroma (Wuidart et al., 2018). It is probable repositioning of progenitor cells through sorting feeds back to regulate cell fate transition and lineage segregation, as seen during blastocyst formation in mice (Rossant et al., 2003). This configuration is then fine-tuned and maintained during subsequent stages of development such as puberty through oriented cell division and cell migration (Neuman et al., 2018, Taddei et al., 2008). I hypothesised affinity to the ECM or repulsion at the apical membrane drives cell sorting in the mammary gland.

In this chapter, I have shown deletion of β 1-integrin in any cell lineage alone in ductal organoids was insufficient to disrupt a proper bilayer formation of inner LE and outer ME cells. MECs ability to position correctly even in the absence of β 1-integrin could be in part due desmosome adhesions between LE and ME cells in the ducts. Unpublished data from our lab group shows the absence of desmosomes between LE and ME cells in the alveoli. Therefore, MECs from pregnant mice were used, as the tissue contains lots of alveoli in preparation for lactation. Interestingly, both WT and β 1-integrin KO alveoli organoids retained the correct cell-type specific positioning even in the absence of desmosomes. These results contrast with that of Runswick et al., (2001), who showed positional sorting of reconstituted primary human MEC is disrupted when treated with desmosome cell adhesion recognition sites blocking peptides. Therefore, MEC clusters present at the time of plating in our study could have been sufficient to retain MEC positioning.

To remove pre-assembled mammary tissue structures, I did a re-plating assay. Pregnant MECs were cultured in 2D and then dissociated to remove pre-assembled structures before plating in a 3D matrix. Under these conditions, a small proportion of luminal only organoids and a significantly larger proportion of mixed type organoids, which all had inner LE and outer ME cell positioning formed. This suggests that cell sorting is not dependent on cell-cell adhesion modulated via desmosomes. Moreover, studies in the intestine have shown that epithelium structure is not altered in the absence of desmoplakin (Sumigraay and Lechler, 2012). Similarly,

other studies demonstrated reconstituted ductal populations of isolated primary human MECs, self-organise to form the correct tissue structure even in the absence of cell-cell adhesion (Carter et al., 2017, Cerchiari et al., 2014).

To better study cell-ECM affinity and repulsion at the apical membrane, I created a new ECM interface by overlaying cells in 2D culture with Matrigel which subsequently disrupted the apical membrane. In the presence of a laminin-rich interface, WT ME cells were found closer to this new surface in concomitant with β 1-integrin repositioning and apical membrane disruption. Interestingly, ME cell repositioning failed in response to a new ECM cue when the apical membrane was intact. Taken together these data suggest that affinity to the matrix is overridden by apical membrane repulsion when driving ME cell positioning. Moreover, studies have revealed apically secreted molecules such as the ZP-domain protein Dumpy and Piopio control cell rearrangement and intercalation in the *Drosophila* trachea and limb bud (Diaz-de-la-Loza et al., 2018, Ray et al., 2015, Jazwinska et al., 2003).

To further test if ME cell position is driven by repulsion at the apical membrane, MECs were plated on top of a confluent Eph4 cell monolayer, originally derived from mouse mammary glands, that exhibits apical-basal polarity in 2D cultures (Yonemura, 2014). Like the recent findings of Pfannenstein and Macara (2023), I show that MECs adhere to a confluent Eph4 cell monolayer and intercalate via protrusions inserted between the Eph4 cells. MECs actively migrated away from the apical membrane towards the basal side, supporting both our hypotheses, repulsion at the apical membrane and differential affinity to the ECM drives MEC positioning. Interestingly, MECs still moved away from this media interface even when the apical membrane was perturbed, suggesting that components secreted apically might be exerting a repulsive force rather than the apical membrane itself. It would be interesting to decipher the composition of the apical matrix in the mammary gland and identify if components known to drive cell rearrangement in other organisms and tissue, such as ZP domain proteins and glycoproteins, are present in the mammary gland. Alternatively, the absence of tight junctions between cells, could be allowing MEC to migrate more freely towards the ECM. Given a ME cell marker was not used, the proportion of ME cells that migrated to the bottom versus the number that were integrated with the Eph4 cells cannot be determined. Use of fluorescence-activated cell sorting (FACS) to get a pure population of

only ME cells to plate on top of an apical membrane will help answer this question (Smalley et al., 2012).

Although data from the repulsion hypothesis experiments suggest MECs use cell movement to migrate towards ECM cues away from apical repulsion, I wanted to examine if oriented cell division of stem cells is important for ME cell positioning. To test this, cell proliferation was inhibited using aphidicolin in the overlay assay. Under these conditions, ME cells still repositioned closer to the new ECM interface, but significantly fewer ME cells were on top compared to the untreated overlay samples, suggesting fewer ME cells were positioned next to the new ECM interface due to the lack of orthogonal oriented cell division. Previously, Huebner et al., (2016) suggested a model for ductal elongation in which proliferation is used as a mechanism to generate migratory cells with high phosphorylated ERK1/2. Therefore, inhibiting proliferation in the overlay assay could have limited the further generation of motile cells capable of migrating towards the new ECM cue. Given, bilayer organoids with inner LE and outer ME were observed despite inhibition of cell proliferation in our replating experiment the latter is more likely. However, studies in which cell division misorientation can be induced, through knockdown of Annexin A1 using small-hairpin RNA, rather than inhibiting cell proliferation completely will help provide a better understanding of the role of oriented cell division in the spatial organisation of the mammary gland (Frankhenal et al., 2023).

Overall, our results suggest that KO of β 1-integrin in ME or LE cell alone is insufficient to disrupt MEC positioning. It is possible other laminin binding receptors such as β 4-integrin or dystroglycan could be involved in driving spatial organisation. The α 6 β 4 preferentially binds to LM-332, however it also interacts with the LMs-511 and 521 (Nishiuchi et al., 2006). Early studies showed β 4-integrin expression is restricted to ME cells *in vitro* (Runswick et al., 2001). However, more recently β 4-integrin expression was shown to be present luminal cells (Akhtar et al., 2013). In agreement with studies by Akhtar and colleagues, I have shown β 4-integrin is expressed in both cell types. Therefore, β 4-integrin mediated signalling could also be involved in MEC positioning in the mammary gland. In other tissues such as the lungs and kidney, β 4-integrin has been implicated in the maintenance of normal tissue architecture (Chi et al., 2022, Viquez et al., 2017). Thus, in the following chapter, I test the role of β 4-integrin in MEC sorting using computational modelling.

In this chapter, I have shown both affinity to the matrix and repulsion at the apical membrane drive ME cell positioning. However, the hierarchy of these two in spatial sorting of MECs needs to be established.

5 Development of an in-silico model to study cell sorting in the mammary gland.

5.1 Introduction

Computational models offer a complementary tool to *in vivo* and *in vitro* experiments and several in-depth reviews have been written on the merits of computational modelling in biology (Montes-Olivas et al., 2019, Sharpe, 2017, Brodland, 2015). In the case of developmental biology, the dynamic complexity of morphological events, arising from interactions from the molecular to the tissue scale, means that computational modelling is increasingly required to help interpret experimental observations and test sufficiency of hypothesised mechanisms.

Computational models can incorporate stochasticity in processes such as cell proliferation, thereby helping us to build up an understanding of the variability observed experimentally in outputs of interest such as tissue size and shape. Furthermore, by increasing the information learned from each experimental observation, computational models can help to reduce the number of animals needed, which is relevant to this thesis as primary cell cultures often require the pooling of mammary epithelial cells from multiple animals for each experiment. Computational modelling thus supports the 3Rs (Replacement, Reduction and Refinement), a set of guiding principles for ethical use of animals in research (Russell and Burch, 1960). Moreover, techniques such as confocal microscopy used for immunofluorescence data collection requires a compromise of the resolution, scan time and the number of images taken to avoid photo-bleaching (St Croix et al., 2005). In contrast, *in silico* observations and data collection from computational models can be made without interfering or damaging the system.

During morphogenesis, different cell populations can self-organise to form distinct tissue compartments through a process known as cell sorting. Cell sorting has been computationally modelled extensively, with many existing models focusing on Steinberg's "differential adhesion hypothesis" that relates differences in relative motion of neighbouring cells to differences in the strength of their surface adhesion (Steinberg, 1963). However, these

models typically feature a single, lumped ‘strength of adhesion’ for each type of interaction rather than considering specific adhesion molecules and their levels or dynamics (Barton et al., 2017). A notable exception to this simplification is the recent work by Tordoff et al., (2021), which presents a model for sorting of a cell population comprising human embryonic kidney (HEK) and Chinese ovary hamster (CHO) cells and compared it to experimental data. The authors find that the degree of cell sorting can be controlled by the relative and absolute numbers of cells of each type present in the population. At high HEK:CHO ratios, simulated cell aggregates self-organised into HEK spheroids engulfed by CHO cells, whilst intermediate HEK:CHO ratios led to more variable patterning. Despite capturing these two design rules, this model fails to include key cellular processes such as cell proliferation, which is evident experimentally and likely to affect the self-organisation process (Huebner et al., 2016).

In the mammary gland, cell-cell adhesion molecules are expressed in a cell type specific manner; E-cadherin is expressed specifically in luminal (LE) cells, whilst P-cadherin is expressed in myoepithelial (ME) cells (Daniel et al., 1995). Inactivation of the E-cadherin gene or homozygous mutation of the P-cadherin gene in mice did not alter the spatial organisation of mammary epithelial cells (MECs), suggesting that cell-cell adhesion is not necessary for correct sorting of LE and ME cells, and raising the question of a possible role for cell-ECM adhesion instead (Radice et al., 1997, Boussadia et al., 2002). To date, Cerchiari et al. (2015) provide the only computational model of mammary gland cell sorting that incorporates differences in cell-ECM adhesion strength between ME and LE cells. They demonstrated that tissue cohesion of the mammary gland is achieved even in the absence of cell-cell adhesion by ME cells appreciably binding to the ECM. However, their model has several limitations, including the use of an overly simplistic description of cell mechanics and the lack of key processes such as proliferation.

In this chapter I implement a cell-based computational modelling framework to study how MEC lineages form a concentric bilayer structure with inner luminal epithelial (LE) and outer myoepithelial (ME) cells. I start by summarising the various cell-based computational modelling approaches that have been used to model self-organisation of multicellular tissues.

5.1.1 Cell-based modelling methods

Unlike continuum models in which tissue dynamics are derived from locally averaged quantities, cell-based models allow for the incorporation of individual cell properties. This framework provides a more biologically accurate description and allows for a better understanding of the complex - and often highly heterogeneous - processes that occur during tissue morphogenesis.

Cell-based models can be divided conceptually into on- and off-lattice models. Cellular automata (CA) (Figure 31A) and the cellular Potts (CP) model (Figure 31B) are examples of on-lattice models; the spatial arrangement of cells in these models is restricted to a fixed lattice geometry (Bull et al., 2020, Zangooei and Habibi, 2017). In contrast, off-lattice models such as the centre-based model and vertex model (VM) (Figure 31C) allow for cells to move continuously in space, in response to mechanical forces acting upon them (Barton et al., 2017, Macnamara et al., 2020). Voronoi tessellation (VT) (Figure 31D) and overlapping spheres (OS) (Figure 31E) models are examples of centre-based models where neighbouring cells are identified in different geometric ways.

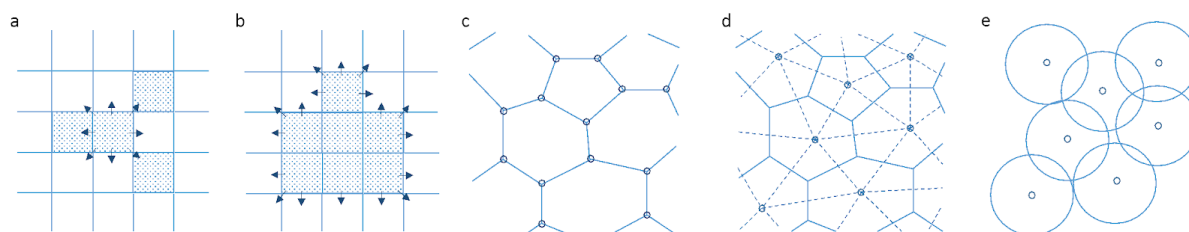


Figure 31: Schematics of different cell-based modelling approaches. (A) Cellular automaton (CA). (B) Cellular Potts (CP) model. (C) Vertex model (VM). (D) Voronoi tessellation (VT) model. (E) Overlapping spheres (OS) model. Figure adapted from Osborne et al., 2017.

OS models offer a good balance between computational simplicity and biophysical realism compared to the other cell-based modelling approaches. For example, in OS models, each cell i is represented as a compressible sphere with an intrinsic radius R_i that may change over time (e.g., due to cell growth); the centre of the sphere is used to track the cell, rather than multiple points in more complex models like VMs. In OS models, two cells, i and j , are defined to be neighbours if their two corresponding spheres overlap. Cell-cell or cell-substrate contacts

result in deformation and displacement of each cell; these force laws are inspired by physical models of colloids and other forms of soft matter (Pathmanathan et al., 2009).

An obvious geometric simplification of OS models is that mammary epithelial cells - and many other cell types - are not spherical, and pack tightly *in vivo* and *in vitro*. LE cells are cuboidal in shape; they line the lumen of ducts and alveoli, whereas ME cells adopt two different cell shapes depending on whether they are ductal or alveolar. Along the long axis of ducts, spindle-shaped ME cells form a continuous layer, whereas in the alveoli, stellate-shaped ME cells form a discontinuous basket-like mesh (Emerman and Vogl, 1986). Ways of mitigating this issue include altering the spherical cell shape to ellipsoidal (Palsson, 2001), using cells of varying radii or using a collection of subcellular elements to represent a single cell (Sandersius and Newman, 2008).

Nonetheless, OS models provide a good starting point for the current study, and their utility as previously been demonstrated in studies of the effects of deregulated proliferation in tumour growth (Galle et al., 2005) and factors required for mammalian blastocyst development (Nissen et al., 2017).

5.1.2 Aims

In the previous results chapters, I have shown that affinity to the matrix and repulsion at the apical membrane drive the spatial organisation of the mammary gland. Experimentally I was only able to test the role of β 1-integrin in LE or ME due to time constraints. Therefore, I could only reach a conclusion regarding the role of β 1-integrin; deletion of this integrin in ME or LE cells alone were insufficient to disrupt the spatial organisation.

To complement and extend these experimental findings, in this chapter I aim to simulate the morphogenesis of mammary tissue and explore the relative contribution of integrin expression and the cellular mechanisms involved. Whilst I have observed experimentally that both cell migration and oriented division could be involved in spatial organisation, I wish to understand the interplay of these two processes and explore the potential role of other mechanisms, such as anoikis, a cell death mechanism induced upon anchorage loss, for maintaining the mammary gland architectural structure.

To that end, in this chapter I present a novel computational model to understand how MECs self-organise to form a bilayer structure in 2D cell culture. I carry out a systematic investigation of the generic properties of the model by simulating selective model knockouts of regulation and control mechanisms to predict what will be seen experimentally. I then build on this model to simulate the formation of 3D organoids to determine the role of different integrin expression between LE and ME cells in driving cell sorting.

5.2 Methods

In this study I use 3D OS models to study spatial organisation of mammary epithelial cells. In the OS models, each cell's centre is represented geometrically by a particle or "node", whose position is tracked over time. For simplicity, in this study I assume that all cells have the same radius.

5.2.1 Initial and boundary conditions

I refer to the collection of nodes as a "mesh". The initial mesh is constructed by specifying the positions of the nodes. I simulate 120 hours of growth in line with our *in vitro* protocol.

Experimentally, the 2D cell cultures are grown in standard Petri dishes coated in a serum-fetuin mix to promote cell adhesion, spreading and growth. Thus, in the simulations I model the bottom of the 2D culture as an impermeable flat surface coated in protein film to permit cell-substrate adhesion. The impermeable flat surface was modelled using a plane boundary condition, which stops nodes moving through the plane $z=0$.

The 3D organoid cultures are grown experimentally in a laminin-rich extracellular matrix, Matrigel and to reflect this in the organoid simulation I model the space surrounding the cells as an extracellular matrix that exerts an adhesion force.

Throughout this study, I non-dimensionalise the models so that the units of space are average cell diameters (CDs), and time is measured in hours. The individual components of the models are described in detail below.

5.2.2 Cell types

The mammary epithelium consists of two differentiated cell types, LE and ME cells that are maintained by lineage-restricted stem cells (Cristea and Polyak 2018). To recapitulate *in vivo* conditions, I allow for up to four distinct cell types in the models: LE, luminal stem cells, ME and basal stem cells. This also allows for a variety of different cell parameters and processes to be cell type-dependent in the models. For example, I can allow for each cell type to express $\beta 1$ and/or $\beta 4$ in each simulation.

I extracted the number of LE and ME cells from the *in vitro* culture and inferred the initial proportion for the models. The initial cell population proportions used in the simulation are: 67% luminal (33.5% LE, 33.5% luminal stem cell) and 33% myoepithelial (16.5% ME, 16.5% basal stem cell).

5.2.3 Mechanical forces

In the models, cells are subject to various mechanical forces that control their motion within the microenvironment. Cells resist compression by other cells (via a cell-cell repulsion force, \mathbf{F}_{ccr}). Cells also form adhesive bonds with adjacent cells (via a cell-cell differential adhesion force, \mathbf{F}_{ccda}) or the ECM (via a cell-ECM force, \mathbf{F}_{cea}). For simplicity, I relate the balance of forces on each cell centre to its velocity \mathbf{v} using Newton's second law, assuming that inertial effects are negligible:

$$m_i \dot{\mathbf{v}}_i = \sum_j (F_{ccda}^{ij} + F_{cea}^{ij}) + F_{ccr}^i \quad (1)$$

where η denotes a viscosity coefficient representing adhesion between the cell and the underlying substrate, and where the sum runs over cells j whose spheres overlap with that of cell i . I implement different cell-ECM adhesion forces to study the influence of differential cell-ECM adhesion in MEC sorting.

5.2.4 Cell-cell repulsion (\mathbf{F}_{ccr})

I assume that cells exhibit mechanical forces on their neighbours due to a combination of cell-cell adhesion and limited compressibility. Here I introduce a cell-cell repulsion force that is

zero when cells are just touching and increases when cells are pressed together. The force experienced by cell i when it overlaps with cell j can be calculated using the Hertz model (Hertz, 1882):

$$F_{ccr}^{ij}(t) = \frac{2x_{ij}^{5/2}}{\frac{3}{4} \left(\frac{1-v_i^2}{E_i} + \frac{1-v_j^2}{E_j} \right) \sqrt{\frac{1}{R_i(t)} + \frac{1}{R_j(t)}} \quad (2)$$

where R_i, R_j are the cell radii and x_{ij} defines the distance between the two cells, and where E_i, E_j and ν_i, ν_j relate to the Young moduli and Poisson ratios of the cells respectively.

5.2.5 Cell-cell adhesion (F_{cca})

I also assume the presence of differential adhesion between luminal and myoepithelial mammary cells. In the models these interactive forces between neighbouring cells are modelled using Hookean linear spring forces. The force experienced by cell i when it overlaps with cell j is given by:

$$F_{ccr}^{ij}(t) = \begin{cases} \mu \hat{r}_{ij}(t) s_{ij}(t) \log \left(1 + \frac{|r_{ij}(t)| - s_{ij}(t)}{s_{ij}(t)} \right), & |r_{ij}(t)| < s_{ij}(t) \\ \mu \hat{r}_{ij}(t) (|r_{ij}(t)| - s_{ij}(t)) \exp \left(-\alpha \frac{|r_{ij}(t)| - s_{ij}(t)}{s_{ij}(t)} \right), & |r_{ij}(t)| \geq s_{ij}(t) \end{cases} \quad (3)$$

Where μ is the stiffness of a given ‘spring’ between two neighbouring cells, known as the “spring constant”, $\hat{r}_{ij}(t)$ is a unit vector pointing from i to j , α is a parameter which defines decay of the attractive force, here set to 5, and $s_{ij}(t)$ is the natural length of the spring connecting cell centre i and j . The $s_{ij}(t)$ is the sum of the radii of the two cells which increases from 0.25 to 0.5 during the first hour of the cell cycle, and thus is a function of time.

5.2.6 Cell-ECM forces (F_{cea})

Cell surface adhesion receptors form heterophilic bonds with specific ECM ligands such as laminins, collagen, and fibronectin. The ECM can be represented as cell-like particles (Cerchiari et al., 2015), as a network of Hookean springs (Zhu and Mogilner, 2016), as a linear elastic medium (Bischofs and Schwarz, 2003) or even as a fibrous matrix (Ahmadzadeh et al.,

2017). However, given many of these approaches are computationally intensive, I modelled cell-ECM force as a simplifying approximation that the ECM exerts an isotropic pressure-like force on cells.

As described and defined in Vittorio and Lowengrub (2010), I assume the strength of the cell-ECM adhesion force is proportional to the expression of $\beta1$ and $\beta4$ integrins by the cell and the ECM density, E . Also, I assume the adhesion force increases as cells get closer to the ECM. Thus, over time I expect cell sorting to occur, to minimise the global interaction energy of the mesh over time, in which ME cells will appreciably interact with the ECM boundary providing a geometric constraint to self-organisation as seen in Cerchiari et al., (2015) model.

I model this adhesion force on cell i by:

$$F_{cea}^i(t) = \alpha_{cea}(t)L_{E,i}E\nabla(d(x_i); R_{cea}^i, n_{cea}) \quad (4)$$

where $L_{B,i}$ is the integrin expression of cell i , d is the distance from cell i to the ECM, and R_{cea}^i is the maximum cell-ECM adhesion interaction distance of cell i , and n_{cea} is the cell-ECM adhesion power. To approximate the cell's limited capacity to deform before breaking all its adhesive bonds I set $R_{cea}^i > r_i$.

5.2.7 Cell division

At birth, the cell cycle time (i.e., age) of cell i is initialised such that $T_i = 0$. The mammary epithelial cells in the models divide according to a stochastic cell cycle model with the duration of the cell cycle drawn from a uniform distribution where the parameter t_{cycle} defines the average cell cycle length, as stated in Table 1. These values were obtained from murine mammary epithelial cells in the adult mammary gland (Shehata et al., 2018).

Epithelial cells grown *in vitro* are only able to divide depending on their adherence to the substrate (Assoian, 1997). Similarly, *in vivo* proliferating cells in multi-layered epithelia are found mostly in contact with the ECM (Tomakidi et al., 1998). Thus, in our 2D models I assume that only cells with a greater contact area to the ECM than some threshold value can enter the cell cycle, $C_{height} < 2$.

The orientation of cell division is important in determining the position of the daughter cells and subsequently the architecture of the tissue. In the absence of quantitative experimental data, computational models in the literature typically assume that the orientation of cell division is uniformly random. In the models I consider two potential unit vectors representing division angle orientation, \mathbf{m} .

First \mathbf{m} is expressed as a unit vector with a random orientation allowing cells to divide in any plane. I model this by:

$$\theta = U[0, 2\pi] \quad u = U[-1, 1], \quad (5)$$

$$\hat{\mathbf{m}} = [\sqrt{1 - u^2} \cos\theta, \sqrt{1 - u^2} \sin\theta, u]. \quad (6)$$

Alternatively, a biologically relevant choice for \mathbf{m} , is the ‘planar division rule’. This rule states that cells can only divide along the plane of the ECM to which they are adhered (x-y plane). I model this by:

$$\theta = U[0, 2\pi], \quad (7)$$

$$\mathbf{m} = [\sin\theta, \cos\theta, 0]. \quad (8)$$

Upon cell division, the daughter cells are placed at half a cell diameter away from the parent cell centre. Their cell cycle times are reset to zero and are assigned new cell cycle durations.

To explore the effects of cell division orientation in the spatial organisation of the mammary tissue I compare these two division rules using the 2D model.

5.2.8 Cell death

Cells are endowed with an innate anchorage-dependent surveillance system that ensures cells that lose adherence to the ECM are targeted for anoikis, a form of caspase-dependent apoptosis (Vachon, 2011). Anoikis is important in maintaining tissue homeostasis and preventing dysplastic cell growth.

In the models I assume that cells whose contact area with the ECM is less than a threshold value, $C_{\text{height}} > 1$, are removed by anoikis at a rate of 0.25 (Grossmann et al., 2001). Thus, I assume

a bilayer culture will form in the models as seen in the 2D cell culture experiments, as the rate of cell death is greater than the rate of cell division (Galle et al., 2005).

5.2.9 Cell polarity

β 1-integrin signalling specifies apical-basal polarity orientation and the formation of lumens in the mammary gland. Endocytosis of apical components from the cell-ECM interface is a continuous process (Akhtar et al., 2013). In the model cell polarity for each cell is implemented using a polarity vector \mathbf{p} . This vector is characterised by a direction, accounting for the apical-basal polarity of the cell, as well as a magnitude. This magnitude accounts for how polarised the cell is.

5.2.10 Data output

The model simulations output .viztypes, .dat and .vtu files at discrete time steps. The .dat file contains each cell's velocity at every time step of the simulation. The .viztypes and .vtu files contain information on the type of cell.

ParaView (<https://www.paraview.org/>) is an open-source, data analysis and visualisation application used to visualise the data and to extract spatial summary statistics associated with cell clustering.

Other summary statistics such as the distance moved by cells are analysed and plotted using MATLAB R2022a. The .dat file is used to calculate the average displacement of cell types over time.

5.2.11 The software

Chaste (Cancer, Heart And Soft Tissue Environment) is an open-source C++ software library used to build and run simulations of biological tissues (Cooper et al., 2020, Gary et al., 2013, Pitt-Francis et al., 2009). The main Chaste repository can be found on GitHub (<https://github.com/Chaste>). To date, biological applications of Chaste have included cardiac electrophysiology and lung ventilation mechanics (Cooper et al., 2020). In the area of developmental biology, Chaste has been used to study processes including tissue size control (Kursawe et al., 2015), axis extension in drosophila (Tetley et al., 2016, Finegan et al., 2019a),

oriented cell divisions (Finegan et al., 2019b), epithelial tube elongation in lung and kidney development (Conrad et al., 2021), cell fate selection (Germano and Osborne, 2021), cell cycle regulation (Murray et al., 2019, Atwell et al., 2015), cell proliferation (Godwin et al., 2017) and crypt fission in the intestinal stem cell niche (Langlands et al., 2016).

We choose to use Chaste in this project because, compared to other popular cell-based modelling software such as CompuCell3D (<https://compuCell3d.org/>) and PhysiCell (<http://physicell.org/>), Chaste gives its users much greater flexibility of implementing different modelling assumptions and approaches (Osborne et al., 2017).

5.2.11.1 Installation

The quickest and easiest way to install Chaste is via [Docker](#), a lightweight virtualisation technology that allows users to run Chaste and all its dependencies in a loosely isolated environment called a container. Docker ensures that users can launch and run Chaste using a single command, despite the hosts operating system or hardware configurations.

5.2.11.1.1 Container directory structure

The Docker container launches in the `chaste` user's home directory at `/home/chaste`, with the following subdirectories:

- `lib` - precompiled Chaste binaries and libraries
- `projects` - a symlink to `/home/chaste/src/projects` for user projects
- `scripts` - convenience scripts for creating, building, and testing projects
- `src` - the Chaste source code
- `testoutput` - the output folder for the project testing framework

5.2.11.1.2 User projects

User projects allow users to modify and use the Chaste source code without altering it directly in the `src` folder. This ensures that, when debugging, any errors can be traced back to either the Chaste source code or users' own code.

User projects can be created using the script `new_project.sh` (in the `scripts` directory) and are stored in the `projects` folder.

Although using a named volume (`chaste_data`) ensures changes made within the home folder (`/home/chaste`) persist between container instances. Resetting Docker results in a loss of all volumes and their contained data. Thus, it is important users push their user projects to a GitHub repository.

5.2.11.2 GitHub

User projects can then be pushed to the user's own GitHub repository. GitHub is a free online cloud-based platform that enables developers to store and manage their code using Git. Version control on GitHub allows developers to safely collaborate with others on projects through branching and merging. Branching allows developers to duplicate part of the source code, which can then be edited safely without affecting the rest of the project. The code can then be merged back with the main source code.

All code used to generate the results presented in this chapter is released under an open source (BSD) licence and is available at: <https://github.com/mdp19pn/PriyaN>.

5.3 Results

5.3.1 2D culture reference model

I first investigated how wild-type MECs organise when grown on a flat substrate in which all the control mechanisms, anchorage dependent growth, planar cell division and anoikis, are present. I ran the simulation with the initial conditions for a simulation time of 120 hr and a time-step of 5 minutes. The age of MECs is randomly assigned. Note that, in the 2-cell type population simulation, all MECs are considered as proliferative. Whereas in the simulation with stem cells, LE and ME cells are considered as differentiated (cannot divide) and only stem cells divide based on cell cycle duration and distance from coverslip. Initial MECs are manually labelled and positioned based on profiling of immunofluorescence images of MEC clusters at the time of plating *in vitro*. The parameter values used for this reference model are given in Table 4.

Table 4: Table of parameters used for 2D culture *in silico* simulations.

Parameter	Description	Value	Reference
t_{cycle}	Mean cell cycle duration	15	(Shehata et al., 2018)
t_{end}	Simulation duration	120	Chosen to reflect <i>in vitro</i> conditions
μ	Spring constant	50	(Dunn et al., 2013, Meineke et al., 2001)
s	Cell spring rest length	1	(Pathmanathan et al., 2009)
w_a	Anoikis rate	0.25	(Grossmann et al., 2001)

5.3.1.1 2D culture morphology of a population comprising of two cell types.

Figure 32 shows top and side views of a growing WT MEC population consisting of two cell types, LE and ME.

The MEC population was characterised by calculating the number of cells in each lineage and cell position of the two cell lineages. Of the monolayer population at $t = 120$ hr 58% of the cells are ME and the remaining 42% of the cells are LE which is opposite to our experimental values. Experimentally in 2D cultures ~61% of the population are LE and ~39% are ME cells at $t = 120$ hr. The difference in results between our *in vitro* and computational simulation is due to the lack of differentiated cell types. In the adult mammary gland only stem cells can proliferate and differentiate.

Despite this, ME cells are still positioned closer to the ECM compared to the LE cells which I have observed experimentally (Figure 33).

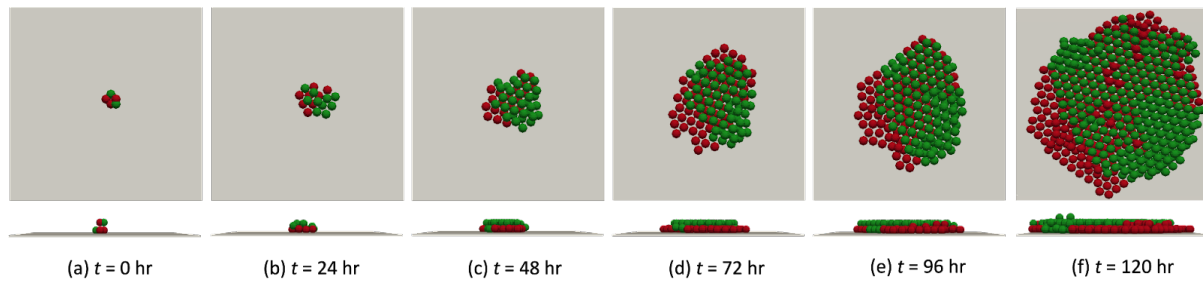


Figure 32: Simulation of WT MEC reference model. Snapshots are shown at selected times, given in hours. Parameter values are given in Table 1.

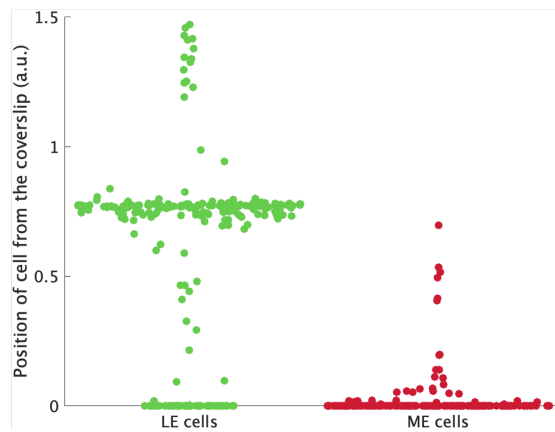


Figure 33: Height distribution of ME and LE cells in the reference population. Plot of cell height from the coverslip at the end of the simulation, $t = 120$ hr.

5.3.1.1.1 Growth kinetics

The total number of cells, number of LE cells, and number of ME cells in the 2D culture as functions of time t are shown in Figure 34A. Fitting an exponential curve to the total number of cells gives $r^2 = 0.98$, indicating clear early exponential growth. However, once a significant amount of anoikis starts to occur due to cells growing away from the coverslip, the rate of growth slows to an approximately linear rate. The exponential growth phase transitioning into linear growth is confirmed by several different cell line experiments (Katwal et al., 2019, Liu et al., 2010, Leggett et al., 2019).

I then investigated the time evolution of the radius of the reference model population. Figure 34B shows initially a diffusion-like growth phase is observed followed by an exponential phase. The growth then becomes approximately linear with a constant expansion velocity.

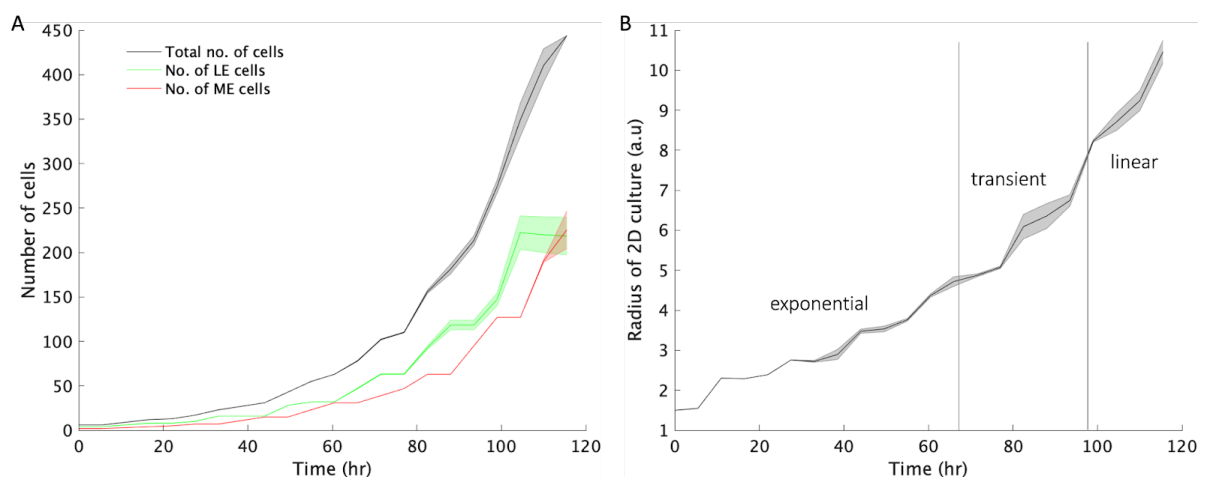


Figure 34: Growth kinetics of WT MEC reference model. (A) Plot of ME, LE and total cell count vs time. **(B)** Plot of monolayer culture radius vs time. Results from 5 simulations. Mean \pm SD.

5.3.1.2 2D culture morphology with addition of stem cells

Mammary stem cells are known to play a key role in postnatal morphogenesis of the mammary gland; thus, I incorporated stem cells into the model to better recapitulate *in vivo* conditions.

Addition of mammary stem cells to the simulation results in a smaller mammary epithelial cell population compared to the WT reference population (Figure 35A). Characterisation of the WT population with stem cells is like what I observe *in vitro* (Figure 35B-C). I find that ME cells lie closer to the ECM compared to the LE cells, in agreement with our experimental findings (Figure 35D). The growth kinetics are different to those of the reference population; population growth is linear as shown in Figure 35E-F.

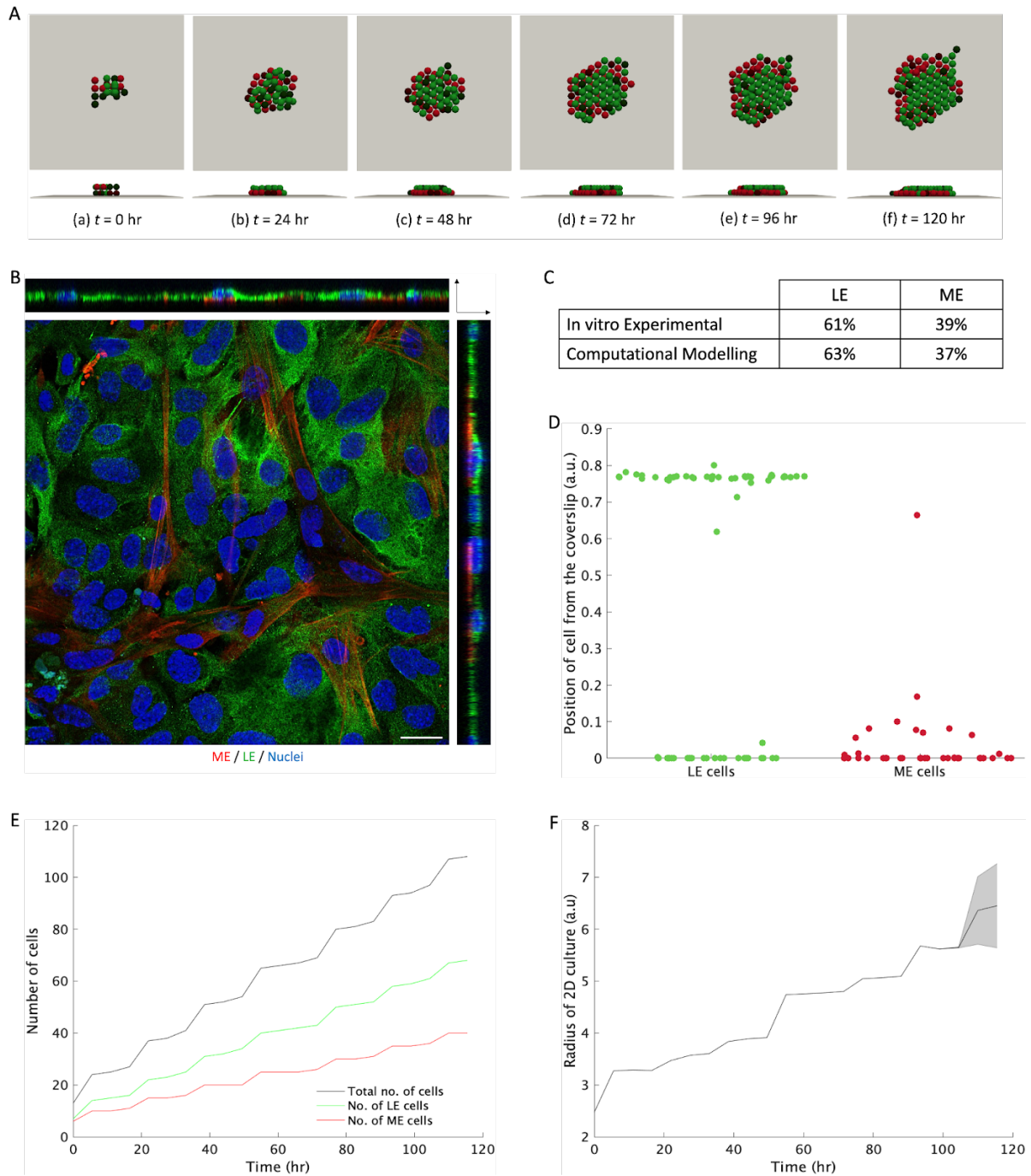


Figure 35: Addition of mammary stem cells better recapitulates in vitro culture. (A) Simulation snapshots are shown at selected times. Time is given in hours. **(B)** Representative confocal image of WT MECs cultured on plastic for 5 days and stained with ME marker: smooth-muscle actin (red), LE marker: K18 (green). Scale bar 20 μ m. **(C)** Table comparing the percentage of LE and ME cells at the end of simulation and in vitro culture Average from 5 simulation and 4 experiments. **(D)** Plot of cell height from the coverslip at the end of the simulation, $t = 120$ hr. **(E)** Plot of ME, LE and total cell count vs time. **(F)** Plot of monolayer culture radius vs time. Results from 5 simulations. Mean \pm SD.

5.3.2 Knockout of control mechanisms

In the following I investigated mammary cell organisation where control mechanisms were knocked out selectively from the reference model with stem cells. I simulated 120 hr of growth using a numerical time-step of 5 minutes. The initial ages of MECs in each simulation are randomly assigned. In the following simulations LE and ME cells are considered as differentiated (cannot divide), while stem cells divide based on cell cycle duration and distance from coverslip (except for the anchorage-dependent growth KO simulation). Initial MECs are manually labelled and positioned based on profiling of immunofluorescence images of MEC clusters at the time of plating *in vitro*.

5.3.2.1 Oriented cell division

Oriented cell division is an important mechanism involved in morphogenesis of tissue. Deregulation of cell division orientation can result in cancer. Cell division orientation is influenced by both intrinsic and extrinsic cues resulting in either planar or perpendicular division to the tissue. *Drosophila* neuroblasts are an example of oriented cell division driven by an intrinsic cue; the plane of division is determined by the apicobasal polarity of the cell (Schaefer et al., 2000). Extrinsic cues such as neighbouring cells, biophysical properties of the ECM, and mechanical forces from the ECM can all influence the orientation of cell division (Chaigne et al., 2013, Gilbert et al., 2010, Théry and Bornens, 2006).

Cell division orientation within the mammary gland varies depending on the stage of development. For example, during pubertal development, *in vivo* and in 3D culture stratification of the bilayer structure is initiated through division of apically positioned luminal epithelial cells perpendicular to the ECM, forming terminal end buds (Huebner et al., 2014). However, during pregnancy, basal cells divide parallel to the ECM (Taddei et al., 2008). Deletion of β 1-integrin in basal cells results in randomised division orientation with some cells dividing perpendicular to the ECM (Taddei et al., 2008).

The mammary gland maintains its bilayer structure despite continual dynamic proliferative changes with each oestrous cycle and pregnancy. Thus, I consider oriented cell division as a mechanism involved in forming and maintaining the concentric bilayer structure in the mammary gland.

To explore the effects of cell division orientation in spatial organisation of mammary tissue *in silico*, I knocked out planar division. Cell division orientation was fully randomised for this simulation.

Figure 36A shows snapshots of a growing mammary epithelial cell population in the absence of oriented cell division. If oriented cell division is present, then cells are only able to divide parallel to the substrate; but in the absence of oriented cell division, cells can divide in any direction, forming three-dimensional aggregates. However, anoikis prevents multilayer aggregates from forming, and thus still maintains a bilayer. The morphology of the cell population, and the proportions of LE and ME cells, are like those observed in the reference model. If cell-ECM adhesion is strong, then ME cells expressing integrins still preferentially adhere to the ECM. In this case ME cells still preferentially position themselves next to the ECM even in the absence of oriented division through migration (Figure 36B).

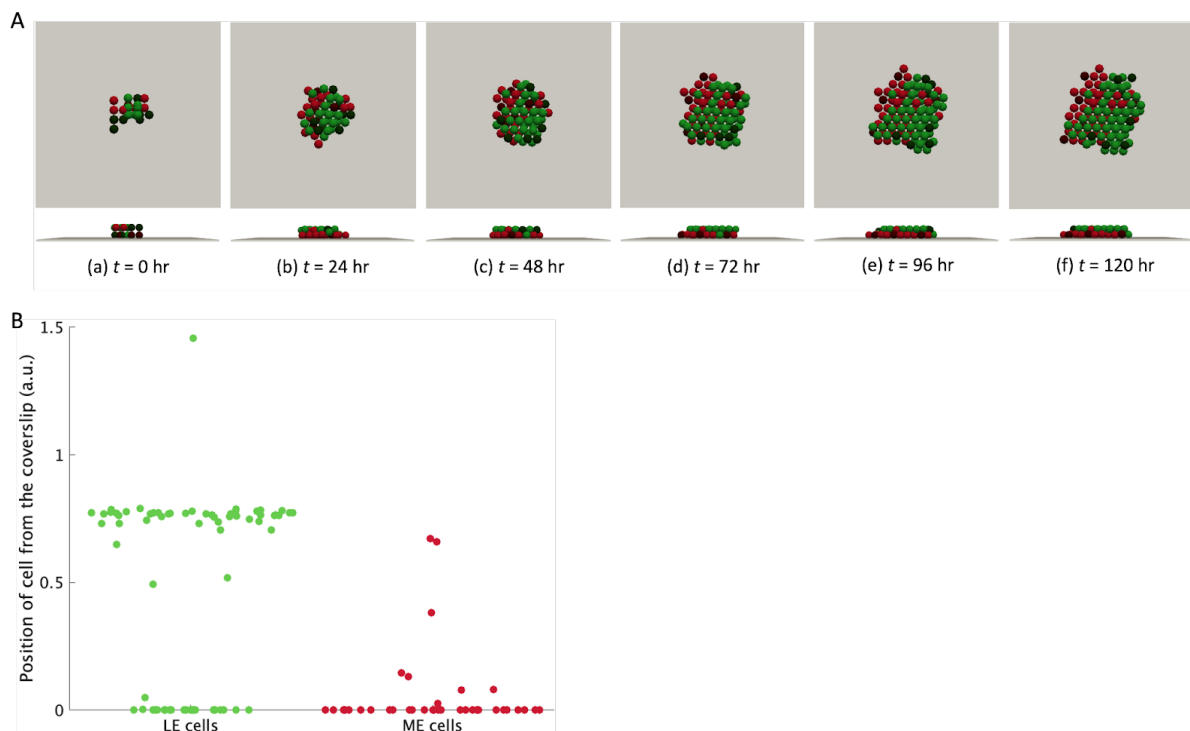


Figure 36: Knockout of oriented planar cell division does not alter cell positioning. (A) Simulation snapshots are shown at selected times. LE cells (green), ME cells (red), basal stem cells (dark red), luminal stem cells (dark green). Time is given in hours. (B) Plot of cell height from the coverslip at the end of the simulation, $t = 120$ hr.

5.3.2.2 Anchorage-dependent growth

Previous experimental observations suggest that cell anchorage to the ECM controls the G1 phase of the cell cycle and regulates progression (Aszodi et al., 2003). Cell-ECM signalling mediated by integrins is necessary for the induction of D-type cyclins and the subsequent phosphorylation of pRB and initiation of DNA synthesis (Böhmer et al., 1996). Furthermore, integrin mediated cell-ECM signalling may control G1 phase progression through activation of other signalling molecules such as Rac1, FAK and Cdc42 (Bao et al., 2002, Li et al., 2005, Jeanes et al., 2012). Moreover, disruption of cell-ECM signalling through integrins prevents proper progression through mitosis (Reverte et al., 2006, Chi et al., 2022, Marek et al., 2010). Thus, I assume that one of the mechanisms involved in spatial organisation of MECs is anchorage-dependent growth.

Figure 37A shows snapshots of a growing mammary epithelial cell population in the absence of anchorage-dependent growth. In this case, the total number of cells is greater than the reference model, as cells away from the basal layer can proliferate. However, anoikis prevents a stratified epithelium from forming. The percentage of each cell lineage is like the reference population: 63% of LE cells and 37% ME cells. Most ME cells are still positioned next to the ECM (Figure 37B).

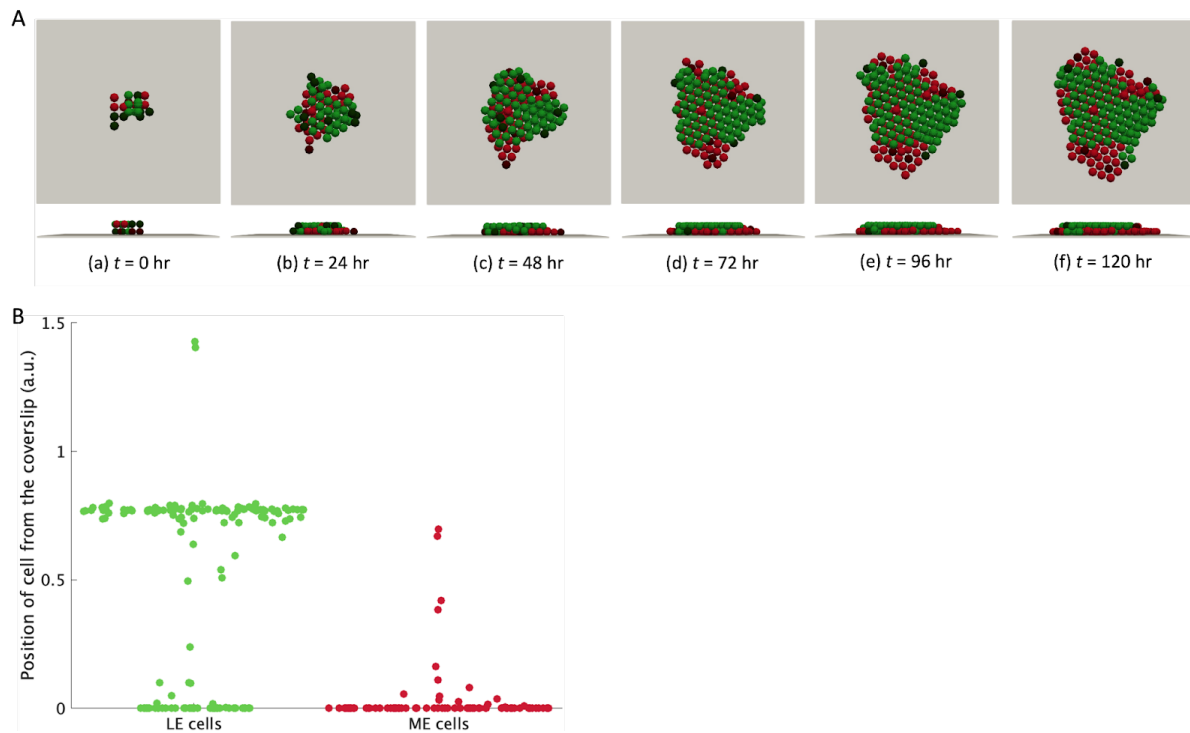


Figure 37: Knockout of anchorage dependent growth does not alter cell positioning. (A) Simulation snapshots are shown at selected times. LE cells (green), ME cells (red), basal stem cells (dark red), luminal stem cells (dark green). Time is given in hours. **(B)** Plot of number of LE and ME cells at end of simulation, $t = 120$ hr. **(C)** Plot of cell height from the coverslip at the end of the simulation, $t = 120$ hr.

5.3.2.3 Anoikis

Apoptosis plays a significant role in development and tissue homeostasis by removing excess and damaged cells (Fuchs and Steller, 2011). Several *in vitro* studies have suggested that anoikis is the main cell death mechanism induced in MECs upon anchorage loss (Boudreau et al., 1995, Farrelly et al., 1999, Debnath et al., 2002, Paulus et al., 2003). Thus, I consider anoikis as a mechanism for maintaining the mammary gland architectural structure.

Figure 38A shows snapshots of a growing mammary epithelial cell population without anoikis. If anoikis is present, cells that lose contact with the ECM undergo apoptosis; but in the absence of anoikis cells remain independent of ECM anchorage. Given that all the other mechanisms are present, the morphology of the cell population is like the reference model as no cells lose contact with the ECM. For our chosen parameter values, I find that 62% of the population is LE whilst the remaining 38% of the population is ME at $t = 120$ hr. I also find that ME cells lie closer to the ECM than LE cells (Figure 38B).

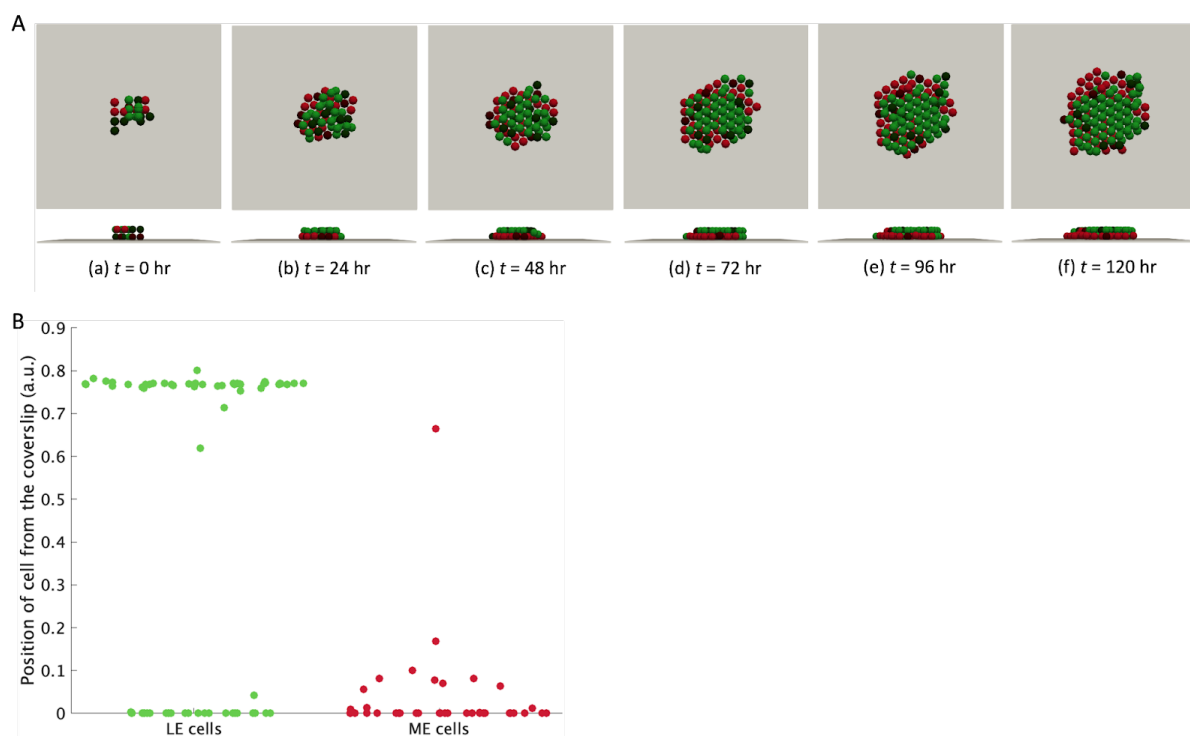


Figure 38: Knockout of anoikis does not alter cell positioning. (A) Simulation snapshots are shown at selected times. LE cells (green), ME cells (red), basal stem cells (dark red), luminal stem cells (dark green). Time is given in hours. (B) Plot of number of LE and ME cells at end of simulation, $t = 120$ hr. (C) Plot of cell height from the coverslip at the end of the simulation, $t = 120$ hr.

5.3.3 Organoid reference model

Next, I investigated how wild-type MECs organise when grown in a 3D matrix in which all the control mechanisms are present. As before, I simulated 120 hr of growth, using a numerical time-step of 5 minutes. The same initial conditions as previous simulations were used. The parameters used for this reference model are given in Table 5.

Table 5: Table of parameters used for 3D culture *in silico* simulations.

Parameter	Description	Value	Reference
t_{cycle}	Mean cell cycle duration	15	(Shehata et al., 2018)
t_{end}	Simulation duration	120	Chosen to reflect <i>in vitro</i> conditions
μ	Spring constant	50.0	(Dunn et al., 2013, Meineke et al., 2001) Meineke et al., 2001)
s	Cell spring rest length	1.0	(Pathmanathan et al., 2009)

5.3.3.1 Morphology and growth kinetics

Figure 39A shows the MEC cluster used at the start of the simulation. Figure 39B shows top and cross-sectional views of a growing reference WT MEC population in a 3D matrix.

Like our *in vitro* 3D organoid cultures (Figure 40A), ME cells in our simulation sit on the outside next to the ECM encompassing the LE cells (Figure 40B). The growth kinetics resemble those of the 2D reference model with stem cells (Figure 40C-D).

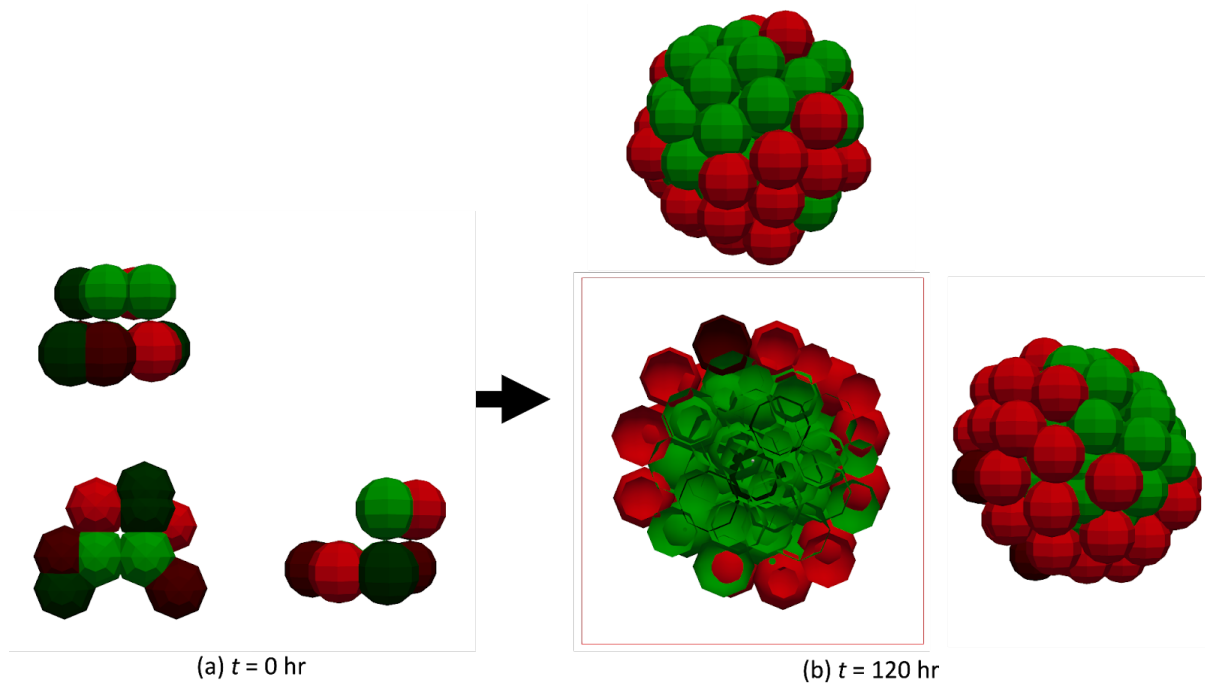


Figure 39: Snapshot of WT organoid reference model at $t = 120$ hr. Parameter values are given in Table 2. LE cells (green), ME cells (red), basal stem cells (dark red), luminal stem cells (dark green). **(A)** Initial condition. **(B)** At the end of the simulation $t = 120$ hr.

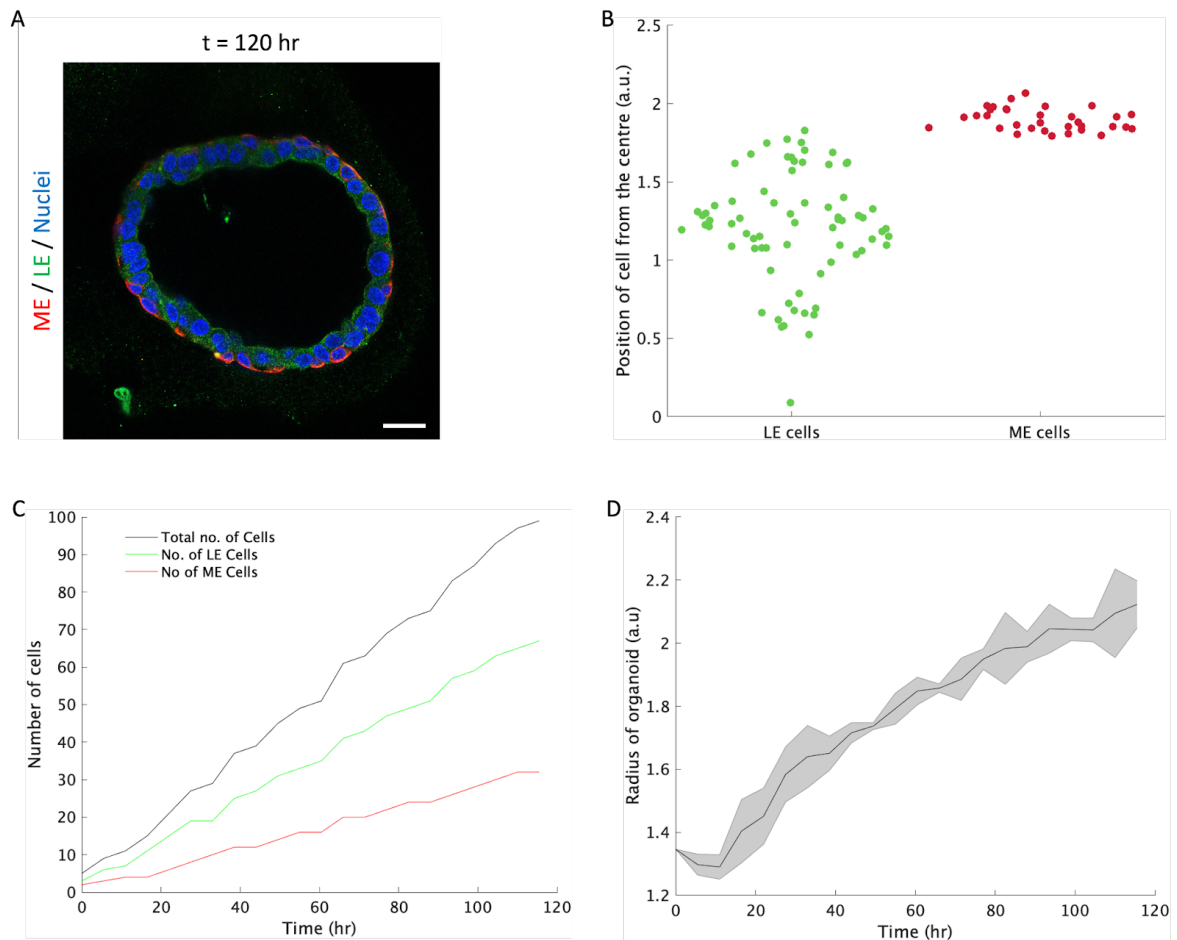


Figure 40: Growth kinetics of WT organoid reference model. (A) Representative confocal image of a WT organoid cultured in a laminin-rich BM (Matrigel) for 5 days and stained with ME marker: smooth-muscle actin (red), LE marker: K18 (green). Scale bar $20\mu\text{m}$. **(B)** Plot of cell position at the end of the simulation, $t = 120$ hr. **(C)** Plot of ME, LE and total cell count vs time. **(D)** Plot of organoid radius vs time. Results from 5 simulations. Mean \pm SD.

5.3.4 Integrin expression variation

I then further investigated how organisation of the epithelial cells depends on cell-specific parameters such as integrin expression. Given there are 16 different $\beta 1$ and $\beta 4$ integrin expression combinations between LE and ME cells, testing these all *in vitro* or *in vivo* is near impossible (Table 6).

Table 6: Combinations of $\beta 1$ and $\beta 4$ expression in luminal and myoepithelial cells.

1.	LE $\beta 1$ KO	LE $\beta 4$ KO	ME $\beta 1$ KO	ME $\beta 4$ KO
2.	LE $\beta 1$ KO	LE $\beta 4$ KO	ME $\beta 1$ KO	ME $\beta 4$ WT
3.	LE $\beta 1$ KO	LE $\beta 4$ KO	ME $\beta 1$ WT	ME $\beta 4$ KO
4.	LE $\beta 1$ KO	LE $\beta 4$ KO	ME $\beta 1$ WT	ME $\beta 4$ WT
5.	LE $\beta 1$ KO	LE $\beta 4$ WT	ME $\beta 1$ KO	ME $\beta 4$ KO
6.	LE $\beta 1$ KO	LE $\beta 4$ WT	ME $\beta 1$ KO	ME $\beta 4$ WT
7.	LE $\beta 1$ KO	LE $\beta 4$ WT	ME $\beta 1$ WT	ME $\beta 4$ KO
8.	LE $\beta 1$ KO	LE $\beta 4$ WT	ME $\beta 1$ WT	ME $\beta 4$ WT
9.	LE $\beta 1$ WT	LE $\beta 4$ KO	ME $\beta 1$ KO	ME $\beta 4$ KO
10.	LE $\beta 1$ WT	LE $\beta 4$ KO	ME $\beta 1$ KO	ME $\beta 4$ WT
11.	LE $\beta 1$ WT	LE $\beta 4$ KO	ME $\beta 1$ WT	ME $\beta 4$ KO
12.	LE $\beta 1$ WT	LE $\beta 4$ KO	ME $\beta 1$ WT	ME $\beta 4$ WT
13.	LE $\beta 1$ WT	LE $\beta 4$ WT	ME $\beta 1$ KO	ME $\beta 4$ KO
14.	LE $\beta 1$ WT	LE $\beta 4$ WT	ME $\beta 1$ KO	ME $\beta 4$ WT
15.	LE $\beta 1$ WT	LE $\beta 4$ WT	ME $\beta 1$ WT	ME $\beta 4$ KO
16.	LE $\beta 1$ WT	LE $\beta 4$ WT	ME $\beta 1$ WT	ME $\beta 4$ WT

Experimentally *in vitro*, I have deleted $\beta 1$ -integrin in ME cells or LE cells and found this alone was insufficient to disrupt spatial organisation (Figure 41A). Similarly in the simulations I observed ME cells preferentially sat on the outside next to the ECM when $\beta 1$ -integrin was deleted in ME or LE cells only, validating the model (Figure 41B). Moreover, deleting $\beta 1$ -integrin in both cell types had no effect on spatial organisation of the two cell lineages indicating the presence of alternate ECM binding receptors that remain competent to direct MEC positioning (Figure 42). To identify compensatory integrins, I ran simulations in the absence of $\beta 4$ -integrin in ME cells and/or LE cells. Like $\beta 1$ -integrin KO, deleting $\beta 4$ -integrin did not alter MEC positioning (Figure 43).

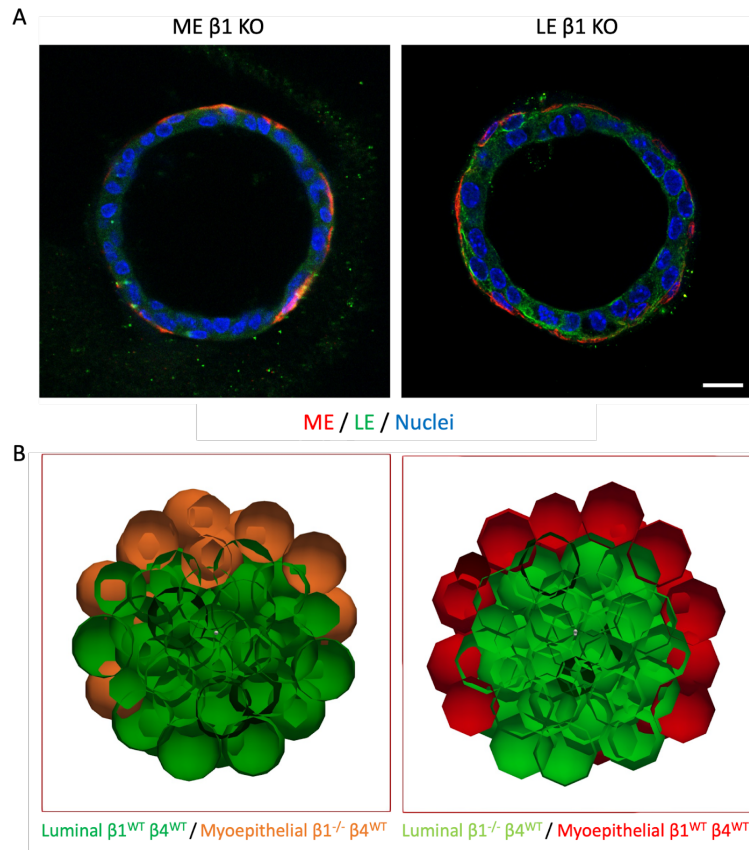


Figure 41: 3D organoid computational model recapitulates in vitro culture of organoids without $\beta 1$ -integrin in ME or LE cells. (A) MECs cultured in a laminin-rich BM (Matrigel) for 5 days and treated with 4-hydroxytamoxifen to delete $\beta 1$ -integrin in ME or LE cells specifically formed organoids with inner LE and outer ME. ME marker: smooth-muscle actin (red), LE marker: K18 (green). Scale bar $20\mu\text{m}$. (B) Snapshot of organoid at the end of the simulation $t = 120$ hr. (i) $\beta 1$ KO in ME cells (orange), WT LE cells (green). (ii) WT ME cells (red), $\beta 1$ KO in LE cells (lime green). Basal stem cells (dark red), luminal stem cells (dark green).

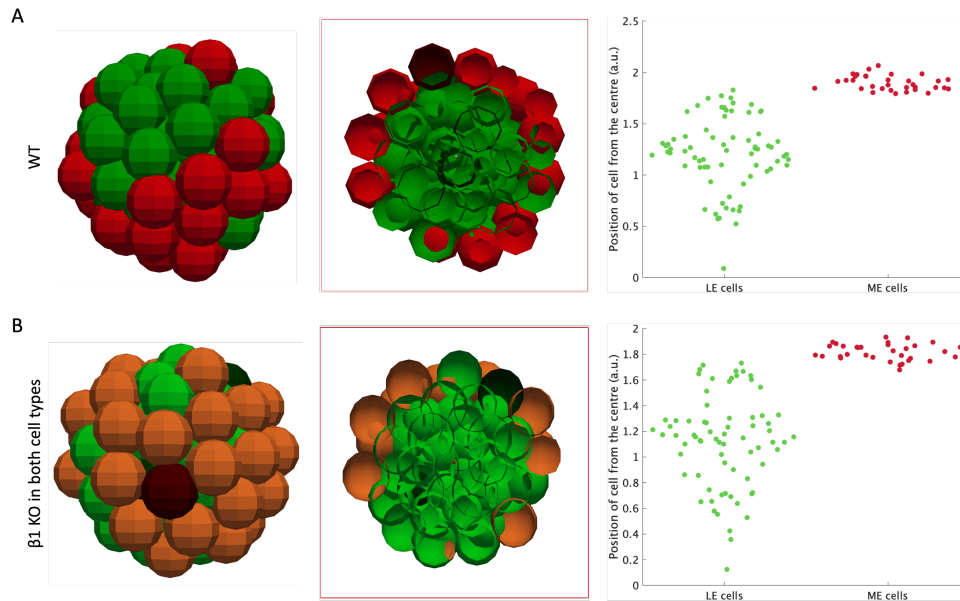


Figure 42: $\beta 1$ -integrin knockout in both cell types does not affect MEC sorting in simulated organoids. Snapshot of organoid at the end of the simulation and plot of cell position from the centre of the organoid at end of simulation, $t = 120$ hr. **(A)** WT ME cells (red), WT LE cells (green). **(B)** $\beta 1$ KO in both cell types, ME (orange), LE (lime green). Basal stem cells (dark red), luminal stem cells (dark green).

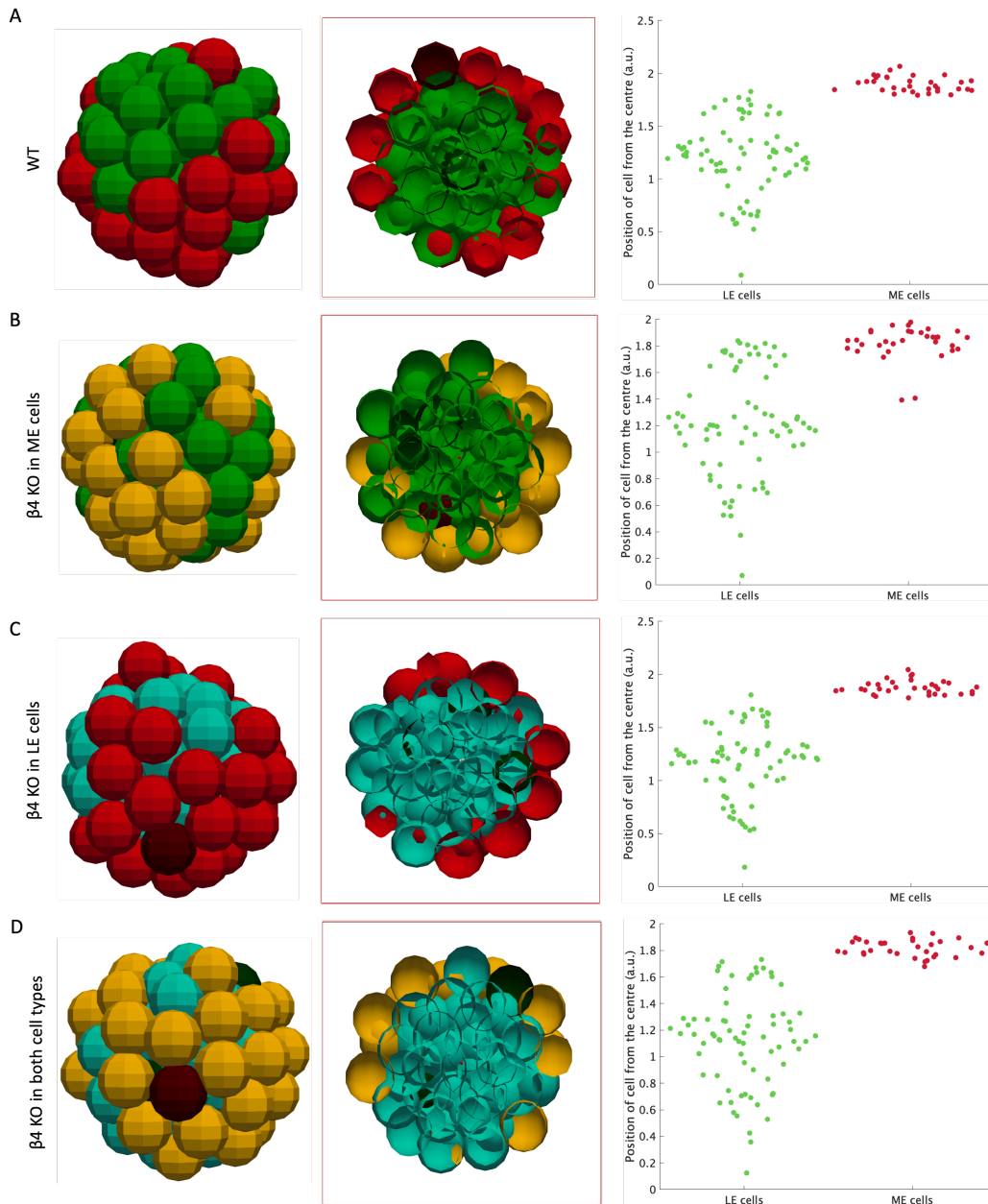


Figure 43: $\beta 4$ -integrin knockout in ME and/or LE cells does not affect MEC sorting in simulated organoids. Snapshot of organoid at the end of the simulation and plot of cell position from the centre of the organoid at end of simulation, $t = 120$ hr. **(A)** WT ME cells (red), WT LE cells (green). **(B)** $\beta 4$ KO in ME cells (amber), WT LE cells (green). **(C)** WT ME cells (red), $\beta 4$ KO in LE cells (aquamarine). **(D)** $\beta 4$ KO in both cell types, ME (amber), LE (aquamarine). Basal stem cells (dark red), luminal stem cells (dark green).

It is probable that β 4-integrin-ECM interaction could be sufficient to drive ME cell spatial organisation in the absence of β 1-integrin and vice versa. To test this, I deleted both β 1 and β 4-integrin in ME cells. Under these conditions ME cells are dispersed throughout the organoid, and there is no clear sorting of the two cell populations (Figure 44B). However, deleting β 1 and β 4-integrin in LE cells produces organoids with two distinct cell population clusters (Figure 44C). The ME cell cluster is nearer the centre surrounded by the LE cells. This result is exciting as it suggests lack of apical membrane could allow ME cells to position near the centre and would be worth testing experimentally. Unsurprisingly when I did a double integrin KO in both cell types, concentric organisation of the two cell types was fully lost (Figure 44D).

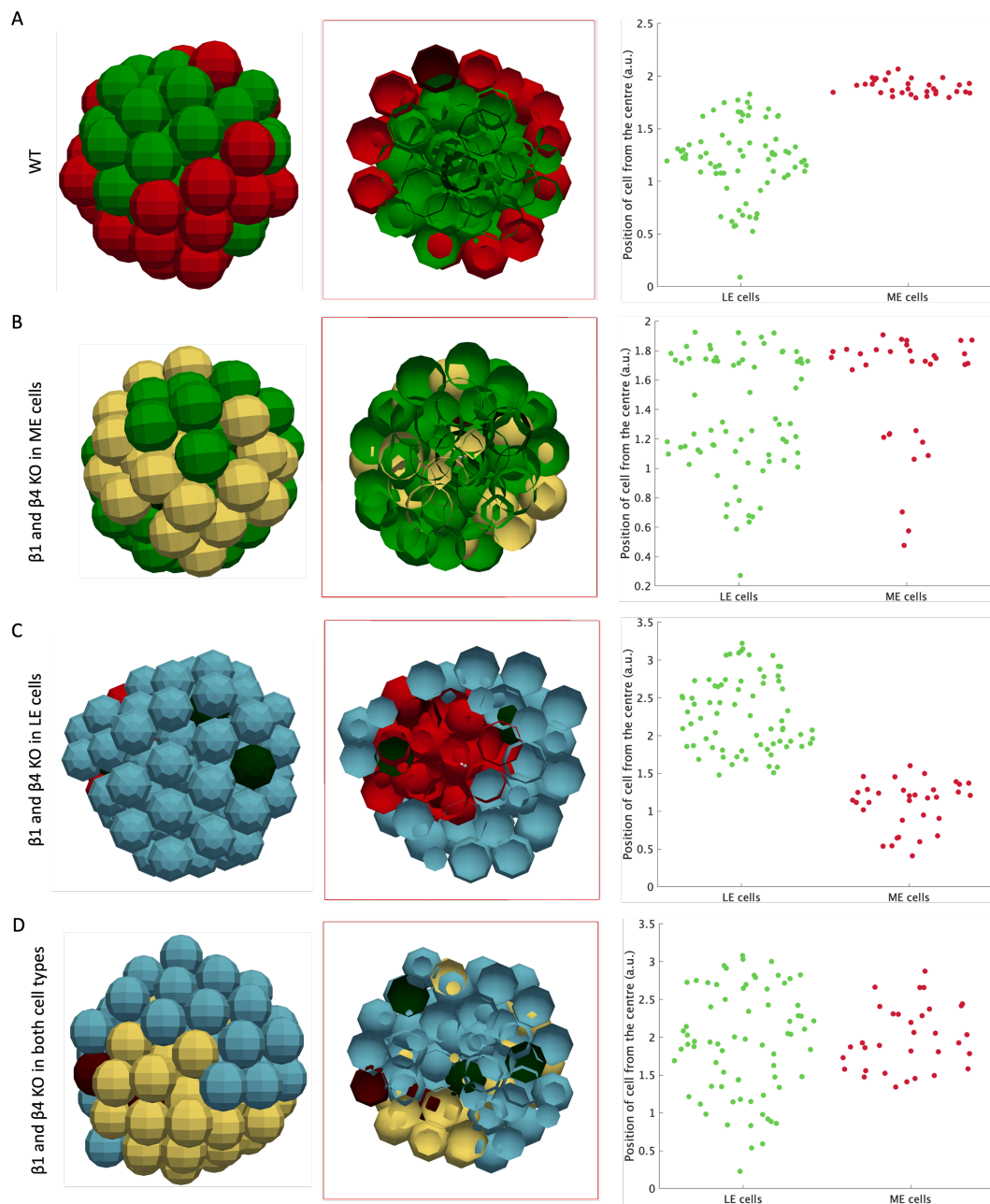


Figure 44: Spatial organisation of organoids with differential integrin expression. Snapshot of organoid at the end of the simulation and plot of cell position from the centre of the organoid at end of simulation, $t = 120$ hr. **(A)** WT ME cells (red), WT LE cells (green). **(B)** $\beta 1$ and $\beta 4$ KO in ME cells (yellow), WT LE cells (green). **(C)** WT ME cells (red), $\beta 1$ and $\beta 4$ KO in LE cells (blue). **(D)** $\beta 1$ and $\beta 4$ KO in both cell types, ME (yellow), LE (blue). Basal stem cells (dark red), luminal stem cells (dark green).

5.3.5 Integrins are necessary for establishing and maintaining cell positioning.

To test whether integrins are required only for establishing spatial organisation or also needed to maintain cell positioning I ran loss of function simulations. WT cells were simulated for 120 hours to establish organoids with correct spatial organisation (Figure 45A), β 1-integrin and β 4-integrin expression was then knocked out in just ME cells, LE cells or in both cell types and the simulations were run for a further 120 hours.

Notably, following cell sorting loss of β 1-integrin and β 4-integrin in ME cells alone does not alter ME cell position (Figure 45B). However, deletion of integrins in LE cells produces a similar phenotype to LE KO of integrins at the time of plating (Figure 45C). Loss of integrins in both cell types results in loss of cellular organisation (Figure 45D). This suggests that deletion of integrins in ME cells alone is insufficient to disrupt spatial organisation once cells have organised, as the apical membrane remains intact providing repulsion.

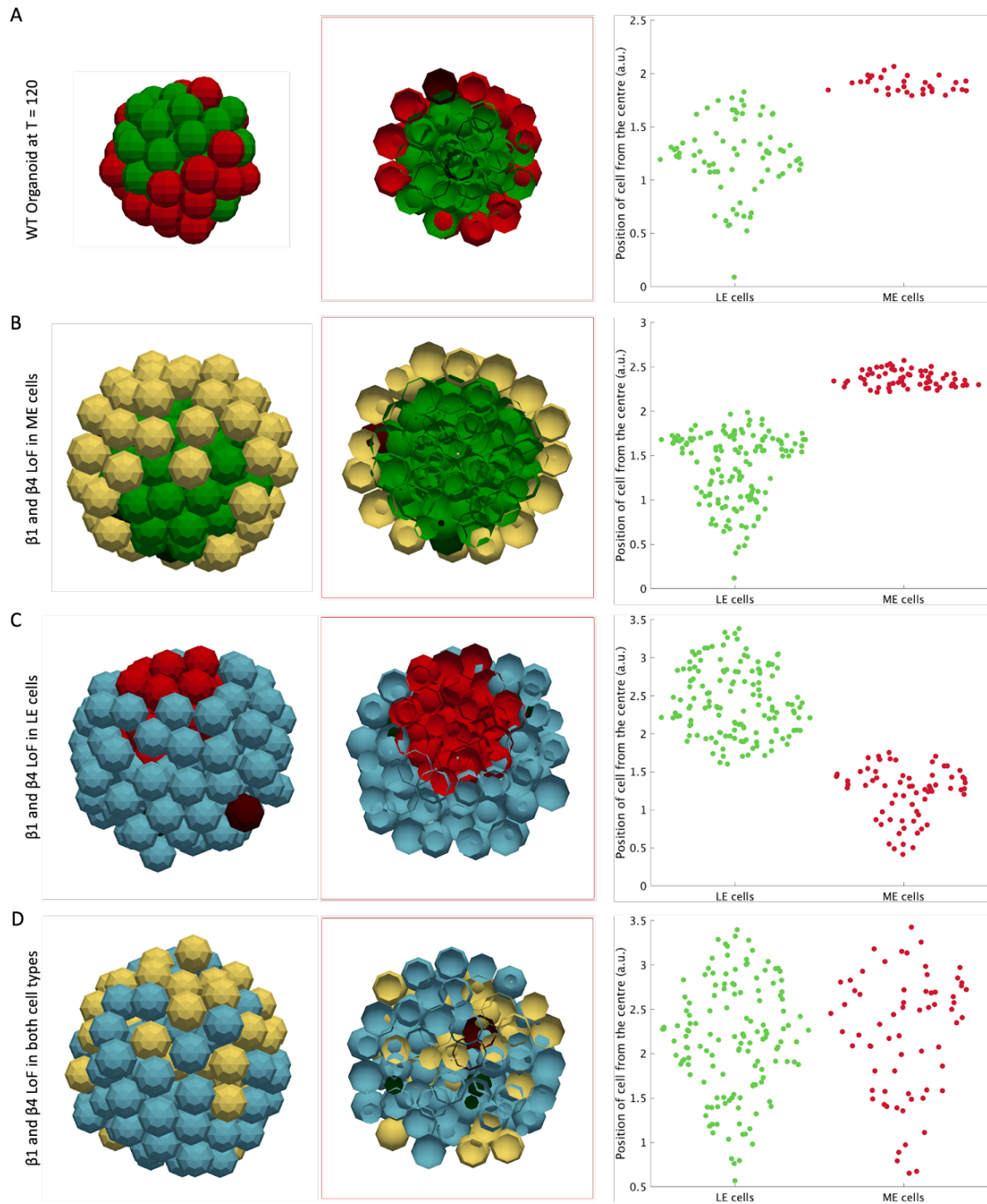


Figure 45: Loss of integrin function simulations from WT organoids. Snapshot of organoid at $t = 120$ hr or the end of the simulation ($t = 240$ hr) and plot of cell position from the centre of the organoid at the respective time point. **(A)** WT ME cells (red), WT LE cells (green). **(B)** $\beta 1$ and $\beta 4$ LoF in ME cells (yellow), WT LE cells (green). **(C)** $\beta 1$ and $\beta 4$ LoF in LE cells (blue), WT LE cells (green). **(D)** $\beta 1$ and $\beta 4$ LoF in both cell types, ME (yellow) and LE (blue). Basal stem cells (dark red), luminal stem cells (dark green).

I then wanted to test whether inner LE and outer ME cell positioning could be restored if I added integrin expression to cells. To do this, integrin null cells were simulated for 120 hours to form disorganised organoids (Figure 46A), after which I re-introduced β 1-integrin and β 4-integrin expression in just ME cells, just LE cells, or in both cell types and the simulations were run for a further 120 hours.

Although adding integrin expression to ME cells caused cell sorting, they did not all position next to the ECM (Figure 46B). Instead, the ME cells all clumped together and were surrounded by LE cells lacking integrins. Interestingly adding β 1- and β 4-integrin expression to LE cells restored ME cell positioning to the outside (Figure 46C). Gain of function in both cell types reverted the disorganised organoid to inner LE and outer ME structure (Figure 46D). These gain of function simulations suggest that disrupted mammary organoid structure can be restored by expressing integrins in LE cells alone or in both cell types.

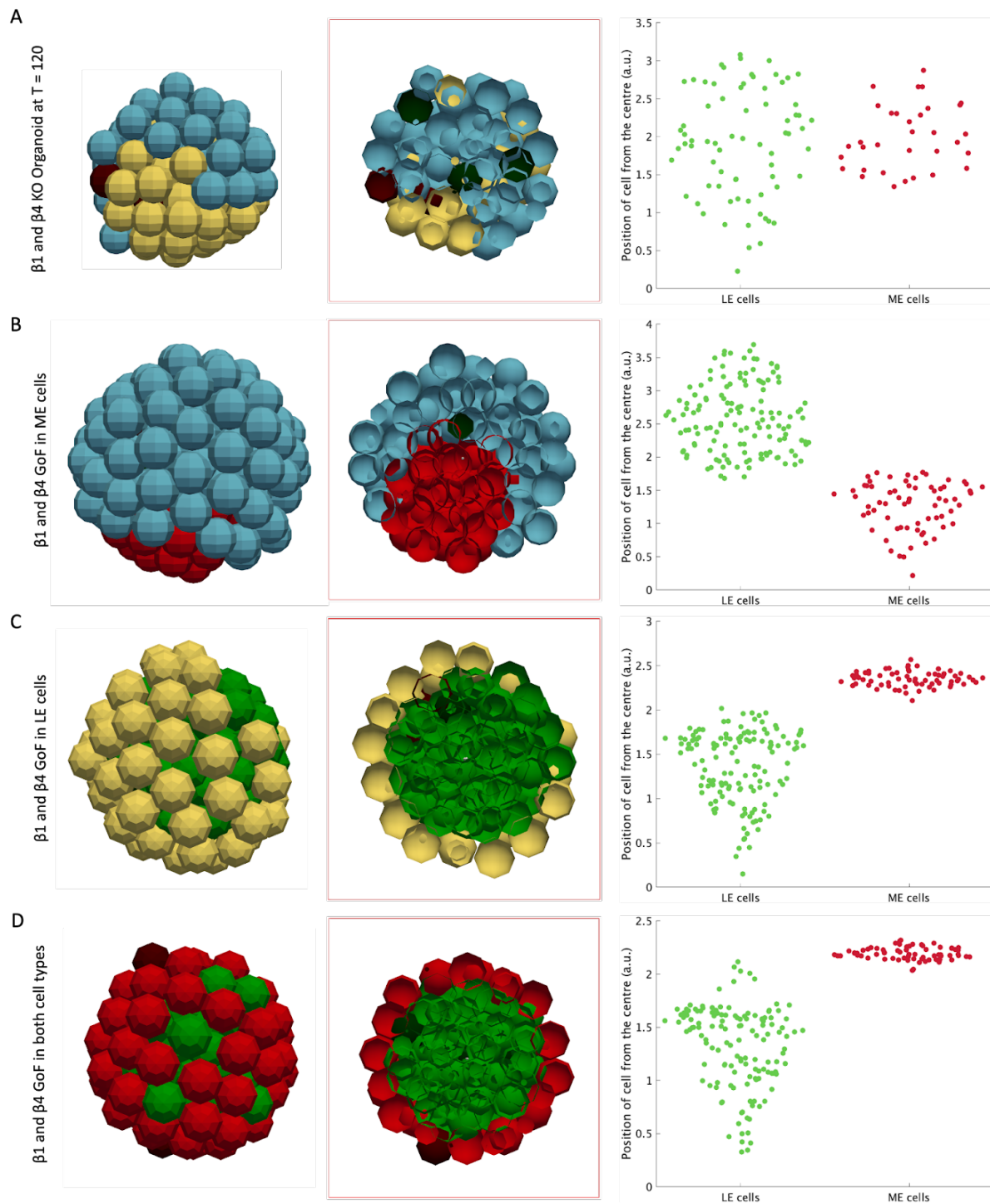


Figure 46: Gain of integrin function simulations from $\beta 1$ and $\beta 4$ KO organoids. Snapshot of organoid at $t = 120$ hr or the end of the simulation ($t = 240$ hr) and plot of cell position from the centre of the organoid at the respective time point. **(A)** $\beta 1$ and $\beta 4$ KO in both cell types, ME (yellow), LE (blue). **(B)** $\beta 1$ and $\beta 4$ GoF in ME cells (red), $\beta 1$ and $\beta 4$ KO LE cells (blue). **(C)** $\beta 1$ and $\beta 4$ GoF in LE cells (green) and LE cells (yellow). **(D)** $\beta 1$ and $\beta 4$ GoF in ME cells (red) and LE cells (green). Basal stem cells (dark red), luminal stem cells (dark green).

5.3.6 Summary of simulated organoid cases

Table 7: Summarises the simulated organoid cases with different integrin expressions.

Scenario	Tissue Organisation	Reference
16. WT Organoid	Inner LE, outer ME	Figure 39
14. ME β 1 KO Organoid	Inner LE, outer ME	Figure 41B(i)
15. ME β 4 KO Organoid	Inner LE, outer ME	Figure 43B
13. ME β 1 & β 4 KO Organoid	LE and ME cells interspersed	Figure 44B
8. LE β 1 KO Organoid	Inner LE, outer ME	Figure 41B(ii)
12. LE β 4 KO Organoid	Inner LE, outer ME	Figure 43C
4. LE β 1 & β 4 KO Organoid	Outer LE, inner ME	Figure 44C
6. β 1 KO Organoid	Inner LE, outer ME	Figure 42B
11. β 4 KO Organoid	Inner LE, outer ME	Figure 43D
1. β 1 & β 4 KO Organoid	LE and ME cells interspersed	Figure 44D

5.4 Discussion

In this chapter, I have introduced a novel cell-based computational model of the mammary epithelial cell population to study cell sorting within the mammary tissue. Unlike previous models, my model explicitly accounts for cell-ECM adhesion via integrins and potential cell sorting mechanisms such as oriented division.

I found that in the presence of all cell sorting control mechanisms and differential adhesion to the ECM, the two-cell population model forms a bilayer structure. However, given this model assumes all cells can proliferate indefinitely and does not account for cell differentiation, it is only reflective of the initial growth phase. As a result, the ratio of ME to LE cells did not reflect *in vivo* conditions. Construction of integrated datasets of mouse and human MEC obtained by scRNAseq suggest postnatally LE and ME cells arise from unipotent progenitors (Saeki et al., 2021). Thus, I introduced unipotent stem cells and differentiation into the model, the growth kinetics and morphology of the population better agreed with my experimental data.

By selective knockout of different cell sorting mechanisms, I studied the interplay of the different mechanisms on the spatial positioning of MECs in the mammary gland. I found that the model was robust to perturbation of any one cell sorting mechanism. This suggests that cell positioning could be driven by a combination of mechanisms and that in the absence of one of the mechanisms, the others could be overriding this loss. Moreover, cell migration could be involved in resolving incorrect spatial organisation of MECs, as seen in my *in vitro* experiments.

In vivo, the ECM surrounds the mammary epithelial cells providing cues in 3D to drive processes such as apical basal polarity, cell proliferation and apoptosis (Akhtar and Streuli 2013, Jeanes et al., 2012, Prince et al., 2002). Similarly, in my 3D cultures *in vitro*, MECs are embedded in a laminin-rich ECM. To better study cell-ECM affinity in cell positioning, I simulated 3D organoid cultures surrounded by an ECM that exerts an isotropic pressure-like force on cells. In future work we could implement a more biophysically detailed description of cell-ECM interactions along the lines of Buske et al (2012). To validate the model, I ran WT, ME β 1-integrin KO and LE β 1-integrin KO simulations to compare the likeness of the simulation results to my *in vitro* experimental data. The spatial patterning from these simulations matched my experimental results, validating the 3D organoid model.

One of the differences between the 3D organoid model and *in vitro* experimental results is the lack of lumen formation. Given the mechanisms of lumen formation in the mammary gland have not been fully elucidated, I have opted not to include this parameter. However, this can be incorporated into the model in the future.

I then used the model to run predictive simulations to assess the role of β 4-integrin in cell sorting as my *in vitro* data had indicated the involvement of another laminin-binding receptor in driving cell sorting. Similar phenotypes were observed in the absence of β 1- and β 4-integrins in both cell types and ME cells only. Surprisingly, deletion of both integrins in LE cells resulted in the engulfment of ME cells by the LE cells, which could be due to inversion of the apical membrane and subsequently the repulsive force. In the mammary gland, β 1-integrin-ILK signalling pathway is utilised for organising apical-basal cell polarity (Akhtar and Streuli 2013). I have shown previously in Chapter 3 that loss of β 1-integrin in LE cells partially inverts the polarity of the organoids. Therefore, in the absence of both integrins, the apical polarity

might be fully inverted, resulting in a loss of the repulsive force at the centre of the organoid that pushes ME cells out towards the ECM. It would be interesting to test this parameter experimentally to further support our apical membrane repulsion hypothesis.

Integrins are known to be important for both establishing and maintaining polarity (Akhtar and Streuli, 2013). Thus, I ran some predictive simulations of integrin knock-in and knock-out scenarios to test whether integrins are also required to maintain cell positioning. Interestingly, following cell sorting loss of β 1- and β 4-integrin in ME cells did not alter ME cell positions suggesting once cells have positioned themselves, they remain there despite loss of affinity to the matrix. However, deletion of both integrins in LE cells caused ME cells to move inwards. This could be because maintenance of polarity is an active process governed by integrins, so when integrins are lost the apical membrane is inverted and repulsion at the centre is lost. These results suggest that repulsion at the apical membrane could be overriding the cues from the ECM when determining positioning of ME cells.

Taken together, the data from the simulations provide new insights into the role of integrins in MEC sorting and the requirement of integrins to maintain correct cell positioning. The data also suggests functional redundancy of integrins in MEC sorting.

6 β 1-integrin is required for myoepithelial cell contractility

6.1 Introduction

During pregnancy, the mammary tissue undergoes major remodelling in preparation for lactation in response to progesterone and prolactin (Brisken, 2002). MECs undergo rapid proliferation to increase cell numbers for the formation of side branches and alveolar units required for milk production. Despite significant changes to the epithelium MECs maintain correct cell positioning, which is essential for normal tissue function. Milk produced by alveolar luminal cells is secreted into the lumen by contracting myoepithelial (ME) cells upon the suckling of the nipple-areolar complex.

ME cells are a specialised smooth muscle like epithelial cells with elevated levels of smooth muscle specific contractile proteins such as α -smooth muscle actin (SMA/ACTA2) and cytoskeletal proteins such as keratin 14 and keratin 5. A growing body of evidence suggests that actin cytoskeleton remodelling is essential for smooth muscle cell contractions. Knockout of ACTA2 impaired ME cell contractility and perturbed milk ejection in the lactating mammary gland (Haaksma et al., 2011).

Contractile assemblies of activated bipolar myosin filaments and actin filaments produce contraction by sliding actin filaments relative to one another. Myosin activation is regulated by myosin light chain kinase (MLCK) dependent phosphorylation of the myosin regulatory light chains. The kinase is regulated by the association of Ca^{2+} bound calmodulin (Moore et al., 1987). In ME cells increase in cytosolic Ca^{2+} is known to be dependent on oxytocin activated phospholipase C (PLC) (Nakano et al., 2001).

ME cell contraction is induced by the activation of the oxytocin receptor by the neuropeptide oxytocin via the Rho/Rock/myosin pathway. Mice with oxytocin or oxytocin receptor knockout have impaired lactation (Takayanagi et al., 2005, Nishimori et al., 1996). The subsequent relaxation of ME cells is modulated by α 3 β 1-integrin signalling via the FAK/Rac/PAK pathway (Raymond et al., 2011). Similarly, α 9 β 1 has been shown to inhibit the contraction of airway smooth muscle cells by recruiting SSAT, which inhibits PIP5K conversion to PIP2 (Chen et al., 2012).

Interestingly several studies have shown integrin-ECM interactions mediate smooth muscle cell contractions. In the arterioles, $\alpha4\beta1$ -fibronectin binding activates L-type Ca^{2+} channels via the tyrosine kinase pathway causing the contraction of smooth muscle cells (Waitkus-Edwards et al., 2002). Similarly, myogenic contractions are triggered by the activation of $\alpha5\beta1$ and $\alphaV\beta3$ integrins and the subsequent activation of Ca^{2+} channels (Martinez-Lemus et al., 2005). More recently, $\alpha2\beta1$ integrin has been shown to control airway constriction independent of smooth muscle cell shortening or actin-myosin (Liu et al., 2021). These studies suggest that integrins could also be involved in mediating contractions in the mammary gland.

Moreover, a study by Lineman et al., 2015 showed that MECs can contract even in the absence of oxytocin, suggesting the involvement of other signalling pathways in moderating ME cell contractility. I investigated the hypothesis that $\beta1$ -integrin can induce contractions in the mammary gland independent of oxytocin stimulation. The aim of this chapter was to assess the functional importance of cell positioning and $\beta1$ -integrin in the mammary gland during lactation, using organoid and collagen gel contraction assays.

The work presented in this chapter identifies that $\beta1$ -integrin moderates the expression of certain ME marker genes and that loss of $\beta1$ -integrin affect ME cell contractility. Interestingly, the deletion of $\beta1$ -integrin in luminal (LE) cells also impaired the contraction of mammary tissue, highlighting potential crosstalk between LE and ME cells.

6.2 Results

6.2.1 $\beta1$ -integrin deletion in ME cells impairs its morphology and transcription of ME cell differentiation markers.

MECs from pregnant $\beta1$ -integrin^{fx/fx}: YFP: K14-CreERTM (BK14) mice were cultured for 5 days +/- 4-OHT in 2D to form a monolayer or embedded in Matrigel to form 3D organoids. I initially analysed for changes in ME cell morphology in 2D and 3D culture using IF staining. The area of each cell was calculated from thresholded images. ME cells in 2D culture appeared relaxed with a large surface area, there was no significant difference in ME cell area between WT and $\beta1$ -integrin KO (Figure 47A-B). The analysis of ME cells was limited to cells that were at the centre of the 2D culture to avoid any differences in ME cell area arising from the attachment

of ME cells to the coverslip versus those on top of luminal cells. Interestingly $\beta 1$ -integrin deleted ME cells embedded in Matrigel had a smaller surface area compared to the WT ME cells (Figure 47C-D). The difference in ME cell shape could be due to the absence of integrin-ECM signalling, as study in the drosophila wing has shown cell-ECM interactions mediated by integrins regulates epithelial cell shape change from columnar to cuboidal during morphogenesis (Domínguez-Giménez et al., 2007). Moreover, recent work in the Drosophila follicular epithelium has revealed stress fibres regulated by integrins control epithelial cell shape (Santa-Cruz Mateos et al., 2020).

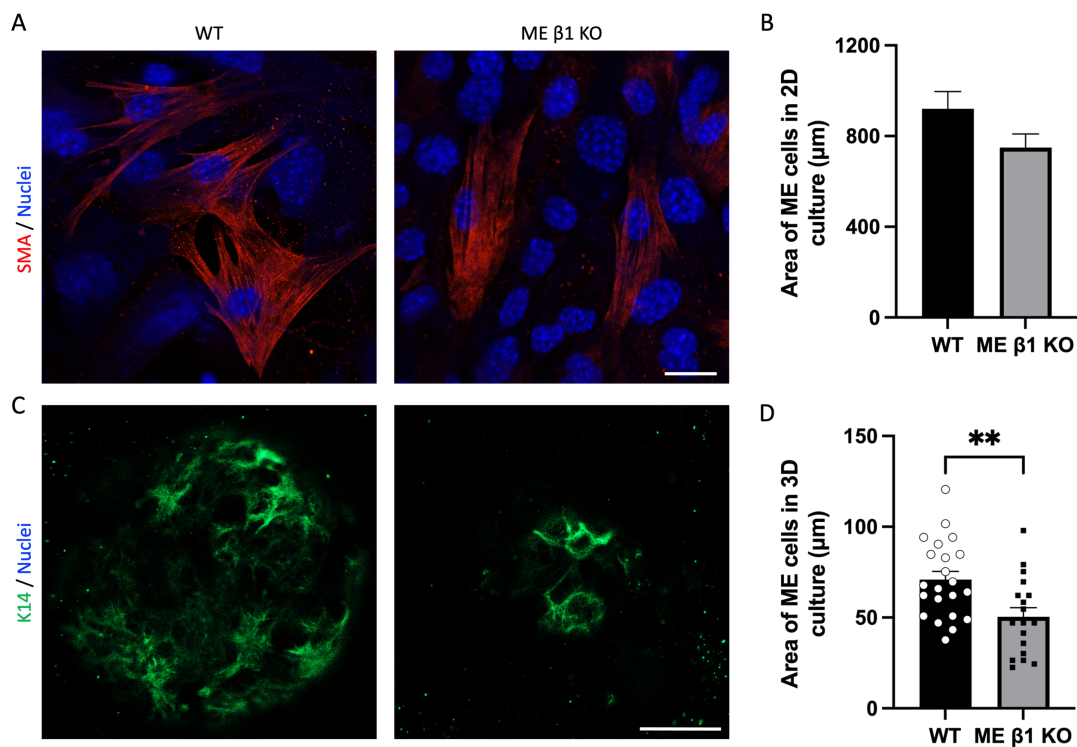


Figure 47: ME $\beta 1$ -integrin^{f/fx} cell area is smaller than WT ME cells in 3D culture. MEC isolated from pregnant BK14 mice were (A) cultured as a monolayer on coverslips or (B) embedded in Matrigel for 5 days +/- 4-OHT. (A) Representative confocal images of MECs stained for SMA (red). Bar: 20 μm . (B) Quantification of average ME cell area in 2D culture from N = 2 independent experiments, 10 ME cells per condition. (C) Representative confocal images of organoids stained for K14 (green). Bar: 20 μm . (D) Quantification of ME area in 3D culture. Minimum N=18 ME cells from N=13 organoids. All data are shown as mean +/- SEM and statistical significant was determined by a Students T-test where **P<0.01.

To test this, I examined ME cell specific markers such as keratin 14 (Krt14), Keratin 5 (Krt5), Tumour related protein 63 (Trp63) and α -smooth muscle actin (ACTA2) at the mRNA level using quantitative PCR. Levels of ACTA2, a smooth muscle contractile protein gene, showed a significant reduction in its expression when β 1-integrin was deleted in ME cells (Figure 48A). However, there was no significant difference in gene expression of the other ME markers (Figure 48A).

Interestingly, deletion of β 1-integrin in virgin ME cells also significantly impaired the expression of the Krt5 gene alongside ACTA2 (Figure 48B). Differences in gene expression between pregnant and virgin samples could be in part due to a smaller proportion of ME cells in pregnant samples making it more difficult to detect slight differences.

Overall, the data suggests that deletion of β 1-integrin in ME cells downregulates expression of some cell specific markers.

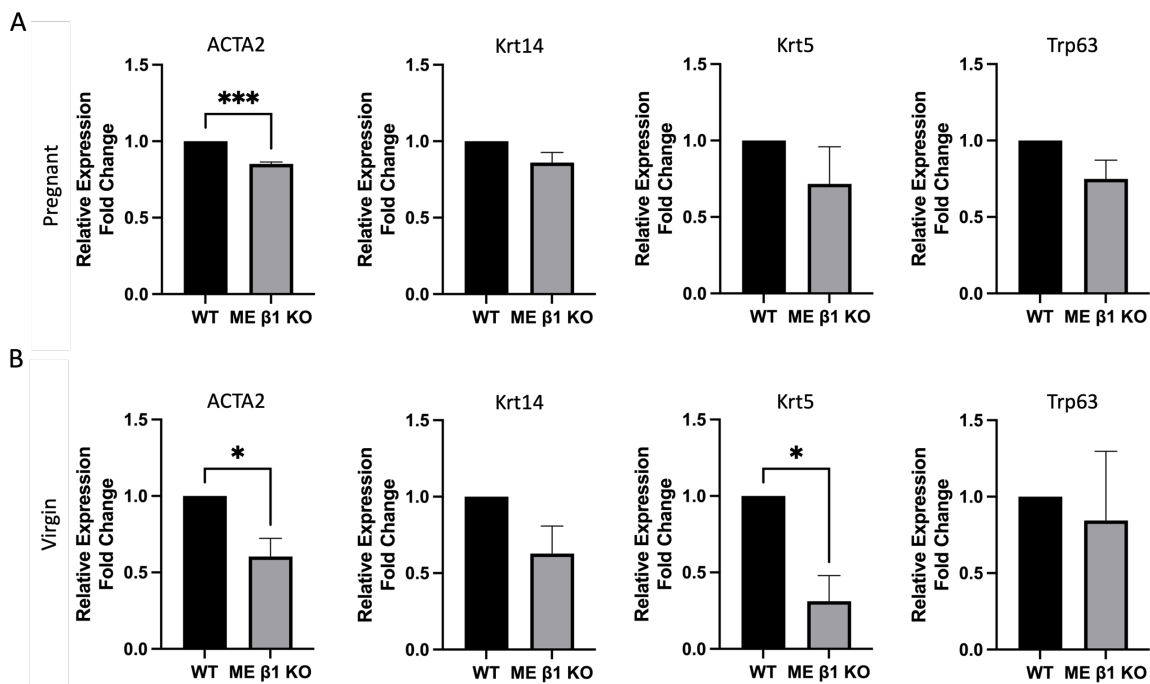


Figure 48: ME β 1-integrin deletion downregulates ACTA2 gene expression. qPCR of ACTA2, Krt14, Krt5 and Trp63 gene in (A) pregnant and (B) virgin MECs cultured in 2D +/- 4-OHT. 3 technical replicates, N = 3 experimental repeats. All data are shown as mean +/- SEM and statistical significant was determined by a Students T-test where *P < 0.05, *** P<0.001.

6.2.2 Deletion of β 1-integrin in ME cells affects its contractility.

MEC organoids were cultured in Matrigel +/- 4-OHT. After four days, the growth media was changed to differentiation media containing the lactogenic hormone prolactin. To induce contractions oxytocin was added to the differentiation media after 24 hours. Organoids were observed using brightfield microscopy after an hour; 120 second videos were captured of each organoid (Figure 49). Organoids not exposed to oxytocin showed relatively static structures, whereas oxytocin treated organoids were contracting (Figure 49). However, fewer ME β 1 KO organoids were contracting compared to WT organoids (Figure 50A). Moreover, the number of contractions per minute was significantly less in ME β 1-integrin KO organoids compared to the WT organoids (Figure 50B).

To better quantify contraction of the organoids the video files were analysed using a custom written MATLAB code and functions (Figure 51A). Pixels from each frame were compared to the subsequent frame to determine moving pixels. A binary map of pixel movement was generated for each frame and averaged to plot organoid contractions over time. This method better accounts for displacement of the organoid that might occur, as it only compares pixels of the organoid and can also detect more subtle changes not visible to the naked eye.

Figure 5B shows the change in organoid area over time of exemplar WT control, WT +oxytocin and ME β 1 KO + oxytocin organoid. The upward line shows an increase in organoid area and downward line shows a decrease in organoid area. There is greater change in the WT organoid area compared to the KO organoid (Figure 51B). The WT control graph highlights the presence of noise as there appears to be slight changes to the organoid area even in the absence of oxytocin. Therefore, this workflow needs further optimisation to reduce the influence of noise on the data.

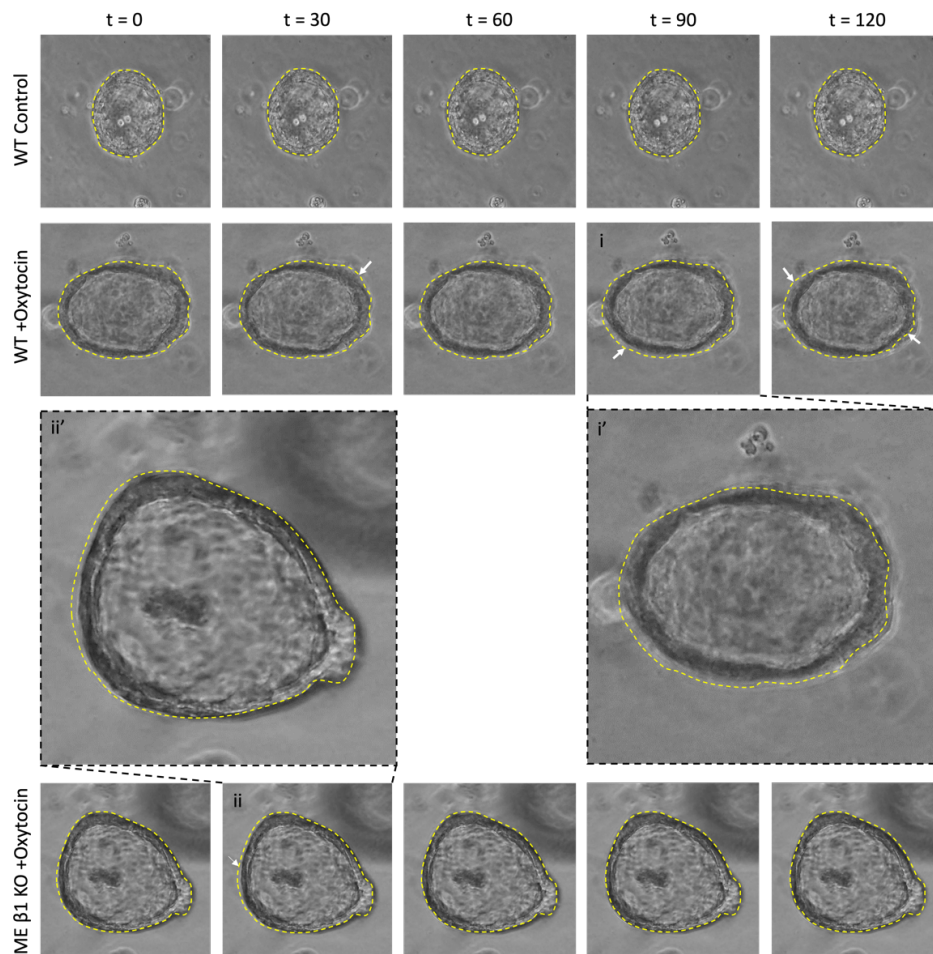


Figure 49: Oxytocin induces contraction of alveolar organoids. MEC isolated from pregnant BK14 mice were embedded in laminin-rich BM (Matrigel) and cultured for 4 days to form organoids before the addition of prolactin. Organoids were either left untreated or oxytocin was added to the media to induce contractions. $t =$ seconds. Yellow dashed line shows the position of the organoid at $t=0$. White arrows indicate areas of contraction.

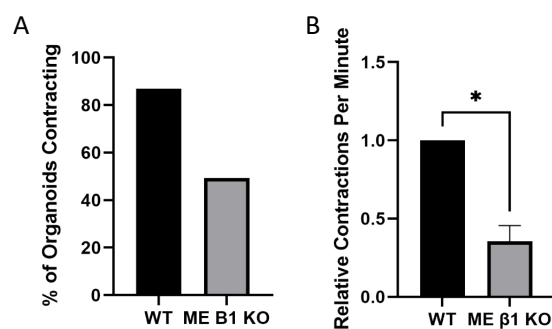


Figure 50: ME β 1-integrin deletion reduces the number of contractions per minute in alveolar organoids. (A) Quantification of the number of organoids contracting. $N = 2$ independent experiments, 15 organoids per condition. (B) Quantification of the number of contractions per minute normalised to the WT. $N = 2$ independent experiments, 15 organoids per condition. All data are shown as mean \pm SEM and statistical significant was determined by a Students T -test where $* P < 0.05$.

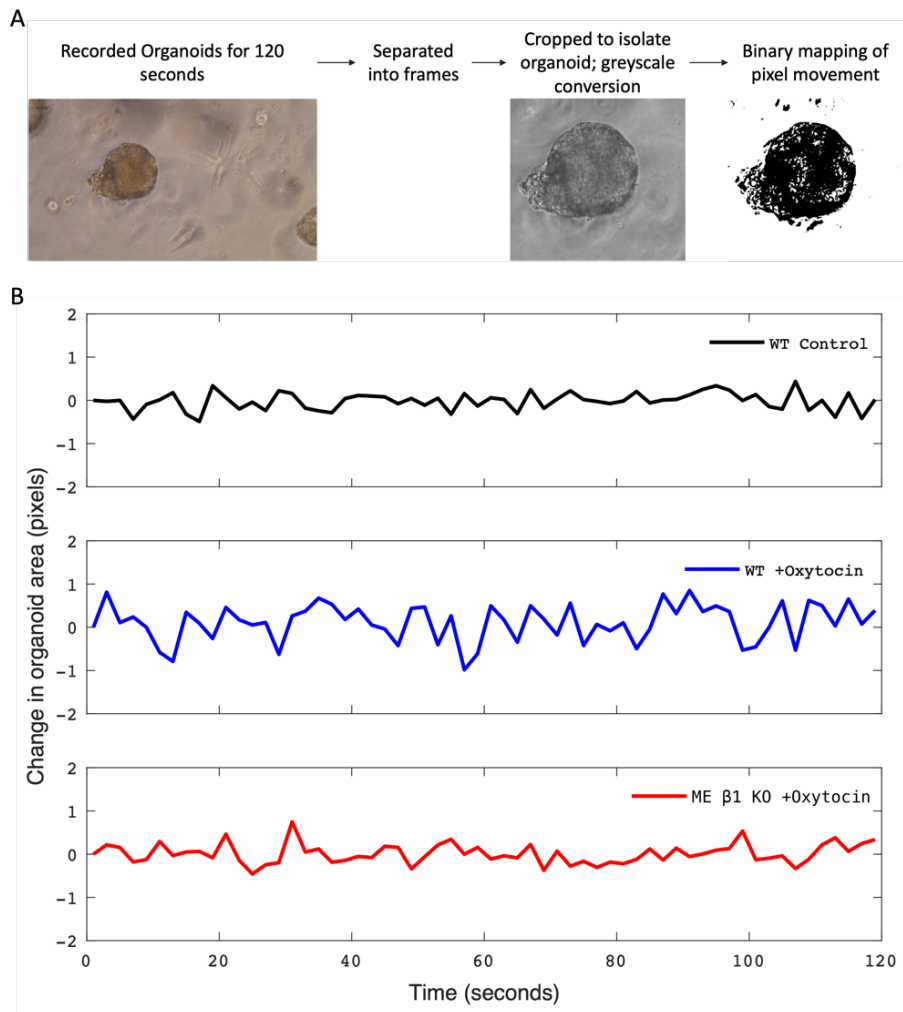


Figure 51: Automatisation of organoid contraction analysis using MATLAB helps detect minute changes not visible to the naked eye. (A) Organoids were recorded for 120 seconds using brightfield microscope. Video files were separated into frames and cropped to isolate the organoid. The images were converted to greyscale and binary mapping of pixel movement was performed. **(B)** Organoid contraction plots of pixel change over time. Black line = WT control, blue line = WT +Oxytocin, red line = ME β 1 KO +Oxytocin.

The lactating organoids were fixed 24 hours after oxytocin addition and stained with K14 to check for ME cells and assess the architectural structure of the organoids. I found that both organoids with and without $\beta 1$ -integrin contained a layer of ME cells on the outside. In WT organoids, ME cells exhibited a spread-out morphology with fine fibres distributed all over the cell (Figure 52A-C). In contrast, $\beta 1$ -integrin KO ME cells were elongated with a smaller surface area and dendritic like projections (Figure 52A-C).

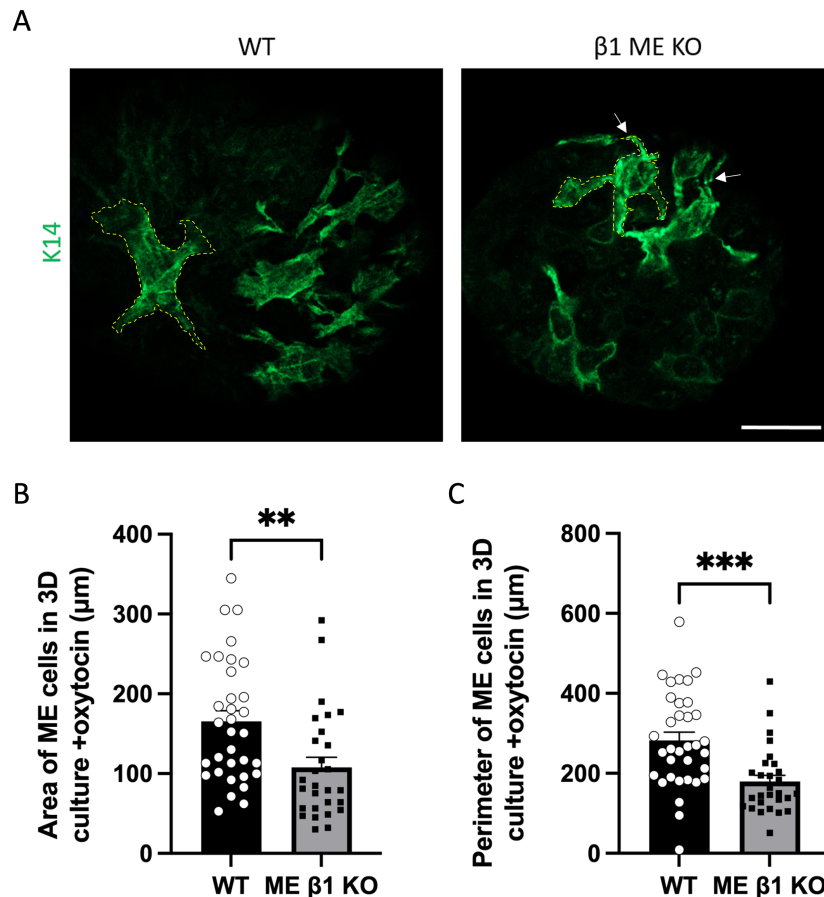


Figure 52: Morphology of ME $\beta 1$ -integrin^{fl/fl} cells is different to WT ME cells when treated with oxytocin. MEC isolated from pregnant BK14 mice were embedded in laminin-rich BM (Matrigel) and cultured for 5 days +/- 4-OHT. **(A)** Representative confocal images of lactating organoids treated with oxytocin and stained for K14 (green). Bar: 20 μm . Arrows indicate dendritic like projections. ME cell shape is outlined by the yellow dashed line. Quantification of **(B)** ME cell area and **(C)** ME cell perimeter. Minimum N = 28 ME cells from 12 organoids. All data are shown as mean +/- SEM and statistical significant was determined by a Students T-test where ** $P < 0.01$, *** $P < 0.001$.

To validate whether the oxytocin used in the above experiments were eliciting contractions of the organoids. MECs were embedded in 80 μ l of collagen and plated on top of a thin layer of set collagen. The collagen gels were imaged on day 5 prior to the addition of oxytocin and again 5, 15, 30, 60 and 180 minutes after oxytocin addition, to calculate the difference in collagen gel area following the addition of oxytocin. At the start of the experiment on day 5, the collagen gels had already shrunk prior to the addition of oxytocin (Figure 53A). This result is in line with a previous study in which they showed ME cells contract even in the absence of oxytocin (Linnemann et al., 2015).

Figure 53B shows the percentage change of the area of the collagen gel with time. Collagen gels treated with oxytocin had a greater reduction in area compared to the gels without oxytocin (Figure 53A-B). Moreover, deletion of β 1-integrin in ME cells reduced the percentage change of the collagen gel area (Figure 53A-B).

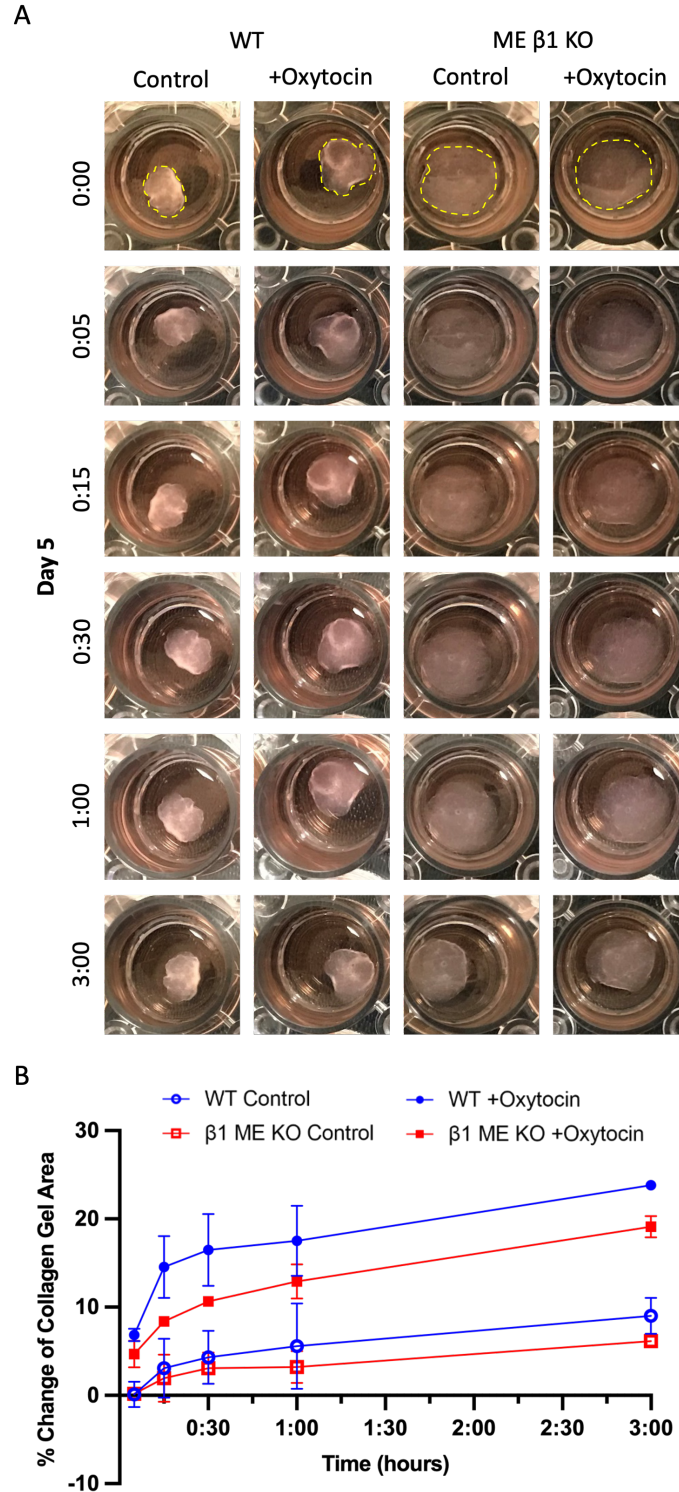


Figure 53: MECs exhibit contractile phenotype even in the absence of oxytocin in collagen gels. MEC isolated from pregnant BK14 mice were embedded in type I collagen and cultured for 5 days +/- 4-OHT. Oxytocin was added to collagen gels on day 5 (0:00) and imaged 5, 15, 30, 60 and 180 minutes after its addition. **(A)** Representative images of collagen gels. Yellow dashed line shows the size of the gel at t=0. **(B)** The percentage change of collagen gel was calculated and plotted over time. Data show mean \pm SEM. N=2 independent experiments.

6.2.3 ME cells cause contraction of collagen gels regardless of oxytocin presence.

To further test if integrins are involved in mediating contractions in the mammary gland I then examined the contractile property of ME cells in the absence of oxytocin using collagen gels. Gels were photographed at the time of plating and again on day 5 once organoids had formed (Figure 54A).

By day 5, WT collagen gels had contracted to about 60% their original size (Figure 54B). However, loss of β 1-integrin in ME cells reduced collagen gel contraction (Figure 54B). I assessed the structure of these organoids, as previous studies have shown MECs cultured in collagen gel can give rise to three types of branched (TDLU-like, thin, star) and non-branched structures (sphere, tubular, multi-sphere) (Linnemann et al., 2015). Majority of the organoids in this study were spherical regardless of β 1-integrin expression in ME cells (Figure 55 A-B). This suggests differences seen in collagen gel contraction are due to β 1-integrin and not due to differences in the organoids structure.

Given qPCR results showed a reduction in the ACTA2 gene in virgin K14 sample, I also assessed contractility of ME cells from virgin mice. WT collagen gels had contracted to a third of their original size which was significantly higher than the β 1-integrin KO sample gels (Figure 56A-B).

These observations suggest that ME cell contractile activity is dependent on β 1-integrin.

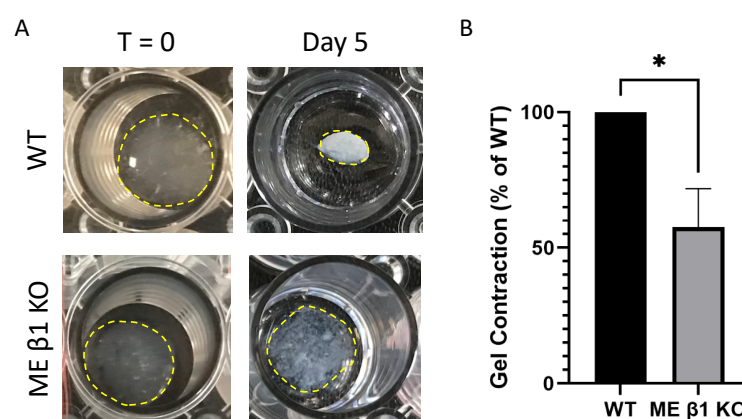


Figure 54: Contractile properties are markedly attenuated in ME β 1-integrin^{f^x/f^x} cells from pregnant mice. MEC isolated from pregnant BK14 mice were embedded in type I collagen and cultured for 5 days +/- 4-OHT. **(A)** Representative images of collagen gels at time of plating (day 0) and time of fixing (day 5). **(B)** Quantification of gel contraction from N = 3 independent experiments. Data is shown as mean +/- SEM and statistical significant was determined by a Students T-test where * P<0.05.

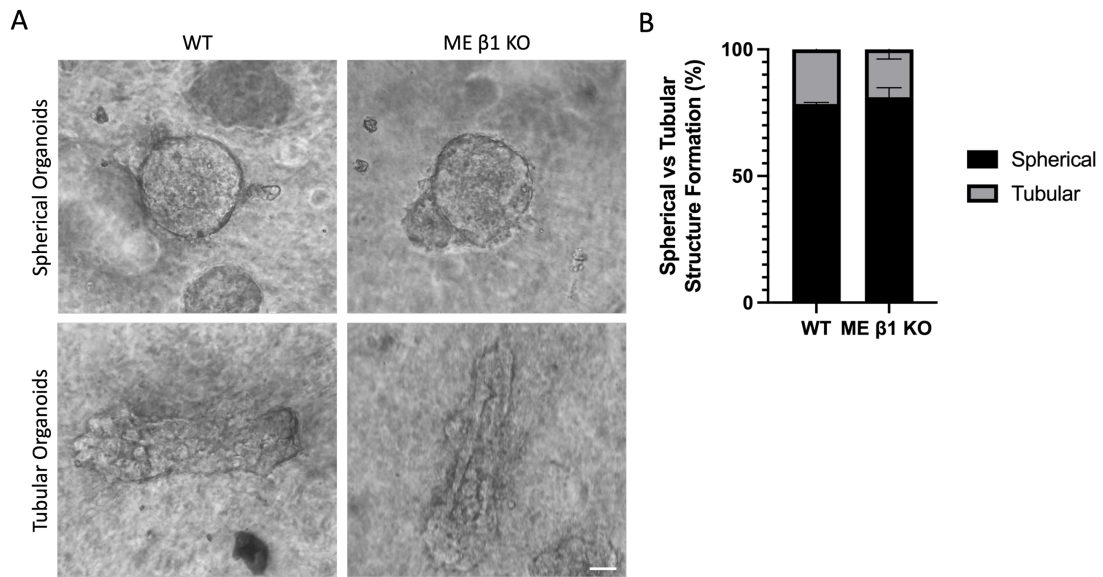


Figure 55: MECs cultured in collagen gel largely formed spherical organoids. MEC isolated from pregnant BK14 mice were embedded in type I collagen and cultured for 5 days +/- 4-OHT. **(A)** Representative brightfield images of spherical and tubular organoids in collagen gel. Bar: 20 μ m. **(B)** Quantification of spherical vs tubular organoid structure. Data show mean \pm SEM. N = 3 independent experiments. Statistical significant was determined by a one way ANOVA.

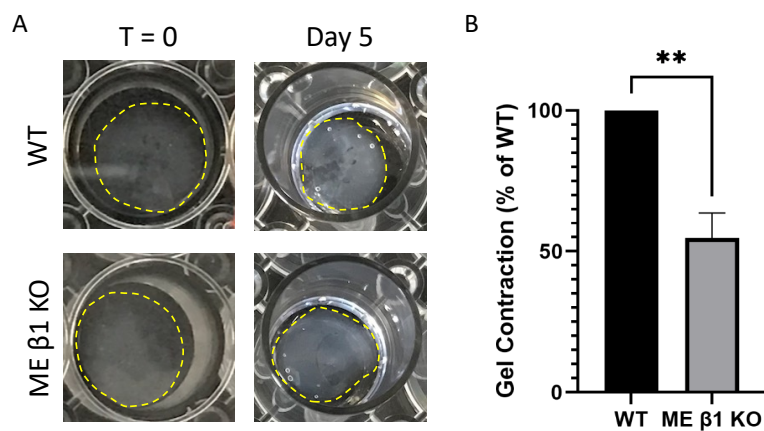


Figure 56: Contractile properties are markedly attenuated in ME β 1-integrin^{fx/fx} cells from virgin mice. MEC isolated from virgin BK14 mice were embedded in type I collagen and cultured for 5 days +/- 4-OHT. **(A)** Representative images of collagen gels at time of plating (day 0) and time of fixing (day 5). **(B)** Quantification of gel contraction from N = 3 independent experiments. Data is shown as mean +/- SEM and statistical significant was determined by a Students T-test where **P<0.01.

6.2.4 Collagen gel contractility is affected by loss of β 1-integrin in LE cells.

Luminal cell-ECM interactions have been shown to enhance expression of genes such as Wnt4 and Rspo-1 (Englund et al., 2021). The products of which then act on ME cells to drive morphogenesis during puberty and pregnancy. Thus, I wanted to assess if LE-ME crosstalk involving integrins plays a role in ME contractions.

MECs from pregnant β 1-integrin^{fx/fx}: YFP: K8-CreERTM (BK8) mice were cultured for 5 days +/- 4-OHT in type I collagen gel to delete β 1-integrin in LE cells. Comparison of the collagen gels on day 5 to the time of plating showed a significant reduction in the size of the WT gels (Figure 57A). Interestingly, compared to the WT, LE β 1-integrin KO collagen gels had a smaller change in gel size (Figure 57B). Assessment of organoid shape revealed no differences between the WT and LE β 1-integrin KO samples (Figure 57C). This suggests that deletion of β 1-integrin in LE cells also affects contractility of alveolar structures.

To investigate whether altered paracrine signalling between LE and ME was affecting functional differentiation of ME cells, I examined the morphology of ME cells using IF staining and mRNA level of ME cell specific markers. IF staining of MECs cultured in 2D and 3D showed no difference in ME area between WT and β 1-integrin LE KO samples (Figure 58A-B, D-E). Similarly, even at the transcription level there was no significant difference in expression of the smooth muscle actin gene, ACTA2, in 2D culture (Figure 58C). However, this result could be due to a smaller proportion of ME cells in pregnant samples making it more difficult to detect slight differences in ACTA2 gene expression. Surprisingly, when treated with oxytocin, the area of ME cells was significantly smaller in LE β 1 KO samples (Figure 58D, F).

Taken together, these data suggest that a paracrine signalling pathway could be modulating ME cell contraction or alternatively LE cells could have contractile properties.

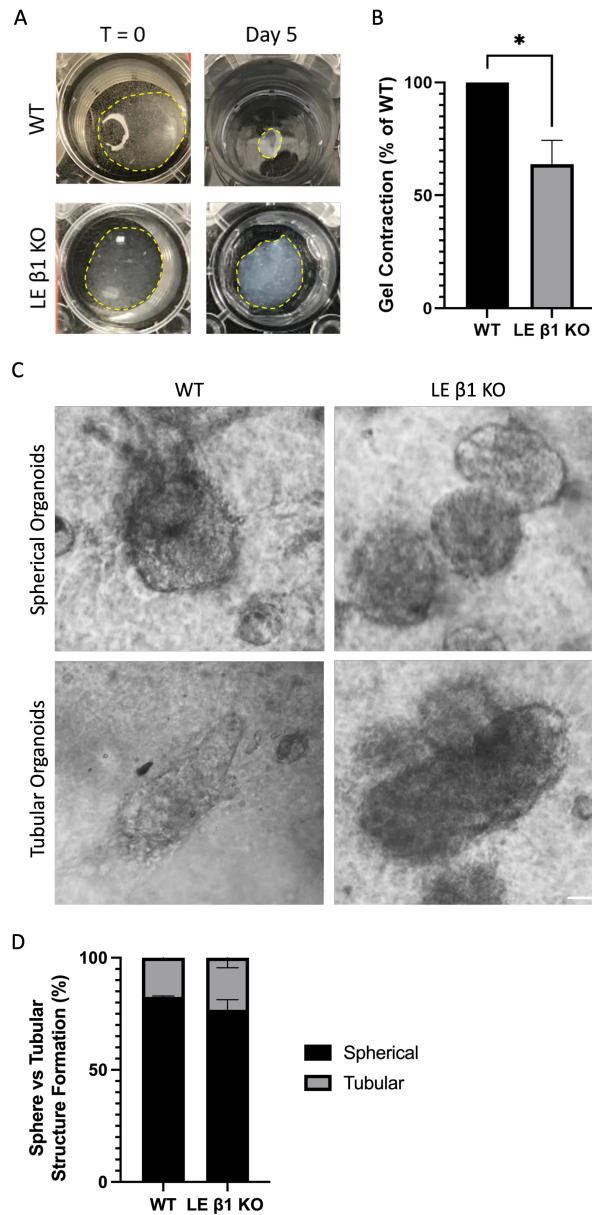


Figure 57: Contractile properties are markedly attenuated in LE $\beta 1$ -integrin^{fl/fl} cells from pregnant mice. MEC isolated from pregnant BK8 mice were embedded in type I collagen and cultured for 5 days +/- 4-OHT. **(A)** Representative images of collagen gels at time of plating (day 0) and time of fixing (day 5). **(B)** Quantification of gel contraction from N = 3 independent experiments. Data is shown as mean +/- SEM and statistical significant was determined by a Students T-test where * P<0.05. **(C)** Representative brightfield images of spherical and tubular organoids in collagen gel. Bar: 20 μ m. **(D)** Quantification of spherical vs tubular organoid structure. N = 3 independent experiments. Data is shown as mean +/- SEM and statistical significant was determined by a one way ANOVA.

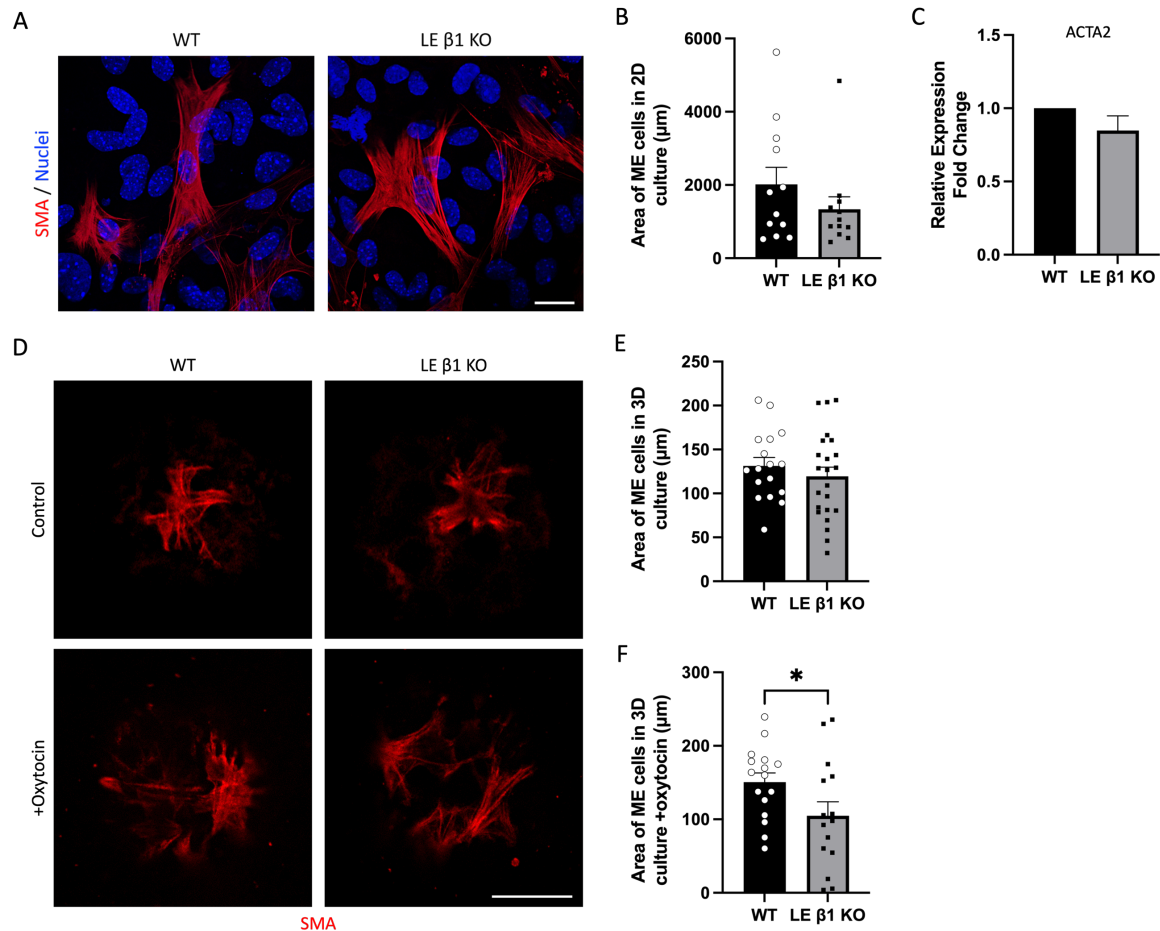


Figure 58: ME cell area is not affected by $\beta 1$ -integrin deletion in LE cells. MEC isolated from pregnant BK8 mice were embedded in type I collagen and cultured for 5 days +/- 4-OHT. **(A)** Representative confocal images of MECs stained for SMA (red). Bar: $20\mu\text{m}$. **(B)** Quantification of ME area in 2D culture. Data show mean \pm SEM. 2D culture: $n = 15$ ME cells. **(C)** qPCR of ACTA2 gene in pregnant MECs cultured in 2D +/- 4-OHT. 3 technical replicates, $N=3$ experimental repeats. **(D)** Representative confocal images of lactating organoids +/- oxytocin, stained for SMA (red). Bar: $20\mu\text{m}$. Quantification of ME area from **(E)** control organoids, minimum $N=17$ ME cells from 13 organoids. **(F)** +oxytocin organoids; minimum $N=15$ ME cells from 10 organoids. All data are shown as mean +/- SEM and statistical significant was determined by a Students T-test where * $P<0.05$.

6.3 Discussion

ME cells play a vital role in ejecting milk during lactation. For normal tissue function, ME cells need contractile activity and to be sat next to the ECM, encompassing LE cells. The mechanisms involved in modulating ME cells contractility are not fully elucidated. The aim of this chapter was to study the role of β 1-integrin in ME cell contractility as it is known to play a key role in other tissues such as the bladder (Yu et al., 2022).

Cell-ECM interactions control cell morphology and gene expression. It was, therefore, important to first determine if there were any differences in ME cell morphology and/or gene expression in the absence of β 1-integrin. The area of ME cells in 2D cultures was reduced, but there was no significant change. However, in 3D culture, the ME cell area was significantly reduced in β 1-integrin KO cells. The difference in ME morphology between 2D and 3D cultures could be due to differences in gene expression between MECs cultured in monolayer compared to cells in 3D culture (Yu et al., 2012). In 2D culture the nuclei of cells are flatter than cells in 3D, therefore the altered nuclear architecture in 2D culture could be affecting gene expression. In this regard, Liu et al., (2022) compared the genomic architecture of mouse hepatocytes cultured in 2D and 3D using in situ Hi-C. They demonstrated growth dimension causes structural changes to the genome some of which are associated with differential gene expression between 2D and 3D cultures (Liu et al., 2022).

Interestingly, gene expression analysis of ME cell markers in 2D culture revealed a downregulation of the ACTA2 gene in pregnant and virgin samples and the Krt5 gene in the virgin samples only. Differential expressions of other genes, such as Krt14 and Trp63, might be present in cells cultured in 3D. Moreover, in α 6 integrin deficient keratinocytes, gene expression of 208 genes was differentially expressed compared to WT, including the downregulation of the SMA gene (Rodius et al., 2007). Thus, it would be interesting to further explore gene expression in ME β 1-integrin KO cells cultured in 3D using Affymetrix oligonucleotide arrays or RNA sequencing.

Previously oxytocin has been used to induce the contraction of a single ME cell (Raymond et al., 2011), as well as in primary organoid cultures (Sumbal et al., 2020, Mroue et al., 2015). In the most recent study, the rate of organoid contraction was determined to be around one

every 10 seconds (Sumbal et al., 2020). However, in this study only a contraction per minute in WT organoids and a contraction every two minutes in ME β 1-Integrin KO organoids was observed. The difference in contraction rates could be due to the number of ME cells encompassing LE cells. Alveolar organoids have significantly fewer ME cells than ductal organoids. Sumbal and colleagues (2020) used ductal organoids, whereas I used alveolar organoids, thus reducing the dynamic shape and size changes of the organoid visible to the human eye. To overcome this issue, I developed a MATLAB code to analyse the organoid contraction video files to quantify contraction. Although mapping pixel movement allows us to detect more minute changes in organoid shape and size, this method also detected noise. The video capturing and analysis workflow needs further optimising as a similar method developed to track and quantify the beating behaviour of cardiac organoids is capable of accurately quantifying 3D cardiac organoid beat rates (Devarasetty et al., 2017).

Studies have shown cells can contract independently of oxytocin, but the mechanism is unclear (Lineman et al., 2015). Given β 1-integrin modulates the contraction of smooth muscle cells in other tissue, I examined ME cell contraction with and without oxytocin using collagen gel contraction assays to test the role of β 1-integrin in ME cell contraction.

Collagen gel contraction assay provides a good model for analysing ME cell contractile ability and the role of integrins on the rate and extent of contraction by measuring the dimensional changes of the collagen gels (Bell et al., 1979). ME cells contracted even in the absence of oxytocin; however, the amount of contraction was significantly less than in oxytocin treated collagen gels. Moreover, deletion of β 1-integrin in ME cells hindered contraction regardless of oxytocin presence. These results are supported by a study in myofibroblasts which showed deletion of β 1-integrin inhibited contraction of the collagen gel matrix (Martin et al., 2016). Focal adhesion and actin stress fibres are required for efficient contractile activity. Downregulation of α -SMA expression in β 1-integrin deficient ME cells leads to a reduction in stress fibres containing α -SMA. This in turn seems to lead to reduced contractility of ME β 1-integrin KO cells. Similar observations were made in vascular smooth muscle cells and mesangial cells after knockdown of α 8-integrin (Marek et al., 2010, Zargham and Thibault, 2006).

Surprisingly, the deletion of β 1-integrin in LE cells also inhibited the contraction of collagen gels. This could be due to paracrine signalling modulating ME cell function, or LE cells could also have contractile properties. However, previously Linnemann et al., 2015 showed that LE cells do not present any contractile activity. To dissect if integrin-mediated paracrine signalling from LE cells controls ME cell function, morphology and gene expression of ME cells were assessed in LE β 1-integrin KO co-cultures. However, there were no significant morphological differences between ME cells in 2D or 3D culture in the absence of β 1-integrin in LE cells. Moreover, there was no difference in the expression of the ACTA2 gene, it would be worth assessing the expression of ACTA2 from a purified population of ME cell in case of subtle differential expression. Surprisingly, in the presence of oxytocin, ME cells had a thinner morphology in the LE β 1-integrin KO organoids. This suggests that LE paracrine signalling could be modulating ME cell function. Secreted ligands, Wnts, have been implicated in various processes in the mammary gland, including stem cell activity by neighbouring LE cells (Rajaram et al., 2015). In the developing kidney, α 3 β 1 integrin regulates Wnt7b transcription in the papilla (Liu et al., 2009). Thus, we propose integrin signalling in LE increases their production of Wnt ligands, which in turn promotes transcription of ME cell-specific genes such as ACTA2 in neighbouring ME cells. However, further functional studies are needed to validate this. Figure 59 summarises the findings in this chapter and shows how cross talk between LE and ME cells could modulate ME cell activity.

Taken together, the data in this chapter provides new insight into the role of β 1-integrin in the contractile activity of ME cells.

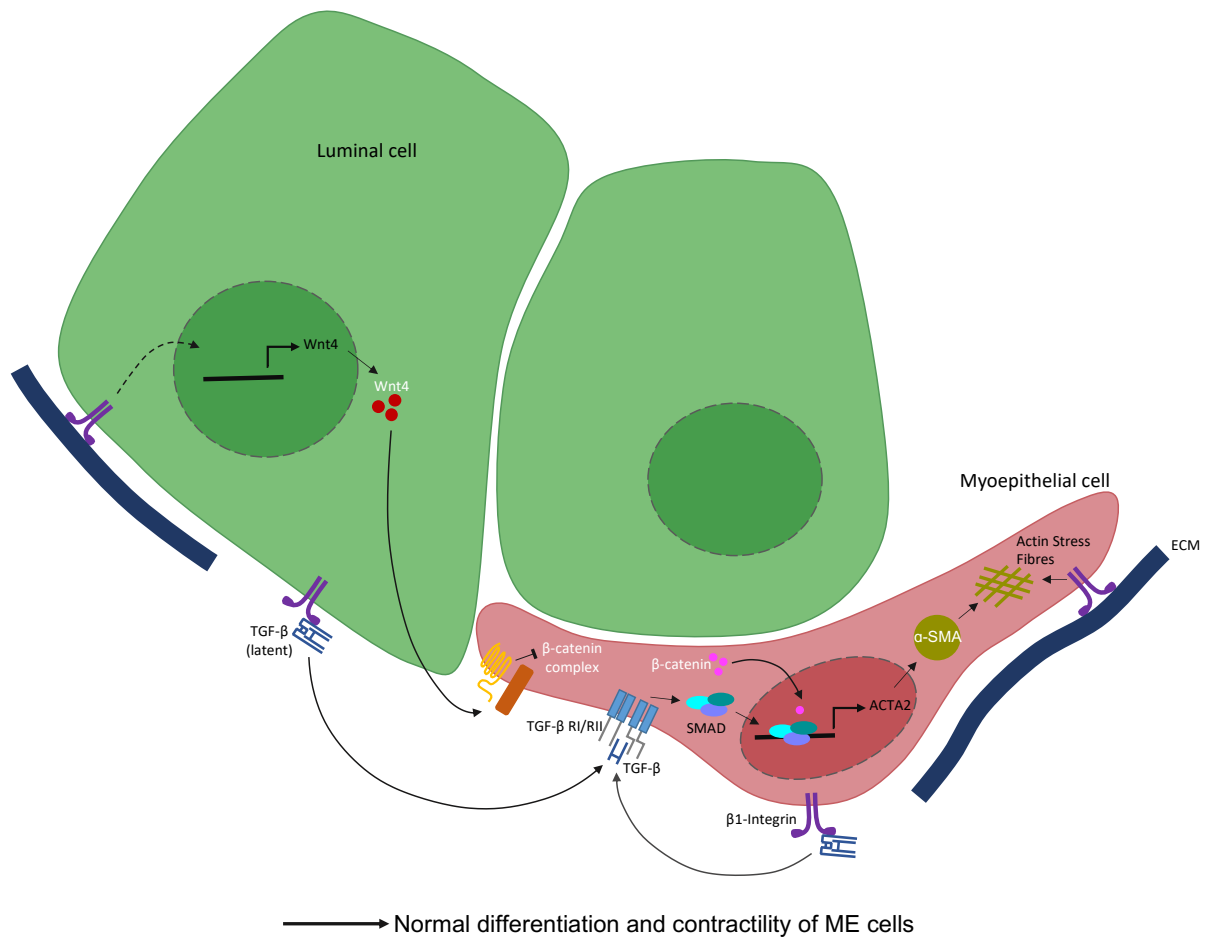


Figure 59: Working model of how integrins modulate differentiation and contractility of ME cells. Schematic showing how ME cell differentiation and contractile activity is modulated by cross talk between LE and ME cells. $\beta 1$ -integrin signalling in LE cells enhances gene expression of Wnt4. The Wnt4 ligand acts on ME cells to inhibit the β -catenin destruction complex, increasing the stabilisation of β -catenin, which in the nucleus activates the transcription of smooth muscle cell specific genes such as ACTA2. Moreover, transcription of the ACTA2 gene is also dependent on TGF- β signalling mediated by integrins such as $\alpha 5\beta 1$ and $\alpha 8\beta 1$. The α -SMA is incorporated into actin stress fibres to give ME cells a strong contractile activity characteristic of smooth muscle cells.

7 General Discussion

7.1 Overview

The focus of this thesis was to understand what drives the spatial organisation of mammary epithelial cells (MECs) in the mammary gland and the mechanisms involved. Identifying the mechanisms involved in positioning MECs is important in breast cancer research, as myoepithelial (ME) cells provide a dynamic barrier capable of restraining invasive luminal (LE) cells and even capturing disseminated cells (Sirka et al., 2018). Therefore, understanding how MECs organise and maintain normal tissue architecture could help elucidate the mechanisms by which this concentric architecture is lost during invasive ductal carcinoma.

Cell sorting is the process through which two or more populations of motile cell sort to form functional tissues. Differences in adhesion are thought to drive the sorting of cells into distinct domains by changing their position relative to each other. An exemplary role of cell sorting in the developmental process is zebrafish gastrulation; internal epiblast cells sort through radial intercalation during the process of epiboly (Kane et al., 2005). Similarly, in the pubertal mammary tissue, intercalation resolves the multilayer epithelium into a bilayer and drives ductal elongation (Neuman et al., 2018). However, even as early as E14, the mammary gland contains a partially segregated population of cells with different induced fates; the outermost cell layer already expresses lower levels of K8 (Wuidart et al., 2018). In the mouse blastocyst, the sorting of progenitor cells feeds back to regulate their cell fate specification (Rossant et al., 2003). Similarly, cell fate specification and tissue patterning of the mammary gland are refined through the interplay of cell positioning during development to achieve inner LE and outer ME configuration. Chimeric recombination model studies have revealed the importance of the stroma and ECM in governing the spatial organisation of the mammary tissue (Cunha et al., 1995, Sakakura et al., 1976).

A recent paper by Cerchiari et al. (2015) elucidated that cell-ECM interactions drive cell sorting and govern tissue architecture in epithelial tissues. However, which ECM adhesion receptor specifically drives cell positioning is unclear. We hypothesised that integrin-mediated affinity to the ECM drives cell positioning as cell-ECM interactions in the mammary

gland are governed mainly by β 1-, β 3- and β 4-integrins. Moreover, MECs express a characteristic set of integrins, which suggests these integrins, and therefore distinct cell-ECM interactions, might have a functional role in MEC sorting (Shehata et al., 2012). β 1-integrin is the most expressed integrin in the mammary gland, and previous studies have shown the importance of this integrin in many aspects of MEC function; therefore, I choose to focus on unravelling the role of this β -integrin in the spatial organisation of the mammary gland. To study this, I used two lineage specific mouse models; β 1-integrin^{fx/fx}: YFP: K14-CreERTM (BK14) and β 1-integrin^{fx/fx}: YFP: K8-CreERTM (BK8). I validated the mouse models showing β 1-integrin gene deletion and protein turnover, specifically in LE or ME cells, following two doses of 4-OHT treatment *in vitro* (chapter 3).

Mammary organoids provide a scalable *in vitro* model that recapitulates *in vivo* tissue architecture and function, making it an ideal model for studying the mechanisms of spatial organisation in the mammary gland. Based on our unpublished TEM data we hypothesise that distinct mechanisms of spatial organisation may exist between the ducts and alveoli in the mammary gland, due to differences in cell-cell adhesion molecules. Desmosomes found between LE and ME cells in ducts could be modulating spatial organisation and maintaining correct cell positioning even in the absence of cell-ECM adhesion. Thus, to define the role of β 1-integrin in the spatial organisation of the mammary gland both ductal (virgin) and alveolar (pregnant) organoids were used to establish how β 1-integrin functions to organise mammary tissue structure independent of cell-cell adhesion.

I first characterised lumen formation in our BK14 and BK8 organoid models, as Bischel and colleagues (2014) have highlighted the importance of including physiologically relevant lumen structures in 3D culture. Moreover, normal mammary tissue function is dependent on a single polarised lumen with the apical surface facing inwards for milk secretion. Previously, Akhtar and Streuli (2013) have shown complete deletion of β 1-integrin lead to inverted polarity and impaired lumen formation *in vitro*. However, *in vivo*, the polarity is rarely inverted despite abnormal lumen formation, and in cases where the apical polarity is inverted, such as invasive micropapillary breast carcinoma (IMBC), the tumour is found in empty stromal space with no ME cells (Hill and Yeh, 2005, Luna-Moré et al., 1994). In chapter 3, I provided evidence for the first time that in the presence of WT ME cells with β 1-integrin, stops the inversion in polarity but does not stop the filled lumen phenotype. Deposition of laminins by WT ME cells could

be engaging with an alternative integrin, such as β 4-integrin in LE β 1-integrin KO cells that provide orientation cues for polarity orientation. Given the control of apical polarity orientation and lumen formation was not the focus of my thesis, I did not investigate this further. However, testing the role of integrins in polarity orientation will potentially expose new targets for diagnosing and treating pathophysiological conditions such as IMBC in the future.

In chapter four, I showed that deletion of β 1-integrin in any one cell lineage was insufficient to disrupt a spatial organisation in ductal or alveolar organoids, suggesting the involvement of an alternative integrin in cell sorting. I used the ECM overlay assay as an alternative method to better study cell-ECM affinity and repulsion at the apical membrane by creating a new ECM interface and subsequently disrupting the apical membrane (Chapter 4). Using this assay, I have shown that ME cell positioning is driven by cues from the ECM received by β 1-integrin. It would be interesting to test if cell sorting is driven by affinity to a specific ECM component. As, even the same integrin, α 3 β 1, can have opposing effects on branching depending on the ECM culture component (Berdichevsky et al., 1994, Stahl et al., 1997). Moreover, temporospatial regulation of ECM components provides specific biochemical and biomechanical signals to support mammary gland morphogenesis and function (Bonnans et al., 2014). For example, β -lactoglobulin and β -casein transcription requires the interaction of MECs with specifically LM-111 for integrin-dependent phosphorylation of the prolactin receptor (Streuli et al., 1995).

Although apically secreted molecules have been shown to control cell rearrangement and intercalation in other organisms, it has not been studied in mammary tissue. In chapter 4, I show for the first time, in the presence of an apical membrane, ME cells fail to position next to the ECM interface despite presence of laminin-rich cues being relayed via β 1-integrin. The apical matrix could be serving a crucial regulatory role in the binding and presenting or sequestering of various cytokines that could be driving ME cells away from the luminal surface (Neptune et al., 2003, Perrimon and Bernfield, 2000). It will be fascinating to decipher the composition of the apical matrix in the mammary gland and the mechanism through which ME cell positioning is driven away from the apical membrane. Moreover, the apical matrix has been identified as a key regulator of lumen expansion. For example, the maturation of the *Drosophila* trachea depends on apically secreted chitin forming fibrils which exerts a

pushing force (Tonning et al., 2005). In vertebrates, lumen formation in developing blood vessels is driven by negatively charged factors such as sialic acid generating an electrostatic repulsion (Tonning et al., 2005, Strilić et al., 2010). Thus, it is possible the apical matrix could play multifaceted role in the spatial organisation of the mammary gland.

The mechanisms by which the concentric preassembled mammary tissue structure is maintained with each oestrous cycle and pregnancy are of great interest. During pubertal branching morphogenesis, the multilayer mammary tissue structures resolve to form inner luminal and outer ME through intercalation (Neuman et al., 2018, Huebner et al., 2016). Studies in *Xenopus* have highlighted the role of cell-ECM affinity in driving cell sorting through intercalation (Marsden and DeSimone, 2001). This mechanism could be conserved in the mammary gland. Other studies in the mammary gland have shown planar oriented division is crucial for epithelial structure as basal cells lacking β 1-integrin have altered cell division orientation resulting in progeny cells being found in the luminal compartment (Taddei et al., 2008, Fankhaenel et al., 2023). This study contributes to this field by showing that both cell movement and oriented cell division might be involved in positioning ME cells next to the ECM. Although it is unclear if both these mechanisms are equally important in driving cell positioning, it will be exciting to determine if cell movement can compensate for aberrant cell division angles in the future.

All the *in vitro* data suggest a potential role for β 4-integrin in driving cell sorting. To better understand the role of cell-ECM affinity in cell sorting, I developed a computational model to run predictive simulations with different integrin expressions (Chapter 5). To date, Cerchiarì et al. (2015) provide the only computational model of mammary gland cell sorting that incorporates differences in cell-ECM adhesion strength between ME and LE cells. However, their model has several limitations, including the use of an overly simplistic description of cell mechanics and the lack of key processes such as cell division. In my model, cellular mechanisms such as cell proliferation and differential integrin expression were incorporated to better reflect *in vivo* conditions. The model was validated by running simulations of β 1-integrin deletion in LE or ME cells to verify the outcome of these with the experimental data. Following this, I ran predictive simulations of different integrin expressions. Deletion of β 4-integrin in LE or ME cells alone was insufficient to disrupt spatial organisation, suggesting there might be functional redundancy between β 1-integrin and β 4-integrin, as deletion of

both integrins in ME cells resulted in no clear sorting of the two cell lineages. Interestingly, the deletion of LE integrins resulted in WT ME cells being positioned near the centre of the organoid, with LE cells encompassing them. Which yet again highlighted the importance of apical polarity in spatial organisation.

ME cells play a vital role in milk ejection during lactation. For normal tissue function, ME cells need contractile activity and to be sat next to the ECM, encompassing LE cells. The mechanisms involved in modulating ME cells contractility are not fully elucidated. This study extends on the published work by Raymond et al. (2011) and shows that β 1-integrin signalling is also involved in moderating ME cell contractility. In contrast to their findings, I showed a difference in ACTA2 and Krt5 gene expression in β 1-integrin KO ME cells. Similar observations of ACTA2 gene downregulation have been made in vascular smooth muscle cells and mesangial cells following the knockdown of α 8-integrin (Marek et al., 2010, Zargham and Thibault, 2006). Our data suggest ME β 1-integrin deletion downregulates the ACTA2 gene reducing α -SMA containing stress fibres and subsequently impairing the contractility of ME β 1-integrin KO cells. Further to this, in chapter 6, I show that loss of integrins in LE cells also affects the contractility of mammary tissue. I hypothesise integrin-mediated paracrine signalling between LE and ME cells could be affecting ME cell contractility through the downregulation of smooth muscle cell markers by Wnt and TGF- β signalling pathways.

7.2 Critical appraisal of key methodology

Although an attempt was made to remove preassembled mammary structures by culturing MECs in 2D, I failed to obtain single cells following trypsinisation and dissociation of the cultures. Moreover, there was also variability in the size of cluster and the number of each cell type between experiments. One way to reduce variability would be to purify populations of ME (CD49^{high} and CD29) and LE (CD24^{high} and EPCAM) cells using FACS and reconstitute them at equal ratios before embedding them in Matrigel. Moreover, using this technique, we could systematically vary the ratio of each cell population to observe any changes in pattern formation (Tordoff et al., 2021).

The experiments to assess repulsion at the apical membrane were done using Eph4 cells and total MECs. It would be interesting to study the activity of each cell population specifically by segregating LE and ME cell populations using FACS. LE and ME cells could then be labelled

with different cell tracker dyes and tracked using live cell imaging to better quantify the number of each cell type that integrates into the Eph4 monolayer and their relative position.

Collagen gel contraction assays are typically one of three types: floating-matrix model, attached-matrix model, and stressed-matrix model. In this study, I used the attached-matrix model as the gels were going to be used for staining thus, they needed to be attached to the coverslips for ease of use. Despite contractions being restricted vertically in an attached-matrix model, I observed contraction of the gels in all directions. This could be due to the collagen gels self-detaching from the coverslip and floating in the media, allowing the gel to contract freely. The floating-matrix model might be a better option to ensure the gels are all released at the same time to avoid any discrepancies. Moreover, I used only change in collagen gel area to quantify contractility, but this does not provide an accurate measurement of the magnitude of cellular contraction. Measurements of the elastic modulus and thickness of the collagen gel will provide a more accurate measure of the cell contraction force (Jin et al., 2015).

7.3 Future work

The work in this thesis suggests β 4-integrin could be involved in driving cell positioning. Development of lineage specific lentiviral vectors or genome editing tools such as zinc finger nucleases would enable us to knockdown β 4-integrin expression in primary MECs alongside β 1-integrin using our existing CreERTM mouse models. This would allow us to examine the effects of deleting both integrins in spatial organisation. If, as predicted by our computational model, we see a disrupted organisation of ME and LE cells following the deletion of both integrins, performing gain-of-function experiments will help validate whether the expression of integrin can rescue cell positioning.

Microinjection of microorganisms into the lumen of gut organoids has been used in several laboratories to study gut microbiota. This technique presents a useful way of accessing and manipulating the apical side of the epithelium by injecting ECM components into the lumen of organoids. However, this technique does present some limitations, such as the number of injections required per organoid or the possibility of ECM components leaking out from the lumen. Alternatively, using the method developed by Co et al., (2019) to engineer apical out

gut organoids could help bypass the need for microinjections. It would be interesting to test if polarity of WT, ME β 1 KO and LE β 1 KO organoids is inverted following dissociation of the organoids embedded in Matrigel, using chelator EDTA to disrupt divalent cation-dependent polymerisation of laminins, and transferring them to suspension culture. Confocal microscopy of organoids fixed and stained from a time course experiment in suspension culture (0, 8, 16, 24, 48, 72 hours) could be used to quantitate lumen formation and polarity orientation. Live imaging of organoids, transduced with LifeAct-mCherry lentivirus and GFP-labelled ME cells, in suspension culture, could also be used to study ME cell movement and visualise apical polarity. Furthermore, the organoids could be resuspended in growth media containing titrated concentrations of ECM components to assess if polarity orientation is matrix specific.

The computational model we have developed in this study has the potential for lots of use and development in the future. For example, our model currently does not have lumen formation encoded, as the mechanisms of lumen formation in the mammary gland are not yet well established. Moreover, lumen formation is a separate process that our model could be used to test different mechanisms and the potential role of integrins in this process.

Transwell migration assays are often used to study the migratory response of cells to chemoattractant such as chemokines and growth factors. To assess if affinity to the ECM drives ME cell positioning via cell migration, transwell assays using WT MEC seeded in the upper chamber and treated with different ECM components in the bottom chamber could be performed. The number of migrated cells can be quantified using crystal violet staining. This assay will also help identify if cell sorting is dependent on a specific $\alpha\beta$ integrin heterodimer. A previous comparison between β 1- and β 3-integrins showed that altered signalling pathways downstream of β -specific integrins controls MEC proliferation and migration (Jeanes et al., 2012). An alternate experiment to study the interplay of oriented cell division and cell migration in the spatial organisation of MECs would be to induce aberrant cell division orientation through knockdown of Annexin A1 using small-hairpin RNA to assess if MEC positioning is impaired or cell migration resolves mispositioned cells (Frankhenal et al., 2023).

In terms of long-term future work, it would be interesting to assess the spatial organisation of the mammary gland *in vivo* using the different mouse models. High resolution 3D imaging of whole-mount mammary tissue will provide a better architectural context of cell positioning

without having to make assumptions, like with thin tissue sections. Further optimisation of whole-mount staining is required to achieve good antibody penetration and better visual clarity whilst imaging.

7.4 Conclusion

In conclusion, in this thesis, I have shown that affinity to the matrix and repulsion at the apical membrane drive ME cell positioning. Moreover, the data indicates some degree of redundancy in MEC integrin function in sorting of the two lineages into inner luminal and outer myoepithelial compartments.

8 References

- AHMADZADEH, H., WEBSTER, M. R., BEHERA, R., JIMENEZ VALENCIA, A. M., WIRTZ, D., WEERARATNA, A. T. & SHENOY, V. B. 2017. Modeling the two-way feedback between contractility and matrix realignment reveals a nonlinear mode of cancer cell invasion. *Proceedings of the National Academy of Sciences*, 114, E1617-E1626.
- AKHTAR, N., MARLOW, R., LAMBERT, E., SCHATZMANN, F., LOWE, E. T., CHEUNG, J., KATZ, E., LI, W., WU, C., DEDHAR, S., NAYLOR, M. J. & STREULI, C. H. 2009. Molecular dissection of integrin signalling proteins in the control of mammary epithelial development and differentiation. *Development*, 136, 1019-27.
- AKHTAR, N. & STREULI, C. H. 2006. Rac1 links integrin-mediated adhesion to the control of lactational differentiation in mammary epithelia. *The Journal of Cell Biology*, 173, 781-793.
- AKHTAR, N. & STREULI, C. H. 2013. An integrin-ILK-microtubule network orients cell polarity and lumen formation in glandular epithelium. *Nat Cell Biol*, 15, 17-27.
- ASZODI, A., HUNZIKER, E. B., BRAKEBUSCH, C. & FASSLER, R. 2003. Beta1 integrins regulate chondrocyte rotation, G1 progression, and cytokinesis. *Genes Dev*, 17, 2465-79.
- ATWELL, K., QIN, Z., GAVAGHAN, D., KUGLER, H., HUBBARD, E. J. A. & OSBORNE, J. M. 2015. Mechano-logical model of C. Elegans germ line suggests feedback on the cell cycle. *Development*, 142, 3902-3911.
- BAO, W. J., THULLBERG, M., ZHANG, H. Q., ONISCHENKO, A. & STROMBLAD, S. 2002. Cell attachment to the extracellular matrix induces proteasomal degradation of p21(CIP1) via Cdc42/Rac1 signaling. *Mol Cell Biol*, 22, 4587-4597.
- BARTON, D. L., HENKES, S., WEIJER, C. J. & SKNEPNEK, R. 2017. Active Vertex Model for cell-resolution description of epithelial tissue mechanics. *PLoS computational biology*, 13, e1005569-e1005569.
- BEITEL, G. J. & KRASNOW, M. A. 2000. Genetic control of epithelial tube size in the Drosophila tracheal system. *Development*, 127, 3271-82.
- BELL, E., IVARSSON, B. & MERRILL, C. 1979. Production of a tissue-like structure by contraction of collagen lattices by human fibroblasts of different proliferative potential in vitro. *Proc Natl Acad Sci U S A*, 76, 1274-8.
- BERDICHEVSKY, F., ALFORD, D., D'SOUZA, B. & TAYLOR-PAPADIMITRIOU, J. 1994. Branching morphogenesis of human mammary epithelial cells in collagen gels. *J Cell Sci*, 107 (Pt 12), 3557-68.
- BERRY, M. G., GUI, G. P., WELLS, C. A. & CARPENTER, R. 2004. Integrin expression and survival in human breast cancer. *Eur J Surg Oncol*, 30, 484-9.
- BISCHOF, I. B. & SCHWARZ, U. S. 2003. Cell organization in soft media due to active mechanosensing. *Proceedings of the National Academy of Sciences*, 100, 9274-9279.
- BOUDREAU, N., SYMPSON, C. J., WERB, Z. & BISSELL, M. J. 1995. Suppression of ICE and apoptosis in mammary epithelial cells by extracellular matrix. *Science*, 267, 891-3.

- BOUSSADIA, O., KUTSCH, S., HIERHOLZER, A., DELMAS, V. & KEMLER, R. 2002. E-cadherin is a survival factor for the lactating mouse mammary gland. *Mech Dev*, 115, 53-62.
- BOX, K., JOYCE, B. W. & DEVENPORT, D. 2019. Epithelial geometry regulates spindle orientation and progenitor fate during formation of the mammalian epidermis. *Elife*, 8.
- BRISKEN, C. 2002. Hormonal control of alveolar development and its implications for breast carcinogenesis. *J Mammary Gland Biol Neoplasia*, 7, 39-48.
- BRISKEN, C. & O'MALLEY, B. 2010. Hormone action in the mammary gland. *Cold Spring Harb Perspect Biol*, 2, a003178.
- BRIZZI, M. F., TARONE, G. & DEFILIPPI, P. 2012. Extracellular matrix, integrins, and growth factors as tailors of the stem cell niche. *Current Opinion in Cell Biology*, 24, 645-651.
- BRODLAND, G. W. 2002. The Differential Interfacial Tension Hypothesis (DITH): a comprehensive theory for the self-rearrangement of embryonic cells and tissues. *J Biomech Eng*, 124, 188-97.
- BRODLAND, G. W. 2015. How computational models can help unlock biological systems. *Seminars in Cell & Developmental Biology*, 47-48, 62 - 73.
- BRYANT, D. M., ROIGNOT, J., DATTA, A., OVEREEM, A. W., KIM, M., YU, W., PENG, X., EASTBURN, D. J., EWALD, A. J., WERB, Z. & MOSTOV, K. E. 2014. A molecular switch for the orientation of epithelial cell polarization. *Dev Cell*, 31, 171-87.
- BUI, T., GU, Y., ANCOT, F., SANGUIN-GENDREAU, V., ZUO, D. & MULLER, W. J. 2022. Emergence of $\beta 1$ integrin-deficient breast tumours from dormancy involves both inactivation of p53 and generation of a permissive tumour microenvironment. *Oncogene*, 41, 527-537.
- BULL, J. A., MECH, F., QUAISER, T., WATERS, S. L. & BYRNE, H. M. 2020. Mathematical modelling reveals cellular dynamics within tumour spheroids. *PLoS computational biology*, 16, e1007961-e1007961.
- BÖHMER, R.-M., SCHARF, E. & ASSOIAN, R. K. 1996. Cytoskeletal integrity is required throughout the mitogen stimulation phase of the cell cycle and mediates the anchorage-dependent expression of cyclin D1. *Mol Biol Cell*, 7, 101-111.
- CENTONZE, A., LIN, S., TIKA, E., SIFRIM, A., FIORAMONTI, M., MALFAIT, M., SONG, Y., WUIDART, A., VAN HERCK, J., DANNAU, A., BOUVENCOURT, G., DUBOIS, C., DEDONCKER, N., SAHAY, A., DE MAERTELAER, V., SIEBEL, C. W., VAN KEYMEULEN, A., VOET, T. & BLANPAIN, C. 2020. Heterotypic cell-cell communication regulates glandular stem cell multipotency. *Nature*, 584, 608-613.
- CERCHIARI, A. E., GARBE, J. C., JEE, N. Y., TODHUNTER, M. E., BROADERS, K. E., PEEHL, D. M., DESAI, T. A., LABARGE, M. A., THOMSON, M. & GARTNER, Z. J. 2015. A strategy for tissue self-organization that is robust to cellular heterogeneity and plasticity. *Proc Natl Acad Sci U S A*, 112, 2287-92.
- CHAIGNE, A., CAMPILLO, C., GOV, N. S., VOITURIEZ, R., AZOURY, J., UMAÑA-DIAZ, C., ALMONACID, M., QUEGUINER, I., NASSOY, P., SYKES, C., VERLHAC, M.-H. & TERRET, M.-E. 2013. A soft cortex is essential for asymmetric spindle positioning in mouse oocytes. *Nat Cell Biol*. LONDON: LONDON: NATURE PUBLISHING GROUP.

- CHANSON, L., BROWNFIELD, D., GARBE, J. C., KUHN, I., STAMPFER, M. R., BISSELL, M. J. & LABARGE, M. A. 2011. Self-organization is a dynamic and lineage-intrinsic property of mammary epithelial cells. *Proc Natl Acad Sci U S A*, 108, 3264-9.
- CHEN, C., KUDO, M., RUTAGANIRA, F., TAKANO, H., LEE, C., ATAKILIT, A., ROBINETT, K. S., UEDE, T., WOLTERS, P. J., SHOKAT, K. M., HUANG, X. & SHEPPARD, D. 2012. Integrin $\alpha 9\beta 1$ in airway smooth muscle suppresses exaggerated airway narrowing. *J Clin Invest*, 122, 2916-27.
- CHI, X., MICHOS, O., SHAKYA, R., RICCIO, P., ENOMOTO, H., LICHT, J. D., ASAI, N., TAKAHASHI, M., OHGAMI, N., KATO, M., MENDELSON, C. & COSTANTINI, F. 2009. Ret-dependent cell rearrangements in the Wolffian duct epithelium initiate ureteric bud morphogenesis. *Dev Cell*, 17, 199-209.
- CHI, Y., CHEN, Y., JIANG, W., HUANG, W., OUYANG, M., LIU, L., PAN, Y., LI, J., QU, X., LIU, H., LIU, C., DENG, L., QIN, X. & XIANG, Y. 2022. Deficiency of Integrin $\beta 4$ Results in Increased Lung Tissue Stiffness and Responds to Substrate Stiffness via Modulating RhoA Activity. *Front Cell Dev Biol*, 10, 845440.
- CHICHE, A., MOUMEN, M., PETIT, V., JONKERS, J., MEDINA, D., DEUGNIER, M.-A., FARALDO, M. M. & GLUKHOVA, M. A. 2013. Somatic loss of p53 leads to stem/progenitor cell amplification in both mammary epithelial compartments, basal and luminal. *STEM CELLS*, 31, 1857-1867.
- CHUNG, J., BACHELDER, R. E., LIPSCOMB, E. A., SHAW, L. M. & MERCURIO, A. M. 2002. Integrin ($\alpha 6\beta 4$) regulation of eIF-4E activity and VEGF translation : a survival mechanism for carcinoma cells. *The Journal of Cell Biology*, 158, 165-174.
- CICALESE, A., BONIZZI, G., PASI, C. E., FARETTA, M., RONZONI, S., GIULINI, B., BRISKEN, C., MINUCCI, S., DI FIORE, P. P. & PELICCI, P. G. 2009. The tumor suppressor p53 regulates polarity of self-renewing divisions in mammary stem cells. *Cell*, 138, 1083-95.
- CONRAD, L., RUNSER, S. V. M., FERNANDO GÓMEZ, H., LANG, C. M., DUMOND, M. S., SAPALA, A., SCHAUMANN, L., MICHOS, O., VETTER, R. & IBER, D. 2021. The biomechanical basis of biased epithelial tube elongation in lung and kidney development. *Development*, 148.
- COOPER, F., BAKER, R., BERNABEU, M. & BORDAS, R. 2020. Chaste: Cancer, Heart and Soft Tissue Environment. *Journal of Open Source Software*, 5, 1848.
- CUNHA, G. R., YOUNG, P., CHRISTOV, K., GUZMAN, R., NANDI, S., TALAMANTES, F. & THORDARSON, G. 1995. Mammary phenotypic expression induced in epidermal cells by embryonic mammary mesenchyme. *Acta Anat (Basel)*, 152, 195-204.
- DANIEL, C. W., DE OME, K. B., YOUNG, J. T., BLAIR, P. B. & FAULKIN, L. J., JR. 1968. The in vivo life span of normal and preneoplastic mouse mammary glands: a serial transplantation study. *Proc Natl Acad Sci U S A*, 61, 53-60.
- DANIEL, C. W., STRICKLAND, P. & FRIEDMANN, Y. 1995. Expression and Functional Role of E- and P-Cadherins in Mouse Mammary Ductal Morphogenesis and Growth. *Dev Biol*, 169, 511-519.

- DAWSON, C. A., MUELLER, S. N., LINDEMAN, G. J., RIOS, A. C. & VISVADER, J. E. 2021. Intravital microscopy of dynamic single-cell behavior in mouse mammary tissue. *Nat Protoc*, 16, 1907-1935.
- DEBNATH, J., MILLS, K. R., COLLINS, N. L., REGINATO, M. J., MUTHUSWAMY, S. K. & BRUGGE, J. S. 2002. The Role of Apoptosis in Creating and Maintaining Luminal Space within Normal and Oncogene-Expressing Mammary Acini. *Cell*, 111, 29-40.
- DELEON, O., PUGLISE, J. M., LIU, F., SMITS, J., TER BEEST, M. B. & ZEGERS, M. M. 2012. Pak1 regulates the orientation of apical polarization and lumen formation by distinct pathways. *PLoS One*, 7, e41039.
- DEVARASETTY, M., FORSYTHE, S., SHUPE, T. D., SOKER, S., BISHOP, C. E., ATALA, A. & SKARDAL, A. 2017. Optical Tracking and Digital Quantification of Beating Behavior in Bioengineered Human Cardiac Organoids. *Biosensors (Basel)*, 7.
- DIAZ, L. K., CRISTOFANILLI, M., ZHOU, X., WELCH, K. L., SMITH, T. L., YANG, Y., SNEIGE, N., SAHIN, A. A. & GILCREASE, M. Z. 2005. Beta4 integrin subunit gene expression correlates with tumor size and nuclear grade in early breast cancer. *Mod Pathol*, 18, 1165-75.
- DIAZ-DE-LA-LOZA, M. D., RAY, R. P., GANGULY, P. S., ALT, S., DAVIS, J. R., HOPPE, A., TAPON, N., SALBREUX, G. & THOMPSON, B. J. 2018. Apical and Basal Matrix Remodeling Control Epithelial Morphogenesis. *Dev Cell*, 46, 23-39.e5.
- DOMÍNGUEZ-GIMÉNEZ, P., BROWN, N. H. & MARTÍN-BERMUDO, M. D. 2007. Integrin-ECM interactions regulate the changes in cell shape driving the morphogenesis of the *Drosophila* wing epithelium. *J Cell Sci*, 120, 1061-71.
- DORNIER, E., RABAS, N., MITCHELL, L., NOVO, D., DHAYADE, S., MARCO, S., MACKAY, G., SUMPTON, D., PALLARES, M., NIXON, C., BLYTH, K., MACPHERSON, I. R., RAINERO, E. & NORMAN, J. C. 2017. Glutaminolysis drives membrane trafficking to promote invasiveness of breast cancer cells. *Nat Commun*, 8, 2255.
- EMERMAN, J. T. & VOGL, A. W. 1986. Cell size and shape changes in the myoepithelium of the mammary gland during differentiation. *Anat Rec*, 216, 405-15.
- ENGLUND, J. I., BUI, H., DINÇ, D. D., PAAVOLAINEN, O., MCKENNA, T., LAITINEN, S., MUNNE, P., KLEFSTRÖM, J., PEUHU, E. & KATAJISTO, P. 2022. Laminin matrix adhesion regulates basal mammary epithelial cell identity. *J Cell Sci*, 135.
- ENGLUND, J. I., RITCHIE, A., BLAAS, L., COJOC, H., PENTINMIKKO, N., DÖHLA, J., IQBAL, S., PATARROYO, M. & KATAJISTO, P. 2021. Laminin alpha 5 regulates mammary gland remodeling through luminal cell differentiation and Wnt4-mediated epithelial crosstalk. *Development*, 148.
- EWALD, A. J., HUEBNER, R. J., PALSDOTTIR, H., LEE, J. K., PEREZ, M. J., JORGENS, D. M., TAUSCHER, A. N., CHEUNG, K. J., WERB, Z. & AUER, M. 2012. Mammary collective cell migration involves transient loss of epithelial features and individual cell migration within the epithelium. *J Cell Sci*, 125, 2638-54.
- FANKHAENEL, M., HASHEMI, F. S. G., MOURAO, L., LUCAS, E., HOSAWI, M. M., SKIPP, P., MORIN, X., SCHEELE, C. & ELIAS, S. 2023. Annexin A1 is a polarity cue that directs

- mitotic spindle orientation during mammalian epithelial morphogenesis. *Nat Commun*, 14, 151.
- FARRELLY, N., LEE, Y.-J., OLIVER, J., DIVE, C. & STREULI, C. H. 1999. Extracellular Matrix Regulates Apoptosis in Mammary Epithelium through a Control on Insulin Signaling. *J Cell Biol*, 144, 1337-1347.
- FATA, J. E., CHAUDHARY, V. & KHOKHA, R. 2001. Cellular turnover in the mammary gland is correlated with systemic levels of progesterone and not 17beta-estradiol during the estrous cycle. *Biol Reprod*, 65, 680-8.
- FATTAH, A. R. A., DAZA, B., RUSTANDI, G., BERROCAL-RUBIO, M., GORISSEN, B., POOVATHINGAL, S., DAVIE, K., BARRASA-FANO, J., CÓNDROR, M., CAO, X., ROSENZWEIG, D. H., LEI, Y., FINNELL, R., VERFAILLIE, C., SAMPAOLESI, M., DEDECKER, P., VAN OOSTERWYCK, H., AERTS, S. & RANGA, A. 2021. Actuation enhances patterning in human neural tube organoids. *Nat Commun*, 12, 3192.
- FINEGAN, T. M., HERVIEUX, N., NESTOR-BERGMANN, A., FLETCHER, A. G., BLANCHARD, G. B. & SANSON, B. 2019a. The tricellular vertex-specific adhesion molecule sidekick facilitates polarised cell intercalation during drosophila axis extension.
- FINEGAN, T. M., NA, D., CAMMAROTA, C., SKEETERS, A. V., NÁDASI, T. J., DAWNEY, N. S., FLETCHER, A. G., OAKES, P. W. & BERGSTRALH, D. T. 2019b. Tissue tension and not interphase cell shape determines cell division orientation in the Drosophila follicular epithelium. *The EMBO Journal*, 38, e100072.
- FUCHS, Y. & STELLER, H. 2011. Programmed Cell Death in Animal Development and Disease. *Cell*, 147, 742-758.
- GALLE, J., LOEFFLER, M. & DRASDO, D. 2005. Modeling the effect of deregulated proliferation and apoptosis on the growth dynamics of epithelial cell populations in vitro. *Biophys J*, 88, 62-75.
- GARY, R. M., CHRISTOPHER, J. A., MIGUEL, O. B., RAFEL, B., JONATHAN, C., ALBERTO, C., YOHAN, D., SARA-JANE, D., ALEXANDER, G. F., DANIEL, G. H., MEGAN, E. M., JAMES, M. O., PRAS, P., JOE, P.-F., JAMES, S., NEJIB, Z. & DAVID, J. G. 2013. Chaste: An Open Source C++ Library for Computational Physiology and Biology: e1002970. *PLoS computational biology*, 9.
- GE, Y., LI, F., HE, Y., CAO, Y., GUO, W., HU, G., LIU, J. & FU, S. 2022. L-arginine stimulates the proliferation of mouse mammary epithelial cells and the development of mammary gland in pubertal mice by activating the GPRC6A/PI3K/AKT/mTOR signalling pathway. *J Anim Physiol Anim Nutr (Berl)*, 106, 1383-1395.
- GEIGER, B., SPATZ, J. P. & BERSHADSKY, A. D. 2009. Environmental sensing through focal adhesions. *Nat Rev Mol Cell Biol*, 10, 21-33.
- GERMANO, D. P. J. & OSBORNE, J. M. 2021. A mathematical model of cell fate selection on a dynamic tissue. *J Theor Biol*, 514, 110535-110535.
- GILBERT, P. M., HAVENSTRITE, K. L., MAGNUSSON, K. E. G., SACCO, A., LEONARDI, N. A., KRAFT, P., NGUYEN, N. K., THRUN, S., LUTOLF, M. P. & BLAU, H. M. 2010. Substrate Elasticity Regulates Skeletal Muscle Stem Cell Self-Renewal in Culture. *Science*, 329, 1078-1081.

- GODWIN, S., WARD, D., PEDONE, E., HOMER, M., FLETCHER, A. G. & MARUCCI, L. 2017. An extended model for culture-dependent heterogenous gene expression and proliferation dynamics in mouse embryonic stem cells.
- GONZALEZ, M. A., PINDER, S. E., WENCYK, P. M., BELL, J. A., ELSTON, C. W., NICHOLSON, R. I., ROBERTSON, J. F., BLAMEY, R. W. & ELLIS, I. O. 1999. An immunohistochemical examination of the expression of E-cadherin, alpha- and beta/gamma-catenins, and alpha2- and beta1-integrins in invasive breast cancer. *J Pathol*, 187, 523-9.
- GROSSMANN, J., WALTHER, K., ARTINGER, M., KIESSLING, S. & SCHÖLMERICH, J. 2001. Apoptotic signaling during initiation of detachment-induced apoptosis ("anoikis") of primary human intestinal epithelial cells. *Cell Growth Differ*, 12, 147-55.
- HAAKSMA, C. J., SCHWARTZ, R. J. & TOMASEK, J. J. 2011. Myoepithelial cell contraction and milk ejection are impaired in mammary glands of mice lacking smooth muscle alpha-actin. *Biol Reprod*, 85, 13-21.
- HART, K. C., TAN, J., SIEMERS, K. A., SIM, J. Y., PRUITT, B. L., NELSON, W. J. & GLOERICH, M. 2017. E-cadherin and LGN align epithelial cell divisions with tissue tension independently of cell shape. *Proc Natl Acad Sci U S A*, 114, E5845-e5853.
- HILL, C. B. & YEH, I. T. 2005. Myoepithelial cell staining patterns of papillary breast lesions: from intraductal papillomas to invasive papillary carcinomas. *Am J Clin Pathol*, 123, 36-44.
- HOGG, N. A., HARRISON, C. J. & TICKLE, C. 1983. Lumen formation in the developing mouse mammary gland. *J Embryol Exp Morphol*, 73, 39-57.
- HUEBNER, R. J., LECHLER, T. & EWALD, A. J. 2014. Developmental stratification of the mammary epithelium occurs through symmetry-breaking vertical divisions of apically positioned luminal cells. *Development*, 141, 1085-1094.
- HUEBNER, R. J., NEUMANN, N. M. & EWALD, A. J. 2016. Mammary epithelial tubes elongate through MAPK-dependent coordination of cell migration. *Development*, 143, 983-993.
- HUMPHRIES, J. D., BYRON, A. & HUMPHRIES, M. J. 2006. Integrin ligands at a glance. *Journal of Cell Science*, 119, 3901-3903.
- ISHIDA, S., TANAKA, R., YAMAGUCHI, N., OGATA, G., MIZUTANI, T., KAWABATA, K. & HAGA, H. 2014. Epithelial sheet folding induces lumen formation by Madin-Darby canine kidney cells in a collagen gel. *PLoS One*, 9, e99655.
- JAYADEV, R. & SHERWOOD, D. R. 2017. Basement membranes. *Curr Biol*, 27, R207-r211.
- JAŻWIŃSKA, A., RIBEIRO, C. & AFFOLTER, M. 2003. Epithelial tube morphogenesis during *Drosophila* tracheal development requires Piopio, a luminal ZP protein. *Nat Cell Biol*, 5, 895-901.
- JEANES, A. I., WANG, P., MORENO-LAYSECA, P., PAUL, N., CHEUNG, J., TSANG, R., AKHTAR, N., FOSTER, F. M., BRENNAN, K. & STREULI, C. H. 2012. Specific beta-containing integrins exert differential control on proliferation and two-dimensional collective cell migration in mammary epithelial cells. *J Biol Chem*, 287, 24103-12.

- JI, H., GOODE, R. J. A., VAILLANT, F., MATHIVANAN, S., KAPP, E. A., MATHIAS, R. A., LINDEMAN, G. J., VISVADER, J. E. & SIMPSON, R. J. 2011. Proteomic profiling of secretome and adherent plasma membranes from distinct mammary epithelial cell subpopulations. *Proteomics*, 11, 4029-4039.
- JONJIC, N., LUCIN, K., KRSTULJA, M., ITERNICKA, Z. & MUSTAC, E. 1993. Expression of beta-1 integrins on tumor cells of invasive ductal breast carcinoma. *Pathol Res Pract*, 189, 979-84.
- KANE, D. A., MCFARLAND, K. N. & WARGA, R. M. 2005. Mutations in half baked/E-cadherin block cell behaviors that are necessary for teleost epiboly. *Development*, 132, 1105-16.
- KERMAN, B. E., CHESHIRE, A. M., MYAT, M. M. & ANDREW, D. J. 2008. Ribbon modulates apical membrane during tube elongation through Crumbs and Moesin. *Dev Biol*, 320, 278-88.
- KLINOWSKA, T. C., ALEXANDER, C. M., GEORGES-LABOUESSE, E., VAN DER NEUT, R., KREIDBERG, J. A., JONES, C. J., SONNENBERG, A. & STREULI, C. H. 2001. Epithelial development and differentiation in the mammary gland is not dependent on alpha 3 or alpha 6 integrin subunits. *Dev Biol*, 233, 449-67.
- KOUKOULIS, G. K., VIRTANEN, I., KORHONEN, M., LAITINEN, L., QUARANTA, V. & GOULD, V. E. 1991. Immunohistochemical localization of integrins in the normal, hyperplastic, and neoplastic breast. Correlations with their functions as receptors and cell adhesion molecules. *Am J Pathol*, 139, 787-99.
- KOUROS-MEHR, H. & WERB, Z. 2006. Candidate regulators of mammary branching morphogenesis identified by genome-wide transcript analysis. *Dev Dyn*, 235, 3404-12.
- KRIEG, M., ARBOLEDA-ESTUDILLO, Y., PUECH, P. H., KÄFER, J., GRANER, F., MÜLLER, D. J. & HEISENBERG, C. P. 2008. Tensile forces govern germ-layer organization in zebrafish. *Nat Cell Biol*, 429-436.
- KURSAWE, J., BRODSKIY, P. A., ZARTMAN, J. J., BAKER, R. E. & FLETCHER, A. G. 2015. Capabilities and limitations of tissue size control through passive mechanical forces. *PLoS Comput Biol*, 11, e1004679.
- LAHLOU, H. & MULLER, W. J. 2011. beta1-integrins signaling and mammary tumor progression in transgenic mouse models: implications for human breast cancer. *Breast Cancer Res*, 13, 229.
- LANGLANDS, A. J., ALMET, A. A., APPLETON, P. L., NEWTON, I. P., OSBORNE, J. M. & NÄTHKE, I. S. 2016. Paneth Cell-Rich Regions Separated by a Cluster of Lgr5+ Cells Initiate Crypt Fission in the Intestinal Stem Cell Niche. *PLoS Biol*, 14, e1002491-e1002491.
- LARSEN, M., WEI, C. & YAMADA, K. M. 2006. Cell and fibronectin dynamics during branching morphogenesis. *Journal of Cell Science*, 119, 3376-3384.
- LECHLER, T. & FUCHS, E. Asymmetric cell divisions promote stratification and differentiation of mammalian skin.

- LEE, S., JILANI, S. M., NIKOLOVA, G. V., CARPIZO, D. & IRUELA-ARISPE, M. L. 2005. Processing of VEGF-A by matrix metalloproteinases regulates bioavailability and vascular patterning in tumors. *J Cell Biol*, 169, 681-91.
- LEE, S. Y., ROBERTSON, C., DIOT, A., MEURAY, V., BOURDON, J. C. & BISSELL, M. J. 2022. $\Delta 133p53$ coordinates ECM-driven morphogenesis and gene expression in three-dimensional mammary epithelial acini. *J Cell Sci*, 135.
- LI, J., SUN, H., FELTRI, M. L. & MERCURIO, A. M. 2015. Integrin beta4 regulation of PTHrP underlies its contribution to mammary gland development. *Dev Biol*, 407, 313-20.
- LI, N., ZHANG, Y., NAYLOR, M. J., SCHATZMANN, F., MAURER, F., WINTERMANTEL, T., SCHUETZ, G., MUELLER, U., STREULI, C. H. & HYNES, N. E. 2005. Beta1 integrins regulate mammary gland proliferation and maintain the integrity of mammary alveoli. *Embo j*, 24, 1942-53.
- LILJA, A. M., RODILLA, V., HUYGHE, M., HANNEZO, E., LANDRAGIN, C., RENAUD, O., LEROY, O., RULANDS, S., SIMONS, B. D. & FRE, S. 2018. Clonal analysis of Notch1-expressing cells reveals the existence of unipotent stem cells that retain long-term plasticity in the embryonic mammary gland.
- LINDSTRÖM, R., SATTA, J. P., MYLLYMÄKI, S.-M., LAN, Q., TRELA, E., PRUNSKAITE-HYYRYLÄINEN, R., VOUTILAINEN, M., KUURE, S., VAINIO, S. J. & MIKKOLA, M. L. 2022. Unraveling the principles of mammary gland branching morphogenesis. *bioRxiv*, 2022.08.23.504958.
- LINNEMANN, J. R., MIURA, H., MEIXNER, L. K., IRMLER, M., KLOOS, U. J., HIRSCHI, B., BARTSCH, H. S., SASS, S., BECKERS, J., THEIS, F. J., GABKA, C., SOTLAR, K. & SCHEEL, C. H. 2015. Quantification of regenerative potential in primary human mammary epithelial cells. *Development*, 142, 3239-51.
- LIU, S., NGO, U., TANG, X. Z., REN, X., QIU, W., HUANG, X., DEGRADO, W., ALLEN, C. D., JO, H., SHEPPARD, D. & SUNDARAM, A. B. 2021. Integrin $\alpha 2\beta 1$ regulates collagen I tethering to modulate hyperresponsiveness in reactive airway disease models. *J Clin Invest*, 131.
- LIU, X., SUN, Q., WANG, Q., HU, C., CHEN, X., LI, H., CZAJKOWSKY, D. M. & SHAO, Z. 2022. Epithelial Cells in 2D and 3D Cultures Exhibit Large Differences in Higher-order Genomic Interactions. *Genomics Proteomics Bioinformatics*, 20, 101-109.
- LIU, Y., CHATTOPADHYAY, N., QIN, S., SZEKERES, C., VASYLYEVA, T., MAHONEY, Z. X., TAGLIANTI, M., BATES, C. M., CHAPMAN, H. A., MINER, J. H. & KREIDBERG, J. A. 2009. Coordinate integrin and c-Met signaling regulate Wnt gene expression during epithelial morphogenesis. *Development*, 136, 843-53.
- LU, S., SIMIN, K., KHAN, A. & MERCURIO, A. M. 2008. Analysis of integrin beta4 expression in human breast cancer: association with basal-like tumors and prognostic significance. *Clin Cancer Res*, 14, 1050-8.
- LUNA-MORÉ, S., GONZALEZ, B., ACEDO, C., RODRIGO, I. & LUNA, C. 1994. Invasive micropapillary carcinoma of the breast. A new special type of invasive mammary carcinoma. *Pathol Res Pract*, 190, 668-74.

- MA, R., GONG, D., YOU, H., XU, C., LU, Y., BERGERS, G., WERB, Z., KLEIN, O. D., PETRITSCH, C. K. & LU, P. 2022. LGL1 binds to Integrin β 1 and inhibits downstream signaling to promote epithelial branching in the mammary gland. *Cell Rep*, 38, 110375.
- MACNAMARA, C. K., CAIAZZO, A., RAMIS-CONDE, I. & CHAPLAIN, M. A. J. 2020. Computational modelling and simulation of cancer growth and migration within a 3D heterogeneous tissue: The effects of fibre and vascular structure. *Journal of computational science*, 40, 101067.
- MALLEPELL, S., KRUST, A., CHAMBON, P. & BRISKEN, C. 2006. Paracrine signaling through the epithelial estrogen receptor alpha is required for proliferation and morphogenesis in the mammary gland. *Proc Natl Acad Sci U S A*, 103, 2196-201.
- MAREK, I., VOLKERT, G., JAHN, A., FAHLBUSCH, F., ZÜRN, C., OZCAN, Z., GOPPELT-STRUEBE, M., HILGERS, K. F., RASCHER, W. & HARTNER, A. 2010. Lack of α 8 integrin leads to morphological changes in renal mesangial cells, but not in vascular smooth muscle cells. *BMC Cell Biol*, 11, 102.
- MARTIN, K., PRITCHETT, J., LLEWELLYN, J., MULLAN, A. F., ATHWAL, V. S., DOBIE, R., HARVEY, E., ZEEF, L., FARROW, S., STREULI, C., HENDERSON, N. C., FRIEDMAN, S. L., HANLEY, N. A. & PIPER HANLEY, K. 2016. PAK proteins and YAP-1 signalling downstream of integrin beta-1 in myofibroblasts promote liver fibrosis. *Nature Communications*, 7, 12502.
- MARTINEZ-LEMUS, L. A., CROW, T., DAVIS, M. J. & MEININGER, G. A. 2005. α 5 β 1-integrin blockade inhibits myogenic constriction of skeletal muscle resistance arterioles. *Am J Physiol Heart Circ Physiol*, 289, H322-9.
- MIECZKOWSKI, K., POPEŁDA, M., LESNIAK, D., SADEJ, R. & KITOWSKA, K. 2022. *FGFR2 controls growth, adhesion and migration of nontumorigenic human mammary epithelial cells by regulation of integrin β 1 degradation.*
- MIRONOV, A., FISHER, M., NARAYANAN, P., ELSAYED, R., KARABULUTOGLU, M. & AKHTAR, N. 2023. Rac1 controls cell turnover and reversibility of the involution process in postpartum mammary glands. *PLoS Biol*, 21, e3001583.
- MONTES-OLIVAS, S., MARUCCI, L. & HOMER, M. 2019. Mathematical Models of Organoid Cultures. *Front Genet*, 10, 873.
- MOORE, D. M., VOGL, A. W., BAIMBRIDGE, K. & EMERMAN, J. T. 1987. Effect of calcium on oxytocin-induced contraction of mammary gland myoepithelium as visualized by NBD-phalloidin. *J Cell Sci*, 88 (Pt 5), 563-9.
- MORI, H., GJOREVSKI, N., INMAN, J. L., BISSELL, M. J. & NELSON, C. M. 2009. Self-organization of engineered epithelial tubules by differential cellular motility. *Proceedings of the National Academy of Sciences*, 106, 14890-14895.
- MROUE, R., INMAN, J., MOTT, J., BUDUNOVA, I. & BISSELL, M. J. 2015. Asymmetric expression of connexins between luminal epithelial- and myoepithelial- cells is essential for contractile function of the mammary gland. *Dev Biol*, 399, 15-26.
- MURRAY, P. J., CARRIERI, F. A. & DALE, J. K. 2019. Cell cycle regulation of oscillations yields coupling of growth and form in a computational model of the presomitic mesoderm. *J Theor Biol*, 481, 75-83.

- MUSCHLER, J. & STREULI, C. H. 2010. Cell-matrix interactions in mammary gland development and breast cancer. *Cold Spring Harb Perspect Biol*, 2, a003202.
- MYAT, M. M. & ANDREW, D. J. 2002. Epithelial tube morphology is determined by the polarized growth and delivery of apical membrane. *Cell*, 111, 879-91.
- MYLLYMÄKI, S. M., KACZYŃSKA, B., LAN, Q. & MIKKOLA, M. L. 2023. Spatially coordinated cell cycle activity and motility govern bifurcation of mammary branches. *J Cell Biol*, 222.
- MYLLYMÄKI, S. M., TERÄVÄINEN, T. P. & MANNINEN, A. 2011. Two distinct integrin-mediated mechanisms contribute to apical lumen formation in epithelial cells. *PLoS ONE*, 6, e19453.
- NAKANO, H., FURUYA, K. & YAMAGISHI, S. 2001. Synergistic effects of ATP on oxytocin-induced intracellular Ca²⁺ response in mouse mammary myoepithelial cells. *Pflugers Arch*, 442, 57-63.
- NAYLOR, M. J., LI, N., CHEUNG, J., LOWE, E. T., LAMBERT, E., MARLOW, R., WANG, P., SCHATZMANN, F., WINTERMANTEL, T., SCHUETZ, G., CLARKE, A. R., MUELLER, U., HYNES, N. E. & STREULI, C. H. 2005. Ablation of beta1 integrin in mammary epithelium reveals a key role for integrin in glandular morphogenesis and differentiation. *J Cell Biol*, 171, 717-28.
- NELSON, C. M., VANDUIJN, M. M., INMAN, J. L., FLETCHER, D. A. & BISSELL, M. J. 2006. Tissue geometry determines sites of mammary branching morphogenesis in organotypic cultures. *Science*, 314, 298-300.
- NEPTUNE, E. R., FRISCHMEYER, P. A., ARKING, D. E., MYERS, L., BUNTON, T. E., GAYRAUD, B., RAMIREZ, F., SAKAI, L. Y. & DIETZ, H. C. 2003. Dysregulation of TGF-beta activation contributes to pathogenesis in Marfan syndrome. *Nat Genet*, 33, 407-11.
- NEUMANN, N. M., KIM, D. M., HUEBNER, R. J. & EWALD, A. J. 2023. Collective cell migration is spatiotemporally regulated during mammary epithelial bifurcation. *J Cell Sci*, 136.
- NEUMANN, N. M., PERRONE, M. C., VELDHUIS, J. H., HUEBNER, R. J., ZHAN, H., DEVREOTES, P. N., BRODLAND, G. W. & EWALD, A. J. 2018. Coordination of Receptor Tyrosine Kinase Signaling and Interfacial Tension Dynamics Drives Radial Intercalation and Tube Elongation. *Dev Cell*, 45, 67-82.e6.
- NGUYEN, D. A., PARLOW, A. F. & NEVILLE, M. C. 2001. Hormonal regulation of tight junction closure in the mouse mammary epithelium during the transition from pregnancy to lactation. *J Endocrinol*, 170, 347-56.
- NISHIMORI, K., YOUNG, L. J., GUO, Q., WANG, Z., INSEL, T. R. & MATZUK, M. M. 1996. Oxytocin is required for nursing but is not essential for parturition or reproductive behavior. *Proc Natl Acad Sci U S A*, 93, 11699-704.
- NISHIUCHI, R., TAKAGI, J., HAYASHI, M., IDO, H., YAGI, Y., SANZEN, N., TSUJI, T., YAMADA, M. & SEKIGUCHI, K. 2006. Ligand-binding specificities of laminin-binding integrins: a comprehensive survey of laminin-integrin interactions using recombinant alpha3beta1, alpha6beta1, alpha7beta1 and alpha6beta4 integrins. *Matrix Biol*, 25, 189-97.

- NISSEN, S. B., PERERA, M., GONZALEZ, J. M., MORGANI, S. M., JENSEN, M. H., SNEPPEN, K., BRICKMAN, J. M. & TRUSINA, A. 2017. Four simple rules that are sufficient to generate the mammalian blastocyst. *PLoS Biol*, 15, e2000737.
- NOSE, A., NAGAFUCHI, A. & TAKEICHI, M. 1988. Expressed recombinant cadherins mediate cell sorting in model systems. *Cell*, 54, 993-1001.
- O'BRIEN, L. E., JOU, T. S., POLLACK, A. L., ZHANG, Q., HANSEN, S. H., YURCHENCO, P. & MOSTOV, K. E. 2001. Rac1 orientates epithelial apical polarity through effects on basolateral laminin assembly. *Nat Cell Biol*, 3, 831-8.
- OLABI, S., UCAR, A., BRENNAN, K. & STREULI, C. H. 2018. Integrin-Rac signalling for mammary epithelial stem cell self-renewal. *Breast Cancer Research*.
- PAINE, I., CHAUVIERE, A., LANDUA, J., SREEKUMAR, A., CRISTINI, V., ROSEN, J. & LEWIS, M. T. 2016. A Geometrically-Constrained Mathematical Model of Mammary Gland Ductal Elongation Reveals Novel Cellular Dynamics within the Terminal End Bud. *PLoS Comput Biol*, 12, e1004839.
- PAINE, I. S. & LEWIS, M. T. 2017. The Terminal End Bud: the Little Engine that Could. *J Mammary Gland Biol Neoplasia*, 22, 93-108.
- PAL, B., CHEN, Y., MILEVSKIY, M. J. G., VAILLANT, F., PROKOPIUK, L., DAWSON, C. A., CAPALDO, B. D., SONG, X., JACKLING, F., TIMPSON, P., LINDEMAN, G. J., SMYTH, G. K. & VISVADER, J. E. 2021. Single cell transcriptome atlas of mouse mammary epithelial cells across development. *Breast Cancer Res*, 23, 69.
- PALSSON, E. 2001. A three-dimensional model of cell movement in multicellular systems. *Future Generation Computer Systems*, 17, 835 - 852.
- PATHMANATHAN, P., COOPER, J., FLETCHER, A., MIRAMS, G., MURRAY, P., OSBORNE, J., PITT-FRANCIS, J., WALTER, A. & CHAPMAN, S. J. 2009. A computational study of discrete mechanical tissue models. *Phys Biol*, 6, 036001.
- PAULUS, J. K., BRUGGE, J. S., REGINATO, M. J., MILLS, K. R., DEBNATH, J., LYNCH, D. K., SGROI, D. C. & MUTHUSWAMY, S. K. 2003. Integrins and EGFR coordinately regulate the pro-apoptotic protein Bim to prevent anoikis. *Nat Cell Biol*, 5, 733-740.
- PERRIMON, N. & BERNFIELD, M. 2000. Specificities of heparan sulphate proteoglycans in developmental processes. *Nature*, 404, 725-8.
- PFANNENSTEIN, A. & MACARA, I. G. 2023. A junction-dependent mechanism drives murine mammary cell intercalation for ductal elongation. *Dev Cell*, 58, 1126-1138.e4.
- PITELKA, D. R., HAMAMOTO, S. T., DUAFALA, J. G. & NEMANIC, M. K. 1973. Cell contacts in the mouse mammary gland. I. Normal gland in postnatal development and the secretory cycle. *J Cell Biol*, 56, 797-818.
- PITT-FRANCIS, J., PATHMANATHAN, P., BERNABEU, M. O., BORDAS, R., COOPER, J., FLETCHER, A. G., MIRAMS, G. R., MURRAY, P., OSBORNE, J. M., WALTER, A., CHAPMAN, S. J., GARNY, A., VAN LEEUWEN, I. M. M., MAINI, P. K., RODRÍGUEZ, B., WATERS, S. L., WHITELEY, J. P., BYRNE, H. M. & GAVAGHAN, D. J. 2009. Chaste: A test-driven approach to software development for biological modelling. *Computer physics communications*, 180, 2452-2471.

- PRESTON, S. E. J., BARTISH, M., RICHARD, V. R., AGHIGH, A., GONÇALVES, C., SMITH-VOUDOURIS, J., HUANG, F., THÉBAULT, P., CLERET-BUHOT, A., LAPOINTE, R., LÉGARÉ, F., POSTOVIT, L. M., ZAHEDI, R. P., BORCHERS, C. H., MILLER, W. H., JR. & DEL RINCÓN, S. V. 2022. Phosphorylation of eIF4E in the stroma drives the production and spatial organisation of collagen type I in the mammary gland. *Matrix Biol*, 111, 264-288.
- RABINOVITZ, I., TOKER, A. & MERCURIO, A. M. 1999. Protein kinase C-dependent mobilization of the alpha6beta4 integrin from hemidesmosomes and its association with actin-rich cell protrusions drive the chemotactic migration of carcinoma cells. *J Cell Biol*, 146, 1147-60.
- RADICE, G. L., FERREIRA-CORNWELL, M. C., ROBINSON, S. D., RAYBURN, H., CHODOSH, L. A., TAKEICHI, M. & HYNES, R. O. 1997. Precocious mammary gland development in P-cadherin-deficient mice. *J Cell Biol*, 139, 1025-32.
- RAJARAM, R. D., BURIC, D., CAIKOVSKI, M., AYYANAN, A., ROUGEMONT, J., SHAN, J., VAINIO, S. J., YALCIN-OZUYSAL, O. & BRISKEN, C. 2015. Progesterone and Wnt4 control mammary stem cells via myoepithelial crosstalk. *Embo j*, 34, 641-52.
- RAY, R. P., MATAMORO-VIDAL, A., RIBEIRO, P. S., TAPON, N., HOULE, D., SALAZAR-CIUDAD, I. & THOMPSON, B. J. 2015. Patterned Anchorage to the Apical Extracellular Matrix Defines Tissue Shape in the Developing Appendages of Drosophila. *Dev Cell*, 34, 310-22.
- RAYMOND, K., CAGNET, S., KREFT, M., JANSSEN, H., SONNENBERG, A. & GLUKHOVA, M. A. 2011. Control of mammary myoepithelial cell contractile function by $\alpha 3\beta 1$ integrin signalling. *Embo j*, 30, 1896-906.
- REVELL, C., BLUMENFELD, R. & CHALUT, K. J. 2019. Force-based three-dimensional model predicts mechanical drivers of cell sorting. *Proceedings. Biological sciences*, 286, 20182495-20182495.
- REVERTE, C. G., BENWARE, A., JONES, C. W. & LAFLAMME, S. E. 2006. Perturbing Integrin Function Inhibits Microtubule Growth from Centrosomes, Spindle Assembly, and Cytokinesis. *J Cell Biol*, 174, 491-497.
- RIOS, A. C., FU, N. Y., LINDEMAN, G. J. & VISVADER, J. E. 2014. In situ identification of bipotent stem cells in the mammary gland. *Nature*, 506, 322-7.
- ROBINSON, E. E., ZAZZALI, K. M., CORBETT, S. A. & FOTY, R. A. 2003. Alpha5beta1 integrin mediates strong tissue cohesion. *J Cell Sci*, 116, 377-86.
- RODIUS, S., INDRA, G., THIBAUT, C., PFISTER, V. & GEORGES-LABOUESSE, E. 2007. Loss of alpha6 integrins in keratinocytes leads to an increase in TGFbeta and AP1 signaling and in expression of differentiation genes. *J Cell Physiol*, 212, 439-49.
- RODRIGUES, M. A., CALDEIRA-BRANT, A. L., GOMES, D. A., SILVEIRA, T. L., CHIARINI-GARCIA, H. & CASSALI, G. D. 2021. Characterization of neoplastic cells outlining the cystic space of invasive micropapillary carcinoma of the canine mammary gland. *BMC Vet Res*, 17, 130.
- ROMAGNOLI, M., CAGNET, S., CHICHE, A., BRESSON, L., BAULANDE, S., DE LA GRANGE, P., DE ARCANGELIS, A., KREFT, M., GEORGE-LABOUESSE, E., SONNENBERG, A.,

- DEUGNIER, M. A., RAYMOND, K., GLUKHOVA, M. A. & FARALDO, M. M. 2019. Deciphering the Mammary Stem Cell Niche: A Role for Laminin-Binding Integrins. *Stem Cell Reports*, 12, 831-844.
- ROONEY, N., WANG, P., BRENNAN, K., GILMORE, A. P. & STREULI, C. H. 2016. The Integrin-Mediated ILK-Parvin-alphaPix Signaling Axis Controls Differentiation in Mammary Epithelial Cells. *J Cell Physiol*, 231, 2408-17.
- ROSSANT, J., CHAZAUD, C. & YAMANAKA, Y. 2003. Lineage allocation and asymmetries in the early mouse embryo. *Philos Trans R Soc Lond B Biol Sci*, 358, 1341-8; discussion 1349.
- RUNSWICK, S. K., O'HARE, M. J., JONES, L., STREULI, C. H. & GARROD, D. R. 2001. Desmosomal adhesion regulates epithelial morphogenesis and cell positioning. *Nat Cell Biol*, 3, 823-30.
- RUSSELL, W. M. S. & BURCH, R. L. 1960. The Principles of Humane Experimental Technique. *Medical Journal of Australia*, 1, 500-500.
- SAEKI, K., CHANG, G., KANAYA, N., WU, X., WANG, J., BERNAL, L., HA, D., NEUHAUSEN, S. L. & CHEN, S. 2021. Mammary cell gene expression atlas links epithelial cell remodeling events to breast carcinogenesis. *Commun Biol*, 4, 660.
- SAKAKURA, T., NISHIZUKA, Y. & DAWE, C. J. 1976. Mesenchyme-dependent morphogenesis and epithelium-specific cytodifferentiation in mouse mammary gland. *Science*, 194, 1439-41.
- SANDERSIUS, S. A. & NEWMAN, T. J. 2008. Modeling cell rheology with the Subcellular Element Model. *Phys Biol*, 5, 015002.
- SANTA-CRUZ MATEOS, C., VALENCIA-EXPÓSITO, A., PALACIOS, I. M. & MARTÍN-BERMUDO, M. D. 2020. Integrins regulate epithelial cell shape by controlling the architecture and mechanical properties of basal actomyosin networks. *PLoS Genet*, 16, e1008717.
- SCHAEFER, M., SHEVCHENKO, A. & KNOBLICH, J. A. 2000. A protein complex containing inscuteable and the G alpha-binding protein Pins orients asymmetric cell divisions in *Drosophila*. *Current biology*, 10, 353-362.
- SCHEDIN, P., MITRENGA, T., MCDANIEL, S. & KAECK, M. 2004. Mammary ECM composition and function are altered by reproductive state. *Mol Carcinog*, 41, 207-20.
- SEDZINSKI, J., HANNEZO, E., TU, F., BIRO, M. & WALLINGFORD, J. B. 2016. Emergence of an Apical Epithelial Cell Surface In Vivo. *Dev Cell*, 36, 24-35.
- SHACKLETON, M., VAILLANT, F., SIMPSON, K. J., STINGL, J., SMYTH, G. K., ASSELIN-LABAT, M. L., WU, L., LINDEMAN, G. J. & VISVADER, J. E. 2006. Generation of a functional mammary gland from a single stem cell. *Nature*, 439, 84-8.
- SHARPE, J. 2017. Computer modeling in developmental biology: growing today, essential tomorrow. *Development*, 144, 4214-4225.
- SHEHATA, M., TESCHENDORFF, A., SHARP, G., NOVČIĆ, N., RUSSELL, I. A., AVRIL, S., PRATER, M., EIREW, P., CALDAS, C., WATSON, C. J. & STINGL, J. 2012. Phenotypic and functional characterisation of the luminal cell hierarchy of the mammary gland. *Breast Cancer Res*, 14, R134.

- SONNENBERG, A., CALAFAT, J., JANSSEN, H., DAAMS, H., VAN DER RAAIJ-HELMER, L. M., FALCIONI, R., KENNEL, S. J., APLIN, J. D., BAKER, J., LOIZIDOU, M. & ET AL. 1991. Integrin alpha 6/beta 4 complex is located in hemidesmosomes, suggesting a major role in epidermal cell-basement membrane adhesion. *J Cell Biol*, 113, 907-17.
- ST CROIX, C. M., SHAND, S. H. & WATKINS, S. C. 2005. Confocal microscopy: comparisons, applications, and problems. *Biotechniques*, 39, S2-5.
- STAHL, S., WEITZMAN, S. & JONES, J. C. 1997. The role of laminin-5 and its receptors in mammary epithelial cell branching morphogenesis. *J Cell Sci*, 110 (Pt 1), 55-63.
- STEINBERG, M. S. 1963. Reconstruction of tissues by dissociated cells. Some morphogenetic tissue movements and the sorting out of embryonic cells may have a common explanation. *Science*, 141, 401-8.
- STERNLICHT, M. D., KOUROS-MEHR, H., LU, P. & WERB, Z. 2006. Hormonal and local control of mammary branching morphogenesis. *Differentiation*, 74, 365-81.
- STINGL, J., EIREW, P., RICKETSON, I., SHACKLETON, M., VAILLANT, F., CHOI, D., LI, H. I. & EAVES, C. J. 2006. Purification and unique properties of mammary epithelial stem cells. *Nature*, 439, 993-7.
- STREULI, C. H., EDWARDS, G. M., DELCOMMENNE, M., WHITELAW, C. B., BURDON, T. G., SCHINDLER, C. & WATSON, C. J. 1995. Stat5 as a target for regulation by extracellular matrix. *J Biol Chem*, 270, 21639-44.
- STRILIĆ, B., EGLINGER, J., KRIEG, M., ZEEB, M., AXNICK, J., BABÁL, P., MÜLLER, D. J. & LAMMERT, E. 2010. Electrostatic cell-surface repulsion initiates lumen formation in developing blood vessels. *Curr Biol*, 20, 2003-9.
- SUMBAL, J., CHICHE, A., CHARIFOU, E., KOLEDOVA, Z. & LI, H. 2020. Primary Mammary Organoid Model of Lactation and Involution. *Front Cell Dev Biol*, 8, 68.
- TADDEI, I., DEUGNIER, M. A., FARALDO, M. M., PETIT, V., BOUVARD, D., MEDINA, D., FÄSSLER, R., THIERY, J. P. & GLUKHOVA, M. A. 2008. Beta1 integrin deletion from the basal compartment of the mammary epithelium affects stem cells. *Nat Cell Biol*, 10, 716-22.
- TAKAYANAGI, Y., YOSHIDA, M., BIELSKY, I. F., ROSS, H. E., KAWAMATA, M., ONAKA, T., YANAGISAWA, T., KIMURA, T., MATZUK, M. M., YOUNG, L. J. & NISHIMORI, K. 2005. Pervasive social deficits, but normal parturition, in oxytocin receptor-deficient mice. *Proc Natl Acad Sci U S A*, 102, 16096-101.
- TALHOUK, R. S., CHIN, J. R., UNEMORI, E. N., WERB, Z. & BISSELL, M. J. 1991. Proteinases of the mammary gland: developmental regulation in vivo and vectorial secretion in culture. *Development*, 112, 439-49.
- TANG, N., MARSHALL, W. F., MCMAHON, M., METZGER, R. J. & MARTIN, G. R. 2011. Control of mitotic spindle angle by the RAS-regulated ERK1/2 pathway determines lung tube shape. *Science*, 333, 342-345.
- TETLEY, R. J., BLANCHARD, G. B., FLETCHER, A. G., ADAMS, R. J. & SANSON, B. 2016. Unipolar distributions of junctional Myosin II identify cell stripe boundaries that drive cell intercalation throughout *Drosophila* axis extension. *eLife*, 5, e12094.

- THÉRY, M. & BORNENS, M. 2006. Cell shape and cell division. *Curr Opin Cell Biol*, 18, 648-657.
- TONNING, A., HEMPHÄLÄ, J., TÅNG, E., NANNMARK, U., SAMAKOVLIS, C. & UV, A. 2005. A transient luminal chitinous matrix is required to model epithelial tube diameter in the *Drosophila* trachea. *Dev Cell*, 9, 423-30.
- TOYOSHIMA, F. & NISHIDA, E. 2007. Integrin-mediated adhesion orients the spindle parallel to the substratum in an EB1- and myosin X-dependent manner. *Embo j*, 26, 1487-98.
- VACHON, P. H. 2011. Integrin signaling, cell survival, and anoikis: distinctions, differences, and differentiation. *J Signal Transduct*, 2011, 738137.
- VAN KEYMEULEN, A., ROCHA, A. S., OUSSET, M., BECK, B., BOUVENCOURT, G., ROCK, J., SHARMA, N., DEKONINCK, S. & BLANPAIN, C. 2011. Distinct stem cells contribute to mammary gland development and maintenance. *Nature*, 479, 189-93.
- WAITKUS-EDWARDS, K. R., MARTINEZ-LEMUS, L. A., WU, X., TRZECIAKOWSKI, J. P., DAVIS, M. J., DAVIS, G. E. & MEININGER, G. A. 2002. alpha(4)beta(1) Integrin activation of L-type calcium channels in vascular smooth muscle causes arteriole vasoconstriction. *Circ Res*, 90, 473-80.
- WALKER, M. R., AMANTE, J. J., LI, J. R., LIU, H. B., ZHU, L., FELTRI, M. L., GOEL, H. L. & MERCURIO, A. M. 2020. Alveolar progenitor cells in the mammary gland are dependent on the beta 4 integrin. *Developmental Biology*, 457, 13-19.
- WARBURTON, M. J., MITCHELL, D., ORMEROD, E. J. & RUDLAND, P. 1982. Distribution of myoepithelial cells and basement membrane proteins in the resting, pregnant, lactating, and involuting rat mammary gland. *J Histochem Cytochem*, 30, 667-76.
- WATANABE, K., VILLARREAL-PONCE, A., SUN, P., SALMANS, M. L., FALLAHI, M., ANDERSEN, B. & DAI, X. 2014. Mammary morphogenesis and regeneration require the inhibition of EMT at terminal end buds by *Ovol2* transcriptional repressor. *Dev Cell*, 29, 59-74.
- WEAVER, V. M., LELIEVRE, S., LAKINS, J. N., CHRENEK, M. A., JONES, J. C., GIANCOTTI, F., WERB, Z. & BISSELL, M. J. 2002. beta4 integrin-dependent formation of polarized three-dimensional architecture confers resistance to apoptosis in normal and malignant mammary epithelium. *Cancer Cell*, 2, 205-16.
- WEAVER, V. M., PETERSEN, O. W., WANG, F., LARABELL, C. A., BRIAND, P., DAMSKY, C. & BISSELL, M. J. 1997. Reversion of the malignant phenotype of human breast cells in three-dimensional culture and in vivo by integrin blocking antibodies. *J Cell Biol*, 137, 231-45.
- WILLIAMS, J. M. & DANIEL, C. W. 1983. Mammary ductal elongation: differentiation of myoepithelium and basal lamina during branching morphogenesis. *Dev Biol*, 97, 274-90.
- WUIDART, A., SIFRIM, A., FIORAMONTI, M., MATSUMURA, S., BRISEBARRE, A., BROWN, D., CENTONZE, A., DANNAU, A., DUBOIS, C., VAN KEYMEULEN, A., VOET, T. & BLANPAIN, C. 2018. Early lineage segregation of multipotent embryonic mammary gland progenitors. *Nat Cell Biol*, 20, 666-676.

- YAO, E. S., ZHANG, H., CHEN, Y. Y., LEE, B., CHEW, K., MOORE, D. & PARK, C. 2007. Increased beta1 integrin is associated with decreased survival in invasive breast cancer. *Cancer Res*, 67, 659-64.
- YING, Z. & BERONJA, S. 2020. Embryonic Barcoding of Equipotent Mammary Progenitors Functionally Identifies Breast Cancer Drivers. *Cell Stem Cell*, 26, 403-419.e4.
- YONEMURA, S. 2014. Differential sensitivity of epithelial cells to extracellular matrix in polarity establishment. *PLoS One*, 9, e112922.
- YU, M., LIN, G., ARSHADI, N., KALATSKAYA, I., XUE, B., HAIDER, S., NGUYEN, F., BOUTROS, P. C., ELSON, A., MUTHUSWAMY, L. B., TONKS, N. K. & MUTHUSWAMY, S. K. 2012. Expression profiling during mammary epithelial cell three-dimensional morphogenesis identifies PTPRO as a novel regulator of morphogenesis and ErbB2-mediated transformation. *Mol Cell Biol*, 32, 3913-24.
- YU, W., DATTA, A., LEROY, P., O'BRIEN, L. E., MAK, G., JOU, T. S., MATLIN, K. S., MOSTOV, K. E. & ZEGERS, M. M. 2005. Beta1-integrin orients epithelial polarity via Rac1 and laminin. *Mol Biol Cell*, 16, 433-45.
- YU, W., MACIVER, B., ZHANG, L., BIEN, E. M., AHMED, N., CHEN, H., HANIF, S. Z., DE OLIVEIRA, M. G., ZEIDEL, M. L. & HILL, W. G. 2022. Deletion of Mechanosensory β 1-integrin From Bladder Smooth Muscle Results in Voiding Dysfunction and Tissue Remodeling. *Function*, 3.
- YU, W., SHEWAN, A. M., BRAKEMAN, P., EASTBURN, D. J., DATTA, A., BRYANT, D. M., FAN, Q. W., WEISS, W. A., ZEGERS, M. M. & MOSTOV, K. E. 2008. Involvement of RhoA, ROCK I and myosin II in inverted orientation of epithelial polarity. *EMBO Rep*, 9, 923-9.
- ZANGOUEI, M. H. & HABIBI, J. 2017. Hybrid multiscale modeling and prediction of cancer cell behavior. *PLoS One*, 12, e0183810-e0183810.
- ZARGHAM, R. & THIBAUT, G. 2006. Alpha 8 integrin expression is required for maintenance of the smooth muscle cell differentiated phenotype. *Cardiovasc Res*, 71, 170-8.
- ZHU, J. & MOGILNER, A. 2016. Comparison of cell migration mechanical strategies in three-dimensional matrices: a computational study. *Interface Focus*, 6, 20160040.
- ZUTTER, M. M., KRIGMAN, H. R. & SANTORO, S. A. 1993. Altered integrin expression in adenocarcinoma of the breast. Analysis by in situ hybridization. *Am J Pathol*, 142, 1439-48.